CRANFIELD UNIVERSITY

Petya K. Ivanova-Mitseva

DEVELOPMENT OF ADVANCED NANOSIZED MOLECULARLY IMPRINTED POLYMERS VIA SURFACE-INITIATED "*LIVING*" RADICAL POLYMERISATION

Cranfield Health

Doctor of Philosophy

Academic Year: 2009 – 2012

Supervisors:
Prof. Sergey A. Piletsky
Dr. Michael J. Whitcombe
Dr. Elena V. Piletska

January 2012

CRANFIELD UNIVERSITY

Cranfield Health

Doctor of Philosophy

Academic Year 2009 - 2012

Petya K. Ivanova-Mitseva

DEVELOPMENT OF ADVANCED NANOSIZED MOLECULARLY IMPRINTED POLYMERS VIA SURFACE-INITIATED "*LIVING*" RADICAL POLYMERISATION

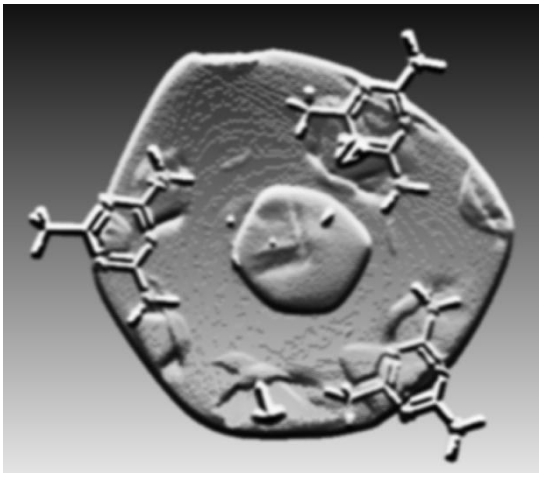

Supervisors:
Prof. Sergey A. Piletsky
Dr. Michael J. Whitcombe
Dr. Elena V. Piletska
January 2012

This thesis is submitted in partial fulfilment of the requirements for the degree of PhD

на Димитрина и Красимир Иванови

„Няма невъзможни неща. Всичко е възможно само желание трябва."

"It's a dangerous business, going out your door.
You step onto the road,
and if you don't keep your feet,
there's no telling where you might be swept off to."

Yours after J. R. R. Tolkien, CBE

Bilbo Baggins: The Lord of the Rings: The Fellowship of the Ring

ABSTRACT

Surface-initiated *photo-iniferter* mediated *controlled* polymerisation was used as a technique for the development of advanced and smart materials. Molecularly imprinted polymer (MIP) shell nanoparticles (NPs) were synthesised in this way from PAMAM dendrimers, used as a graftable core, in 2 min irradiation time. Surprisingly the so-synthetised NPs were around 200 nm and had a cubic shape. The NPs showed dissociation constant, K_d calculated via Biaevaluation software (Biacore), of 1.76×10^{-10} M for MIP, and 1.11×10^{-8} M for Blank (control) for the template compound (acetoguanamine). The apparent K_d calculated for MIP NPs to a close analogue to the template: atrazine desisopropyl, was 3×10^{-8} M and 3.2×10^{-5} M for Blank. Fluorescent core NPs were prepared using the same composition but using a dendrimer core partially modified with a fluorescent label (dansyl). They showed high affinity and selectivity towards fluorescent sensing of the template in solution after just 10 min incubation time. The limit of detection was calculated to be 3×10^{-8} M. A new monomer: *N*-(*N'*,*N'*-diethyldithiocarbamoyl ethyl amido ethyl)-aniline (NDDEAEA), that combines a dithiocarbamate ester (DTCE) part and an aniline part was synthsised and fully characterised. *N*-substituted polyaniline (PANI) was synthesised by both chemical and electrochemical polymerisation. Successful UV-initiated *grafting from* polymerisation of different monomers (styrene, methacrylic acid, lauryl methacrylate and acrylamido-2-methylpropane sulfonic acid) was achieved from different substrate supports (gold, glass, polypropylene, polystyrene). Poly (NDDEAEA) was further analysed for conductivity enhancement during UV irradiation. This material performance was compared with PANI and with another synthesised polymer: poly (*S*-methyl-*N*-methyl-*N*-ethyl (2-(phenylamino)) dithiocarbamate ester) (poly (MEPDTC)). Greater enhancement in the conductivity of poly (MEPDTC) was measured. This result was attributed to the fact that poly (MEPDTC) forms *dormant* (stable) radicals that induce doping effect in the polymer. These versatile new materials can be used in biosensing as materials with integrated functionalities (*e.g.* conductivity, molecular recognition, catalysis and controlled transport properties *etc.*).

Keywords: grafting from, dithiocarbamate ester group, *N*-substituted polyaniline, conductivity, fluorescent core MIP nanoparticles.

ACKNOWLEDGEMENTS

Above all, I would like to thank Prof. Sergey Piletsky, Dr. Michael Whitcombe and Dr. Elena Piletska, for supervising my work and for being motivating, enthusiastic and loyal supervisors that provide enough freedom and support for the development and realisation of own ideas. I would like to thank the whole Smart Materials Group for the nice and sympathetic ambience in the laboratory, who helped me feel at home in Cranfield Health from the very first day. I would also like to thank Dr. Antonio Guerreiro for the adequate and professional laboratory assistance, to Dr. Frank Davis for his creative comments and critical review of the writing of papers and of this thesis and to Dr. Dhana Lakshmi for reasons too numerous to detail here. I would also like to thank Dr. Kal Karim for the computational modelling assistance and for being the assessor of my work. Dr. Mathew Karsaw is gratefully acknowledged for his assistance with XPS and SEM analysis as well as Dr. Zhaoxia Zhou (University of Loughborough, UK) for the TEM and EDX analysis. I am grateful to Prof. Seamus Higson for being chairman of my work. Prof. Ian Nicholls (University of Kalmar, Sweden) is kindly acknowledged for the warm and smooth hospitality during my stay in his laboratory where radioactive scintillation measurements were performed. Dr Victor Chechik (University of York, UK) is acknowledged for the ESR analysis. Thanks also go to Mr. David Titmus for the fast deliveries and to Susan and David Johnston and Rita and Tom O'Brien that were making my resultless days sunny. Thanks also to all the master students that I had the pleasure to work with during this period, whose optimism and scientific innocence were so refreshingly inspiring. Thank you, Chem. Eng. Diana Ivanova, Dr. Konstantinos Karras and Miss. Andrea Schmolzer. I would also like to acknowledge the committee of this thesis. I thank the EU Commission (Seventh Framework Programme, Water Treatment by Molecularly Imprinted Materials (WATERMIM), with grant agreement number CP-FP 226524) for the provided financial support. Without any of the listed above, what is going to follow after this tiny page, would have never happened in this way.

TABLE OF CONTENTS

ABSTRACT v
ACKNOWLEDGEMENTS vii
AIMS AND OBJECTICES xiii
LIST OF FIGURES xv
LIST OF TABLES xxi
LIST OF SCHEMES xxiii
LIST OF APPENDIX FIGURES xxv
LIST OF APPENDIX TABLES xxix
LIST OF ABBREVIATIONS xxxi
1 Literature Review 1
1.1 Introduction 3
1.2 Molecularly Imprinted Polymers (MIPs) 5
1.3 Nano-MIPs 9
1.4 Surface-Initiated Controlled Radical Polymerisation (SI-CRP) 11
1.4.1 Surface-initiated nitroxide-mediated f*ree-radical* polymerisations (SI-NMP) 14
1.4.2 Surface-initiated nitroxide-mediated *free-radical* polymerisations (SI-NMP) and MIPs 21
1.4.3 Surface-initiated atom transfer radical polymerisation (SI-ATRP) 23
1.4.4 Surface-initiated atom transfer radical polymerisation (SI-ATRP) and MIPs 26
1.4.5 Surface-initiated reversible addition-fragmentation chain-transfer (SI-RAFT) polymerisation 29
1.4.6 Surface-initiated reversible addition-fragmentation chain-transfer (SI-RAFT) polymerisation and MIPs 33
1.4.7 Surface-initiated *photo-iniferter* mediated polymerisation (SI-PIMP) 36
1.4.8 Surface-initiated *photo-iniferter* mediated polymerisation (SI-PIMP) and MIPs 40
1.5 Conclusions 45
2 Cubic MIP Nanoparticles – Building Blocks for a Bright Future 47
2.1 Introduction 49
2.2 Results and Discussion 55
2.2.1 Surface modification and characterisation of PAMAM dendrimers 55
2.2.2 Synthesis of MIP NPs 62
2.2.3 Polymer affinity testing 67
2.2.4 Fluorescent sensing 70
2.3 Experimental Details 74
2.3.1 Materials 74

2.3.2 Apparatus 74
2.3.3 Synthesis of *S*-(carboxypropyl)-*N,N*-diethyl-dithiocarbamic acid (CNDDA) .. 76
2.3.4 Surface modification and characterisation of PAMAM dendrimers 77
2.3.5 Synthesis of MIP and Blank NPs 78
2.3.6 Preparation of affinity adsorbent 79
2.3.7 Affinity separation on a glass beads column 79
2.3.8 Polymer affinity testing 80
2.3.9 Treatment of gold chips 80
2.3.10 Scanning electron microscopy (SEM) and transmission electron spectroscopy (TEM) 81
2.3.11 Fluorescent labelling of PAMAM dendrimers 81
2.3.12 Synthesis of fluorescent core MIP and Blank NPs 82
2.4 Conclusions 83
3 Conjugated Polymers with Pendant *Iniferter* Units – Versatile Materials for Grafting 85
3.1 Introduction 87
3.2 Results and Discussion 95
3.2.1 Synthesis of *N*-(*N´,N´*-diethyldithiocarbamoyl ethyl amido ethyl)-aniline (NDDEAEA) 95
3.2.2 Electropolymerisation of NDDEAEA 100
3.2.3 Molecular modeling of NDDEAEA and poly (NDDEAEA) 103
3.2.4 Surface-confined photo grafting of various polymers 105
3.2.5 Deposition of poly (NDDEAEA) films using chemical oxidation 110
3.2.6 Grafting of poly (*N*-(3-aminopropyl)-methacrylamide) over chemically polymerised poly (NDDEAEA) through a TEM grid 114
3.3 Experimental Details 115
3.3.1 Materials 115
3.3.2 Apparatus 115
3.3.3 Synthesis of *N*-(*N´,N´*-Diethyldithiocarbamoyl ethyl amido ethyl)-aniline (NDDEAEA) 116
3.3.4 Electropolymerisation of the aniline group of NDDEAEA 117
3.3.5 Molecular Modeling of NDDEAEA and poly (NDDEAEA) 118
3.3.6 Surface-confined photo grafting of various polymers onto electropolymerised films of NDDEAEA 118
3.3.7 Chemical oxidative polymerisation of NDDEAEA on polypropylene (PP) ultra-filtration membranes (thinner films) 120
3.3.8 Photografting by UV polymerisation of monomers onto chemically oxidized poly (NDDEAEA)-modified PP membranes and glass slides 120
3.3.9 Surface-confined photo grafting of various monomers on poly (NDDEAEA)-modified microtitre plates 121

3.3.10 Spatially-confined grafting of poly (*N*-(3-aminopropyl)-methacrylamide) over chemically polymerised poly (NDDEEA) using a TEM grid as a photomask. 122
3.4 Conclusions 123
4 Enhancement of Conductivity by UV Irradiation in Polyanilines *N*-Substituted with *Dormant* or Active Radical Species 125
4.1 Introduction 127
4.2 Results and Discussion 132
4.2.1 Synthesis of *S*-methyl-*N*-methyl-*N*-ethyl (2-(phenylamino)) dithiocarbamate ester (MMDTCE) 133
4.2.2 Conductivity enhancement of chemically polymerised poly (NDDEAEA) and poly (MMDTCE) during UV irradiation 135
4.2.3 UV spectroscopy of chemically polymerised poly (NDDEAEA) and poly (MMDTCE) before and after UV irradiation 141
4.2.4 Electron spin resonance (ESR) of chemically polymerised poly (NDDEAEA), poly (MMDTCE) and PANI 144
4.2.5 Confocal laser scanning microscopy of chemically polymerised poly (NDDEAEA), poly (MMDTCE) and PANI 147
4.2.6 Conductivity measurements of electrochemically polymerised poly (NDDEAEA), poly (MMDTCE) and PANI during UV irradiation 152
4.3 Experimental Details 159
4.3.1 Materials 159
4.3.2 Apparatus 159
4.3.3 Synthesis of *N*-methyl-*N*'-phenyl-1,2-ethylenediamine (MPEDA) 160
4.3.4 Synthesis of *S*-methyl-*N*-methyl-*N*-ethyl (2-(phenylamino)) dithiocarbamate ester (MMDTCE) 161
4.3.5 Polymer deposition over interdigitated microsensor electrodes (IMEs) 162
4.3.6 Measuring the electrical properties of poly (NDDEAEA), poly (MMDTCE) and PANI during UV irradiation 163
4.3.7 UV spectroscopy of chemically polymerised poly (NDDEAEA), poly (MMDTCE) and PANI before and after UV irradiation 164
4.3.8 Cyclic voltamometry of electrochemically polymerised poly (NDDEAEA), poly (MMDTCE) and PANI during UV irradiation 164
4.4 Conclusions 166
5 General Conclusions and Future Work 169
REFERENCES 175
APPENDICES 213
Appendix A Cubic MIP Nanoparticles – Building Blocks for a Bright Future 213
Appendix B Conjugated Polymers with Pendant Iniferter Units – Versatile Materials for Grafting 219

Appendix C Enhancement of Conductivity by Ultraviolet Irradiation in Polyanilines *N*-substituted with *Dormant* or Active Radical 234

AIMS AND OBJECTICES

The aim of the present project is to prepare molecularly imprinted polymer (MIP) nanomaterials for the selective adsorption and sensing of environmental pollutants. The project forms part of the EU FP7 Network Project "WATERMIM", which involves seven research groups from five EU countries. The aim of this EU project is to develop MIP recognition element in sensors for water pollutants (pesticides, pharmaceutical active compounds). The key challenges to overcome in the project are to achieve high specificity of the sensor to selected pollutants and to make clear detection of analytes at concentrations in the order of μg L^{-1} so it would fulfil the rapidly changing regulations. It is evident that innovative methods for the synthesis of advanced functional materials with high selectivities are urgently required. This is why as part of this project the present PhD thesis would involve an exploration of the chemistry of new monomers and initiation systems for *living free* radical polymerisation and their application to the synthesis of molecularly imprinted nanoparticles, nanolayers and membranes with potential application in biosensing technology. The specific objectives for the proposed three years study will be:

1. To synthesise new compounds that can act as *photoiniferters* and to characterise them by NMR, MS, FT-IR and UV-visible spectroscopy.

2. To synthesise and characterise new *photoiniferters* which also incorporate polymerisable functionality.

3. To investigate the polymer chemistry of these materials as initiators and macroinitiators.

4. To synthesise well-defined MIP nanoparticles, nanolayers, and molecularly imprinted membranes and to characterise their chemical and physical properties.

6. To investigate the application of the synthesised materials in applications such as sensing, sequestering and separation.

7. To communicate the results of these studies through meetings and reports to the other EU project partners, through presentation at international conferences and the preparation of patents and of papers for submission to refereed journals.

The structure of the present thesis is organised as a series of results chapters, each dealing with an individual aspect of the research and comprising introduction, results and discussion, experimental and conclusions sections. The introduction of each chapter focuses on a review of the literature specific to the work presented in that chapter. A more general literature review is provided at the beginning of the thesis as Chapter 1.

LIST OF FIGURES

Figure 1.1: Bar graphics showing the number of MIPs publications and patents for the period 1994-2011 (the data is obtained from *mipdatabase.com*, last accessed on 19/12/2011)..... 6

Figure 1.2: Schematic representation of the molecular imprinting process showing some of the interactions used in creating template-monomer complex (a-e). (a) reversible covalent interaction; (b) semi-covalent method; (c) electrostatic interaction; (d) non-covalent interaction; (e) ligand exchange interaction. The scheme is adapted from Alexander *et al*. (2006). 7

Figure 1.3: Schematic representation of nitroxide-mediated *living* radical polymerisation mechanism. 15

Figure 1.4: Preparation of cholesterol-imprinted polymer using NMP. The transient *free* radicals generated from **4** (Step **a**) initiate chain polymerisation of **5** and divinylbenzene (Step **b**). The majority of the growing chain radicals are stabilised by their reversible association with TEMPO (Step **c**), so that permanent chain termination is avoided. This *living* polymerisation finally leads to the formation of imprinted sites in the cross-linked polymer network (Step **d**), which after hydrolysis (Step **e**) afford specific cholesterol binding cavities. The scheme is adapted from Boonpangrak *et al.* (**2006**). 22

Figure 1.5: Schematic representation of the catalytic cycle in ATRP: X=Cl, Br; P=polymer; M=monomer; L=N-ligand. 24

Figure 1.6: Schematic representation of the process of modification of nanotube membranes via SI-ATRP to achieve MIP nanotubes (Wang *et al.* 2006): a) Silanisation with 3-aminomethyltrimethoxysilane; b) Grafting of the ATRP agent on the membrane via substitution reaction with 2-bromo-2-methylpropyl bromide; c) Polymerisation of 4-vinylpyridine as functional monomer, ethylene glycol dimethacrylate as cross-linking agent in the presence of β-estradiol as template. CuBr/1,4,8,11-tetraazacyclotetradecane were used as ATRP initiators. The reaction was performed in acetonitrile under nitrogen atmospere at 70°C for 24 hours; d) Removal of estradiol from the imprinted polymer via washing with acetonitrile, methanol-acetic acid (9:1, v/v), and methanol, followed by drying *in vacuo*. 27

Figure 1.7: Schematic representation of the *living* character of RAFT polymerisation. 31

Figure 1.8: Schematic representation of the process of modification of silica gel particles (presented by pink rods on the diagram) via SI-ATRP to achieve MIP film (Li *et al*. 2009): a) Silanisation with 4-(chloromethyl) phenyltrimetoxysilane (Cl-Silica); b) Substitution reaction with phenylmagnesium bromide and carbon disulfide to prepare PhC(S)SMgBr, which reacted with Cl-Silica; c) Grafting of MIP film on the RAFT agent modified silica gel particles using bulk technique. Methacrylic acid, divinylbenzene, and azobis-(isobutylonitrile) were polymerised

in chloroform under nitrogen atmoshere at 60 °C for 24 hours. Theophylline was used as a template; d) The template was washed away and the polymer was dried *at vacuo* at 50 °C for 12 hours. 34

Figure 1.9: Schematic representation of *photoiniferter*-mediated polymerisation mechanism. 37

Figure 2.1: Schematic representation of the structure of polyamidoamines (PAMAM) 25% C_{12} (*N*-(2-hydroxydodecyl) groups) dendrimers, generation 4..... 53

Figure 2.2: Dynamic light scattering (DLS) size distribution for (blue diamonds) PAMAM, 25 % C_{12} with maximum peak intensity at 6.5 nm and (pink squares) *macroiniferter*, with an intensity peak maximum at 10.1 nm. 57

Figure 2.3: ^{1}H NMR spectra; A. CNDDA; B. *macroiniferter*; C. PAMAM 25% C_{12}, generation 4, dendrimer. All spectra were recorded in methanol – D_4. The arrows (in A and B) indicate the signals assigned to the methylene groups of the diethyldithiocarbamate residue ethyl substituents. 58

Figure 2.4: ^{13}C NMR spectra; A. *macroiniferter*; B. PAMAM 25% C_{12} dendrimer. All spectra were recorded in methanol – D_4. The characteristic peak of the carbonyl residue from the dialkyldithiocarbamate group at around 200 ppm is shown circled in red. 59

Figure 2.5: Fluorescence spectrum: A. 3D spectrum of isoindole complex the periphery of PAMAM 25% C_{12} dendrimer in methanol; B. Emission spectra of isoindole dendrimers in methanol: (pink solid line) PAMAM 25% C_{12} dendrimer and (blue dashed line) *macroiniferter*. 61

Figure 2.6: Size distribution of (blue diamonds) Blank NPs separated on affinity column at 4-6 minutes with mean hydrodynamic diameter of 220 nm and (pink squares) MIP NPs, affinity separated with mean hydrodynamic diameter of 246 nm. 63

Figure 2.7: (A) SEM micrographs of MIP NPs (scale bar 200 nm); (B) SEM micrographs of Blank NPs (scale bar 200 nm); (C) TEM of Blank NPs (scale bar 200 nm); (D) SEM micrographs of MIP NPs prepared by one minute irradiation time (scale bar 100 nm); (E) SEM micrographs of MIP NPs prepared by thirty seconds irradiation time (scale bar 100 nm); (F) Electron diffraction pattern of a cube-like particle; (G) EDX spectrum of a cube-like particle suggested it is rich in both carbon and oxygen.. 66

Figure 2.8: Above: Sensogram showing binding of MIP NPs to the specific ligand (melamine, solid line) and to a non-specific analogue (atrazine desisopropyl, dashed line) immobilised on Biacore sensor chips. Concentration of surface-accessible imprinted binding sites estimatedto be present in the undiluted dispersion of MIP NPs in PBS was 2.19 mM (Figure_Apx A.1, 5A.2, page 224). Injections were made in order of increasing concentration using dilutions of: 1/10000; 1/1000; 1/100; 1/10; 1 with respect to the stock NPs dispersion. Below: schematic representation of the binding between the immobilised ligand (A. melamine and B. atrazine desisopropyl) and MIP NPs. 69

Figure 2.9: Scanning electron micrographs of fluorescent core NPs prepared by one minute irradiation time of: A. MIP and B. Blank (scale bar 500 nm). 71

Figure 2.10: Intensity of the fluorescent response of MIP and Blank NPs to different concentrations of the template and close analogues (Atrazine Desisopropyl or Simazine) in acetonitrile after ten minutes incubation time. I_0 is the intensity of the emission maximum of the NPs without the template and I is the intensity of the emission maximum of the NPs with different concentrations of the template. Error bars represent ±1 standard deviation (n=3). 73

Figure 3.1: 400 MHz ^{1}H NMR spectrum of NDDEAEA (2) in DMSO-D_6 and 100 MHz ^{13}C NMR spectrum of NDDEAEA in DMSO-D_6 at 25 °C showing two peaks due to two conformations for the NDDEAEA around the N-C(=S) single bond. 97

Figure 3.2: 400 MHz ^{1}H NMR spectrum of NDDEAEA (2) in DMSO-D6 and 100 MHz ^{13}C NMR spectrum of NDDEAEA in DMSO-D_6 at 100 °C showing single high resolution peaks. 98

Figure 3.3: 400 MHz ^{1}H NMR spectrum of NDDEAEA (2) in DMSO-D_6 and 100 MHz ^{13}C NMR spectrum of NDDEAEA in DMSO-D_6 at 130 °C. 99

Figure 3.4: Cyclic voltammogram obtained during deposition of electropolymerised NDDEAEA films on gold screen-printed electrodes. Electropolymerisation of NDDEAEA (0.1 M in 0.75 M hydrochloric acid 25% acetonitrile in water) on a screen printed gold electrode by cyclic voltammetry (potential range: -0.2 V to 0.9 V versus Ag/AgCl, at 100 mV s^{-1} scan rate, 20 sweeps), under nitrogen atmosphere and in the dark, giving rise to poly (NDDEAEA). 102

Figure 3.5: The energy minimized structure of neutral (left) and protonated (right) NDDEAEA showing intramolecular hydrogen bonding. 104

Figure 3.6: Postulated structure of poly (NDDEAEA) (n=16) which shows polyaniline chains with DTCE side groups. 105

Figure 3.7: Electropolymerised poly (NDDEAEA) films UV irradiated for twenty minutes in the presence of styrene or methacrylic acid (0.1 M, acetonitrile), leading to surface-confined grafted polymer layers. Also the layer-by-layer (block copolymer) grafting of poly (styrene) over a grafted poly (methacrylic acid) layer is displayed. The static water contact angle shows changes consistent with the uppermost surface layer of the grafted polymer, such that polystyrene grafted over poly (MAA) shows the same contact angle as a single polystyrene grafted layer (Ivanova-Mitseva *et al.* 2010). 106

Figure 3.8: XPS spectra of electropolymerised film of poly (NDDEAEA) on a gold screen-printed electrode before UV irradiation (solid line) and after UV irradiation (dotted line). 109

Figure 3.9: a) polypropylene membrane (left) and poly (NDDEAEA)-coated membrane (right) and b) microtitre plate showing deposition of poly (NDDEAEA) in the wells. 112

Figure 3.10: Water contact angle image of chemically polymerised poly (NDDEAEA) over glass slide after UV grafting of poly (acrylamido-2-methylpropane sulfonic acid) (left) and polystyrene (right). 113

Figure 3.11: Confocal micrograph of poly (aminopropyl methacrylamide) grafted over poly (NDDEAEA) cast film over gold sputtered glass slide through chemical polymerisation. a) Before the removal of the TEM grid and b) after the removal of the TEM grid. Features are of the dimensions 200 μm × 200 μm. 114

Figure 4.1: Simple band energy dsiagram, showing the difference between insulator, semiconductor, PANI after UV irradiation, PANI before UV irradiation and metal (W: work function). 129

Figure 4.2: Conductivity measurements experimental set up diagram and principal idea behind the expected result. 136

Figure 4.3: Change in conductivity observed for poly (NDDEAEA), doped with 1 M hydrochloric acid, coated onto IMEs during UV irradiation. The intensity of the UV source was varied from 10 to 50 %. Each intensity level was repeated three times per electrode. 137

Figure 4.4: Change in conductivity observed for poly (MMDTCE) coated IMEs doped with 1M hydrochloric acid, during UV irradiation. The intensity of the UV source was varied from 10 to 50 %. Each intensity level was repeated three times per electrode..... 138

Figure 4.5: Change in conductivity observed for PANI, doped with 1 M hydrochloric acid, coated IMEs during UV irradiation. The intensity of the UV source was varied from 10 to 50 %. Each intensity level was repeated three times per electrode.. 139

Figure 4.6: UV spectra of chemically polymerised PANI, poly (NDDEAEA) and poly (MMDTCE) deposited on the walls of quarts cuvettes. For reference nitrogen gas was used. 142

Figure 4.7: ESR spectrum of poly (NDDEAEA) before (solid line) and after (dotted line) UV irradiation at 120 K. 144

Figure 4.8: ESR spectrum of poly (MMDTCE) before (solid line) and after (dotted line) UV irradiation at 120 K. 145

Figure 4.9: ESR spectrum of PANI before (solid line) and after (dotted line) UV irradiation at 120K. 146

Figure 4.10: Confocal 3D laser topography of PANI layer deposited over 96 % Al_20_3 support (blue top corner). 147

Figure 4.11: Confocal 3D laser colour model of PANI showing a blue, fine structure continuous organic layer over 96 % Al_20_3 support (the white top corner). 148

Figure 4.12: 2D laser monochromatic con-focal surface reproduction of PANI at a 2300 times magnification (scale bar 15 µm). 149

Figure 4.13: 2D laser monochromatic con-focal image of poly (NDDEAEA) (left) over an Al_2O_3 96% substrate support (right) (scale bar 20 µm). 150

Figure 4.14: 3D laser con-focal surface topography model of poly (MMDTCE). 151

Figure 4.15: 3D laser con-focal surface texture model of poly (MMDTCE). 151

Figure 4.16: Cyclic voltammogram obtained during deposition of electropolymerised poly (NDDEAEA) films on gold screen-printed electrodes. The electropolymerisation of NDDEAEA (0.1 M in 0.75 M hydrochloric acid 25% acetonitrile in water) was obtained by cyclic voltammetry (potential range: -0.2 V to 0.9 V versus Ag/AgCl, at 100 mV s^{-1} scan rate, 20 sweeps), under nitrogen atmosphere and in the dark which afforded the generation poly (NDDEAEA). .. 153

Figure 4.17: Cyclic voltammogram of electropolymerised poly (NDDEAEA) films obtained during UV irradiation (light intensity 0%, 10% and 50 %) in hydrochloric acid (0.1 M, 5 mL solution) on gold screen-printed electrodes by cyclic voltammetry (potential range: -0.2 V to 0.9 V versus Ag/AgCl, at 100 mV s^{-1} scan rate), under nitrogen atmosphere and in the dark. 154

Figure 4.18: Cyclic voltammogram obtained during deposition of electropolymerised poly (MMDTCE) films on gold screen-printed electrodes. The electropolymerisation of MMDTCE (0.1 M in 0.75 M hydrochloric acid 25% acetonitrile in water) was obtained by cyclic voltammetry (potential range: -0.2 V to 0.9 V versus Ag/AgCl, at 100 mV s^{-1} scan rate, 20 sweeps), under nitrogen atmosphere and in the dark which afforded the generation poly (MMDTCE). ... 155

Figure 4.19: Cyclic voltammogram of electropolymerised poly (MMDTCE) films obtained during UV irradiation (light intensity 0%, 10% and 50 %) in hydrochloric acid (0.1 M, 5 mL solution) on gold screen-printed electrodes by cyclic voltammetry (potential range: -0.2 V to 0.9 V versus Ag/AgCl, at 100 mV s^{-1} scan rate), under nitrogen atmosphere and in the dark. 156

Figure 4.20: Cyclic voltammogram obtained during deposition of electropolymerised PANI films on gold screen-printed electrodes. The electropolymerisation of PANI (0.1 M in 0.75 M hydrochloric acid 25% acetonitrile in water) was obtained by cyclic voltammetry (potential range: -0.2 V to 0.9 V versus Ag/AgCl, at 100 mV s^{-1} scan rate, 20 sweeps), under nitrogen atmosphere and in the dark which afforded the generation poly (PANI). 157

Figure 4.21: Cyclic voltammogram of electropolymerised PANI films obtained during UV irradiation (light intensity 0 %, 10 % and 50 %) in hydrochloric acid (0.1 M, 5 mL solution) on gold screen-printed electrodes by cyclic voltammetry (potential

range: -0.2 V to 0.9 V versus Ag/AgCl, at 100 mV s^{-1} scan rate), under nitrogen atmosphere and in the dark. 158

LIST OF TABLES

Table 2.1: Measured size and zeta potential for MIP and Blank NPs in different solvents. 65

Table 2.2: Static water contact angle in air for surface-modified gold Biacore chips after each stage of modification. 67

Table 3.1: Static water contact angles in air for various substrates, substrates modified with poly (NDDEAEA) and after surface-grafting of polymers..... 108

Table 3.2: XPS element composition (wt %) of the NDDEAEA monomer and its polymers. 110

Table 4.1: Measurement of the electrode surface temperature with thermocouple with nitrogen gas flow and in air. The readings were taken at the end of a five minutes irradiation period. 141

LIST OF SCHEMES

Scheme 1.1: Synthetic scheme for the SG1-based alkoxyamine initiator 1, used as a *free* initiator and initiator 3 used as grafted initiator in the work of Blas *et al.* (2011). N-butyl acrylate was reacted with BlocBuilder alkoxyamine in *tert*-butanol as a solvent at 100 °C for 1.24 hours to form the alkoxyamine 1. The alkoxyamine 2 was synthesised by reacting 1 with *N*-hydroxysuccinimide and dicyclohexylcarbodiimide in THF at 0 °C for 24 hours. The alkoxyamine 3 was synthesised by reacting 2 with 3-aminopropyldimethylethoxysilane in dichloromethane at ambient temperature for two hours. 20

Scheme 2.1: Schematic representation of the synthesis of the NPs. *S*-(carboxypropyl)-*N*,*N*-diethyldithiocarbamic acid (CNDDA) was reacted with the primary amino groups at the surface of the dendrimer via EDC coupling. The *macroiniferter* formed in this way was used further in a UV-initiated *living* radical polymerisation to create MIP NPs. The template was acetoguanamine which is known to form complexes with methacrylic acid (functional monomer). The resultant NPs were fractionated by affinity chromatography. 52

Scheme 2.2: The surface modification of PAMAM, 25% C_{12}, generation 4, dendrimer (4) with *iniferter* groups (CNDDA, 1) via standard EDC (2) coupling reaction leading to the formation of *macroiniferter* (5). 55

Scheme 2.3: The reaction between *o*-phaldialdehyde (7), a mercaptan (8) and a primary amine (10), *via* a hemithioacetal intermediate (9), leading to the formation of a fluorescent isoindole (11). 60

Scheme 2.4: Schematic representation of the synthesis of fluorescent *macroiniferter* (15). PAMAM dendrimer, generation 4 (12) was 50% surface modified with CNDDA (1) to form the product (13). The rest of the free amino groups from the periphery of (13) were modified with the fluorescent dye dansyl chloride (14). 71

Scheme 2.5: Schematic representation of the chemical structures of: Acetoguanamine (16); Melamine (17); Atrazine desisopropyl (18) and Simazine (19). 73

Scheme 3.1: Molecular structure formulas of PANI in its various states of oxidated or protonated forms. The scheme is adopted form MacDiarmid, 1997. 89

Scheme 3.2: Pathways for the initial steps of aniline oxidation and deprotonation and mechanism of aniline polymerisation, proposed by Wei *et al.* (1990). . 91

Scheme 3.3: Schematic representation of different polymerisation techniques and polymer structure of NDDEAEA monomer. 94

Scheme 3.4: Schematic representation of the synthesis of NDDEAEA (13) from CNDDA (12) and its polymers. Poly (NDDEAEA) (14) formed via electrochemical polymerisation or chemical oxidative polymerisation giving rise to polyaniline chains with pendant DTCE moieties. Addition of monomer (M), by UV grafting giving rise to poly (M)/poly (NDDEAEA) graft copolymers (15). 95

Scheme 4.1: Schematic representation of the designed structures of monomers in terms of the structures of their individual sub-units and their polymerisation to *N*-substituted PANIs. 131

Scheme 4.2: Schematic representation of the structures of the monomers NDDEAEA (13) and MMDTCE (16) and their oxidative polymerisation leading to the formation of the corresponding *N*-substituted PANIs (14 and 17). During UV irradiation the polymers will form active and *dormant* radicals, respectively along the PANI chain. 132

Scheme 4.3: Schematic representation of the synthesis of MMDTCE (16) via electrophilic substitution of MPEDA (18) with carbon disulfide. Methyl iodide was added to the dithiocarbamate salt to form the ester. 133

Scheme 4.4: Schematic representation of the mechanism for the synthesis of MPEDA hydrochloride (23). The mechanism is adapted from Poindexter *et al.* (1992). 135

LIST OF APPENDIX FIGURES

Figure_Apx A.1: Calibration curve obtained from gravimetric analysis of dried samples. 217

Figure_Apx A.2: Copy of spreadsheet calculation used to estimate concentration of *binding sites* (in mol L^{-1}) from concentration of *nanoparticles* (in mg mL^{-1}, obtained from the calibration plot shown in Figure_Apx A.1). In the worked example, an absorbance of 0.18 at λ = 197.4 nm gives a particle concentration of 0.023 mg mL^{-1}. From the measured diameter (Nanosizer) of 278 nm, the volume of an individual particle (assuming a sphere) is 1.12×10^{-14} cm^3. Assuming a density of 1 g mL^{-1}, the mass of one particle is calculated to be 1.12×10^{-14} g. This gives a figure of 2.0×10^{15} particles in 1 mL or 3.33×10^{-9} moles of particles per mL, from which a molar concentration of particles: 3.33 μM can be estimated. A further assumption is that there will be one binding site per 100 $Å^2$ of particle surface. Calculation of the surface area, gave a figure of 2.4×10^7 $Å^2$ per particle or 2.4×10^5 binding sites per particle. Multiplying this figure by the molar particle concentration gives a binding site concentration of 0.8 M. This figure was used in the Biacore software to provide the estimates of K_d for the imprinted nanoparticles. 218

Figure_Apx B.1: Infra-red spectra of NDDEAEA monomer (Scheme 3.4, 2). 219

Figure_Apx B.2: MS spectrum of NDDEAEA (Scheme 3.4, 2), actual mass: 362. 1352; calculated mass: 362.1337. 219

Figure_Apx B.3: SEM images of surface morphology of (left) pre-treated gold screen-printed electrode and (right) electropolymerised NDDEAEA electrode (0.2 M NDDEAEA and 0.75 M hydrochloric acid in 25% acetonitrile). 220

Figure_Apx B.4: SEM images of surface morphology of electropolymerised NDDEAEA grafted with (left) MAA, (centre) AMPSA and (right) styrene. ... 220

Figure_Apx B.5: AFM of (A and B) bare pre-treated gold SPE, mean roughness 285.54 nm; (C and D) electropolymerised NDDEAEA film on pre-treated gold SPE, mean roughness 124.15nm; (E) electropolymerised NDDEAEA, after fifteen minutes of UV-irradiation, mean roughness 164.26 nm; (F and G), poly (methacrylic acid) film grafted over electropolymerised NDDEAEA by *iniferter* activation using UV irradiation mean roughness 7.474 nm; (H and I), poly (AMPSA) film grafted over electropolymerised NDDEAEA by *iniferter* activation using UV irradiation, mean roughness 155.33 nm; (J and K), poly (styrene) film grafted over electropolymerised NDDEAEA by *iniferter* activation using UV irradiation, mean roughness 116.12nm; (L), layer by layer grafting of poly (styrene) film over poly (methacrylic acid) over electropolymerised NDDEAEA by *iniferter* activation using UV irradiation, mean roughness 65.097nm. 226

Figure_Apx B.6: Chemical polymerisation conditions (condition A): (A) The effect of monomer concentration and hydrochloric acid concentration on the optical density of chemically polymerised films of poly (NDDEAEA) at constant (0.0183 M) ammonium persulphate concentration (measured at pH 1) and (B) the effect of monomer concentration and ammonium persulphate concentration on the optical density of chemically polymerised films of poly (NDDEAEA) at constant (0.225 M) hydrochloric acid concentration (measured at pH 1)..... 228

Figure_Apx B.7: Absorption (at 550 nm) of chemically polymerised poly (NDDEAEA) films deposited on a microtitre plate with variation of the concentration of the monomer (0.5 M, 0.43 M, 0.36 M, 0.29 M, 0.22 M, 0.15 M, 0.08 M, 0.01 M) and of the ammonium persulfate (0.05, 0.043, 0.036, 0.029, 0.022, 0.015, 0.008, 0.001). The concentration of the hydrochloric acid was kept constant at 0.6 M in 25% acetonitrile in water..... 230

Figure_Apx B.8: Absorption of chemically polymerised poly (NDDEAEA) films deposited on a microtitre plate (condition B) with variation of the concentration of the monomer (0.08 M, 0.07 M, 0.06 M, 0.05 M, 0.04 M, 0.03 M, 0.02 M, 0.01 M) and of the ammonium persulfate (0.05, 0.043, 0.036, 0.029, 0.022, 0.015, 0.008, 0.001). The concentration of the hydrochloric acid was kept constant at 0.6 M in 25% acetonitrile in water. 231

Figure_Apx B.9: Confocal microscopic images of chemically polymerised poly (NDDEAEA) (the green material) using condition B on microtitre plate (the white part of the image). 231

Figure_Apx B.10: IR spectra of chemically polymerised poly (NDDEAEA) scraped off a microtitre plate and redispersed in KBr. 232

Figure_Apx B.11: UV spectrum of poly (NDDEAEA) solution 1 mg mL^{-1} in methanol in a quartz cuvette..... 232

Figure_Apx B.12: SEM images of chemically polymerised poly (NDDEAEA) on (top left) microtitre plates, (top right) as bulk polymer (showing bead type structure of the polymer) and (below) over PP membranes..... 233

Figure_Apx C.1: ^{1}H NMR (400 MHz, MeOH-D_3, 25 °C) of MPEDA. 234

Figure_Apx C.2: ^{13}C NMR (100 MHz, MeOH-D_3, 25 °C) of MPEDA. 235

Figure_Apx C.3: DEPT 135 NMR (100 MHz, MeOH-D_3, 25 °C) of MPEDA..... 236

Figure_Apx C.4: ^{1}H NMR (400 MHz, DMSO-D_6, 25°C) of MMDTCE. 237

Figure_Apx C.5: ^{1}H NMR (400 MHz, DMSO-D_6, 130 °C) of MMDTCE. 238

Figure_Apx C.6: ^{13}C NMR (100 MHz, DMSO-D_6, 25 °C) of MMDTCE..... 239

Figure_Apx C.7: ^{13}C NMR (100 MHz, DMSO-D_6, 130 °C) of MMDTCE. 239

Figure_Apx C.8: DEPT 45 NMR (100 MHz, DMSO-D_6, 25 °C) of MMDTCE. 240

Figure_Apx C.9: DEPT 90 NMR (100 MHz, DMSO-D_6, 25 °C) of MMDTCE. 241

Figure_Apx C.10: DEPT 135 NMR (100 MHz, DMSO-D_6, 25 °C) of MMDTCE. 242

Figure_Apx C.11: Mass spectrum of MMDTCE..... 242

Figure_Apx C.12: Absorption (at 550 nm) of chemically polymerised poly (MMDTCE) films deposited on a microtitre plate with variation of the concentration of the monomer (0.08 M, 0.07 M, 0.06 M, 0.05 M, 0.04 M, 0.03 M, 0.02 M, 0.01 M) and of the ammonium persulfate (0.05, 0.043, 0.036, 0.029, 0.022, 0.015, 0.008, 0.001). The concentration of the hydrochloric acid was kept constant at 0.6 M in 25% acetonitrile in water. 244

Figure_Apx C.13: Absorption (at 550 nm) of chemically polymerised PANI films deposited on a microtitre plate with variation of the concentration of the monomer (0.5 M, 0.43 M, 0.36 M, 0.29 M, 0.22 M, 0.15 M, 0.08 M, 0.01 M) and of the ammonium persulfate (0.05, 0.043, 0.036, 0.029, 0.022, 0.015, 0.008, 0.001). The concentration of the hydrochloric acid was kept constant at 0.6 M in 25% acetonitrile in water. 245

LIST OF APPENDIX TABLES

Table_Apx A.1: Calculated values based on theoretical prediction of the perfect structure of dendrimer PAMAM 25 % C_{12}, generations from 0 to 5, of the molecular weight, molecular formula, and number of different groups, including number of different non-equivalent protons from the different methylene groups presented. 213

Table_Apx A.2: Calculated values based on theoretical prediction of the perfect structure of dendrimer PAMAM 25 % C_{12} – modified (*macroiniferter*), generations from 0 to 5, of the molecular weight, molecular formula, and number of different groups, including number of different non-equivalent protons from the different methylene groups presented. 215

LIST OF ABBREVIATIONS

AMPSA	Acrylamido-2-methylpropane
ATRP	Atom transfer radical polymerisation
AFM	Atomic force microscopy
Blank	Control polymer
CNDDA	*S*-(carboxypropyl)-*N*,*N*-diethyldithiocarbamic acid
CPs	Conducting polymers
CV	Cyclic voltammetry
DLS	Dynamic light scattering
DMSO	Dimethyl sulfoxide
DMF	Dimethylformamide
DTCE	Dithiocarbamate ester
EDC	1-Ethyl-3-(dimethylaminopropyl)-carbodiimide hydrochloride
EDX	Energy-dispersive X-ray
EU	European Union
iniferter	Initiator, transfer agent, and terminator
IR	Infrared
K_d	Dissociation constant
MAA	Methacrylic acid
MEPDTC	*S*-Methyl-*N*-methyl-*N*-ethyl (2-(phenylamino)) dithiocarbamate ester
MIP	Molecularly imprinted polymers
MS	Mass spectroscopy
NDDEAEA	*N*-(*N´,N´*-Diethyldithiocarbamoyl ethyl amido ethyl)-aniline
NMP	Nitroxide-mediated polymerisation
NMR	Nuclear magnetic resonance
NPs	Nanoparticles
NPEDMA	*N*-Phenylethylenediamine methacrylamide
PAMAM	Polyamidoamine
PANI	Polyaniline
PBS	Phosphate buffered saline
PIMP	Photo-iniferter mediated polymerisation

RAFT	Reversible addition-fragmentation chain-transfer
SEM	Scanning electron microscopy
SI-ATRP	Surface-initiated atom transfer radical polymerisation
SI-CRP	Surface-initiated controlled radical polymerisation
SI-NMR	Surface-initiated nitroxide-mediated polymerisation
SI-PIMP	Surface-iniferter mediated polymerisation
SI-RAFT	Surface-initiated reversible addition-fragmentation chain-transfer
SPR	Surface plasmon resonance
TEM	Transmission electron microscopy
TEMPO	(2,2,6,6-Tetramethylpiperidin-1-yl)oxyl
THF	Tetrahyrofuran
UV	Ultraviolet
XPS	X-Ray photoelectron spectroscopy

1 Literature Review

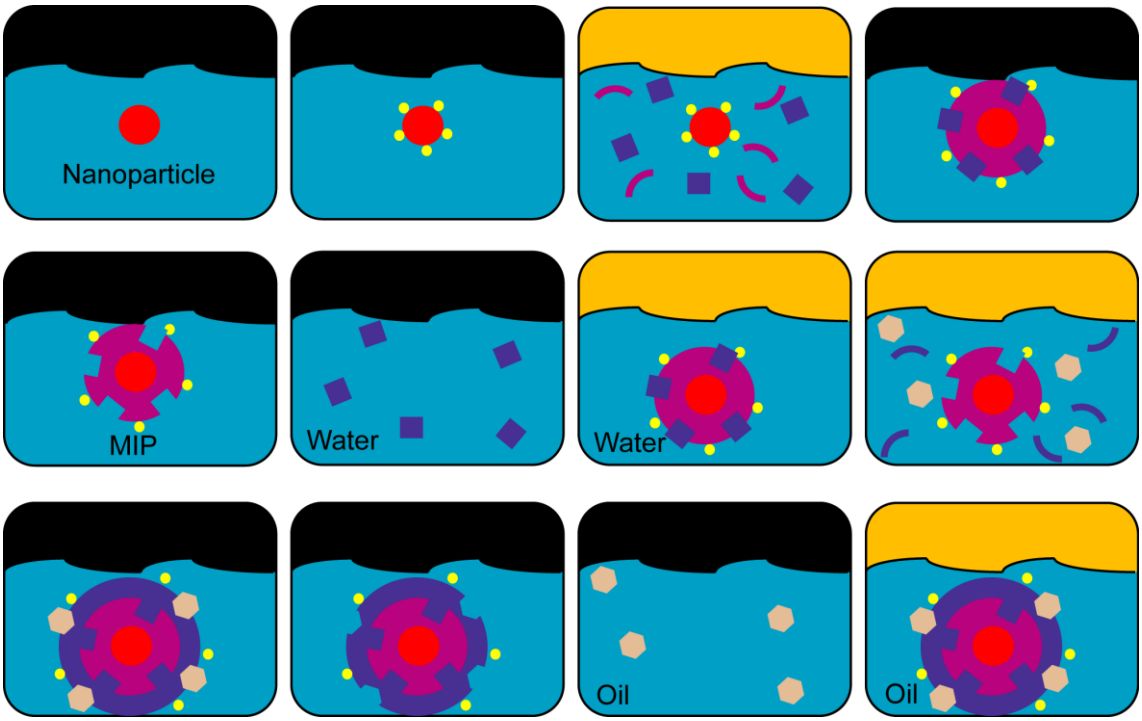

1.1 Introduction

In recent years, the extensive exploitation of natural resources and widespread use of chemicals has led to the accumulation of various pollutants in the environment. This has lately received much attention due to the adverse effects of pollutants on human health. In particular several synthetic organic compound such as pesticides and pharmaceutically active compounds are emerging contaminants. A series of medicines employed in the treatment of various diseases, such as cancer, hormone imbalance, osteoporosis *etc.* end up in the aquatic environment via domestic and industrial wastewater. This is why the existing regulations for drinking water are constantly changing (for pesticides the EU regulations for drinking water at present are not more than 0.1 μg L^{-1}). The existing water treatment methods need to be more flexible and more sensitive ways of detecting of a wider variety of different pollutants need to be developed.

It is evident that novel smart and very specific materials with high selectivities and sensitivities for toxic and other contaminants in the sensing technologies are urgently required. More specifically, innovative methods for the synthesis of advanced *"tailor-made"* functional materials with long-term performance stability are demanded. One of the most promising classes of new and highly selective functional materials is molecularly imprinted polymers (MIPs). MIPs can be used as selective sorbents for a wide range of biological, pharmaceutical and environmental applications. These developments underline the potential use of MIPs in detection and environmental monitoring of pollutants at very low concentrations (below 0.1 ppb).

This review will largely be concerned with chemical aspects of the design and synthesis of MIPs in nano-format via surface initiated *living* radical polymerisation as a way of synthesis of well defined materials and composites. Each one of the sub-sections will describe the basic concept behind each type of *living* radical polymerisation: nitroxide-mediated *free* radical polymerisation (NMP), atom transfer radical polymerisation (ATRP), reversible addition-fragmentation chain-transfer (RAFT) polymerisation and *poto-iniferter* mediated polymerisation (PIMP). Surface-initiated reactions would be

the focus for the technologies listed above. Each one of them would be considered for its application to the creation of MIPs, with examples taken from the recent literature. The aspect of creating MIPs via different surface initiated *living* radical polymerisations would be discussed in details in respect not only to the enhanced imprinting effect and of the format of the synthesised materials (nanoparticles, nanolayers, nanotubes *etc.*) but also from a technological point of view (reaction conditions, reagents, technological time *etc.*) which would provide a better idea for the exploitation characteristics of the process in future applications. The molecular imprinting philosophy would be explained briefly due to the numerous reviews on the subject. The different techniques used for the preparation of MIPs in nano-formats (beads, nanoparticles, nanolayers) will also be discussed briefly herein. In conclusion a critical comparison between the different methods for polymerisation techniques will be presented.

1.2 Molecularly Imprinted Polymers (MIPs)

Molecular recognition is a fundamental process for all living systems, being involved in the translation of the genome, enzymatic catalysis and the workings of the immune system, among others. Technological exploitation of the phenomenon has, to a large part, exploited naturally-derived systems (particularly antibodies) as the selective component of immunoassays, affinity phases and biosensors and as therapeutic agents. While these technologies already have extensive commercial use, the search continues for alternatives to antibodies and enzymes which combine their selective molecular recognition capabilities with greater stability to temperature, pH and humidity, extremes of which can rapidly degrade protein receptors. Recognition of organic compounds is a great challenge as the interactions involved are the weak hydrophobic and van der Waals interactions, and hydrogen bounding.

The first work on molecular imprinting is attributed to Polyakov in **1931**. He studied the polymerisation of sodium silicate in water with ammonium carbonate as gelating agent. When the polymerisation process was accompanied by an additive such as benzene or toluene, the silica particles ultimately formed, showed a higher uptake of this additive than for structurally related ligands. Some kind of memory for the additives was apparent.

The interest in this new approach of polymerisation, its development and the range of applications of molecularly imprinted polymers (MIPs) increased dramatically during the years, which can be easily observed from the number of publications and patents produced each year (**Figure 1.1**).

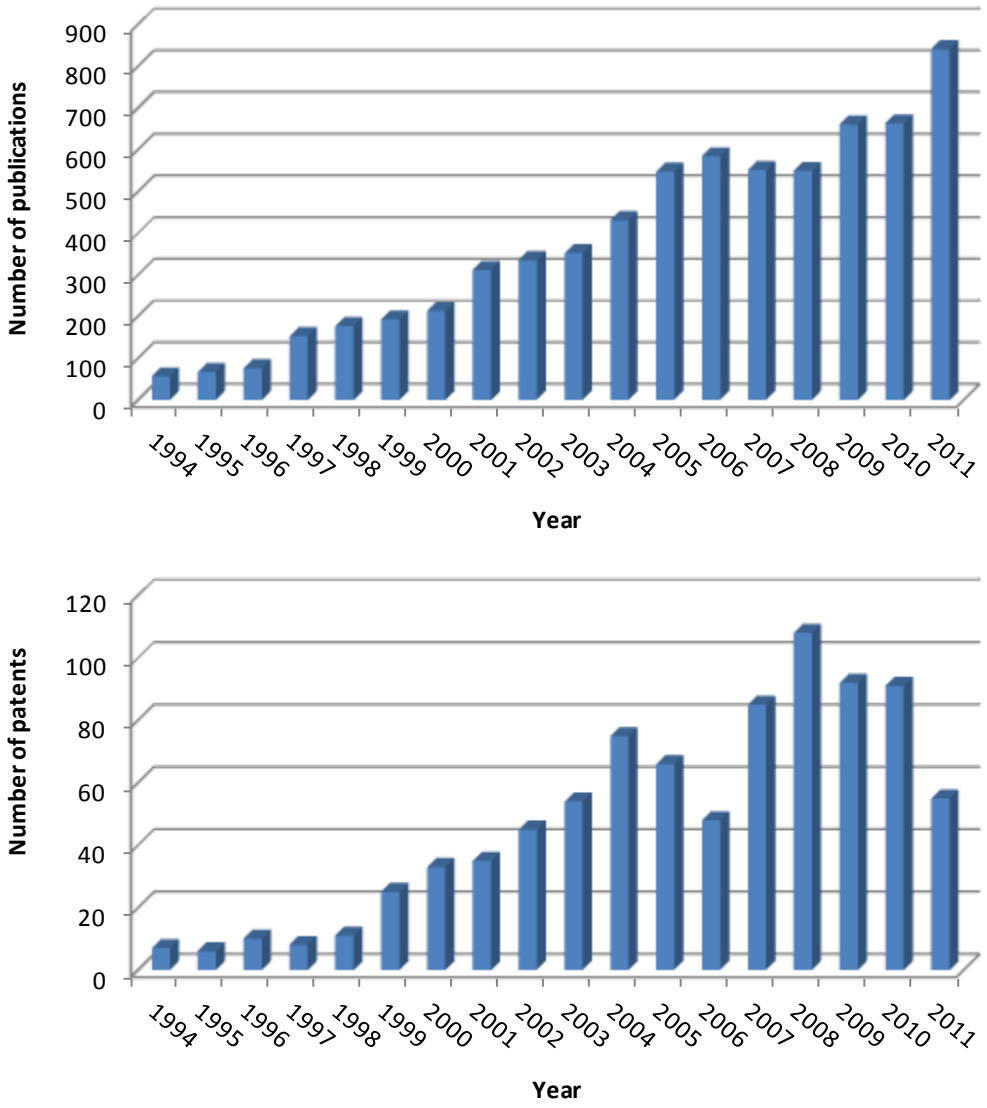

Figure 1.1: Bar graphics showing the number of MIPs publications and patents for the period 1994-2011 (the data is obtained from *mipdatabase.com*, last accessed on 19/12/2011).

The modern science defines the concept of molecular imprinting as a process of polymer formation in the presence of another compound (*template*) (**Figure 1.2**). The template forms a complex with a functional polymerisable monomer. The nature of the template-monomer interactions can vary (covalent, semi-covalent, non-covalent, ligand exchange (Mayes and Whitcombe, **2005**)). The monomer is crosslinked to form a polymer mould around the template compound. After removal of the template from the polymer matrix under certain conditions, cavities complementary in size, shape and chemistry (*binding sites*) are created. These binding sites can selectively rebind the

specific template compound (Chen *et al.* **2011**; Lasakova and Jandera, **2009**; Kloskowski *et al.* **2009**; Ye *et al.* **2008**; Alexander *et al.* **2006**; Haupt and Mosbach *et al.* **1998**; Wulff, **1995**; Guan *et al.* **1931**). Among all the other imprinting techniques, non-covalent imprinting uses the same forces of interactions between template and monomer typical for biological systems, such as hydrogen bonds, van der Waals forces, dipole-dipole interactions *etc*. This method of imprinting originates from the early 80's with the work of Mosbach (Arshady and Mosbach, **1981**; Norrlow *et al.* **1984**) and is the predominant method of imprinting used nowadays. It offers more flexible choice of templates for imprinting and less complex chemistry involved in the formation and dissociation of the template-monomer complex. There are some drawbacks, including heterogeneity of the receptor sites produced (huge range of receptor affinity), non-specific interactions, very low yield of high-affinity receptors and template leaching (Mayes and Whitcombe **2005**). The current trend line of the contemporary imprinting research focuses on overcoming these problems.

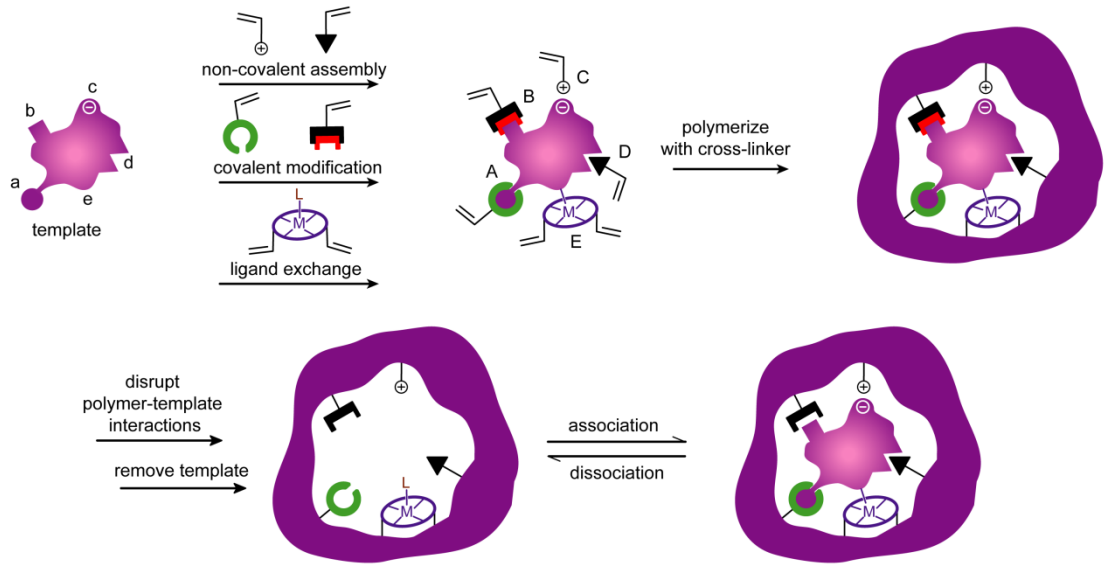

Figure 1.2: Schematic representation of the molecular imprinting process showing some of the interactions used in creating template-monomer complex (**a**-**e**). (**a**) reversible covalent interaction; (**b**) semi-covalent method; (**c**) electrostatic interaction; (**d**) non-covalent interaction; (**e**) ligand exchange interaction. The scheme is adapted from Alexander *et al.* (**2006**).

MIPs are man-made tailored organic materials that actually represent the creation of synthetic holes for the molecular key. They combine selective recognition with chemical robustness (Mayes and Whitcombe **2005**). MIPs have already been successfully applied in solid phase extraction (Beltran *et al.* **2010**; Tamayo *et al.* **2007**) and in biosensors (Kim *et al.* **2011**; Lautner *et al.* **2011**; Suryanarayanan *et al.* **2010**; Al-Kindy *et al.* **2000**). The synthesis of these types of materials with molecular architectures which are well defined on the molecular level is a future priority development. The imprinting of low molecular weight compounds in MIPs has been extensively studied. A recent trend has been the development of methods for the imprinting of proteins which demonstrates the robustness of these systems (Whitcombe *et al.* **2011**; Zeng *et al.* **2010**; Ge and Turner, **2008**). Even more recent contemporary approach in the application of MIPs is as nucleants for protein crystallisation where faster formation of large single crystals with improved diffraction pattern in the presence of MIPs hydrogels was observed (Saridakis *et al.* **2011**; Whitcombe *et al.* **2011**).

1.3 Nano-MIPs

The application of traditional MIPs as substitutes for antibodies in many applications is restricted by their bulk format. The preparation of MIPs in the form of nanoparticles (NPs) would enable their development for applications such as drug delivery or the development of novel drug leads (Hoshino *et al.* **2010**), as well as in diagnostics and in drug delivery (Cunliffe *et al.* **2005**). The size and the shape of the particles used for such applications are of a vital importance. NPs would of course possess the usual advantages that MIPs have over their natural counterparts such as stability at low and high pH, pressure and high temperature. NPs however would possess higher surface area per unit volume and hence a larger number of accessible binding sites than their bulk counterparts (Poma *et al.* **2010**). This would lead to increased sensitivity in biosensors.

NPs can be prepared by a number of methods, including precipitation polymerization (Chaitidou *et al.* **2008**; Yoshimatsu *et al.* **2007**), pre-dilution (Maddock *et al.* **2004**), post-dilution (Wulff *et al.* **2006**), mini- (Curcio *et al.* **2009**) and micro-emulsion (Shen *et al.* **2005**), polymerisation grafting from a core nanoparticle (Gao *et al.* **2007**; Carter and Rimmer, **2005**) or early termination of the polymerisation (Guerreiro *et al.* **2009**). Each of these methods have some disadvantages which include: production of particles with irregular shapes and sizes, heterogeneous binding sites, decreased affinity due to the use of surfactants and high polymerisation temperature, long polymerisation time, relatively low yield, *etc*.

Molecular imprinting technology could be used in future nanosized devices for separation, reaction and detection because of its chemical and physical robustness and its straightforward method of synthesis. Nano-science and imprinting technology are integral, interdisciplinary fields for the development of these future technologies. Manipulation, visualization and interorganisation of nanostuctured objects and devices in highly precise, sensitive and specific manners are some of the anticipated outputs of contemporary science (Tokonami *et al.* **2009**; Ozin and Arsenault, **2005**). MIP nanostuctures in the form of nanoparticles/nanospheres, nanofibres, nanodisks and

thin films have great promise for a range of applications, such as environmental clean-up and detection and in nanomedicine. Thus particles with diameters in the nanometer range provide dramatically increased total surface areas per unit weight of material and highly active surfaces as well as better accessibility to the imprinted cavity that leads to a fast analyte equilibration which is important in sensing and separation events.

A number of reports describing the synthesis of MIP nanoparticles have been published recently, among these is the synthesis of nanoparticles prepared by MIP grafting to core-shell silica and latex particles (Gao *et al.* **2007**; Perez-Moral *et al.* **2007**). The main advantages of the core-shell approach are that the MIP layers could be very thin and uniform and that other functionalities, such as magnetic and fluorescent properties could be integrated into the core particle. Other nanobeads preparation techniques such as precipitation and miniemulsion polymerisation have also been reported (Cucio *et al.* **2009**; Zhu *et al.* **2007**; Yoshimatsu *et al.* **2007**; Wei *et al.* **2006**; Vaihinger *et al.* **2002**; Ye *et al.* **2001**). MIP nanofibres and nanobrushes have been reported using sacrificial alumina membranes as the templates (Berti *et al.* **2010**; Vandevelde *et al.* **2007**; Li *et al.* **2006**; Xie *et al.* **2006**). Other 2D nanostructures such as nanodisks and squares in MIP format have not yet been reported. This could be done using appropriate format support by patterning techniques, focusing on microsensor applications. Monolayer MIP nanofilms deposited on gold substrates using self assembly process have been reported, and frequently used for the construction of nano devices (Tabushi *et al.* **1987**; Mirsky *et al.* **1999**; Chen and Nagaoka, **2000**; Takonami *et al.* **2009**).

MIP nano-technology is a very recent development and is a promising tool for future technologies. Despite the many advantages this technique could bring, it still suffers from the disadvantage that synthesis of as many different nano-MIPs as the number of analyte targets would be required. One of the most promising approaches in the grafting of MIPs to nanoparticles as well as sensor surfaces is the use of *controlled* radical polymerisation, which will be analysed in the next part of this chapter.

1.4 Surface-Initiated Controlled Radical Polymerisation (SI-CRP)

The use of well defined polymer structures in various contemporary applications of polymers such as biomedical and biosensing applications is of vital importance. The investigation of the effect of the polymer architecture, size, charge, charge distribution *etc.* on the material's performance depends on the preparation of well defined polymers. The ability to control such parameters would have huge impact on their performance on a molecular level.

The architecture, complexity and functionality which can be introduced into a polymer depend significantly on the chosen type of surface-initiated polymerisation. Surface-initiated polymerisations can be classified into *"controlled/living"* and *noncontrolled/conventional* chain growth polymerisations. Depending on the type of polymerisation rather simple (linear homo- or co-polymers) or more complex (linear or branched block-copolymers, *etc.*) macromolecular architectures can be realised. Furthermore the type of polymerisation will determine whether a broad and ill-defined or narrow and well defined molecular weight distribution of the grafted chains will be obtained (Barz *et al.* **2011**; O'Reilly, **2010**; Blencowe *et al.* **2009**; Gao and Matyjaszewski **2009**; Moad *et al.* **2008**).

The typical characteristics of conventional chain growth polymerisations can be illustrated by considering a conventional *"free-radical"* chain-growth polymerisation. Random or gradient copolymer *"brushes"* are the most complex macromolecular architectures that can be realised with this type of polymerisation. The molecular weights of the polymer chains within the *"brush"* usually show broad molecular weight distribution, i.e. polydispersities. The polydispersity of a polymer is usually expressed by the polydispersity index, which is defined as the ratio between the weight and the number average molecular weight (M_w/M_n). In an ideal conventional *free-radical* polymerisation the lowest theoretical polydispersity index values that can be obtained depend on the type of termination reaction. Polydispersity index values as low as 2 can be achieved for termination by disproportionation or chain transfer, while a minimum value of 1.5 can be expected when termination of chain growth is caused by

recombination. Practical conventional *"free-radical"* polymerisations however are often far from ideal and especially for structurally more complex monomers, higher polydispersity index values and less defined products with increased batch to batch variability might be obtained. The origin of these broad molecular weight distributions can be explained by the random molecular processes that are occurring in *"free-radical"* polymerisation. After initiation, the polymer chains grow very quickly by stepwise addition of monomer units. The lifetime of this propagation process is however restricted by irreversible termination reactions of the propagating radicals and typically lies in the range of 5-10 seconds. The random fashion and the pure statistical distribution of termination reactions lead to the formation of relatively low as well as high molecular weight polymer chains, which is finally expressed by the relatively high polydispersity index values of the isolated polymer.

By contrast to a non-controlled polymerisation, in an ideal *"living polymerisation"* all polymer chains are initiated at the same time, grow at the same rate and active chain ends are retained at the end of the polymerisation, without any irreversible chain transfer or termination. Consequently, the final polymer is characterised by a homogenous, narrow and well defined distribution of molecular weight. In *"living polymerisation"* systems especially, the rate of initiation is much higher or at least comparable to the rate of chain growth, which causes the ensemble of polymer chains to grow homogenously and simultaneously, resulting in a narrow molecular weight distribution of the final product. The term *"living polymerisation"* was first introduced by Szwarc in 1956 describing the fact, that chain braking reactions, i.e. termination and transfer reactions, are virtually absent in these systems (Webster, **1991**; Szwarc *et al.* **1956**; Szwarc **1956**).

By contrast *"free-radical"* polymerisations are characterised by the tendency of *free-radical*s to recombine and terminate the polymerisation. The main strategy to achieve a *"living free-radical"* polymerisation is therefore based on the reduction of the number of propagating radicals, which leads to an effective retardation of the polymerisation process. Consequently, modern *"living free-radical"* polymerisation techniques are based on the use of special polymerisation mediators, which

temporarily and reversibly transform propagating radicals into *dormant/stable* species. This reversible transformation is either accomplished by reversible deactivation or by reversible chain transfer. A fast transformation between *dormant* and propagating radical species ensures the homogeneous growth of the overall ensemble of polymer chains. As a result *"living polymerisations"* are characterised by a linear evolution of molecular weight with time (for low conversions). Moreover polydispersity values of typically 1.1 are obtained.

The term *controlled polymerisation* is used for *"living polymerisation"* systems, which yield polymers with well-defined topologies, terminal functionality, composition and arrangement of comonomers into statistical, periodic, block, graft and gradient polymers or polymer brushes. Moreover in *controlled* polymerisations the molecular weights of the final polymers are predetermined by the ratio of monomer to initiator.

The use of the terms *"living"* and *"controlled"* in the concept of the described polymerisations, according to The International Union of Pure And Applied Chemistry (IUPAC) *"living polymerisation"* is "a chain polymerisation from which irreversible chain transfer and irreversible chain termination (deactivation) are absent" and the term *"controlled"* means a particular form of polymerisation.

Controlled surface-initiated radical polymerisation techniques represent the most powerful tools for the fabrication of well-defined polymers since they allow control over the composition, molecular weight, polydispersity, macromolecular architecture, grafting density and chemical nature of end groups of tethered polymer chains at the molecular level. Mechanistically *controlled radical polymerisation* (CRP) techniques proceed via the same steps as conventional *"free-radical"* polymerisations: initiation of the polymerisation by generation of radicals, propagation steps, and termination reactions. Especially termination processes lead to the loss of control over the properties of the envisaged final product. However in CRPs termination reactions are suppressed by a simple but effective strategy, *i.e.* by decreasing the number of *free-radical*s that is simultaneously present in the reaction medium to a minimum amount. This decrease of *"free-radicals"* is achieved by a temporary and reversible

transformation of *"free-radicals"* into *dormant* species. Ideally the final product polymer is also isolated in the form of a *dormant* species, which allows reinitiation of the polymerisation with other monomers and therefore to allow the fabrication of block-copolymers.

The techniques for *"living polymerisation"* through reversible deactivation include the *iniferter* method, nitroxide-mediated polymerisation (NMP), atom-transfer radical polymerisation (ATRP), reversible addition-fragmentation polymerisation (RAFT). All of them will be discussed in the next sections in respect to surface-initiation processes. Recent combinations of the above mentioned methods of polymerisation and MIPs in respect to the system architecture and the format of the imprinted polymer are also presented.

1.4.1 Surface-initiated nitroxide-mediated f*ree-radical* polymerisations (SI-NMP)

In nitroxide-mediated polymerisation (NMP) propagating *free-radical* chain ends are reversibly transformed into the corresponding *dormant* nitroxide capped species (Scheme 1.1) (Bertin *et al.* **2011**; Grubbs **2011**; Alemdar *et al.* **2010**; Neslihan *et al.* **2009**; Brinks and Studer **2009**; Chen *et al*. **2007**; Konn *et al.* **2007**; Zhao *et al.* **2006**; Studer and Schulte **2005**; Hawker *et al.* **2001**; Weimer *et al.* **1999**; Mansky *et al.* **1997**; Hawker *et al.* **1996**). The key mechanism reveals reversible thermal C-O bond homolytic cleavage of a polymer alkoxyamine to generate the corresponding polymeric radical and a nitroxide (*dormant*) radical. Monomer insertion with subsequent nitroxide trapping leads to chain-extended polymeric alkoxyamine.

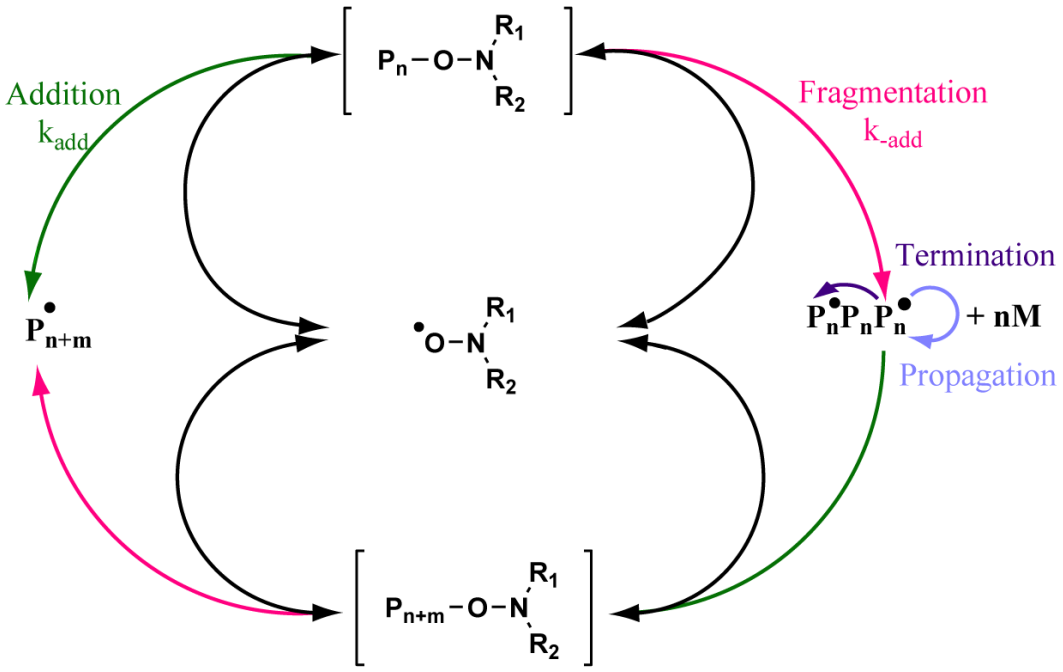

Figure 1.3: Schematic representation of nitroxide-mediated *living* radical polymerisation mechanism.

Hussemann *et al.* (**1999**) reported the first example for surface-initiated nitroxide-mediated polymerisation (SI-NMP). Up to 120 nm thick film of polystyrene brushes from initiator self-assembled monolayers of 2,2,6,6-tetramethyl-1-piperidinyloxy (TEMPO) functional chlorosilane supported on silicon substrates was prepared within sixteen hours polymerisation time and at a reaction temperature of 120 °C. Under these conditions, the C-ON-bond of the initiator dissociates into a reactive benzyl radical, which undergoes monomer addition, and a sterically stabilised persistent TEMPO radical (Hawker *et al.* **2001**). The reversible recombination of the propagating chain ends and the persistent TEMPO radicals results in a homogeneous chain growth and a low molecular weight distribution of the final ensemble of polymer chains within the brush. In SI-NMP the maximum number of persistent TEMPO-radicals that can be formed is limited by the total number of initiator moieties on the substrate surface. However especially for planar surfaces with low specific surface areas this total amount of initiator is relatively low and the reversible capping becomes ineffective due to quasi infinite dilution of persistent radicals in the reaction medium. As a consequence a pseudo conventional *free-radical* polymerisation is observed for these

systems. In order to increase the concentration of persistent radicals Husseman *et al.* (**2000**) therefore added predetermined amounts of *"free"* alkoxyamine initiator to the reaction mixture. An advantage of systems including "*free* initiator" is that the ratio of monomer to initiator can be readily used to control the molecular weight of grafted chains and brush thickness. However the *free* polymer formed in solution needs to be removed by thoroughly extracting the brushes after the polymerisation. The polydispersity index of grafted polymer was found to be slightly lower than the value found for the polymer formed in solution. This difference was attributed to autopolymerisation, which increases the polydispersity index of the resulting polymer in solution but does not influence the polymer formed from surface-initiated polymerisation. Additionally block copolymer brushes were fabricated by reinitiating the polymerisation from polystyrene brushes with mixtures of styrene and methyl methacrylate to form polystyrene-b-(polystyrene-*co*-poly (methylmethacrylate)) block copolymer brushes.

A drawback of the TEMPO-based initiators lies in their limitation to styrenic monomers. As a consequence TEMPO based NMP and copolymerisation of acrylic monomers has been found to yield polymers with only low molecular weights and relatively high polydispersity index compared to polymers from styrenic monomers (Listigovers *et al.* **1996**). Especially irregular polymers were produced with acrylic and methacrylic monomers due to chain growth and reversible deactivation competing with β-H-elimination of the growing polymer chain (Goto *et al.* **2002**).

In order to achieve better control over the NMP of acrylic monomers several studies analysed the effect of the steric and electronic properties of the nitroxide chain growth moderator on the polymerisation kinetics and the molecular weights and polydispersities of the resulting polymers (Goto *et al.* **2002**; Benoit *et al.* **1999**). From these studies the highly sterically hindered open-chain phosphonate alkoxyamine *N*-*tert*-butyl-*N*-[1-diethylphosphono-(2,2-dimethylpropyl)] nitroxide was identified as a lead candidate for the *controlled* polymerisation of acrylic, methacrylic and styrenic monomers. However slightly higher percentages of termination reactions were

observed for the *N-tert*-butyl-*N*-[1-diethylphosphono-(2,2-dimethylpropyl)] nitroxide-mediated polymerisation of styrenic monomers (Benoit *et al.* **2000**).

Bartholome *et al.* (**2003**) used grafting of polystyrene-brushes from silica nanoparticles. However the *N-tert*-butyl-*N*-[1-diethylphosphono-(2,2-dimethylpropyl)] nitroxide-mediated polymerisation yielded polystyrene brushes with lower molecular weight and higher polydispersity index compared to the TEMPO-mediated system presented by Husseman *et al.* (**2000**) and therefore provided further evidence for the preferred suitability of the *N-tert*-butyl-*N*-[1-diethylphosphono-(2,2-dimethylpropyl)] nitroxide-mediator for the polymerisation of acrylic and methacrylic monomers. Husemann *et al.* (**2000**) reported the successful use of α-hydrido nitroxide (2,2,5-trimethyl-3-(1-phenylethoxy)-4-phenyl-3-azahexane) as "*free initiator*" for the SI-NMP of *tert*-butyl acrylate brushes from TEMPO-initiator functionalised substrates. This class of nitroxide initiators and moderator was previously identified to yield well-*controlled* bulk polymerisations of acrylic monomers (Benoit *et al.* **1999**). The used approach is based on a fast interchange of TEMPO and α-hydrido nitroxides between polymer chains growing in solution and from the surface. Ignatova *et al.* (**2004**) used the same mediator exchange strategy to grow polystyrene and poly (2-dimethylamino) ethyl acetate brushes as well as poly (2-dimethylamino ethyl acrylate)-b-poly-(butyl acrylate) block copolymer brushes from stainless steel substrates. Typically researchers always try to avoid using TEMPO for the polymerisation of acrylates and methacrylates. Instead of the commercially available poly (oligoethylene glycol) methacrylate the authors used a 4-(oligoethyleneoxy) oxymethylstyrene monomer to prepare brushes with high polyethylene glycol content via TEMPO mediated SI-NMP (Andruzzi *et al.* **2005**).

Nevertheless examples of the polymerisation of acrylates and methacrylates using this approach exist. Li *et al.* (**2005**) reported the TEMPO-mediated surface-initiated vapour deposition polymerisation of various acrylic monomers including *N*-isopropyl acrylamide and styrene. The authors also reported the synthesis of diblock and triblock-copolymer brushes, *e.g.* of poly (acrylic acid)-b-polystyrene (polystyrene)-b-poly (*N*-(2-hydroxypropyl)-methacrylamide) brushes. A particular difference was noted

from the comparison between the fabrication of poly (*N*-isopropylacrylamide) brushes via surface-initiated vapour deposition polymerisation and the conventional SI-NMP. While the latter approach completely failed poly (*N*-isopropylacrylamide) brushes could be readily prepared from the surface-initiated vapour deposition polymerisation approach. Unfortunately molecular weights and PDI values of the grafted polymer chains obtained from the surface-initiated vapour deposition polymerisation approach were not reported. This prevents making a direct comparison between the degree of control that can be achieved with surface-initiated vapour deposition polymerisation and the conventional SI-NMP approach.

Hybrid silica particles comprised of an inorganic core and an organic polymer shell were synthesized by SI-NMP in the presence of a grafted alkoxyamine as initiator. It was demonstrated that the "grafting from" or "grafting to" SI-NMP exhibits a control character with a very low polydispersity and good agreement between theoretical/experimental molecular weights (Ghannam *et al.* **2006**). 2-(Dimethylamino) ethyl acrylate was grafted from the surface of alkoxyamine-functionalised crosslinked poly (styrene-*co*-chloromethylstyrene) microspheres by NMP in *N,N*-dimethylformamide at 112 °C (Bian and Cunningham **2006**). Polystyrene-grafted-titanium dioxide (TiO_2) nanoparticles with a diameter of 15 nm were prepared by the "grafting-from" method using the SI-NMP (Matsuno *et al.* **2006**). When the polystyrene-grafted-TiO_2 particles were finely dispersed, the ultraviolet absorption due to TiO_2 was strong and the difference in absorbance between the visible and ultraviolet regions was ten or more times greater than that for non-grafted TiO_2.

The synthesis of monodisperse zinc-sulfide high refractive index nanoparticles and their subsequent coating with concentrated polystyrene brush using SI-NMP, which proceeded with good control over the molecular weight and polydispersity index of the grafted chains, was performed (Ladmiral *et al.* **2006**). Polymer grafting of polystyrene on nanotubes using the technique *"grafting onto"* has been done and the result was narrower distribution of the external diameters and their solubilisation in organic solvents was greatly improved (Dehonor *et al.* **2007**). Wang *et al.* (**2008**) have reported polymer grafting onto nanosilica using TEMPO as mediator. The authors

reported well controlled grafting with narrow molecular weight distributions of the poly (styrene-*co*-maleic anhydride) chains.

Poly (styrene) brushes were grafted from montmorillonitrite surfaces in a three step procedure using TEMPO-mediated SI-NMP (Shen *et al.* **2010**). The polymerisation was carried out at 50 °C for 24 hours and this new route demonstrated an easy control of molecular weight distributions, and architecture of the grafted polymer.

4-Vinylpyridine was polymerised by SI-NMP via TEMPO-mediated polymerisation on the surface of 3-methacryloxyproyltrimethoxysilane-modified magnetic nanoparticles at 130 °C (Chen *et al.* **2010**). After the polymerisation the size of the particles increased from 30 to 150 nm.

SI-NMP of styrene was performed from various types of ordered mesoporous silica particles (500 nm with different pore sizes and morphologies) using SG1-based alkoxyamine initiator (Blas *et al.* **2011**) (Scheme 1.1). The polymerisation was performed at 115 °C for 300 minutes in *tert*-butanol as a solvent. The polymerisation kinetics were followed with ^{1}H NMR analysis of the remaining styrene and was similar in all cases. The most important result was observed in the molar mass distribution. The authors reported that pore diameters of 2 nm are too small to ensure good diffusion of reactants, 5 nm seemed to be satisfactory, and for more than 5 nm, the porous morphology of the particles was of high importance.

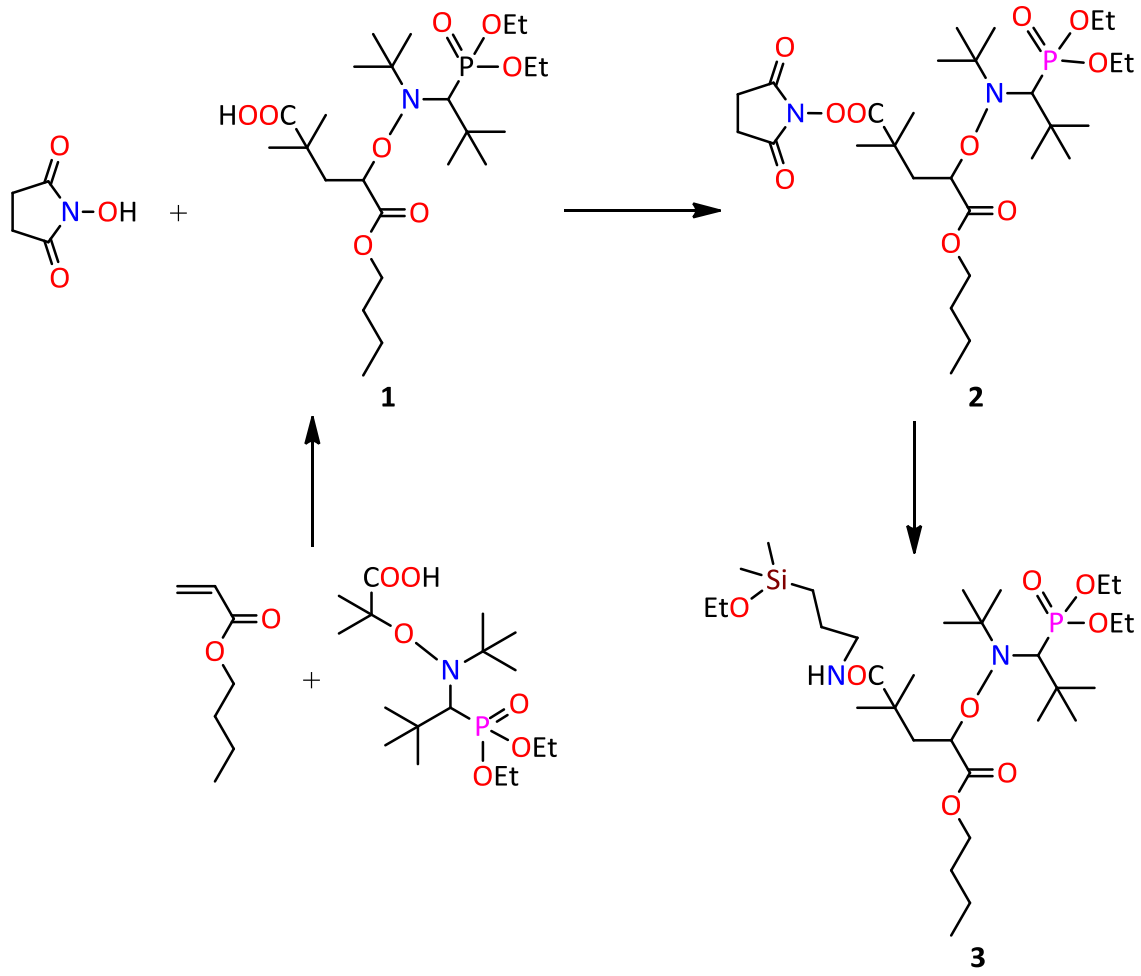

Scheme 1.1: Synthetic scheme for the SG1-based alkoxyamine initiator **1**, used as a *free* initiator and initiator **3** used as grafted initiator in the work of Blas *et al.* (**2011**). N-butyl acrylate was reacted with BlocBuilder alkoxyamine in *tert*-butanol as a solvent at 100 °C for 1.24 hours to form the alkoxyamine **1**. The alkoxyamine **2** was synthesised by reacting **1** with *N*-hydroxysuccinimide and dicyclohexylcarbodiimide in THF at 0 °C for 24 hours. The alkoxyamine **3** was synthesised by reacting **2** with 3-aminopropyldimethylethoxysilane in dichloromethane at ambient temperature for two hours.

In conclusion, SI-NMP represents a valuable method for the controlled fabrication of polymer brushes with well-defined polydispersity and molecular architecture of grafted polymer chains. NMP does not require the use of special polymerisation catalysts or chain transfer reagent, which becomes especially important for sensitive applications *e.g.* in the electronics or in the biomedical sector. In addition, NMP can also be used for multistep grafting of different monomers which can be used *e.g.* in

improving of the surface compatibility with different solvents or adding other functionality (catalytic, or signalling) to the sensor systems. A clear advantage of the SI-NMP initiators compared to *e.g.* azo-initiators is their higher thermal stability. However this increased stability of NMP initiators also requires higher polymerisation temperatures of typically 120 °C and might cause problems with polymerisation of thermally sensible monomers, although new low temperature NMP initiator are being developed.

The major disadvantage of NMP and SI-NMP is related to strong dependence of the polymerisation on the combination of monomer type and initiator, i.e. mediator type that is used. Also NMP initiators are usually not commercially available and have to be prepared by multistep synthetic procedures.

1.4.2 Surface-initiated nitroxide-mediated *free-radical* polymerisations (SI-NMP) and MIPs

Few examples exist describing the use of NMP for MIPs preparation. Boonpangrak. *et al.* (**2006**) and Isarakura-Na-Ayudhya *et al.* (**2005**) reported the successful synthesis of a MIP for cholesterol using semi-covalent imprinting technique and NMP (Figure 1.4). The nitroxide mediator 3-(4-*tert*-butylphenyl)-1,1'-dimethyl-3-(2,2',6,6'-tetramethylpiperidinooxy) propyl cyanide was used to assist the polymerisation of divinylbenzene in the presence of the template. Cholesterol template was covalently bounded to a monomer during its copolymerisation with cross-linker at 125 °C for 48 hours under argon atmosphere. The template was removed by hydrolytic cleavage. The resulted MIPs had specific binding sites that could interact with cholesterol via non-covalent hydrogen bond interactions in a non-polar solvent. The obtained polymer in the form of a monolith was then ground to small particles. Radio-scintillation was used as an analytical tool for quantification of the binding capability of the material for sensor devices application. The efficiency of the MIPs was improved compared with the same MIPs prepared via traditional radical initiator.

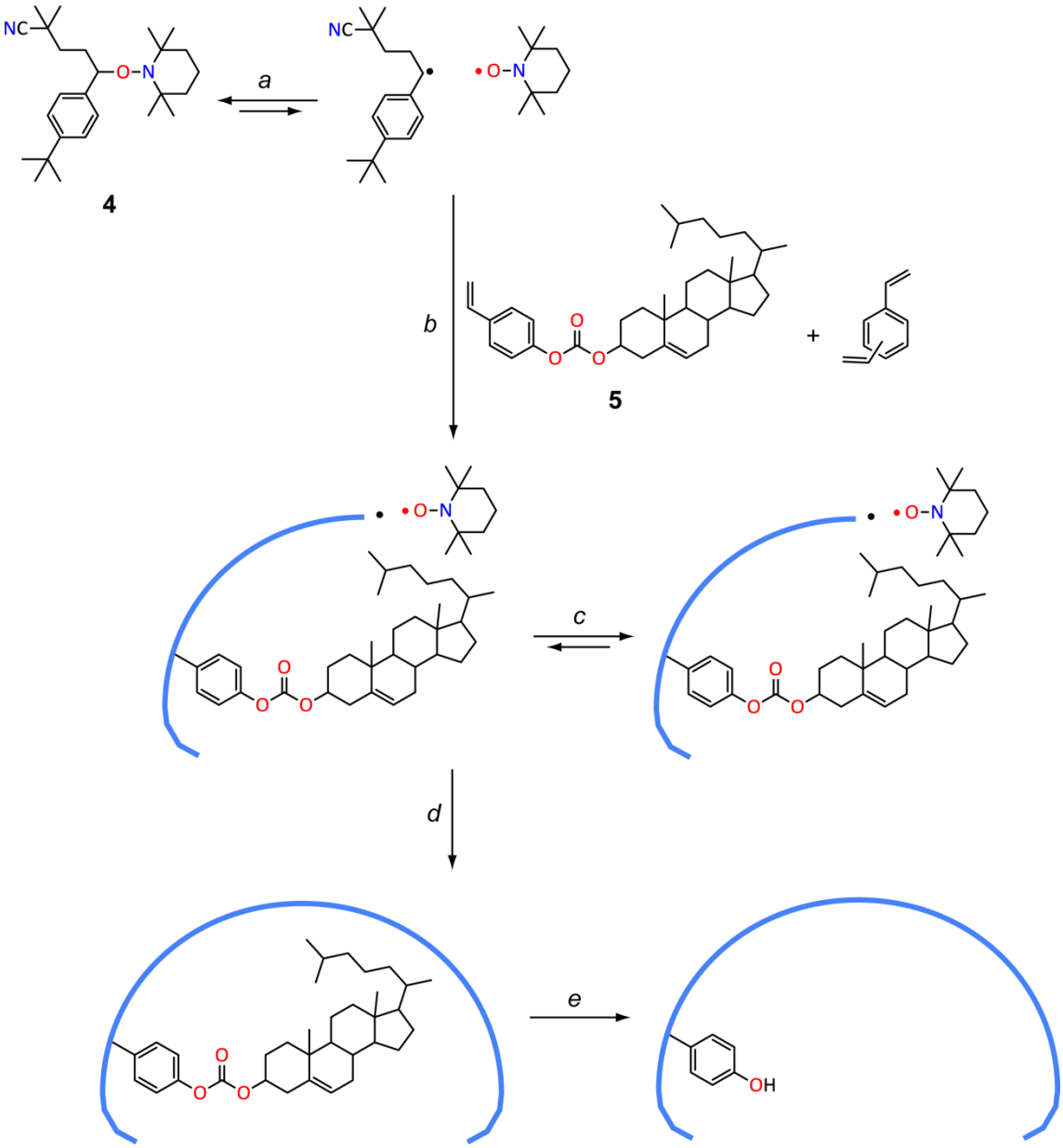

Figure 1.4: Preparation of cholesterol-imprinted polymer using NMP. The transient *free* radicals generated from **4** (Step **a**) initiate chain polymerisation of **5** and divinylbenzene (Step **b**). The majority of the growing chain radicals are stabilised by their reversible association with TEMPO (Step **c**), so that permanent chain termination is avoided. This *living* polymerisation finally leads to the formation of imprinted sites in the cross-linked polymer network (Step **d**), which after hydrolysis (Step **e**) afford specific cholesterol binding cavities. The scheme is adapted from Boonpangrak *et al.* (**2006**).

With the development of NPM initiators applicable to low temperature polymerisations, NMP can be applied to other systems for the preparation of MIPs,

using different techniques, formats and a bigger variety of monomers. At the moment however the high temperatures required for initiating polymerisation with NMP will limit its application to non-covalent MIPs since high temperature is detrimental to the strength of the complex between template and functional monomers (Piletsky *et al.* **2002**).

1.4.3 Surface-initiated atom transfer radical polymerisation (SI-ATRP)

Atom transfer radical polymerisation (ATRP) is based on the concept that the presence of *dormant* radicals in the polymerisation process could be used to reduce the stationary concentration of active radicals and minimize termination, which represents the *living* properties of the process (Ayres, **2011**; Min and Matyjaszewski, **2009**; Rosen and Percec, **2007**; Kamigaito *et al.* **2001**; Patten and Matyjaszewski, **1998**). ATRP employs atom transfer from an organic halide to a transition-metal complex to generate the reacting radicals and a back transfer from the transition metal to the product-radical to form the final product (**Figure 1.5**). It is chemically versatile procedure, due to its compatibility with a large variety of monomers (Czaun *et al.* **2008**), including styrenes (Lui and Su *et al.* **2006**), methacrylates (Saito, **2008**), dienes, and acrylonitrile with good control over the molecular weight and molecular weight distribution of the final product (Wu *et al.* **2009**). It is used for the preparation of chain end-functionalised polymers. ATRP tolerates a relatively high degree of impurities and consequently can be performed without the need of ultrapure, anhydrous monomers or solvents and proceeds even when a small amount of oxygen is present.

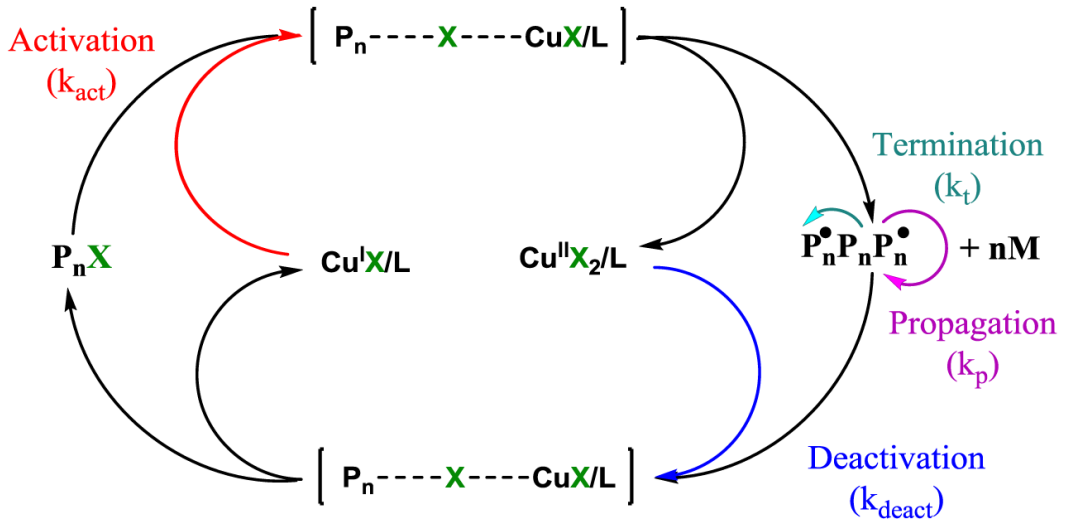

Figure 1.5: Schematic representation of the catalytic cycle in ATRP: **X**=Cl, Br; **P**=polymer; **M**=monomer; **L**=N-ligand.

The mechanism of ATRP, involves rapid activation/deactivation process which is represented as the equilibrium between active, propagating macroradical, ($P_n^{\bullet}$), and *dormant*, halide-terminated propagating macroradical, (**P_n-X**) (Patten and Matyjaszewski, **1998**). It involves various oxidation states of a copper (or other metal) catalyst and proceeds with activated monomers. The activator is **Cu^IX/L**, and the deactivator is **$Cu^{II}X_2/L$**, where **X**=Cl, Br, and **L**=N-ligand (**Figure 1.5**). The activation/dissociation process involves transfer of **X** atom from the initiator (**P-X**), or the *dormant* polymer halide (**P_n-X**) to **Cu^IX/L** via intermediary reduction of the halogen radical to the halide anion, generating the initiating radical **$P^{\bullet}$** or the propagating radical **$P_n^{\bullet}$** and oxidation of the catalyst to **$Cu^{II}X_2/L$** via an cyclic electron transfer process. The deactivation step involves the reverse process of atom transfer of halogen anion back to the propagating radical, which regenerates the *dormant* polymer chain and the reduced **Cu^I/L** catalyst. K_{act} for **P_n/P-X** depends on the nature of the halide. This is due to the fact that from iodine to bromine to chlorine the bond dissociation energies of homolytic cleavage increase sharply.

SI-ATRP could be performed at ambient temperature, which is especially favourable for the functionalisation of temperature-sensitive substrates. Under these conditions thermal autopolymerisation in solution is nearly absent. The first example for SI-ATRP

at ambient temperature was reported by Kim *et al.* (**2000**), who prepared 35 nm thick poly (methyl methacrylate) brushes within twelve hours of polymerisation time using *tris* [(2-dimethylamino) ethyl] amine as ligand. Interestingly no deactivating Cu^{II} species was used in this approach. The grafted chains showed relatively low polydispersities.

Moreover SI-ATRP can be carried out as surface-confined polymerisation, i.e. without the addition of *"free initiator"* (Edmondson and Armes, **2008**). Most of the standard ATRP catalyst systems, as well as surface immobilisable initiators such as *e.g.* benzylchloride functional silanes are commercially available in ready-to-use quality. Additionally the important reaction parameters, i.e. the type, ratio and concentration of the ATRP catalyst, the solvent, the monomer, the polymerisation temperature, the initiator type, *etc.* can be readily adapted to the demands of a specific polymerisation system, which adds to the flexibility of the process. The need for a determination of the correct conditions for each system could however require more time and effort. The only restriction on the use of ATRP comes from the necessity to use metal complexes, such as Cu (I) halide, Ni, Pd, Ru, Fe and other metals, which could be a problem for some applications.

ATRP was first reported in 1995 simultaneously by Wang and Matyjaszewski (**1995**) and Kato et al. (**1995**).ATRP was described as series of consecutive occurring atom transfer radical additions (ATRA) (Bellus, **1985**; Ancher and Vofsi, **1963**). The authors reported the *controlled* polymerisation of styrene using 1-phenylethyl chloride as initiator and CuCl and 2,2'-bipyridine, which represents one of the most common catalyst pairs in ATRP. The main difference between ATRA and ATRP is the molar ratio of alkene to alkylhalide. While ATRA is based on equimolar ratios of alkene to alkylhalide, in ATRP the alkene monomer is used in large excess compared to the initiating alkyl halide (De Clercq and Verpoort, **2003**).

The first example of SI-ATRP was reported by Ejaz *et al.* in **1998** and comprised the SIP of poly (methacrylic acid) from 2-(4-chlorosulfonylphenyl) ethyl silane SAMs supported on silicon substrates. In order to achieve a *controlled* polymerisation *p*-toluenesulfonyl chloride was used as *"free initiator"* to generate a sufficient amount of deactivator. In

order to estimate the molecular weight of the tethered polymer chains the authors compared the polymer layer thickness with the molecular weight of poly (methyl methacrylate) that formed simultaneously in solution. By this metod a polymer layer thickness of 70 nm was correlated to M_w of 100 000 Da or a degree of polymerisation of ~1000.

1.4.4 Surface-initiated atom transfer radical polymerisation (SI-ATRP) and MIPs

ATRP was used by Li and Husson (**2006**) and Wei *et al.* (**2005**) for synthesis of an ultrathin (>10nm), surface-confined, MIP film on gold substrates via ATRP. 2-Vinylpyridine was used as the functional monomer, ethylene glycol dimethacrylate was the cross-linker and *N*,*N'*-didansyl-L-cystine and *N*,*N'*-didansyl-L-lysine were used as template molecules. The MIPs films were selective to the template, compared to the non-imprinted polymer (NIP) films, and the template removal from this imprinted films appeared to be 100% efficient. The film parameters: solution pH, polymer layer thickness and adoption kinetics, were analysed.

Porous anodic alumina oxide nanotube membranes, prepared through template synthesis, were modified with MIPs via ATRP (Wang *et al.* **2006**) for bioseparations (ions and drug molecules, DNA and proteins) (Siwy *et al.* **2005**). The 60 µm thick membrane was first modified with 3-aminopropyltrimethoxysilane (**Figure 1.6**). The ATRP initiator, 2-bromo-2-methylpropionyl bromide, was then grafted onto the silanised membrane. The formed macroinitiator was used for the imprinting process using β-estradiol as template, 4-vinylpyridine as monomer, ethylene glycol dimethacrylate as crosslinker and CuBr and 1,4,8,11-tetraazacyclotetradecane (1 to 2 ratio) as organometallic catalyst.

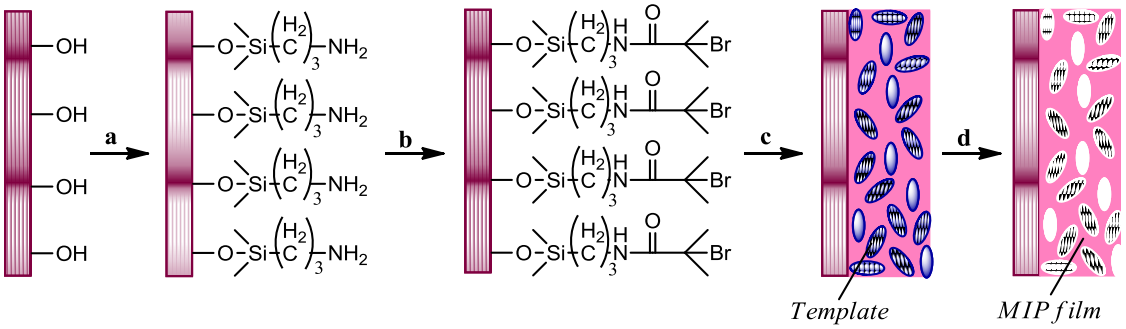

Figure 1.6: Schematic representation of the process of modification of nanotube membranes via SI-ATRP to achieve MIP nanotubes (Wang *et al.* **2006**): a) Silanisation with 3-aminomethyltrimethoxysilane; b) Grafting of the ATRP agent on the membrane via substitution reaction with 2-bromo-2-methylpropyl bromide; c) Polymerisation of 4-vinylpyridine as functional monomer, ethylene glycol dimethacrylate as cross-linking agent in the presence of β-estradiol as template. CuBr/1,4,8,11-tetraazacyclotetradecane were used as ATRP initiators. The reaction was performed in acetonitrile under nitrogen atmospere at 70°C for 24 hours; d) Removal of estradiol from the imprinted polymer via washing with acetonitrile, methanol-acetic acid (9:1, v/v), and methanol, followed by drying *in vacuo*.

Silica gel particles were grafted with MIP via ATRP (Wei and Husson, **2007**). High-performance liquid chromatography column packed with MIP grafted from silica gel particles showed higher column efficiency and better resolution of the enantiomers compared to MIP prepared by conventional *free* radical polymerisation. The formed materials showed improved mass-transfer properties and also higher binding capacity per unit mass of polymer.

Nanolayers of the cation-exchanger poly (acrylic acid) were grown from the surface of regenerated cellulose membranes (average pore diameter 1 µm) via SI-ATRP (Singh *et al.* **2008**). CuCl/2-bromoisobutyryl bromide was used as ATRP initiator and the protein lysozyme, as template. Measurements of pore-size distributions and permeability showed that the modification of the membranes resulted in decreased pore size and permeability. The modified membranes had high static and dynamic binding capacities for lysozyme, comparable to the commercially available ion-exchange membranes.

The combination of ATRP and precipitation polymerisation in the MIPs field was described, which produced spherical particles with a mean diameter of 3 µm (Zu *et al.*

2009). 4-Vinylpyridine was polymerised in the presence of bisphenol A as a template at 60 °C for 24 hours with CuCl/2-chloropropionate as ATRP initiator.The produced material showed fast template binding kinetics, high-affinity binding site densities on the surface and high selectivity over structurally related compounds. It also showed higher high-affinity site densities in comparison with MIP prepared via traditional radical polymerisation techniques.

The first time ATRP was applied in *"bulk"* polymerisation of MIPs was described by Zu *et al.* (**2010**). Bisphenol A was imprinted using both ATRP and conventional bulk *free* radical polymerisation. The authors obtained MIPs via ATRP that showed lower binding capacities and similar binding association constants by comparison with the conventional *free* radical polymer. This result was explained with the occurrence of fast gelation process in ATRP, which restricted the mobility of the chemical species, leading to interruption of the equilibrium between *dormant* and active radicals and heterogeneous polymer networks. This example demonstrates that applying *controlled* radical polymerisation (CRP) in molecular imprinting does not always benefits the binding properties of the resultant material.

Gai *et al.* (**2010**) showed the imprinting of the protein, lysozyme, on magnetic particles via SI-ATRP in aqueous media. The magnetic nanoparticles (Fe_3O_4 at SiO_2) were surface modified with 2-bromoisobutyryl bromide to achieve the ATRP initiator (Fe_3O_4 at initiator). *N*-isopropylacrylamide was crosslinked in the presence of the template and CuCl in phosphate buffered saline (PBS) for twelve hours at ambient temperature. The polymer thickness was about 15 nm and the size of the particles was estimated to be around 120 nm. The obtained polymer was endowed with higher specific recognition and selectivity to template when placed in a mixture of standard proteins and real sample (egg white). Due to the magnetic support, the imprinted material could be used in fast and easy protein separation processes.

Theophylline imprinted polymers were synthesised on the surface of multiwalled carbon nanotubes via SI-ATRP (Xu *et al.* **2011**). The thickness of the film was 5 nm which was determined by transmission electron microscopy. The so synthesised

polymer demonstrated rapid dynamics and good selectivity towards theophyline, compared to caffeine.

The *controlled* polymerisation technique ATRP has been proven to allow the growth of uniform MIP films with adjustable thicknesses, improving diffusion mass transfer and achieving relatively higher binding capacities. ATRP has a good potential for the preparation of MIPs with tailor-made structures and improved binding capacities. This combination of techniques has been applied to different formats (nanolayer on gold surface (Wu *et al.* **2009**; Saito **2008**), layers on silica gel particles (Wei and Husson, **2007**), layers in nanotube membranes (Li and Husson **2006**), nanolayers on cellulose membranes (Singh *et al.* **2008**), micro particles via precipitation polymerisation (Zu *et al.* **2009**), nanolayers on magnetic nanoparticles Gai *et al.* (**2010**), nanolayers on multiwalled carbon nanotubes (Xu and Chen *et al.* **2011**)) recently. This combination of techniques is relatively new and promising for future development. It has demonstrated improved imprinted qualities of the synthesised materials, improved control over various polymer parameters and increased variety of polymer formats. Compared to SI-NMP, SI-ATRP could be applied to a wider variety of templates for noncovalent imprinting, because of the milder synthesis conditions. The preference in using these techniques should be given to the imprinted materials whose performance would not be affected by the presence of metal ions in the polymerisation mixture. The disadvantage of using metals in the polymerisation process could be important in cases where the synthesised materials are to be used in environmental applications.

1.4.5 Surface-initiated reversible addition-fragmentation chain-transfer (SI-RAFT) polymerisation

Reversible-addition fragmentation chain-transfer (RAFT) polymerisation was first reported in 1998 (Le *at al.* **1998**; Chiefari *et al.* **1998**). It is a *controlled/living* polymerisation process with respect to the type of monomers and the reaction conditions which enable the formation of polymer with *controlled* molecular weight,

low polydispersity and complex polymeric microstructure (Gregory and Stenzel **2011**; Moad *et al.* **2011**; Destaras **2011**; Moad *et al.* **2008**; Barner-Kowollic *et al.* **2006**).

RAFT process is not based on the reversible termination by recombination but on reversible termination by degenerative chain transfer, in which propagating polymer chains are reciprocally transformed into *dormant* chains and *vice versa* (**Figure 1.7**). In RAFT polymerisation special reagents such as dithioesters, trithiocarbonates, dithiocarbamates and xanthates, are used as chain transfer agents to achieve a *controlled free*-radical polymerisation by providing cycled addition-fragmentation chain-transfer during polymerisation (Chiefari *et al.* **2003**; Chong *et al.* **2003**). These unsaturated compounds with the general structure of **7** or **9** act as transfer agents by a two step addition-fragmentation mechanism. In these compounds C=X should have a double bond that is reactive towards radical addition. **X** is most often a $=CH_2$ group or sulfur. **Z** is a group chosen to give the transfer agent an appropriate reactivity towards propagating radicals and convey appropriate stability to the intermediate radicals (**8** or **11**, respectively). Examples of **A** are CH_2, CH_2=$CHCH_2$, oxygen or sulfur. **R** is a homolytic leaving group and $\mathbf{R}^{\bullet}$ should be capable of efficiently reinitiating polymerisation. In all known examples of transfer agents **B** is oxygen. The overall RAFT polymerisation mechanism is divided into two sets of reactions that is the so-called *pre-equilibrium*, which involves *initialisation* of the *living* process starting from RAFT agent and the *main equilibrium* between growing and *dormant* polymer chains (Barner-Kowollic *et al.* **2006**). In the *pre-equilibrium*, which takes place in the early stages of the RAFT polymerisation, propagating oligomeric macro radicals ($\mathbf{P_n^{\bullet}}$, **6**) react with the double bond of the RAFT agent resulting in formation of a carbon-centred intermediate RAFT radical (**8**). The adduct radical undergoes homolytic fragmentation, either to the back reaction or to the formation of active radical and polymeric unsaturated compound **9**, which constitutes the *dormant* species. In the *main equilibrium* a similar set of reactions takes place in which a propagating macroradical ($\mathbf{P_n^{\bullet}}$, **6**), reacts with the polymeric RAFT agent (**7**). Recurring RAFT events establish the equilibrium between *dormant* and *living* radicals. The individual reactions of these equilibria are described kinetically via *addition rate coefficients* (k_{add}) and *fragmentation rate coefficients* (k_{-}

$_{add}$). The values of each reaction (each cycle) should be considered separately, because chemically different radical species are involved as attaching and leaving group radicals.

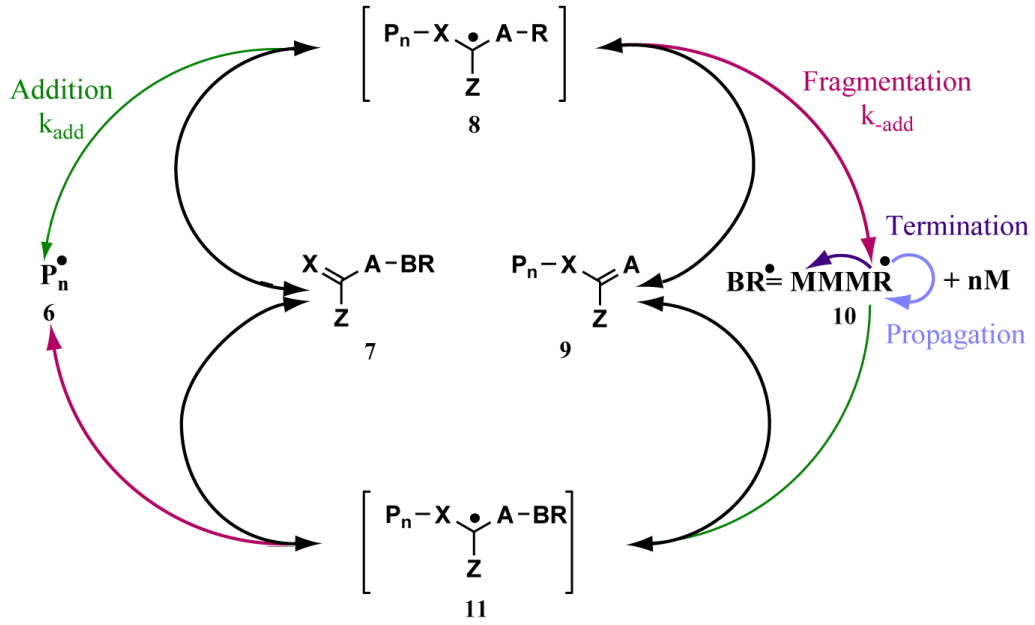

Figure 1.7: Schematic representation of the *living* character of RAFT polymerisation.

A distinct advantage of RAFT polymerisation is its experimental simplicity and versatility since conventional *free-radical* polymerisations can be readily converted to RAFT polymerisations by the addition of an appropriate RAFT agent, while other reaction parameters (monomers, initiators, solvents and temperatures) can be kept constant. RAFT polymerisations show all characteristics of a *living* polymerisation, *i.e.* all chains are initiated simultaneously and grow homogeneously until the monomer is consumed. Furthermore active chain ends are retained at the end of the polymerisations, which gives access to block copolymers or block *copolymer brushes*. Furthermore RAFT polymerisations are compatible with a large variety of monomers and polymers with the capability to produce a broad range of molecular weights. The resulting polymer is *a priori* relatively *free* of contaminants, which is especially advantageous compared to ATRP that often requires additional steps to achieve complete removal of the polymerisation catalyst. As an addition to that which has already been stated concerning RAFT polymerisation; it can be performed in aqueous

media and at *ambient temperature* (Skrabania *et al.* **2008**; Zhang and Deng *et al.* **2007**; McCormic and Lowe, **2004**).

A representative example of SI-RAFT polymerisation was presented by Baum and Brittain (**2002**), who polymerised methyl methacrylate, dimethylaminopyrolidine and styrene from azo-initiator functionalized SiO_x substrates in the presence of the chain transfer agent 2-phenylpropyl-2-yl-dithiobenzoate to form 28 nm thick poly (methyl methacrylate) *brushes* in twenty-four hours polymerisation time. Alternatively SI-RAFT could be performed by grafting a RAFT functional silane on a substrate surface and by initiating the polymerisation from a conventional *free-radical* initiator in solution. This strategy was explored to functionalise silica nanoparticles with RAFT agent to form core-shell particles (Pearson *et al.* **2009**; Li *et al.* **2006**). A significant advantage of this approach is the ability to control the surface density of RAFT functional silane. Li *et al.* (**2006**) compared to the rate of solution phase RAFT polymerisation with the rate of SI-RAFT for methyl methacrylate on colloidal silica nanoparticles. The rate of solution phase RAFT was reported to be significantly slower than the rate of SI-RAFT. This was attributed to the high local RAFT agent concentration on the *brush* surface as well as to the unique structure and steric constrains of the transitional dithioester radical, which in SIP *bridges* two surface tethered polymer chains (Li *et al.* **2006**). Yoshikawa *et al.* (**2005**) reported SI-RAFT of poly (2-hydroxyethyl methacrylate) *brushes* from plasma treated poly (tetrafluoroethylene-*co*-hexafluoropropylene) films. The plasma treatment was used to create peroxo-groups on the surface of the poly (tetrafluoroethylene-*co*-hexafluoropropylene), which were used to initiate the polymerisation in the presence of a RAFT-agent. The SI-RAFT of charged monomers from silicon substrates in aqueous medium was reported by Zhai *et al.* (**2004**).

By contrast to other *living* polymerisation techniques, which are based on reversible recombination, the total number of radicals in RAFT polymerisation and SI-RAFT is constant and therefore more prone to termination reactions and impurities that might induce termination reactions. Due to constant number of radicals, the termination of a single polymer chain will affect the polymerisation rate of the whole polymer ensemble since it will increase the ratio of chain-transfer agent to radicals in the

polymerisation mixture and slow down the overall polymerisation process. Compared to the other SIP techniques SI-RAFT remains experimentally demanding since surface-immobilisable conventional *free-radical* initiators or functional RAFT agents are required, which have to be prepared by multistep synthetic procedures. Another problem of SI-RAFT is linked to the fact that the rates of termination by recombination are dependent on the grafting densities of the *brushes*. This point might restrict the chemical flexibility of SI-RAFT since the amount of control of the SIP process becomes dependent on the *brush* parameters.

1.4.6 Surface-initiated reversible addition-fragmentation chain-transfer (SI-RAFT) polymerisation and MIPs

Recently, significant interest has been shown in the use of surface initiated *controlled* reversible addition-fragmentation chain-transfer (SI-RAFT) radical polymerisation for the preparation of MIPs (Gonzato *et al.* **2011**; Pan *et al.* **2011**; Chang *et al.* **2010**; Pan *et al.* **2010**; Li *et al.* **2009**; Pan *et al.* **2009**; Liu *et al.* **2008**; Li *et al.* **2008**; Southard *et al.* **2007**, *Macromolecules*; Southard *et al.* **2007**, *Analitica Chimica Acta*; Titirici and Sellegren, **2006**). Titirici and Sellergren (**2006**) reported the successful grafting of cross-linked MIP films on the surfaces of mesoporous silica beads through RAFT polymerisation. Lu *et al.* (**2007**) described a general protocol for preparing surface imprinted core-shell nanoparticles using RAFT agent functionalized silica nanoparticles as the chain transfer agent. Southard *et al.* (**2007**, *Macromolecules and Analyticachimica Acta*), prepared europium (III) containing insoluble or soluble MIPs for the luminescent sensing of organophosphates by RAFT polymerisation or by a combination of RAFT polymerisation and ring-closing metathesis. Liu *et al*. (**2008**) prepared a molecularly imprinted monolithic column for selective separation of enrofloxacin through liquid chromatography via RAFT-mediated *living* radical polymerisation. Pan *et al.* (**2009**) reported the first combination of RAFT polymerisation and precipitation polymerisation (RAFTPP), which provided MIP microspheres with imprinting effect towards the template: 2,4-dichlorophenoxyacetic

acid. The microspheres also demonstrated fast template binding and high selectivity over MIPs synthesised via traditional radical precipitation polymerisation. Li *et al.* (**2009**).described the use of SI-RAFT technique to graft thin (1.98 nm) MIP films of copolymers of methacrylic acid and divinyl benzene in the presence of theophylline as template from the surface of silica gel particles, which were used as the sorbent in solid-phase extraction with recovery of more than 90 % (Figure 1.8).

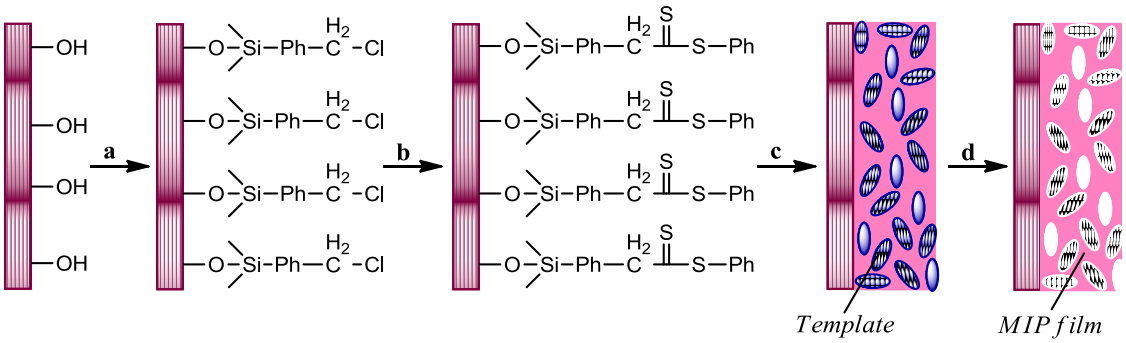

Figure 1.8: Schematic representation of the process of modification of silica gel particles (presented by pink rods on the diagram) via SI-ATRP to achieve MIP film (Li *et al.* **2009**): a) Silanisation with 4-(chloromethyl) phenyltrimetoxysilane (Cl-Silica); b) Substitution reaction with phenylmagnesium bromide and carbon disulfide to prepare PhC(S)SMgBr, which reacted with Cl-Silica; c) Grafting of MIP film on the RAFT agent modified silica gel particles using bulk technique. Methacrylic acid, divinylbenzene, and azobis-(isobutylonitrile) were polymerised in chloroform under nitrogen atmoshere at 60 °C for 24 hours. Theophylline was used as a template; d) The template was washed away and the polymer was dried *at vacuo* at 50 °C for 12 hours.

Core-shell molecularly imprinted beads were prepared via a combination of SI-RAFT polymerisation and click reaction (Chang *et al.* **2010**). The RAFT agent was synthesised and attached to the silica particles surface via click chemistry. Imprinted thin films were prepared in the presence of 2,4-dichlorophenol as template. The polymerisation was carried out at 55 °C for 24 hours under a nitrogen atmosphere. The imprinted beads were characterised with a homogeneous polymer film with thickness of around 2.27 nm. The synthesised material demonstrated an imprinted effect towards the template, fast template rebinding kinetics, and good selectivity over structural analogues.

MIPs with both water compatibility (for application in environmental water) and stimuli-responsive binding properties were described by Pan *et al.* (**2010**). SI-RAFT polymerisation of *N*-isopropylacrylamide from the MIP nanoparticles to form polymer brushes was performed in order to increase the hydrophilicity of the nanoparticles and their thermo-responsive binding properties. Their binding properties were investigated in both methanol/water (4/1, v/v) and pure water. This approach has great potential for the preparation of MIP films with functional polymer brushes, for application as chemical sensors in aqueous environments or as MIP nanoparticles for stimuli-responsive drug-delivery. Furthermore, the authors reported a continuation of this work in the shape of the synthesis of narrowly dispersed pure-water-compatible MIP microspheres with surface-grafted hydrophilic polymer brushes by a one-pot RAFT precipitation polymerisation (Pan *et al.* **2011**). The synthesised materials showed an enhancement in their ability to recognise the template in aqueous solutions.

Magnetic molecularly imprinted nanoparticles were synthesised via SI-RAFT polymerisation (Gonzato *et al.* **2011**). Nanocomposite materials with 40 nm diameter and 7 nm MIP shell were prepared from commercially available amino functionalised Fe_3O_4 nanoparticles. The last were surface modified with trithiocarbonate agent from which SI-RAFT polymerisation was initiated. *S*-propranolol was imprinted at 65 °C for six hours. The active RAFT fragments present on the surface of the synthesised materials were further used to functionalise the particles with ethylene glycolmethacrylate phosphate polymer brushes. The resulting materials retained both a good imprinting effect and superparamagnetic behaviour.

So far, RAFT polymerisation has shown great potential in preparing MIPs with improved properties (e. g., faster binding kinetics (Pan *et al.* **2011**; Gonzato *et al.* **2011**; Chang *et al.* **2010**; Pan *et al.* **2009**; Titirici and Sellergren, **2006**), high selectivity and efficiency (Pan *et al.* **2011**; Gonzato *et al.* **2011**; Chang *et al.* **2010**; Pan *et al.* **2009**; Liu *et al.* **2008**), uniform pore size distribution (Liu *et al.* **2008**), larger surface area (Liu *et al.* **2008**), improved mass-transfer properties (Li *et al.* **2009**)), water-compatibility (Pan *et al.* **2011**; Pan *et al.* **2010**), tailor-made structures (Liu *et al.* **2008**; Li *et al.* **2006**; Southard *et al.* **2007**, *Analitica Chimica Acta and Macromolecules*; Titirici and

Sellergren, **2006**), and more adjustable conditions for making monolithic materials with different morphologies (Pan *et al.* **2009**; Liu *et al.* **2008**)). Disadvantages are the need for the synthesis of new chain transfer agents and to adjust the polymerisation conditions for each system. Temperatures reported for RAFT polymerisation are between ambient and 140 °C (Barner-Kowollik, **2006**). Higher temperatures allow higher rates of polymerisation and shorter reaction times. Higher pressure (5 kbar) results in higher molecular weight polymers and higher rates of polymerisation compared with the same reaction at ambient temperature (Barner-Kowollik, **2006**). It should be of great importance to extend the application of RAFT polymerisation to the synthesis of MIPs with different formats in order to show its versatility.

1.4.7 Surface-initiated *photo-iniferter* mediated polymerisation (SI-PIMP)

Conventional *free* radical *photo-polymerisation* represents a widely used technique in the field of coatings technology since it brings with it some intrinsic advantages over thermally initiated polymerisations. Besides their faster initiation rates, photo-initiated polymerisation systems work under *ambient* conditions and can therefore be readily used for the functionalisation of thermally labile substrates or the polymerisation of thermally labile monomers, like *e.g.* liquid crystalline materials. Moreover the polymerisation temperature itself might be varied as a valuable parameter to fine tune the properties of the final polymeric material without influencing significantly the rate of polymerisation or the underlying mechanism of the polymerisation (Deng *et al.* **2009**; Ishizu and Katsuhara, **2006**; Dyer, **2006**).

In surface-initiated *"photo-iniferter"* mediated polymerisation (SI-PIMP), in contrast to the previously discussed SIP techniques, photons are used as the energy source to initiate the polymerisation and to control the position of the equilibrium between *dormant* and propagating species via the utilization of "*photo-iniferters*" as reported by Matsuda *et al*. (Matsuda and Otsu, **2005**; Nakayama and Matsuda, **1996**; Nakayama *et al.* **1993**).

The first *iniferter*, an abbreviation of *initiator*, *transfer* agent, and *terminator*, was reported by Otsu and Yoshida (**1982**). The *controlled* nature of the polymerisation mechanistically relies on the photolytic dissociation of the *iniferter* molecule into a reactive carbon centered *(active)* and a relatively stable *(dormant)* dithiocarbamoyl centered radical. While the carbon centred radical readily undergoes addition of monomer units to initiate chain propagation, the persistent *(dormant)* dithiocarbamoyl radical does not participate in initiation but acts as a transfer agent and induces reversible termination of the growing polymer chain *(iniferter)*. In the absence of termination or transfer reactions the polymerisation proceeds only during irradiation of light and via a predominantly *controlled* radical polymerisation mechanism, which is based on reversible termination (**Figure 1.9**).

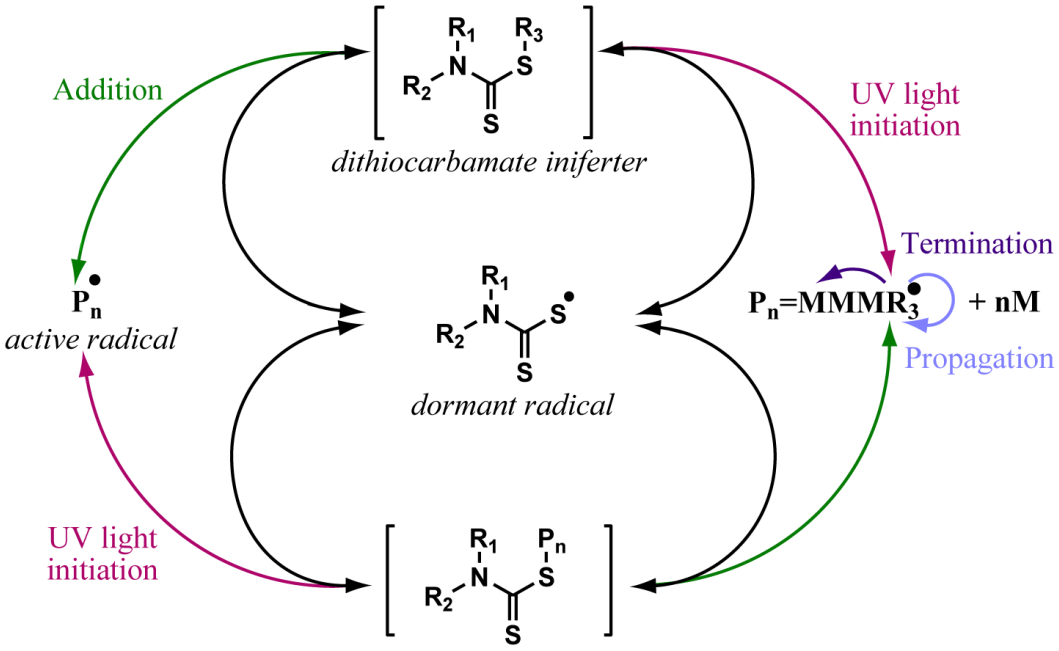

Figure 1.9: Schematic representation of *photoiniferter*-mediated polymerisation mechanism.

The mechanism of SI-PIMP starts with the photolysis of the surface-immobilised *photo-iniferter* yielding a reactive carbon-centred radical on the substrate surface as well as a relatively stable dithiocarbamoyl radical in solution. After the addition of a certain number of monomer units the reactive radical at the end of the propagating chain recombines with the dithiocarbamoyl radical to restore the *dormant* species and to reversibly terminate the polymerisation. The absorption of a new photon leads to

photolysis of the *dormant* species and to a reinitiation of the polymerisation. The concept of SI-PIMP was presented by de De Boer *et al.* (**2000**). In this work glass or silicon substrates were functionalised with the *iniferter*-functional silane, benzyl-*N*,*N'*-(diethylamino)-dithiocarbamoyl-(trimethoxy)-silane. SI-PIMP was initiated from the resulting substrates in the presence of monomer by irradiation with 365 nm UV light. Typically 100 nm thick poly (styrene) *brushes* were obtained within fifteen hours of polymerisation time. These poly (styrene) *brushes* were subsequently used as *macro-initiators* for the SI-PIMP of methyl methacrylate to realise poly (styrene)-block-poly (methyl methacrylate) block copolymer *brushes* with block thicknesses of ~100 nm and ~170 nm, respectively. The possibility to reinitiate *brush* growth as well as a linear increase of *brush* thickness with polymerisation time evidenced the presence of a "*living*" *free-radical* polymerisation.

In SI-PIMP the concentration of radicals and therefore the rate of polymerisation are directly correlated to the intensity of irradiating light. In other words the polymerisation is spatially and temporally coupled to the location, intensity and duration of irradiation (Rhane *et al.* **2005**). SI-PIMP can be therefore readily combined with photolithographic techniques to realize polymer *brush* surfaces with regionally precise topographical and chemical micro patterns. Hagashi *et al.* **1999** and Nakayama and Matsuda, **1999** extensively used this feature of SI-PIMP to realize complex polymer *brush* micro patterns with up to five chemically different zones on polystyrene-*co*-poly (vinylbenzyl-*N*,*N`*-diethyldithiocarbamate)-coated poly (ethylene terephthalate) surfaces. The authors explicitly point out the advantage of SI-PIMP to achieve complex surface patterns compared to conventional patterning techniques, such as soft lithography, which offer the possibility to realize patterns consisting of more than two chemically different zones. Furthermore polymer *brushes* with lateral thickness, i.e. molecular weight gradients were realized via SI-PIMP by either spatially varying the light intensity using a gradient UV-filter or by spatial variation of the light exposure time by means of an X-Y controlled step motor. In contrast to the mainly 2D structured patterns that can be realized by thermal SIP, SI-PIMP therefore offers the additional possibility to realize 3D microstructured *brush* surfaces.

The fact that SI-PIMP is usually carried out without additional *"free"* deactivating species has induced a controversial discussion about the *controlled* nature of this technique since the concentration of the deactivating dithiocarbamoyl-radicals is supposed to be not sufficiently high to effectively convert propagating polymer chains to the corresponding *dormant* species. Studies of the kinetics of SI-PIMP of methyl methacrylate performed by Haris and Metters (**2006**) indicated a pseudo-*living* behaviour of the polymerisation, which was mainly attributed to the presence of bimolecular termination reactions. The same authors interpreted the observed linear increase of *brush* thickness with polymerisation time during SI-PIMP as an increase in *grafting* density and not as an increase in molecular weight of *grafted chains*. However grafting densities as well as molecular weights of *grafted chains* were only determined indirectly in these studies and a significant experimental proof of this hypothesis is still missing. The elucidation of the exact nature of the polymerisation mechanism will surely require further experimental efforts.

The limitations of SI-PIMP are connected to the fact, that only photostable and optically transparent surfaces and monomers can be used. Furthermore microchannels, tubes or small cavities are difficult to functionalise since UV light cannot be easily coupled into these structures or an inhomogeneous distribution of light intensity might cause inhomogeneous *brush* growth on the surfaces of these structures.

SI-PIMP represents a valuable alternative to the thermally driven SIP approaches that were previously presented. SI-PIMP especially offers the possibility to realize 2D and 3D micro patterned polymer *brushes* with versatile lateral and horizontal patterns of chemically different zones. Additionally SI-PIMP is not particularly limited to special types of monomers. Furthermore SI-PIMP does not require the removal of polymerisation catalysts as *e.g.* in SI-ATRP and was therefore proposed to be especially suitable for the functionalisation of materials surfaces for biomedical or bioanalytical applications.

1.4.8 Surface-initiated *photo-iniferter* mediated polymerisation (SI-PIMP) and MIPs

Photo-grafting methods have been applied in molecular imprinted membranes. In the work of Wang *et al.* (**1997**) a surface layer containing molecular imprinted sites of theophylline was produced on a polyacrylonitrile membrane using acrylic acid as monomer and *N*, *N'*-methylenebisacrylamide as cross-linker. After the removal of the template the membrane showed high efficiency recognition. Piletsky *et al.* (**2000**) prepared MIP membranes with desmetryn as template. The produced membrane could be used in a fast preconcentration step and solid phase extraction (Sergeyeva *et al.* **2001**). SI-PIMP based on dithiocarbamate *iniferters* has been used to create molecularly imprinted multi-layer core-shell nanoparticles with propranolol, morphine and naproxen imprints in aqueous media (Pérez-Moral *et al.* **2001**).

Oxelbark *et al.* (**2007**) compared four different MIP formats using a common monomer-template formulation, in term of their chromatographic performance. Chromatography was exploited to assess and compare both the degree of imprinting and thermodynamic parameters such as efficiency, imprinting factors, water compatibility and reproducibility. For this reason MIPs were prepared in five different ways: crushed monolith, microspheres via precipitation polymerisation, silica-based composites using *iniferter*-modified mesoporous silica beads by *"grafting from"* technique, and capillary monoliths using *"grafting to"* approach. All materials were imprinted with bupivacaine. The *iniferter* used was dithiocarbamate-based with UV irradiation time two hours. The crushed monolith procedure is well established technique that has some drawbacks to be overcome, such as binding site heterogeneity, mass transport limitations, selectivity, and water compatibility. In this particular case the bulk polymer synthesised exhibited high imprinting factors including in aqueous environments, but also exhibited a significant non-specific binding. The capillary monoliths provided a miniaturised format which benefited from low reagent consumption, short run times, and high selectivity. The *"grafting from"* technique by *controlled* radical polymerisation provided tuneable size and porosity of the synthesised materials. Much faster analysis, good reproducibility, and low non-

specific binding were observed with both *iniferter* composites and capillary monoliths. Among all the different formats only the microparticles did not exhibit significant imprinting effect.

Sulfamethazine imprinted silica beads were prepared via SI-PIMP (Su *et al.* **2008**). Methacrylic acid was used as a functional monomer, ethylene dimethacrylate was used as cross-linker, and *N*,*N*-diethyldithiocarbamate was used as *iniferter*. The polymerisation was UV-initiated at 10 °C under a nitrogen atmosphere. The resulting polymer had good selectivity and high column efficiency in HPLC analysis of sulfamethazine in milk.

MIP layer was *"grafted from"* the periphery of polystyrene beads via SI-PIMP (Gai *et al.* **2008**). Acrylamide was used as a functional monomer, bovine hemoglobin was used as a template and *N*,*N'*-methylenebisacrylamide as crosslinker in PBS as solvent. The authors demonstrated that the polymer prepared by SI-PIMP exhibited better selectivity for the template when compared with composites prepared by a traditional radical polymerisation method.

Lysozyme protein molecularly imprinted polymer beads were prepared in aqueous media, creating material with well-distributed pores on the surface (Qin *et al.* **2009**). Mesoporous chloromethylated polystyrene beads containing dithiocarbamate *iniferter* were used as supports for the grafting process via SI-PIMP. The polymerisation was performed in an ice bath during UV irradiation with various irradiation times in order for different sizes to be compared. The synthesised materials exhibited better imprinting effect than the MIP beads prepared via traditional radical polymerisation. In this study it was shown that *iniferter-modified* supports could be used successfully to prepare protein imprinted MIPs. These materials were applied as a stationary phase for the separation of bioactive compounds in aqueous mobile phases.

Lee and Kim (**2009**) and Lee *et al.* (**2008**) used *iniferter-modified* carbon nanotubes to prepare a MIP nanocomposite. Ethylene glycol dimethacrylate was used as cross-linking agent, methacrylic acid as functional monomer, DTCE as *iniferter*, and theophylline as template. The MIP nanotubes showed higher binding capacity and

selectivity for theophylline over caffeine and theobromine (close structural analogues). This new material could be incorporated as protein-based sensing elements into biosensors.

Vaughan *et al.* (**2010**) reported for first time the combination of SI-PIMP and MIPs in order to achieve enhanced template loading, higher affinity and delayed release in weakly crosslinked gels. Two gel systems were studied: poly (diethylaminoethyl methacrylate-*co*-2-hyroxyethylmethacrylate-*co*-polyethylene glycol 200 dimethacrylate) gel imprinted with diclofenac sodium and poly (methacrylic acid-*co*-ethylene glycol dimethacrylate) gel imprinted with ethyladenine-9-acetate. Tetraethylthiuram disulfide was used as *iniferter*. The polymerisation was carried out at 14 °C during UV-irradiation. The experimental evidence provided showed that the template diffusion coefficients are strongly influenced by the binding affinity of the template. It was shown that in the case of SI-PIMP MIPs the affinity to the template is higher and the release is slower by at least two times when compared with MIPs prepared by conventional *free-radical* polymerisation. In this work for first time anti-inflammatory imprinted hydrogels were prepared which could have applications in anti-inflammatory therapeutic contact lenses.

Barahona *et al.* (**2010**) imprinted thiabenzadole using two different imprinting formats: core-shell microspheres by precipitation polymerisation and grafted MIP layers via SI-PIMP with DTCE as *photo-inifeter*. SI-PIMP was carried out at 15 °C for four hours under UV-irradiation whereas the precipitation polymerisation was in two steps at 60 °C for 26 hours. The two types of materials were loaded in to HPLC columns as the stationary phases. Both materials demonstrated good imprinted properties. SI-PIMP MIPs were prepared in a one step fast procedure and using only a fraction of the reagents typically used to prepare particles from bulk polymers.

A novel restricted access MIP was synthesised using SI-PIMP (Xu *et al.* **2010**). The material was prepared by *"grafting from"* polymerisation via DTCE *iniferter* of two layers of polymers with different functions on a silica support. The internal polymer layer was imprinted poly (methacrylic acid) with sulfamethazine template during UV

irradiation in ice-water bath. On the exterior of the material the hydrophilic poly (glycidyl methacrylate) was grafted during UV irradiation at 40 °C. The result showed that this restricted access MIP structure had good selectivity for the template and the ability to exclude bovine serum albumin. This result demonstrated that the thus synthesised material could be successfully applied to sample extraction and clean-up of sulphonamides in real samples such as bovine milk.

The first report of precipitation polymerisation via SI-PIMP to produce MIPs was also introduced (Li *et al.* **2010**). The imprinted 2 µm diameter poly (ethylene glycol dimethacrylate) microspheres for the herbicide 2,4-dichlorophenoxyacetic acid were characterised with narrow polydispersity, high selectivity over structural analogues, and fast template rebinding kinetics. As *iniferter* benzyl dithiocarbamate was used. The polymerisation was performed at 37 °C for ten hours under UV irradiation. The *iniferter* surface groups were further used in the *"grafting from"* technique to form polymer brushes of poly (*N*-isopropylacrylamide) which contributed to the polymer water compatibility.

Molecularly imprinted membranes for the selective transport and separation of lysozyme were synthesised in a novel way (Chen *et al.* **2010**). The poly (acrylonitrile-*co*-*N*,*N'*-diethylaminodithiocarbamoylmethylstyrene) imprinted membrane was prepared via a phase inversion method and surface modified with the photosensitive DTCE group for SI-PIMP. The results indicated excellent selectivity and separation performance of the membrane that were assigned to the size and structure of the imprinted sites, which offers great potential for separation and purification in commercial applications.

Prasad *et al.* (**2011**) reported the creation of a biosensor for L-histidine produced via "grafting from" approach with *iniferter*. The electrocatalytic activity of the material was enhanced due to the Cu^{2+} ion-mediated imprinting on graphite electrodes. The limit of detection was as low as 1.98 ng mL^{-1}. The authors reported no cross-reactivity and non-specific binding in real samples for enantioselective sensing.

The combination of SI-PIMP and MIP is beneficial due to the improved characteristics of the materials, more flexible systems in terms of variety of MIP formats and better control over the process. The evidence for this fact over the last five years lies in the extremely rapid increase in the number of the publications related to the topic. The better control over the polymerisation process contributes to better imprinted properties of the materials. Nevertheless the production processes are shorter and simpler. There is no need to apply high temperature during polymerisation which is favourable for non-covalent imprinting and increases the number of templates available for imprinting and the affinity to the template. There is no need for the use of extra compounds such as initiators or metal ions that are not incorporated into the structure of the synthesised polymer that will affects the purity of the resultant polymer, thus more thorough washing procedures could be avoided and more environmentally friendly materials could be synthesised. The use of a specific *iniferter* is not directly connected to a monomer which could be polymerised in a certain system. This provides a very flexible polymerisation technique that does not need to be connected with good synthetic chemistry abilities. Future work on the topic should contribute to the development of different formats of MIPs with higher binding energies and enhanced selectivity.

1.5 Conclusions

MIPs are a promising tool for the development of *"tailor-made"* sensing elements. Their formulation in nanoscale formats, such as nanoparticles and nanolayers, could be advantageous for their better processability and sensitivity. The application of SI-CRP techniques in the production of MIPs leads to enhancements of their imprinted properties. It also leads to very well tunable thickness of the polymer layer and also to the possibility of reinitiation of the process to provide layer-by-layer grafting of different polymer layers. The last could provide a better tuning of the compatibility of a specific composite in different polarity media and change in the surface properties of a particular material. SI-CRP also introduces specific surface functionalities on the synthesised materials which could be further used for additional surface modification.

From the known SI-CRPs, SI-NMP has received the least attention due to the need of high polymerisation temperatures (above 100 °C) during the polymer synthesis process. This restricts its application in non-covalent imprinting because of the detrimental influence of high temperatures on the non-covalent monomer-template interaction. The number of templates that could be applied in SI-NMP is very limited as well. In SI-ATRP the polymerisation temperatures are significantly reduced but the use of metal ions is required as part of the initiation mechanism, which requires longer washing procedures of the resulting polymer. SI-RAFT polymerisation involves a number of organic initiators that require precise and specific tuning of the polymerisation conditions for each target-monomer mixture. SI-PIMP is the most promising tool for the synthesis of well defined MIPs. It is the fastest and the simplest of all. It could be conducted even at sub-zero temperatures, does not involve any additional initiators or metal ions that are not incorporated in the polymer matrix, and does not require additional tuning of the polymerisation conditions for the different template-monomer mixtures. A disadvantage of this technique could be the restricted application for UV sensitive templates such as proteins, although there are examples in the literature of the successful application of the technique in protein imprinting.

For the reasons stated above SI-PIMP with DTCE was chosen as the most appropriate polymerisation technique for the work presented in this thesis. In Chapter 2 it was applied in the form of the *"grafting from"* technique where dendrimers, modified on their periphery with DTCE groups, were used as the core in the synthesis of core-shell MIP NPs, imprinted with the pesticide acetoguanamine. In Chapter 3 a new *N*-substituted polyaniline (PANI) was synthesised. Each of the polymer units contains a DTCE unit in the side chain that can be used in surface-confined grafting of different polymer layers. The technique provides a rapid metod of surface modification of the conductive polymer layer that could be deposited for example, on a sensor surface. The enhancement of conductivity upon UV irradiation in variety of *N*-substituted PANIs bearing DTCE groups is discussed in Chapter 4.

2 Cubic MIP Nanoparticles – Building Blocks for a Bright Future

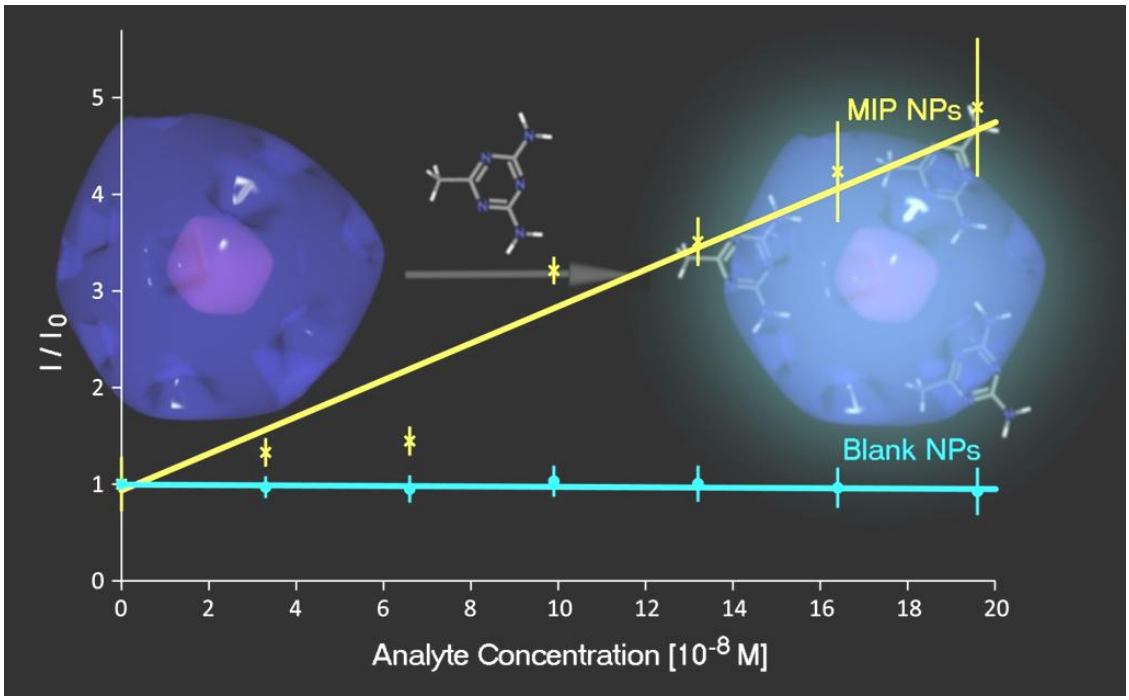

2.1 Introduction

The fast, sensitive and selective detection of organic pollutants is of a vital importance for human health and for the environment. Molecularly imprinted polymers (MIPs) are one of the leading contenders, combining selective recognition with chemical robustness (Mayes and Whitcombe **2005**; Chen *et al.* **2011**; Ye and Mosbach, **2008**; Alexander *et al.* **2006;** Haupt and Mosbach, **1998**; Wulff **1995**). MIPs have already been exploited in biosensors (Kim *et al.* **2011;** Lautner *et al.* **2011**; Suryanarayanan *et al.* **2010**; Al-Kindy *et al.* **2000**). The synthesis of these types of materials with molecular architectures which are well defined on the molecular level is a future priority development. For this reason preparation of MIPs via surface-initiated controlled radical polymerisation (SI-CRP) has been extensively studied during the last decade (see Chapter 1, Literature Review). Preparation of MIPs in nanoformats would benefit from increased surface area per unit mass and hence a larger number of accessible binding sites (Poma *et al.* **2010**).

Recognition of organic compounds is a great challenge as the involved interactions are the weak hydrophobic and van der Waals interactions, and hydrogen bonding. Fluorescence sensing is so far the dominant analytical tool for environmental analysis and for biological imaging (Liu *et al.* **2011**; Basable-Desmonts *et al.* **2007**). The direct detection of binding in MIPs and other artificial receptors would be a desirable property and one method of achieving this aim is through allowing binding to influence the fluorescent properties of the material. Fluorescent MIP nanoparticles (NPs), with their large surface areas, enable them to amplify the fluorescent signal of detection for higher sensitivity in bioassays. The fluorescent label could be incorporated in the template, in the MIP shell, or in the core of MIP NPs.

When the template is fluorescently-labelled a precise physical quantification of the binging events could be achieved (Harz *et al.* **2011**; Lalo *et al.* **2010**; Gultekin *et al.* **2009**; Wang *et al.* **2008**; Lu *et al.* **2007**). All examples characterise the binding event with a quenching of fluorescence. In this approach each binding event would be characterised with direct fluorescent responce. It has the drawback of requiring

additional synthetic steps in order to chemicaly modify of the target analyte, which is not convenient in many cases.

In the preparation of fluorescent MIP shell NPs in general two approaches have been introduced. In the first one a fluorescent functional monomer is used for the synthesis of the composite (Liu *et al.* **2011**; Hoshino and Koide *et al.* **2010**). In the second approach the fluorescent label is attached to the accesible part of the MIP shell after the synthesis (Yang et *al.* **2009**; Gao *et al.* **2008**). In these approaches quenching of fluorescence was observed when binding occurred. An interesting approach was that used by Frasconi *et al.* (**2010**) where thioaniline-functionalized gold NP composites were prepared during electropolymerisation in the presence of different template molecules that had π-acceptor groups, the latter forming fluorescent π-donor-acceptor complexes between the substrates and the thioaniline units of the NPs. Fluorescent quenching was induced when the template molecule was rebound. These approaches also involve additional synthetic modification steps, but this time of the polymer matrix itself, rather than to the monomers prior to synthesis. This leads to limitations in the choice of imprinted molecules. When the fluorescent modification is done after polymerisation it could influence the binding event in case of modification occurring in the binding sate. Another disadvantage could be the enhanced fluorescent leaching of the dye when exposed to direct contact with different solvents.

There are only two different reported approaches for florescent core MIP NPs. In one of the cases this was the cost ineffective quantum dots coated with MIP (Ye *et al.* **2011**; Zhang *et al.* **2011**). And in the second two layer NPs were created, where the first layer was a fluorescently-labelled polymer and the second, outer layer was the MIP (Li *et al.* **2011**). Fluorescent quenching was observed when binding occurred. The advantage of this approach is that the fluorescent label is shielded in a polymer shell where it is protected from the environment, and also there is no restriction on the type of template chosen or the monomer used in the imprinting process. In both of the given examples though, no precise control over the fluorescent labelling could be established.

The approach we applied was to use dendrimers as the core from which to graft a MIP shell to form imprinted NPs (Scheme 2.1). Dendrimers are biocompatible, soluble, highly-branched well defined and organised structures that have low solution viscosity compared to linear polymers of the same molecular weight, with a strictly defined number of surface functionalities, and regular shape and size (Suarez *et al.* **2011**; Klajnert and Bryszewska, **2007**) (Figure 2.1). Using dendrimers as the core in a controlled or *"living"* polymerisation would ensure precise control of grafting at the molecular level. An earlier example of the use of dendrimers in the production of MIP NPs was reported in the work of Zimmerman *et al.* **2002**: a dendrimer bearing allylic terminal groups was cross-linked, by olefin metathesis, around a single porphyrin template at the core of the molecule. The method had the advantage of thermodynamic control during the cross-linking process, but necessitated the use of covalent imprinting. In addition the monomolecular imprinted NPs formed had only one binding site at the centre of the particles and involved a long and tedious synthesis. The use of dendrimer-based macro-initiators for the synthesis of star polymers and NPs using atom transfer *living* radical polymerisation (Ogawa *et al.* **2010**) and microemulsion polymerisation (Yi *et al.* **2004**) have been reported. Unfortunately the polymerisation conditions are mostly incompatible with the imprinting process (high temperature, presence of ions *etc*.). Much more favourable conditions are associated with use of *iniferters* (initiation, transfer agent, termination) (Otsu, **2000**) and nitroxide-mediated polymerisation (NMP). TEMPO-based stable radicals were attached to the interior of dendrimers of various sizes and used to initiate NMP of styrene, vinyl acetate, and (meth) acrylates at 90 °C (Matyjaszewski *et al.* **1996**), however as pointed out in Capter 1, the high temperatures demanded by NMP are unsuitable for use in imprinting. For these reasons the iniferter method was chosen for the work presented in this chapter.

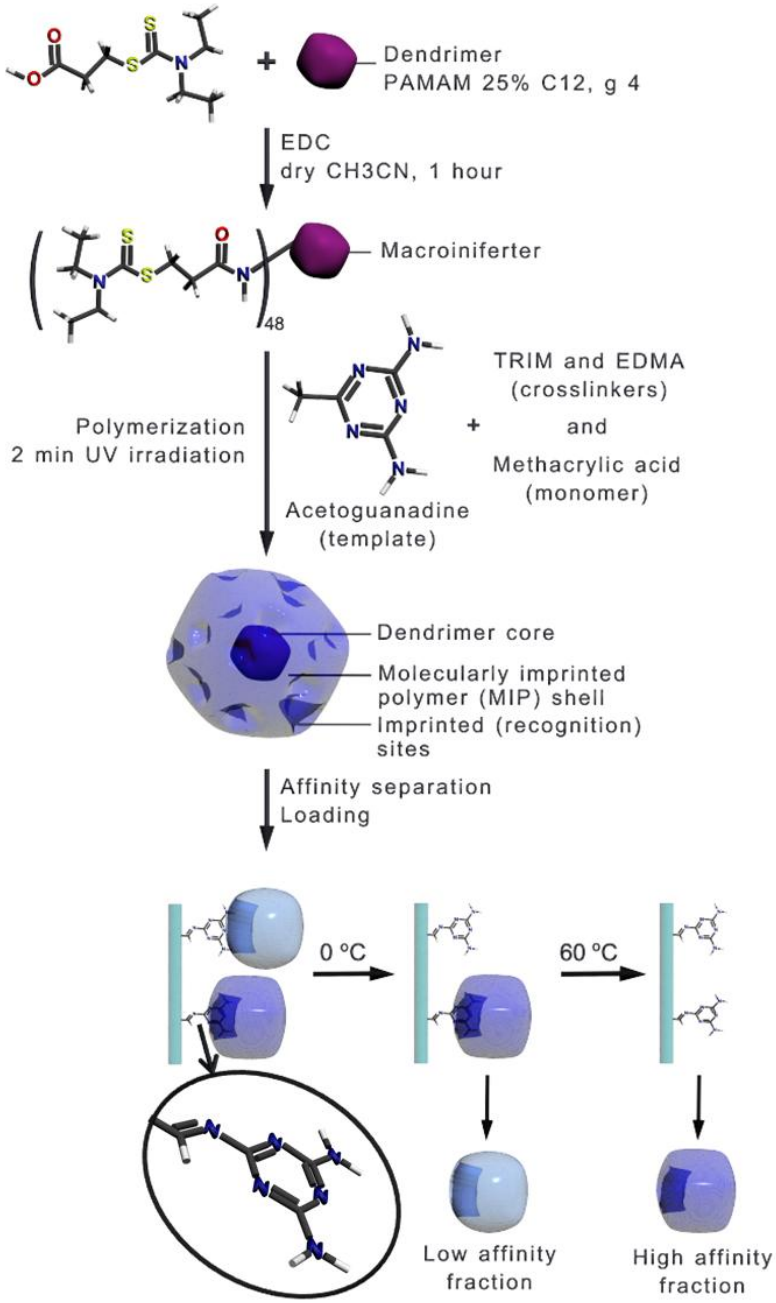

Scheme 2.1: Schematic representation of the synthesis of the NPs. *S*-(carboxypropyl)-*N*,*N*-diethyldithiocarbamic acid (CNDDA) was reacted with the primary amino groups at the surface of the dendrimer via EDC coupling. The *macroiniferter* formed in this way was used further in a UV-initiated *living* radical polymerisation to create MIP NPs. The template was acetoguanamine which is known to form complexes with methacrylic acid (functional monomer). The resultant NPs were fractionated by affinity chromatography.

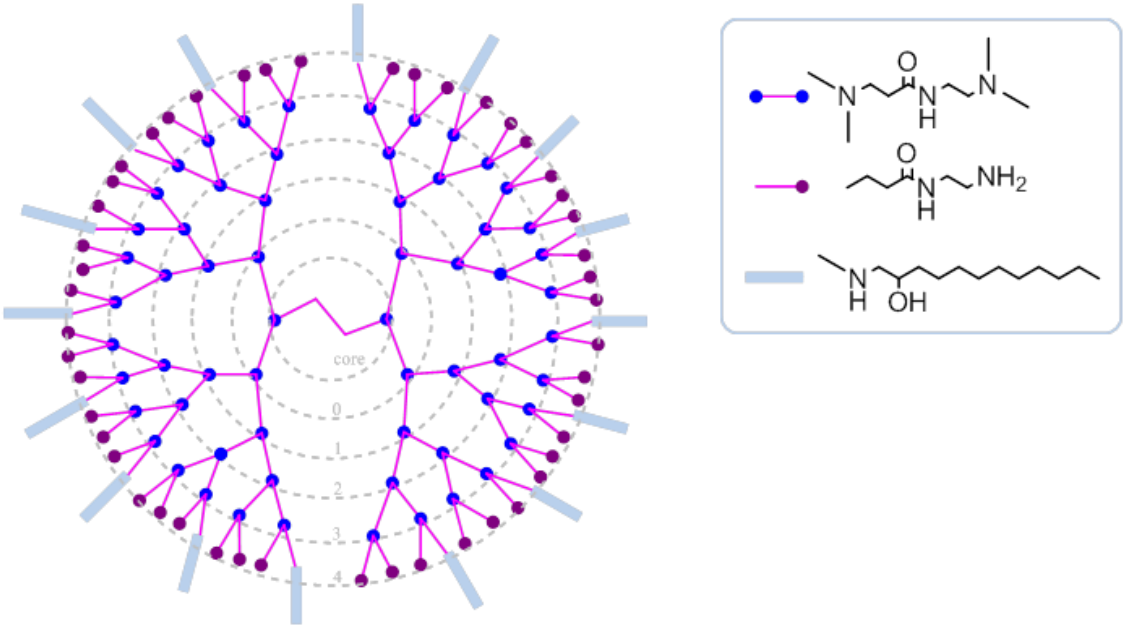

Figure 2.1: Schematic representation of the structure of polyamidoamines (PAMAM) 25% C_{12} (*N*-(2-hydroxydodecyl) groups) dendrimers, generation 4.

In this chapter a novel approach towards the synthesis of water compatible MIP NPs will be discussed and described in details. Surface-initiated *photo-inifeter* mediated polymerisation (SI-PIMP) will be applied in the preparation methodology. The preparation protocol does not use surfactants or high temperatures and is achieved in just two minutes polymerisation time. A unique versatile and highly controlled technique combining dendrimer *macroiniferters*, *living* polymerisation, nanotechnology, molecular imprinting and fluorescent sensing is demonstrated herein.

The organic compound acetoguanamine (6-methyl-1,3,5-triazine-2,4-diamine) was used as the imprinted template. It is a triazine-based compound that is a close structural analogue of melamine (Wang *et al.* **2011**) and of the herbicide atrazine (Xu *et al.* **2011**). When melamine is combined with cyanuric acid and related compounds it forms melamine cyanurate and related crystal structures, which were implicated as contaminants in recent cases of food adulterations, such as the contamination of dried milk that occurred in China (www.bbc.co.uk, "China milk poisoning cases rise", 22/09/2008). Melamine was involved in poisoning due to its illegal addition to food stuffs. It was discovered that melamine-adulterated food causes severe kidney

damages in children and pets. Atrazine is one of the most widely used herbicides worldwide. Its use is banned in the EU due to widespread contamination of drinking water and its associations with birth defects and menstrual problems when consumed by humans.

2.2 Results and Discussion

2.2.1 Surface modification and characterisation of PAMAM dendrimers

Dendrimers are biocompatible macromolecules possessing highly defined regularly-branched structures, a well defined shape, size and number of peripheral functionalities. *Iniferter* units were attached on the periphery of polyamidoamine (PAMAM) dendrimers, (25% C_{12} [*N*-(2-hydroxydodecyl)], generation 4), (Scheme 2.2, **4**) creating a soluble *macroiniferter* which was then used as a core for the synthesis of the nanoparticles (NPs). As *iniferter* *S*-(carboxypropyl)-*N*,*N*-diethyldithiocarbamic acid (CNDDA, **1**) was used. CNDDA was synthesised following a protocol described in a previous work (Ivanova-Mitseva *et al.* **2011**). The dithiocarbamate ester (DTCE) functionalised with carboxylic acid was coupled to the peripheral primary amino groups of the dendrimers via 1-ethyl-3-(dimethylaminopropyl)-carbodiimide hydrochloride, (EDC, **2**) coupling reaction. The modified dendrimers were characterised by nuclear magnetic resonance (NMR), fluorescence-labelling to determine primary amino groups and dynamic light scattering (DLS) measurements of the hydrodynamic diameter, before and after modification.

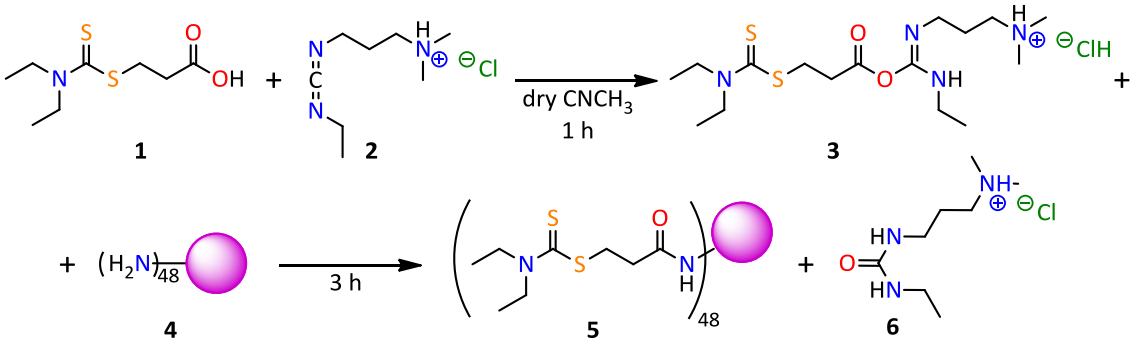

Scheme 2.2: The surface modification of PAMAM, 25% C_{12}, generation 4, dendrimer (**4**) with *iniferter* groups (CNDDA, **1**) via standard EDC (**2**) coupling reaction leading to the formation of *macroiniferter* (**5**).

EDC is a water-soluble derivative of carbodiimide. EDC reacts with carboxyl groups to form reactive *o*-alkylisourea intermediates (**3**). In the absence of water these intermediates form stable amide bonds by reaction with primary amines. The only by-

product of this reaction is a water- soluble urea derivative **(6)**, which is easily removed by extraction. Different methods for the product purification were tried: ethyl acetate/water extraction, filtration through a 20,000 M_w centrifuge filter, Saphadex size-exclusion column separation and dialysis. Ethyl acetate/water extraction had some disadvantages: namely poor solubility of the dendrimers and very slow phase separation, on the other hand the method has the advantages of simplicity and relative speed. For the filtration method, the process was very slow and part of the product could not be recovered from the membrane. The Sephadex size-exclusion approach needed optimisation, involved long separation times, and required large volumes of solvent. The procedure chosen for the isolation of the product was extraction, as it was the fastest and simplest method.

The hydrodynamic size of the macromolecules was measured and compared using DLS (Nano-S, Malvern Instruments, Malvern, UK, **Figure 2.2**). A clear increase of particle diameter of approximately 4 nm was observed. This was good evidence that some structural changes occurred which resulted in an increase of the particles hydrodynamic diameter. Both of the samples analysed demonstrated narrow size distributions.

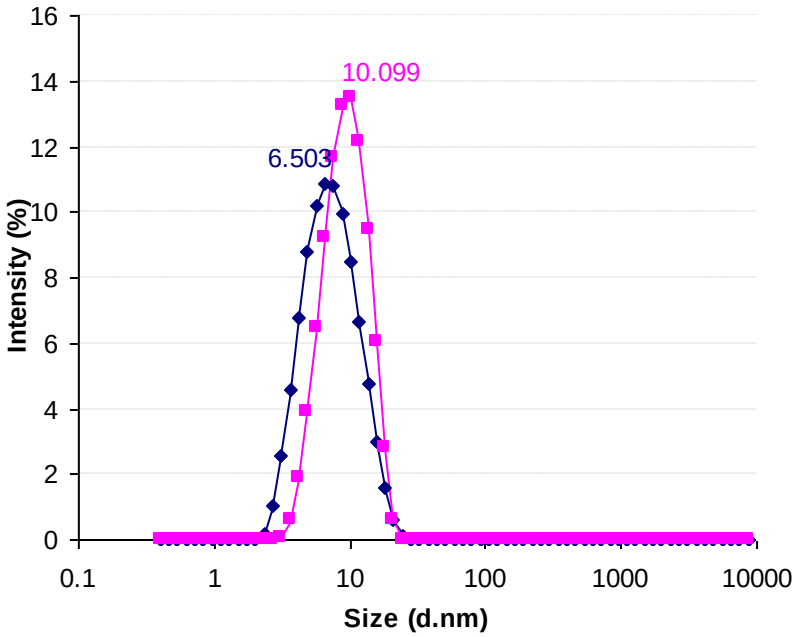

Figure 2.2: Dynamic light scattering (DLS) size distribution for (blue diamonds) PAMAM, 25 % C_{12} with maximum peak intensity at 6.5 nm and (pink squares) *macroiniferter*, with an intensity peak maximum at 10.1 nm.

The isolated *macroiniferter* was characterised using ^{1}H and ^{13}C NMR spectroscopy (**Figure 2.3** and **Figure 2.4**, respectively). **Figure 2.3** shows the appearance of two broad signals at around 3.9 ppm and around 3.7 ppm in the spectrum of the modified dendrimer. These two signals were as assigned to the two methylene groups from the ethyl groups connected to the nitrogen of the DTCE residues. They are non-equivalent due to restricted rotation around the -C(=S)-N- bond. The broadening of the peaks as compared to the native spectrum of CNDDA was also an expected characteristic when this functional group is attached to macromolecular species such as dendrimers.

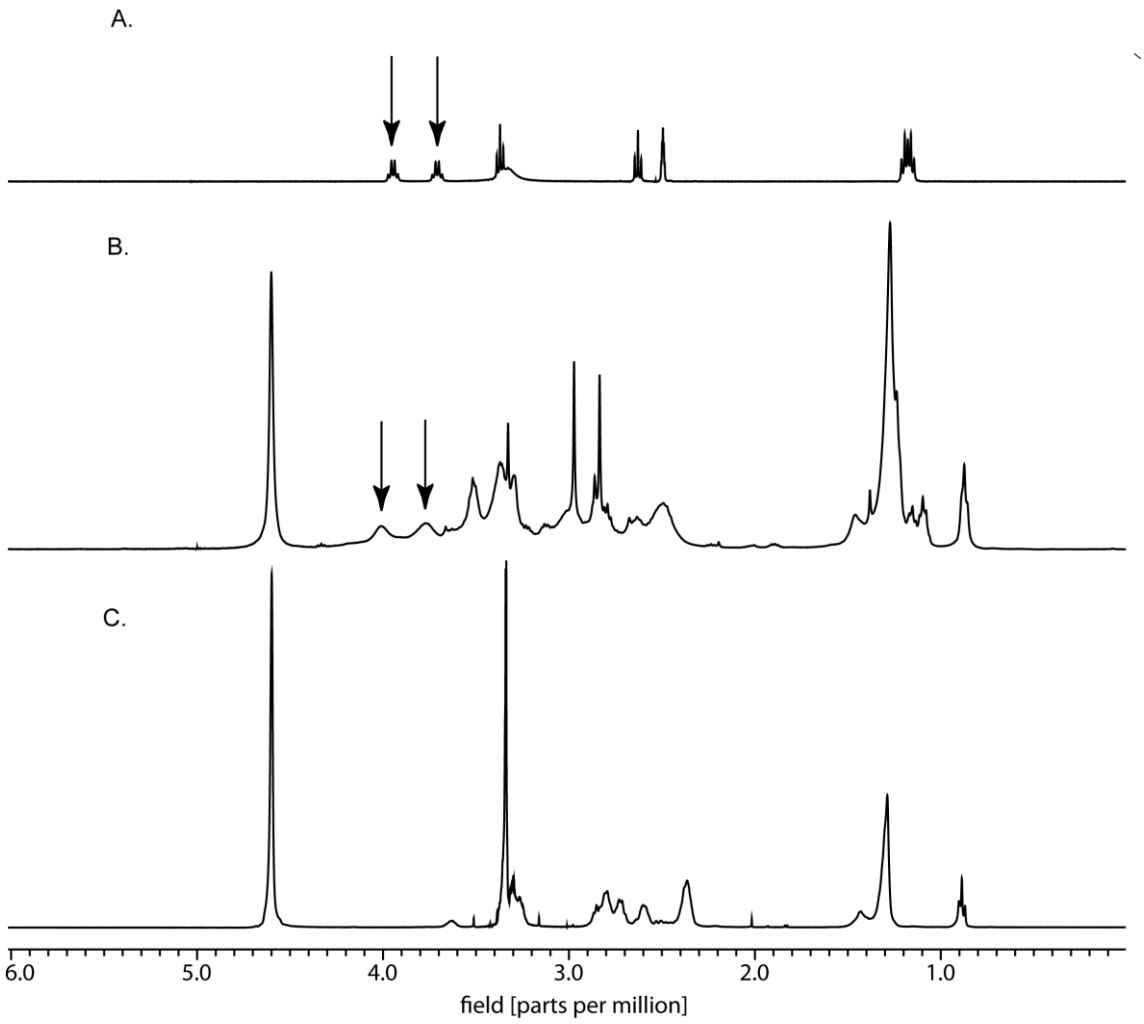

Figure 2.3: ^{1}H NMR spectra; A. CNDDA; B. *macroiniferter*; C. PAMAM 25% C_{12}, generation 4, dendrimer. All spectra were recorded in methanol – D_4. The arrows (in A and B) indicate the signals assigned to the methylene groups of the diethyldithiocarbamate residue ethyl substituents.

Figure 2.4 shows the appearance of a peak at around 200 ppm in the spectrum of the modified dendrimers, assigned to the diethyldithiocarbamate thiocarbonyl residue, which is absent on the spectrum of the unmodified dendrimers. This was taken as clear evidence that the modification was successful and the CNDDA unit was present.

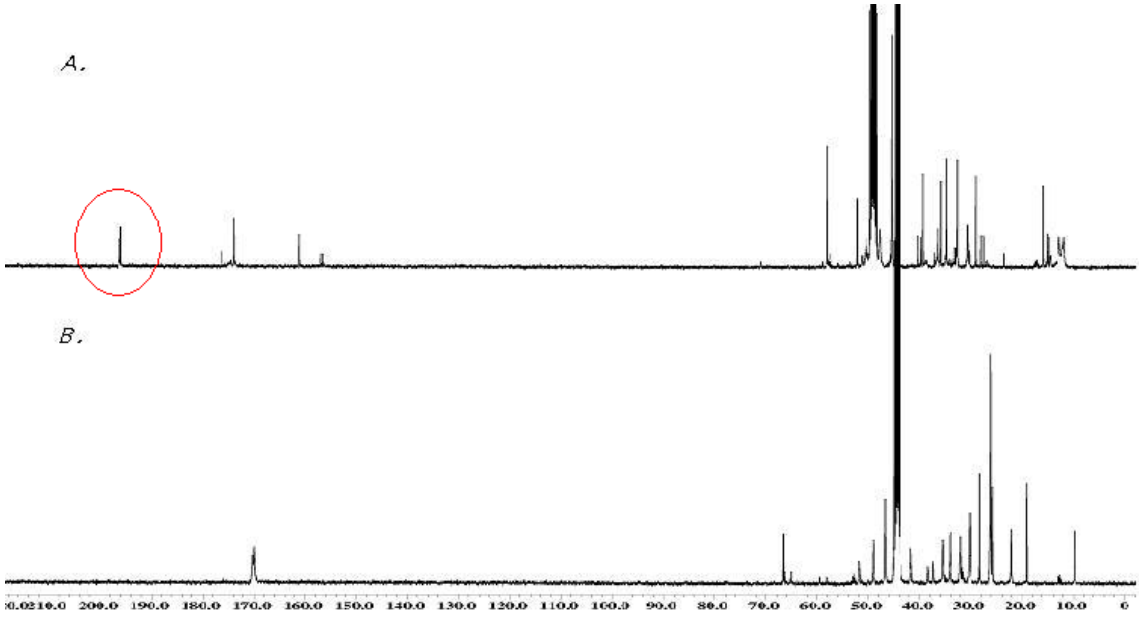

Figure 2.4: ^{13}C NMR spectra; A. *macroiniferter*; B. PAMAM 25% C_{12} dendrimer. All spectra were recorded in methanol – D_4. The characteristic peak of the carbonyl residue from the dialkyldithiocarbamate group at around 200 ppm is shown circled in red.

The interpretation of the spectra of such macromolecules as dendrimers is a challenge even for specialists in the field of NMR spectroscopy. The explanation of this is the presence of groups with similar shifts in multiple repeat units. One peak in the spectrum could therefore be due to several groups in structurally and magnetically similar environments. **Table Apx A.1** (5A.1, page 213) shows the theoretically calculated values of the molecular weight, molecular formula and number of different groups, including the number of different non-equivalent protons from the different methylene groups present in perfect dendrimers of the PAMAM type with 25 % C_{12} substitution, for generations from 0 to 5. **Table Apx A.2** (5A.1, page 213) includes the same type of information but for the synthesised *macroiniferter*.

In order to evaluate the degree of modification of the dendrimers the quantification of the number of primary amine groups on the dendrimer surface was performed. The chemistry used was based on nucleophilic addition of a mercaptan (**Scheme 2.3**, **8**) to *o*-phthaldialdehyde (**7**) which resulted in the formation of hemithioacetal (**9**), which reacted almost immediate with the free primary amino groups (**10**) to form a

fluorescent isoindole (**11**) at *ambient temperature*. The rate of the chemical reaction was monitored as a function of time by measuring the fluorescence intensity maximum after twenty minutes, as by this the reaction was judged to be complete (no further increase in fluorescence emission intensity, data not shown).

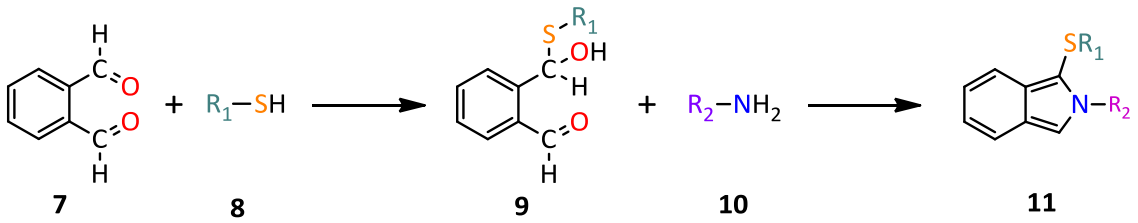

Scheme 2.3: The reaction between *o*-phaldialdehyde (**7**), a mercaptan (**8**) and a primary amine (**10**), *via* a hemithioacetal intermediate (**9**), leading to the formation of a fluorescent isoindole (**11**).

The protocol was adapted from Piletska *et al.* **2000**. Methanol was used as solvent due to the limited solubility of the dendrimers in water. In order to maintain the basic environment required for this reaction to proceed, triethylamine was used in place of phosphate buffer, due to the nature of the solvent used. The excitation and emission spectra were different from those reported in the cited work. The excitation and emission maxima were 250 and 430 nm, respectively (instead of 347 and 400-460 nm) (Piletska *et al.* **2000**) as can be seen from the 3D spectrum shown below (**Figure 2.5**, A). The shift in the excitation maximum could be explained by the fact that there was a different format of spherical macro fluorescent species, namely dendrimers. This phenomenon could be due to the presence of tertiary amino groups in the dendrimer core and in the branches. It could be assumed that the backbone of the dendrimer plays a key role in forming the novel fluorescent centre with strong blue photoluminescence in pH range down to 6 (Dongjun and Imae, **2004**).

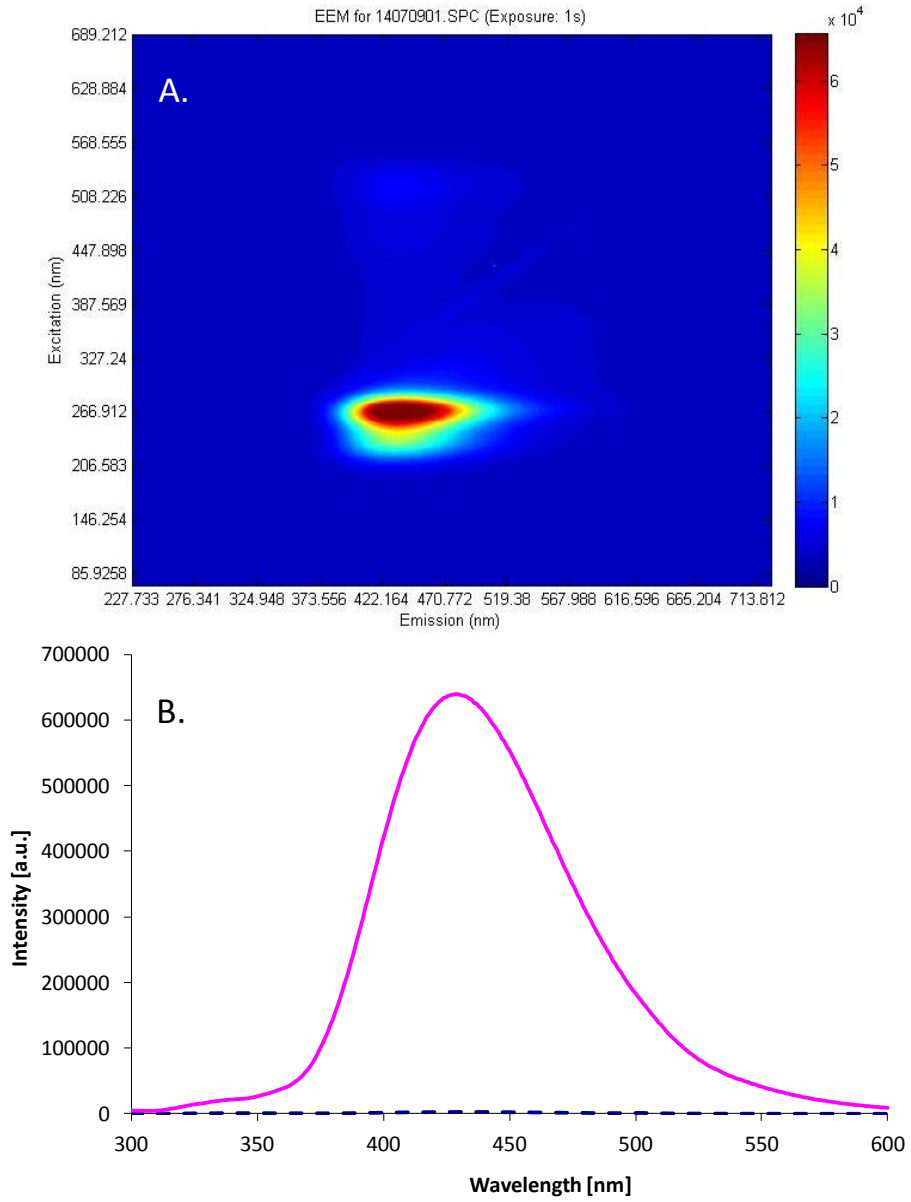

Figure 2.5: Fluorescence spectrum: A. 3D spectrum of isoindole complex the periphery of PAMAM 25% C_{12} dendrimer in methanol; B. Emission spectra of isoindole dendrimers in methanol: (pink solid line) PAMAM 25% C_{12} dendrimer and (blue dashed line) *macroiniferter*.

The strong blue luminescence produced after the treatment of the dendrimers with thioacetal, originates from the derivatised surface amino groups of the PAMAM dendrimers. From the 2D emission fluorescence spectrum (**Figure 2.5**, B) it could be seen that there was almost no fluorescence after modification with DTCE groups. This result was attributed to the fact that there were no free amino groups left on the surface of the dendrimers after the modification with CNDDA. The excitation maximum

was set to 250 nm and the emission spectrum was measured between 300 and 600 nm. Lee *et al.* (**2004**) reported that the surface groups bring highest impact on dendrimer fluorescence. Although he did the experiments with hydroxyl-surfaced dendrimers, the results shown in this work represents the same conclusion. This blue-luminescent chemical species may have potential applications as a novel fluorophore for molecular diagnostic, chemosensors and optoelectronics (Georgiev and Bojinov, **2010**; Grabchev *et al.* **2010**).

Based on the experiments shown above, (^{1}H and ^{13}C NMR spectra, DLS hydrodynamic diameter measurements and fluorescence spectroscopy), it can be concluded that the modification of the dendrimers was successfully accomplished.

2.2.2 Synthesis of MIP NPs

In order to first characterise the properties of dendrimer-core NPs, a non-fluorescent core was first used. The polymerisation was initiated simultaneously from potentially 48 points per dendrimer moiety by activation with UV light (Scheme 2.1). In just two minutes irradiation time the organic MIP NPs were synthesised. The use of UV-initiated *living* radical polymerisation, besides imparting better control over the size distribution, has another fundamental advantage. The polymerisation process can be re-initiated by UV exposure, where the already synthesised NPs will act as a *macroinitiator* (Otsu, **2000**), allowing many possibilities for further modification of the particle surface properties.

A model system based on crosslinked methacrylic acid polymers imprinted with the triazine derivative 2,4-diamino-6-methyl-1,3,5-triazine (acetoguanamine), which is a close structural analogue to melamine, was chosen. Triazines have been successfully imprinted before, using similar monomer compositions (Guerreiro *et al.* **2009**; Sergeyeva *et al.* **1999**; Muldoon and Stanker, **1997**). The use of high monomer concentration in the present method favours the formation of stable template-monomer interactions and should lead to the formation of high affinity binding sites in

the MIP (Guerreiro *et al.* **2009**). Control (Blank) polymers were prepared following the same protocol but in the absence of template. The NPs produced were characterised by DLS measurements (Figure 2.6). UV initiation was utilized to ensure the formation of polymer recognition binding sites in a controlled manner. Grafting from the surface of the dendrimer *macroiniferter* was achieved in solution and without the use of surfactants. The NPs were separated by affinity purification to isolate a fraction with high affinity for the template (Guerreiro *et al.* **2009**).

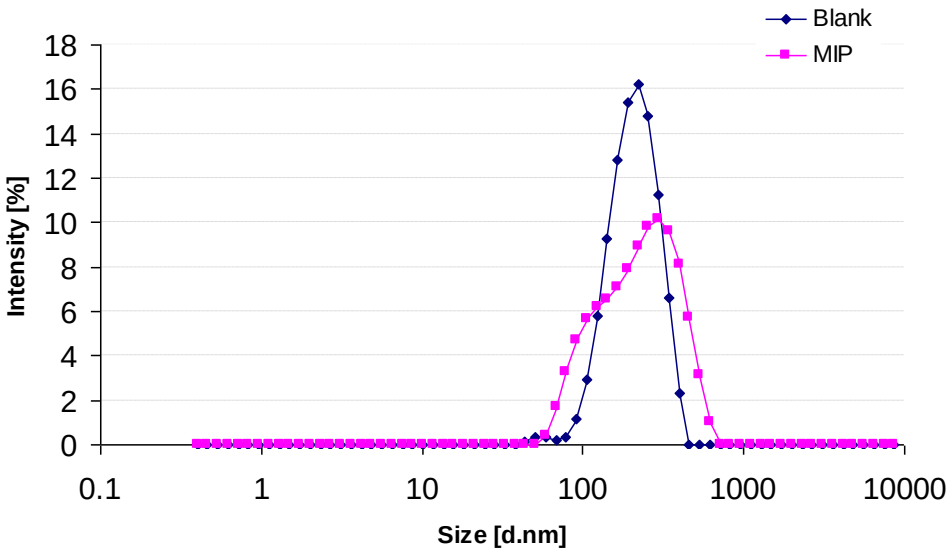

Figure 2.6: Size distribution of (blue diamonds) Blank NPs separated on affinity column at 4-6 minutes with mean hydrodynamic diameter of 220 nm and (pink squares) MIP NPs, affinity separated with mean hydrodynamic diameter of 246 nm.

The zeta potential of MIP and Blank NPs, dispersed in three different solvents, was determined using a Zetasizer Nano ZS. A summary of the results shows significant variation in the zeta potentials, depending upon the solvent used (Table 2.1). These results correlate with and help to explain the changes in observed particle size of the samples. It was shown that both sample types (MIP and Blank) exhibit particle sizes of around 250-350 nm when dispersed in acetonitrile, however apparent particles size increased after replacing the solvent with water or phosphate buffered saline (PBS). The size of the MIP NPs in acetonitrile was measured as 341.9 nm, however sizes of 662.7 or 827.8 nm were measured in PBS or water respectively. Similarly the diameter

of Blank NPs in acetonitrile was 253.7 nm, increasing to 905.8 nm in PBS and 765.4 nm in water. This observation correlates well with the zeta potential measured for both samples. Zeta potential gives an indication of a material's stability in suspension and liability to agglomeration. A large zeta potential indicates a high degree of repulsion between adjacent particles and assures that the dispersion will be stable. A small zeta potential means the attraction between particles will exceed repulsion and the dispersion will tend to flocculate or aggregate. Zeta potential values between ±10 and ±30 are characteristic for dispersions which are considered as incipiently unstable (Callejas-Fernández *et al.* **1993**). Blank NPs shows a high zeta potential in acetonitrile, indicating a well dispersed and stable suspension, but in water/PBS the zeta potential is fairly low, suggesting the sample may be aggregating which explains the increase in particle size. Although the magnitudes of zeta potential of MIP NPs are similar in both aqueous and organic media, the sample exhibits a positive zeta potential when dispersed in acetonitrile and negative zeta potentials in water/PBS. This means that, upon displacement of the acetonitrile, the sample must pass through 0 mV, allowing aggregation of the particles to occur and hence resulting in an increase in the observed particle size. This inversion of charge was not observed with Blank NPs. The explanation of this could be due to the fact that these are two different polymers although synthesized in a similar but not exact manner. The recorded low values are still near ±30, which means that the process of aggregation is not fast. Despite the observed change in diameter dependant on the solvent used, the synthesised NPs show narrow size distributions, comparable to that of the dendrimers. This is as a result of the controlled polymerisation.

Table 2.1: Measured size and zeta potential for MIP and Blank NPs in different solvents.

type NPs		**MIP**			**Blank**	
solvent	**PBS**	**water**	**acetonitrile**	**PBS**	**water**	**acetonitrile**
size[nm]	662.7	827.8	341.9	905.8	768.4	253.7
PDI*	0.408	0.251	0.457	0.243	0.216	0.725
zeta potential [mV]	-23.7	-16.5	17.5	-22.8	-20.5	-56.8

*Poly-dispersity index (PDI)

MIP and Blank NPs were analysed by SEM (Figure 2.7.A and Figure 2.7.B). Surprisingly, the analysed samples were found to contain particles approximately cubic in shape, with sizes between 200 and 300 nm. Reducing the irradiation time for formation of the imprinted shell to one minute resulted in the formation of 100 nm, and to thirty seconds of 60 nm, NPs. The shape however was consistent in all cases (Figure 2.7.D and Figure 2.7.E). Additional images and electron diffraction patterns of Blank NPs were recorded using transmission electron microscopy (TEM) (Figure 2.7.C). The cubic shape and size are consistent with the scanning electron microscopy (SEM) images. Electron diffraction of the particles suggested they are amorphous rather than crystalline in nature (Figure 2.7.F). Chemical analysis using energy-dispersive X-ray (EDX) showed major peaks for carbon and oxygen, with a weak peak due to silicon (Figure 2.7.G). Peaks assigned to copper came from the support grid. No other elements were observed to be present. The weak silicon peak may come from the detector (Smith, **1979**) or may be present in the sample. Glassy SiO_2 can show an amorphous structure, however, the peak due to silicon would be much larger in the case of a glassy SiO_2 particle. The possibility of glassy SiO_2 particle can be completely excluded on the basis of the sample preparation as well. Thus the organic nature of the cubic-shaped organic NPs could be unambiguously confirmed. A survey of the literature failed to show any similar morphology in organic polymer particles from homogenious solution, suggesting that the cube-like appears to be a novel

observation, the shape presumably arises as a result of polymerisation from a dendrimer core.

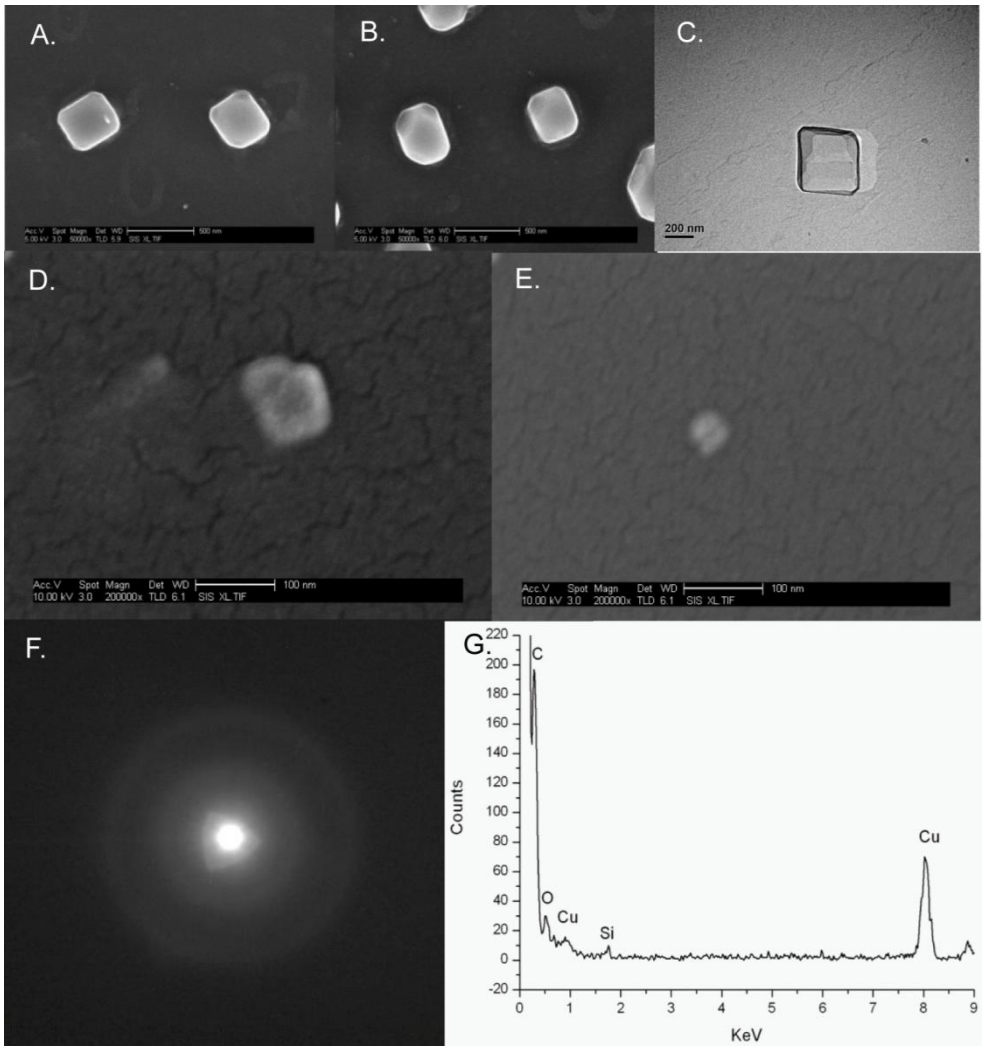

Figure 2.7: (A) SEM micrographs of MIP NPs (scale bar 200 nm); (B) SEM micrographs of Blank NPs (scale bar 200 nm); (C) TEM of Blank NPs (scale bar 200 nm); (D) SEM micrographs of MIP NPs prepared by one minute irradiation time (scale bar 100 nm); (E) SEM micrographs of MIP NPs prepared by thirty seconds irradiation time (scale bar 100 nm); (F) Electron diffraction pattern of a cube-like particle; (G) EDX spectrum of a cube-like particle suggested it is rich in both carbon and oxygen.

2.2.3 Polymer affinity testing

The ability of the synthesised NPs to bind to the target compound was demonstrated by surface plasmon resonance (SPR) using the Biacore 3000 instrument. The surface of the Biacore chip was modified with melamine, a structural analogue of the template compound. Melamine (1,3,5-triazine-2,4,6-triamine) is similar to acetoguanamine (6-methyl-1,3,5-triazine-2,4-diamine) in that both possess the diamino-triazine motif imprinted into the polymer, but the former has an additional amino group (useful for attachment to the sensor chip) whereas the latter has a methyl group. Attachment of melamine via one of its amino groups to an aldehyde-functionalised SPR chip exposed the common recognition motif at the sensor surface. The aldehyde-modified surface was prepared by reaction of glutaraldehyde with a self-assembled monolayer (SAM) of 2-mercaptoethylamine on the gold surface (Jiang *et al.* **2003**). This modification procedure was followed by static contact angle measurements of the surface at each stage of modification (Table 2.2).

Table 2.2: Static water contact angle in air for surface-modified gold Biacore chips after each stage of modification.

nature of surfaces	**biacore gold chip**	**2-mercapto ethylamine**	**glutaraldehyde**	**melamine**	**atrazine deisopropyl**
	13.4	57.7	49.9	57.2	45.7
Water contact angle [deg]	13.1	57.3	49.0	57.2	46.0
	12.1	57.3	48.6	57.0	45.1
Average [deg]	12.9	57.4	49.2	57.1	45.6
Standard deviation	0.71	0.26	0.65	0.13	0.48

Representative SPR sensorgrams, obtained during a series of MIP sample injections of increasing concentration, is shown in Figure 2.8. The concentration of the NPs in PBS was determined by UV/Vis spectrometry (λmax = 277.5 nm) using a calibration curve, obtained from gravimetric analysis of dried samples. The concentration of accessible

binding sites was estimated using the method described in 5A.2 (page 217, Figure Apx A.1 and Figure Apx A.2)**.** The estimates of binding site concentration were based on a number of assumptions; hence the calculated dissociation constants should not be regarded as absolute values, rather they provide a valid basis for comparison of materials. On the basis of these estimates, the apparent dissociation constant, K_d, was determined using the Biaevaluation software, provided by Biacore, to be 1.76×10^{-10} M for MIP, and 1.11×10^{-8} M for Blank NPs. Since Blank particles were also subjected to affinity separation some binding to the melamine chip would be expected. Indeed Shea and co-workers (Hoshino and Haberaecker *et al.* **2010**) recently showed that the high affinity NPs for a complex biological target could be selected from a population of non-imprinted NPs by affinity separation alone. However, as it is proven in the present case, the affinity of Blank NPs is clearly not as high as the affinity of MIP NPs which originates from the imprinting process itself.

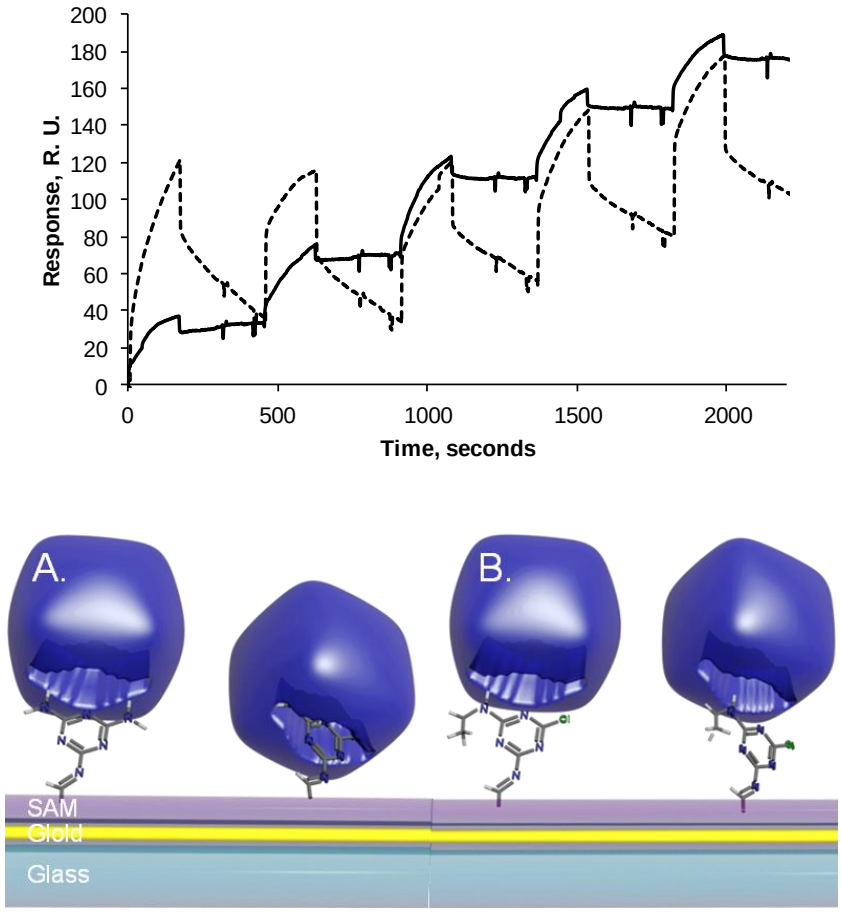

Figure 2.8: Above: Sensogram showing binding of MIP NPs to the specific ligand (melamine, solid line) and to a non-specific analogue (atrazine desisopropyl, dashed line) immobilised on Biacore sensor chips. Concentration of surface-accessible imprinted binding sites estimatedto be present in the undiluted dispersion of MIP NPs in PBS was 2.19 mM (**Figure_Apx A.1**, 5A.2, page 217). Injections were made in order of increasing concentration using dilutions of: 1/10000; 1/1000; 1/100; 1/10; 1 with respect to the stock NPs dispersion. Below: schematic representation of the binding between the immobilised ligand (A. melamine and B. atrazine desisopropyl) and MIP NPs.

To assess the selectivity of the MIP NPs, an analogue of the template, 2-amino-4-chloro-6-ethylamino-1,3,5-triazine (also known as atrazine desisopropyl) was used to modify the surface of the Biacore chip, in place of melamine, following the fictionalisation procedure described above. Both compounds possess a triazine core but have different substituents. Analogously to the above experiment, SPR sensorgram, obtained during a series of MIP NPs sample injections of increasing

concentrations, is shown in Figure 2.8. The apparent K_d calculated for MIP NPs was 3×10^{-8} M and 3.2×10^{-5} M for Blank on the non specific surface. The MIP NPs showed higher affinity (lower K_d) for both surfaces compared with Blank, however the affinity of MIP NPs for the non-specific surface was lower than that of the Blank NPs to the specific surface. The K_d for MIP binding to the specific surface is 2 orders of magnitude lower than that of the Blank binding to the same, while the K_d for MIP binding to the non-specific surface is 2 orders of magnitude higher than that for MIP binding to the specific surface. Therefore the MIPs show 100-fold higher selectivity for the template with respect to an analogue and with respect to the Blank binding to the template.

2.2.4 Fluorescent sensing

In order to investigate how NPs made by this approach would perform as a fluorescent sensor, a fluorescent label (dansyl, Scheme 2.4, **14**) was covalently attached to 50 % of the core dendrimer peripheral amine groups (**13**) by coupling with dansyl chloride before polymerisation of the shell to form the fluorescent *macroiniferter* (**15**). Prior to this modification 50% of the amino groups of the PAMAM dendrimer (**12**) were modified with *iniferter* group (**1**) to form the graftable core (**13**). MIP shell was created over the dendrimer core by irradiation for one minute using a polymerisation mixture four times more diluted than previously used in order to create a thinner polymer shell. A better sensitivity of the core would be achieved in this way. Cubic NPs with the dimensions of 50 nm were created in this way (Figure 2.9).

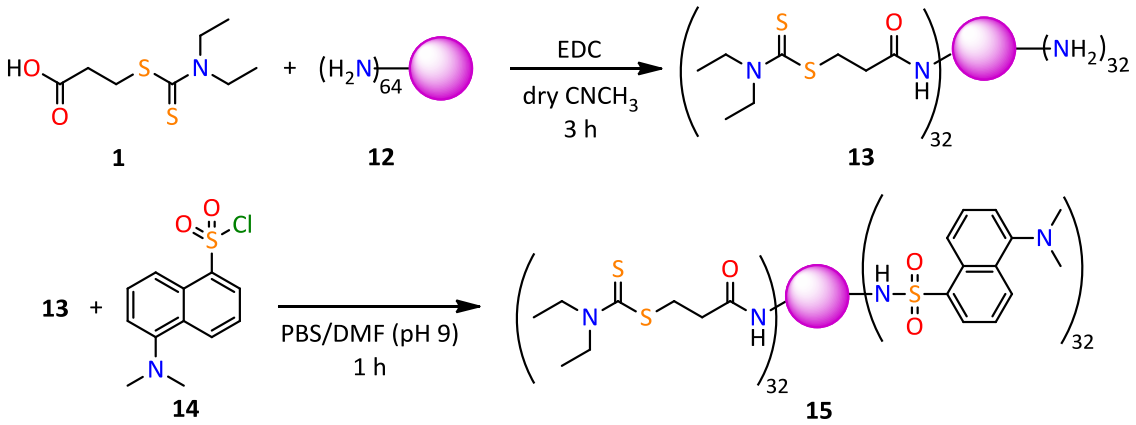

Scheme 2.4: Schematic representation of the synthesis of fluorescent *macroiniferter* (**15**). PAMAM dendrimer, generation 4 (**12**) was 50% surface modified with CNDDA (**1**) to form the product (**13**). The rest of the free amino groups from the periphery of (**13**) were modified with the fluorescent dye dansyl chloride (**14**).

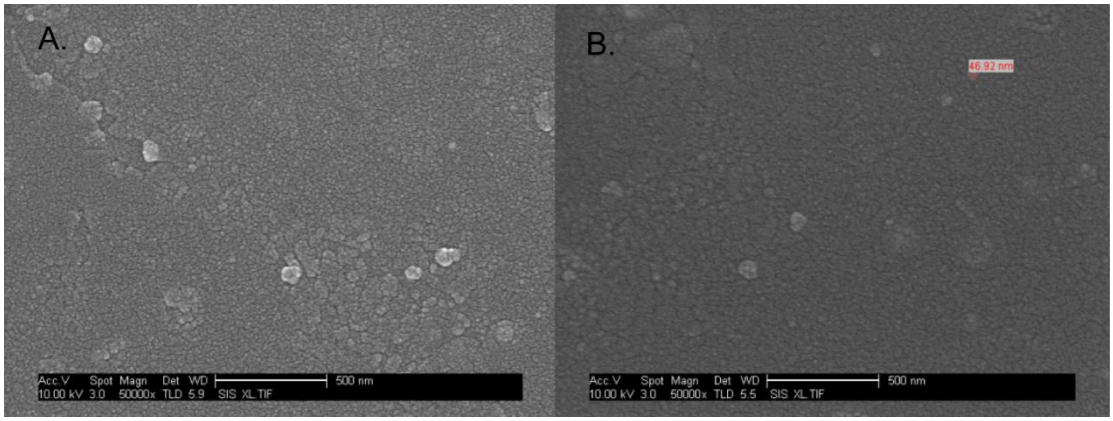

Figure 2.9: Scanning electron micrographs of fluorescent core NPs prepared by one minute irradiation time of: A. MIP and B. Blank (scale bar 500 nm).

The method allows the formation of NPs with a precisely controlled quantity of fluorescent label per each particle. Covalent attachment of the flourophore to the core prevents their migration within the polymer shell and shields them from the environment. The template was removed with series of washes (acidic and basic) using centrifuge filtration tubes.

Exposing the fluorescent-core NPs to solutions containing different concentrations of the template (Scheme 2.5, (**16**)) for just ten minutes resulted in a concentration dependant increase in the NPs fluorescence (Figure 2.10). The local environment of the

dansyl group, including the hydrophilic/hydrophobic nature of the solvent, determines its fluorescent properties (Srivastava *et al.* **2011**). Binding of template to the imprinted polymer shell will lead to expulsion of solvent molecules and changes in conformation of the polymer shell which have an indirect effect on the fluorophores located at the core-shell boundary. In this particular case this led to an observed increase in fluorescence of dansyl-labeled NPs on interaction with *e.g.* haemoglobin have been reported (Liu *et al.* **2011**). Almost no response was detected under the same conditions with the Blank NPs. Almost no change in the level of fluorescence was seen under the same conditions with Blank NPs, or with MIP or Blank NPs in the presence of analogues of the template (Scheme 2.5, Atrazine desisopropyl (**18**) or Simazine (**19**)). Both of the polymers were used without affinity separation. The limit of detection was calculated to be 3×10^{-8} M.

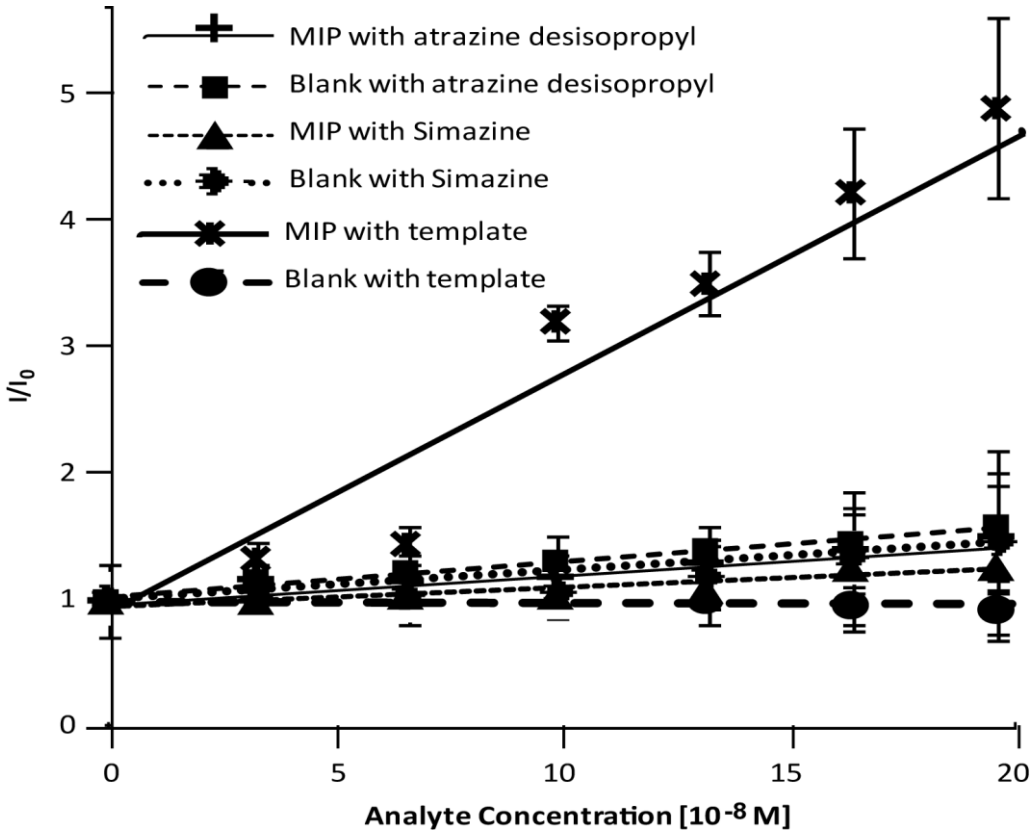

Figure 2.10: Intensity of the fluorescent response of MIP and Blank NPs to different concentrations of the template and close analogues (Atrazine Desisopropyl or Simazine) in acetonitrile after ten minutes incubation time. I_0 is the intensity of the emission maximum of the NPs without the template and **I** is the intensity of the emission maximum of the NPs with different concentrations of the template. Error bars represent ±1 standard deviation (n=3).

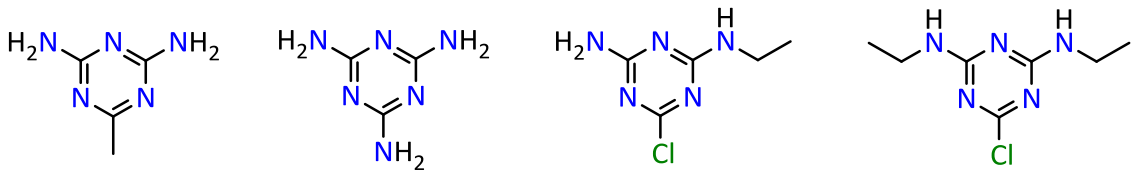

Scheme 2.5: Schematic representation of the chemical structures of: Acetoguanamine (**16**); Melamine (**17**); Atrazine desisopropyl (**18**) and Simazine (**19**).

2.3 Experimental Details

2.3.1 Materials

PAMAM – 25% C_{12} dendrimer, generation 4 (10 wt. % in methanol), 1,1'-azobis-(cyclohexenanecarbonitrile), 1-(3-dimethylaminopropyl)-3-ethyl-carbodiimide hydrochloride, acetic acid, acrylic acid, ethyleneglycol dimethacrylate, methacrylic acid, trimethylolpropane trimethacrylate, 2-mercaptoethanol, o-phthaldialdehyde, sodium diethyldithiocarbamate trihydrate, 3-aminopropyl trimethyloxysilane, extra dry dimethylformamide (DMF), and extra dry acetonitrile were purchased from Sigma Aldrich (UK). Sodium hydroxide and hydrochloric acid were purchased from Fisher Scientific (UK). Atrazine desisopropyl was purchased from Riedel-de-Haen (Germany). Glass beads (75 μm) were purchased from Supelco Analytical (Bellefonte PA, USA). NMR solvents were obtained from Goss Scientific (UK). Ultrapure water (Millipore) was used for analysis. All chemicals and solvents were analytical or HPLC grade and used without further purification unless stated otherwise.

2.3.2 Apparatus

NMR measurements were made using a JEOL ECX 400 MHz NMR and FT-IR spectra were recorded using KBr disks on a ThermoNicolet Avatar-370 spectrometer (Nicolet, US). For UV irradiation, a Philips type HB 171/A self-tanning UV lamp, fitted with 4 CLEO 15W UVA fluorescent tubes (Philips) with continuous output in the region 300-400 nm, delivering 0.09 W cm^{-2} at a distance of 8 cm, was used. Sessile water contact angle (CA) measurements were made using a Cam 100 optical Angle Meter (KSV Instruments Ltd., Finland) along with the software provided. Elemental analyses were provided by Medac Ltd, Egham, UK. Mass spectra were obtained using a Waters LCT Premier XE mass spectrometer. Optical densities were recorded using a UV/VIS spectrophotometer (UV-1800 Schimadzu, Japan).

Dynamic light scattering (DLS) was used to characterize variation of the size of the species using a Nano-S (Malvern Instruments, Malvern, UK) at 25 °C in a 10 mm path

length glass cuvette. The data were analysed using the solvent parameters for acetonitrile (dielectric constant 37.5, viscosity 0.343 mPa s, refractive index 1.34). The parameters for the measured material, polystyrene latex was chosen (refractive index 1.59; absorption 0.01), as being the closest approximation to the present system. The instrument was allowed to automatically select the attenuator position based upon the observed scattering. The measurement duration and the number of runs were also set to automatic. Three measurements were made per sample.

The analysis of zeta potentials for Blank and MIP NPs in acetonitrile was performed using the technique of photon correlation spectroscopy using a Zetasizer Nano ZS in conjunction with a zeta dip cell and 10 nm glass cuvettes at 25 °C. Five measurements were done per sample. For the calculation of zeta potential, Henry's function F (ka) (the function of the dimensionless parameter) (Zaucha *et al.* **2011**) was set to 1.0 (Hückel approximation). The data were analyzed using the same solvent parameters as for DLS analysis. The instrument was allowed to automatically select the attenuator position based upon the observed scattering. The voltage was fixed to 5 V.

Detailed examination of surface nanostructures (1.5 nm resolution) has been achieved with a high resolution FEI XL30 SFEG analytical SEM. A JEOL 2000FX TEM equipped with an Oxford Inca energy dispersive X-ray (EDX) was used to analyze the sample microstructure and chemical composition.

Excitation and emission of solutions were measured in a 3 cm^3 quartz cuvette using a FluoroMax-2 fluorimeter (ISA Instruments S.A (UK) Ltd., Jobin Yvon-Spex, Middlesex, England) with Datamax software (v2.20; GRAMS/32 v4.11 level II) by Jobin Yvon-Spex.

A Biacore 3000 (G.E. Healthcare, UK), which is a surface plasmon resonance (SPR) instrument with a continuous flow system and four flow channels, and Au-coated chips (SIA Kit Au) purchased from Biacore (Sweden) were used in this work. All the experiments were performed at 25 °C. The change in Biacore response units (RU) is directly proportional to the change of surface mass (1 RU is approximately equivalent to 1 pg mm^{-2}). Typically each experiment was held at a flow rate of 15 μL min^{-1} and 75 μL injection volume (MIP and Blank NPs suspensions in PBS, pH 7.4). Prior to use the

gold chips were cleaned for three minutes using oxygen plasma at 40 W in a plasma chamber (Emitech, UK).

2.3.3 Synthesis of *S*-(carboxypropyl)-*N,N*-diethyl-dithiocarbamic acid (CNDDA)

S-(carboxypropyl)-*N,N*-diethyl-dithiocarbamic acid (CNDDA) (Scheme 2.2, **1**) was synthesised using a method adapted from the patent disclosed by Hook *et al*. (**1957**) Acrylic acid (0.5 mol, 36.0 g, 1 equiv), diethylamine (0.5 mol, 36.5 g, 1 equiv) and carbon disulfide (0.6 mol, 41.5 g, 1.1 equiv) were added dropwise in that order to a cooled (0 °C) solution of sodium hydroxide (0.5 mol, 20.0 g, 1 equiv) in 200 mL water. The mixture was stirred for thirty minutes at ambient temperature and then for thirty minutes at 60 °C (bath temperature). After cooling in ice, the solution was acidified with hydrochloric acid to pH 5.5. The oil formed in the reaction solidified on vigorous stirring. This solid was filtered off and washed well with distilled water. The pale yellow crystals (30% yield) were dried. UV (acetonitrile): λ_{max} = 275 nm, (ε = 4280 M^{-1} λ^{-1}); 334 nm, (ε = 73 M^{-1} λ^{-1}).

Spectroscopic data (CNDDA) (Scheme 2.2, **1**)*:*

IR (KBr) cm^{-1} 700-600 (C-S), 1500-1470 (N-C=S), 1420-1210 (COOH), 1700 (C=O);.

^{1}H NMR (400 MHz, DMSO-D_6, 25 °C) δ 4.23-4.18 (2H, m, **CH_2**CH_3), 3.99-3.94 (2H, m, **CH_2**CH_3), 3.63 (2H, t, J = 6.88, CH_2**CH_2**COOH), 2.89 (2H, t, J = 5.96, **CH_2**CH_2COOH), 1.45-1.4 (6H, m, N(CH_2**CH_3**)$_2$) ppm.

^{1}H NMR (400 MHz, DMSO-D_6, 130 °C) δ 3.88 (4H, t, N(**CH_2**CH_3)$_2$), 3.45 (2H, t, **CH_2**S), 2.64 (2H, t, HOOC**CH_2**), 1.23 (6H, t, N(CH_2**CH_3**)$_2$ ppm.

^{13}C NMR (400 MHz, DMSO-D_6, 25°C) δ 193.56 (C(S)S), 172.77 (C(O)OH), 50.00 N(**CH_2**CH_3)$_2$, 48.00 N(**CH_2**CH_3)$_2$, 33.38 (HO(O)C**CH_2**), 31.38 (CH_2S), 12.29 (N(CH_2**CH_3**)$_2$), 12.33 (N(CH_2**CH_3**)$_2$) ppm.

^{13}C NMR (400 MHz, DMSO-D_6, 130 °C) δ 193.88 (C(S)S), 171.52 (C(O)OH), 47.80 N(**CH_2**CH_3)$_2$, 31.50 (HOOC**CH_2**), 30.50 (CH_2S), 11.20 (N(CH_2**CH_3**)$_2$) ppm (The assignments were based on COSY, DEPT and HMQC experiments made in DMSO-D_6).

HRMS (ES) Exact mass calculated $C_{15}H_{22}N_2O_3S_2$ [M+H]+: m/z: 221.05 (100.0%), 223.05 (9.1%), 222.06 (8.9%), 222.05 (2.0%), found: 221.05.

2.3.4 Surface modification and characterisation of PAMAM dendrimers

S-(carboxypropyl)-*N*-diethyl-dithiocarbamic acid, (CNDDA, prepared as described (Ivanova-Mitseva *et al.* **2010**) (20.77 × 10^{-3} mol, 4.57 g, 1.2 equiv) and 1-(3-dimethylaminopropyl)-3-ethyl-carbodimide hydrochloride (EDC, 31.16 × 10^{-3} mol, 5.97 g, 1.5 equiv) were added in that order to 60 mL extra dry acetonitrile, in a round-bottomed flask, equipped with magnetic stirring bar and septa under an argon atmosphere (Scheme 2.2). The mixture was left to stir at ambient temperature for one hour in the dark. Polyamidoamine (PAMAM) dendrimer, 75% amino and 25% *N*-(2-hydroxydodecyl) surface groups (25% C_{12}), generation 4 (9.94 × 10^{-6} mol dendrimer, representing 0.017 mol free surface primary amino groups, 2 mL, 10 wt. % in methanol, 1 equiv) was added to the mixture. The mixture was left to stir for three hours. The solvent was evaporated *in vacuo*. The residue was dissolved in 200 mL ethyl acetate and twice extracted with 200 mL water. The organic layer was collected and this solution was evaporated to remove ethyl acetate and the product dissolved in absolute ethanol (50 mL) and evaporated again to remove the ethanol. This dissolution/evaporation procedure was repeated five times to remove water as an azeotrope. The product was characterized using ^{1}H and ^{13}C NMR (Figure 2.3 and Figure 2.4). Measurements of particles size via dynamic light scattering (DLS) were performed using a Nano-S (Figure 2.2).

The covalent reaction between a dialdehyde, a mercaptan and free amino groups of the dendrimers was used to evaluate the degree of the modification by measuring the fluorescence of the isoindole product. Solutions of 2-mercaptoethanol (0.3 mL of a

0.35 mg ml^{-1} solution in methanol) and *o*-phthaldialdehide (0.3 mL of a 0.7 mg mL^{-1} solution in methanol), methanol (2.4 mL) and triethylamine (3 μL) were prepared and combined. This solution (3 mL) and PAMAM 25% C_{12}, generation 4, dendrimer (5 μL, 10 wt. % in methanol) were mixed and the fluorescence spectrum was taken as a function of time (excitation wavelength, Eex = 250 nm, emission 300-700 nm) (Scheme 2.3 and Figure 2.5). All measurements were made in triplicate. Excitation and emission of solutions were measured in a 3 cm^3 quartz cuvette using a FluoroMax-2 fluorimeter. The procedure is adopted from (Piletska *et al.* **2000**).

2.3.5 Synthesis of MIP and Blank NPs

A mixture of freshly vacuum distilled methacrylic acid (monomer, 3.16 × 10^{-3} mol, 0.176 g), 2,4-diamino-6-methyl-1,3,5-triazine (template, 1.909 x 10-4 mol, 2.388 x 10-2 g), trimethylolpropane trimethacrylate (crosslinker, inhibitor removed by passing through an Al_2O_3 column, 5.263 x 10^{-4} mol, 0.178 g), ethylene dimethacrylate (crosslinker, inhibitor removed by passing through an Al_2O_3 column, 9.474 x 10^{-4} mol, 0.188 g) and the surface modified PAMAM dendrimer 25% C_{12}, generation 4 (1 mL 10 wt. % solution in DMF) were mixed in 0.24 mL DMF. The mixture was degassed under high vacuum with nitrogen via a triple freeze/pump/thaw method and polymerized under UV radiation, for two minutes in a closed 12 mL glass bottle whilst stirring. An identical procedure was used for the preparation of the Blank NPs but in the absence of the template. This method was adapted from (Guerreiro *et al.* **2009**). The NPs suspensions were then separated on an affinity column packed with glass beads surface-modified with melamine, a template analogue. The hydrodynamic size of the obtained fractions of MIP and Blank NPs were measured using DLS using the Nano-S instrument.

2.3.6 Preparation of affinity adsorbent

Glass beads (75 μm), were activated by boiling in 4 M sodium hydroxide for ten minutes, washed with deionized water and acetone and then dried at 80 °C for two hours. The beads were then incubated in toluene containing 2% (v/v) 3-aminopropyl trimethoxysilane for three hours, washed with acetone and dispersed in PBS buffer (pH 7.2) containing 7% (v/v) glutaraldehyde for thirty minutes followed by washing with water. The template (melamine) was then immobilised on the surface of the beads by incubation in a solution of melamine (0.1 mg mL^{-1}) in PBS (pH 7.2) containing *N*-methyl-2-pyrrolidone (10% v/v) for four hours. The resulting melamine coated particles were washed with water, dried and then used for affinity chromatography.

2.3.7 Affinity separation on a glass beads column

The beads surface-modified with melamine (see previous section, 1.2 g) were loaded into an empty SPE cartridge (polypropylene, 1 cm^3, Phenomenex) with frit for 1 cm^3 SPE tube (polyethylene, 20 μm porosity, Phenomenex). The end of the cartridge was supplied with a needle. The crude solution after polymerisation (0.5 mL) was sonicated twenty minutes prior to dilution with acetonitrile (50 %). Half of this mixture (0.5 mL) was loaded on the column and 0.5 mL of fresh acetonitrile was added. The column was closed by inserting the needle end into a rubber bung, and the cartridge was placed in an ice bath for five minutes. The column was then washed to remove the particles with no affinity to the template. The affinity fractions were collected by adding a fresh portion of acetonitrile (0.5 mL) to the column which was then closed and placed in a hot water bath (60 °C) for five minutes. The solvent was eluted and another portion of acetonitrile (0.5 mL) was added to the column for flushing. Five fractions were collected in the described manner one after another. The column was washed for the next loading from the same crude mixture. This was done by loading of fresh acetonitrile (5 mL) in the column and placing it in the hot water bath for five minutes, thereby washing away any residues. The same procedure was applied to both MIP and Blank NPs. Fresh columns were used for the two materials. After fractionating, the

solvent was exchanged following concentration in centrifuge filtration cartridges (molecular weight cut-off 50 000, Millipore, USA). Prior to loading in the filtration cartridges, the fractions were diluted with PBS. The resulting concentration of acetonitrile was 20 %.

2.3.8 Polymer affinity testing

A Biacore 3000, which is a surface plasmon resonance (SPR) instrument was used in this work. Prior to injection, each sample was sonicated for five minutes. Each injection was repeated three times per channel. Different concentrations of the NPs were injected one after another in order of increasing concentration. MIP and Blank NPs surface binding sites concentration was 2.19 mM and 3.34 mM respectively (5A.2, page 217, Figure Apx A.2). Dilutions in increasing order were: 1/10000; 1/1000; 1/100; 1/10; 1. The concentration of the NPs was determined by UV/Vis spectrometry using a calibration curve of the maximum absorbance at 277.50 nm of gravimetric samples. The concentration of binding sites was calculated as a function to the surface area of the particles (5A.2, page 217, Figure Apx A.1). MIP NPs used were from the fifth fraction eluted from the affinity column, Blank NPs were from the first fraction.

2.3.9 Treatment of gold chips

Biacore sensor chips were used in order to assess the ability of the synthesized organic NPs to bind to the analyte used. For that purpose the chips were surface modified with an analogue of the template. Prior to use the chips were cleaned for three minutes using oxygen plasma at 40 W in a plasma chamber. After this procedure was completed the chips were immersed in ethanol for ten minutes. The procedure for the chip modification was adopted from (Jiang *et al.* **2003**). The cleaned chip was immersed in a solution of 0.2 mg mL^{-1} 2-mercaptoethylamine in ethanol at 4 °C for 24 hours. After thorough rinsing with water, the modified electrode was treated with a 7% (v/v) aqueous solution of glutaraldehyde solution (10 mM in PBS, pH 7.0) at 25 °C

for twenty minutes and then rinsed with water and acetone and dried under a flow of nitrogen. The electrode was then immersed in 1/10 (v/v) melamine (for the affinity test) or Atrazine Desisopropyl (for the selectivity test) diluted in PBS (pH 7.0). The chips were thoroughly rinsed with water and dried with nitrogen gas. Each of the described modification steps was followed using static contact angle measurements (Table 2.2).

2.3.10 Scanning electron microscopy (SEM) and transmission electron spectroscopy (TEM)

Detailed examination of surface nanostructures (1.5 nm resolution) has been achieved with a high resolution FEI XL30 SFEG analytical SEM. Samples of MIP and Blank NPs suspended in water were prepared in the following way: (1) samples were ultrasonicated for five minutes, (2) using a Pasteur pipette, a drop of the solution was placed on a piece of microscope glass slide, (3) the sample was allowed to dry in air for 12 hours, (4) samples were sputter-coated with carbon prior to analysis. The TEM preparation procedures involved: (1) ultrasonication of the sample solution for five minutes, (2) application of a drop of the solution to a carbon-film coated copper mesh grid, (3) drying of the sample in air for thirty minutes, after which it was ready for TEM characterization. TEM equipped with an energy dispersive X-ray (EDX) was used to analyze the sample microstructure and chemical composition. Copper was always present in the EDX spectra because carbon film coated copper grids were used to support the samples.

2.3.11 Fluorescent labelling of PAMAM dendrimers

S-(carboxypropyl)-*N*-diethyl-dithiocarbamic acid (CNDDA, prepared as described (Ivanova-Mitseva *et al.* **2010**) (0.225×10^{-3} mol, 0.049 g, 0.5 equiv) and 1-(3-dimethylaminopropyl)-3-ethyl-carboimide hydrochloride (EDC, 0.338×10^{-3} mol, 0.065 g, 1 equiv) were added in that order to 2 mL extra dry acetonitrile, in a round-bottomed flask, equipped with magnetic stirring bar and septa under an argon

atmosphere (Scheme 2.4). The mixture was left to stir at ambient temperature for one hour in the dark. Polyamidoamine (PAMAM) dendrimer, generation 4 (0.45×10^{-3} mol free surface primary amino groups, 1 mL, 10 wt. % in methanol, 1 equiv) was added to the mixture. The mixture was left to stir for three hours. The solvent was evaporated *in vacuo*. The residue was dissolved in 200 mL ethyl acetate and twice extracted with 200 mL water. The organic layer was collected and this solution was evaporated to remove ethyl acetate and the product dissolved in absolute ethanol (50 mL) and evaporated again to remove the ethanol. This dissolution/evaporation procedure was repeated five times to remove water as an azeotrope. The remaining approximately 50 % of the surface free amino groups were used to attach the fluorescent label, using dansyl chloride as described from Tanaka *et al.* (**2007**).

2.3.12 Synthesis of fluorescent core MIP and Blank NPs

The so modified dendrimers (as described above) were used as a fluorescent *macroiniferter* for the synthesis of MIP and Blank NPs. The procedure was analogous to the one described previously. The only modifications done were that four times dilution of the polymerisation mixture was used and the irradiation time was decreased to one minute. Centrifuge filtration cartridges were used to separate the particles from any impurities (MW cut off 50 000). In order to remove the template from the MIP NPs and to process the Blank NPs in the same manner, both materials were washed with 1% acetic acid (three times), 1 M sodium hydroxide (three times), and water (three times). Both of the synthesised materials were concentrated to 2 mL volume. No further affinity separation was done. 10 µL out of these volumes were placed in 3 mL quartz cuvette for the fluorescent measurements.

2.4 Conclusions

In conclusion, the present work has demonstrated the synthesis of organic NPs with regular and reproducible shape and size for both MIP and Blank polymers. For the first time cube-like organic NPs are reported. Cubic NPs were an unexpected result and the origin of this morphology could be the subject of future study, however this shape may be an advantage where close-packing of NPs-based material is required, such as in dense coatings. This result was achieved by employing a unique combination of advances in the modern polymer chemistry. Dendrimer-based *macroiniferters* were used as the core in the synthesis of core-shell NPs, imprinted in the shell. Photochemical *living* radical polymerisation was used to imprint template compound (acetoguanamine) in the shell. The use of nano-sized dendrimer-based *macroiniferter* cores gave excellent control over the size and the shape of the final core-shell particles. It proved possible to process the NPs as if they were biological entities, including fractionation according to their affinity for the target compound and characterisation by surface plasmon resonance (SPR). We demonstrated very good specificity of the synthesised material to the specific template via SPR. High selectivity of the particles over close analogue to the template was also successfully demonstrated. Assumptions made in order to fit the Biacore data probably resulted in an underestimate of the affinity of the imprinted particles to the target. Fluorescent core cubic MIP NPs were prepared. They demonstrated excellent selectivity and affinity after just ten minutes incubation time with the template and with close analogues to the template. Advantageous such as precise control of the number of the covalently attached fluorescent label per particle and its polymer shielding are reported for first time as a new technique. Particles prepared in this way are promising materials to replace antibodies in sensors and immunoassays and in drug delivery and diagnostics.

3 Conjugated Polymers with Pendant *Iniferter* Units – Versatile Materials for Grafting

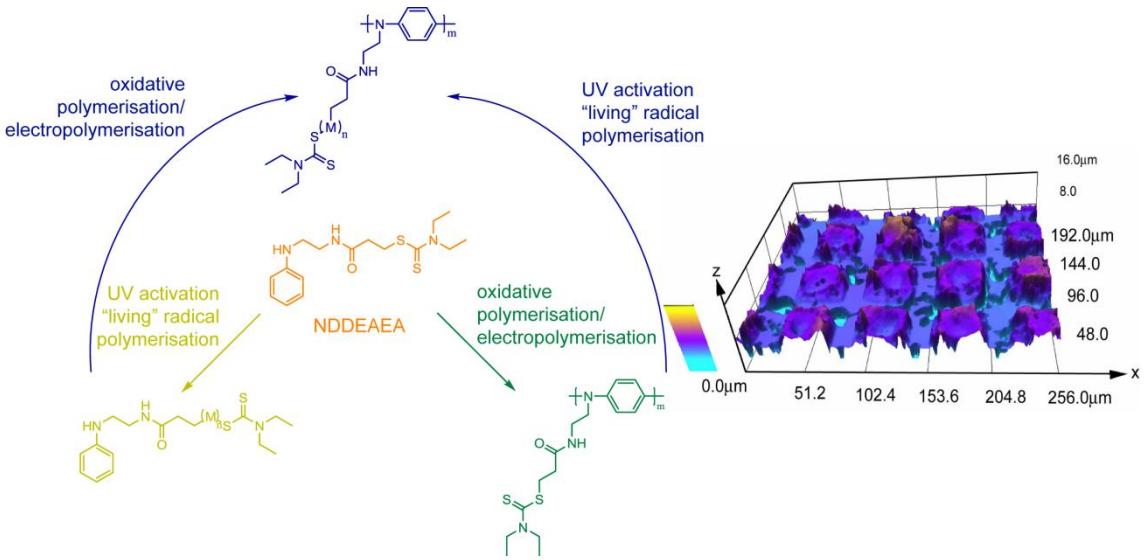

3.1 Introduction

Surface grafting of polymers is an important process for introducing interfacial and functional properties to both microscopic and macroscopic objects. Examples include modifying the hydrophilicity/hydrophobicity, adhesive, electronic or electrical properties of the surface and the introduction of features, such as molecular recognition or fluorescence. In this context, *"living"* polymerisation processes (Barbey *et al.* **2009**; Moad *et al.* **2008**; Braunecker and Matyjaszewski, **2007**) (atom-transfer radical polymerisation (ATRP) (Gam-Derouich *et al.* **2010**; Coessens *et al.* **2001**), reversible addition-fragmentation chain transfer (RAFT) (Smith *et al.* **2010**; Li *et al.* **2009**; Southard *et al.* **2007**; Chiefari *et al.* **1998**), nitroxide-mediated polymarisation (NMP) (Brinks and Studer **2009**; Boonpangrak *et al.* **2006**) and *photo-iniferter mediated* polymerisation (PIMP) (Barahona *et al.* **2010**; Bossi *et al.* **2010**; Perez-Moral *et al.* **2007**; Sellergren *et al.* **2002**; Otsu, **2000**) offer a number of advantages (see Chapter 1, Literature Review). These include: control of the grafting process due to the step-wise addition of monomers, resulting in a more homogeneous growth of polymer and the possibility to prepare block copolymer architectures by re-initiation in the presence of new monomers (Borner *et al.* **2001**). Of these, the use of *photo-iniferters*, based on dithiocarbamate esters (DTCE), is especially convenient for selective grafting to surfaces, since the process can readily be controlled and confined by the selective application of long wavelength UV light.

Grafting by any of these methods however requires the immobilisation of a suitable initiator species on the surface to be grafted. In the case of *iniferters*, this requires the *in situ* formation or attachment of a suitable DTCE. This has been achieved in the past by polymer analogous reaction of side chain residues, such as chloromethylstyrene groups, with a dithiocarbamate salt (Perez-Moral *et al.* **2007**; Sellergren *et al.* **2002**), by use of a polymer bearing DTCE groups (Garcia-Con *et al.* **2010**; Luo *et al.* **2002**; Qin and Qiu, **2001**; Otsu *et al.* **1986**), by attachment of a surface-reactive DTCE, such as a silane derivative (Bossi *et al.* **2010**; Kobayashi *et al.* **1992**) or by photochemical activation of surface-confined double bonds with a soluble DTCE (Mijangos *et al.* **2009**; Lakshmi *et al.* **2009**). In this chapter the application of a novel conjugated polymer with pendant

iniferter groups synthesised from a polyaniline precursor bearing a DTCE group is presented.

Conducting polymers (CPs), especially polyanilines (PANIs) have received much attention as a result of their promise in optical and electronic applications such as solar cells, sensors, and light-emitting diodes (Malkaj *et al.* **2006**; Mu *et al.* **1997**; Novak *et al.* **1997**). PANI was recognised as one of the most promising materials with its air and moisture stability in its doped, conducting form and in its de-doped, insulating form (MacDiarmid, **1997;** Salaneck *et al.* **1985**; MacDiarmid *et al.* **1985**). It is also unique in its easy doping/de-doping chemistry (Scheme 3.1). It shows sensitivity to the proton activity of its environment because of the nitrogen atom, which is part of the aromatic ring system. Upon oxidation and protonation of the polymer, positively charged macromolecules are formed. For compensation of the charge, anions from the supporting electrolyte, called dopant ions or counterions, are incorporated. The different oxidation states of the polymer chains also determine the properties of the material. Only the emeraldine base is a conductive material.

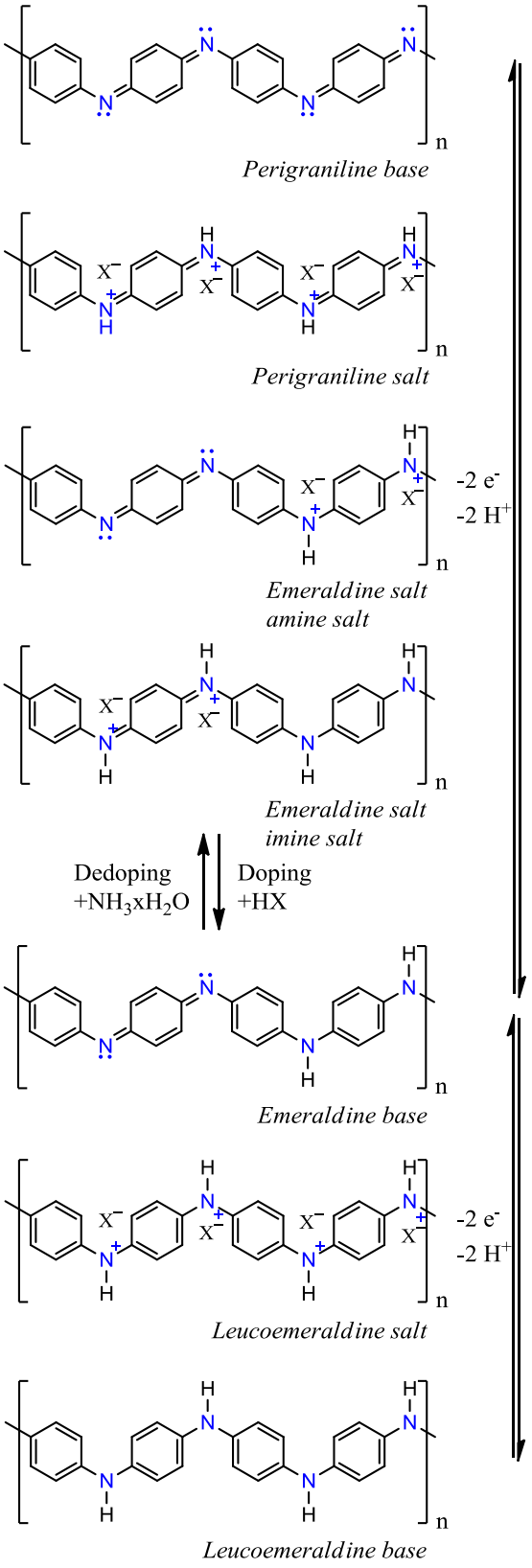

Scheme 3.1: Molecular structure formulas of PANI in its various states of oxidated or protonated forms. The scheme is adopted form MacDiarmid, **1997**.

PANI and the polymers of substituted anilines can be formed by chemical or electrochemical oxidation. The mechanism of polymerisation of PANI has been subject of many investigations, devoted to identify the steps of the process and the intermediates. Knowledge of the polymerisation mechanism could contribute to the better control over the properties of the polymer. Formation of a nitrenium cation is believed to be the first step of the process (Scheme 3.2) (Nalwa, **2001**). Once the nitrenium ion is formed, it leads to all the three possible dimers that is, head-to-tail, tail-to-tail, and head-to-head which are capable of growing into polyaniline in the presence of aniline.

In fact, the oxidation of the aniline to *N*-phenyl-1,4-benzequinonediimine can happen in acidic, neutral and alkaline media, when ammonium peroxidisulfate is used, as its oxidation potential does not depend on the pH of the medium. This is not the slowest step, but a step that requires the highest electrochemical potential (Gospodova *et al.* **1998**). The formation of N^1-phennylbenzene-1,4-diamine has lower potential and is considered as the initiation stage of the aniline polymerisation. The formation of new growing sites occurs probably at the initial stage of the polymerisation only.

The propagation of the polymer chains proceeds through a redox process between the growing chain, as an oxidant, and aniline, as a reductant, with addition of a monomer to the chain end. The polymerisation, as a whole, is an exothermic process. The termination is a result of the establishment of a thermodynamic equilibrium in the redox process, corresponding to chain propagation. Aniline polymerisation can be considered as a redox process, characterised by a sequence of defined oxidation potentials. Their value is determined by the degree of protonation of the chain. The value of the oxidation potential of PANI chains determines the direction of the redox process.

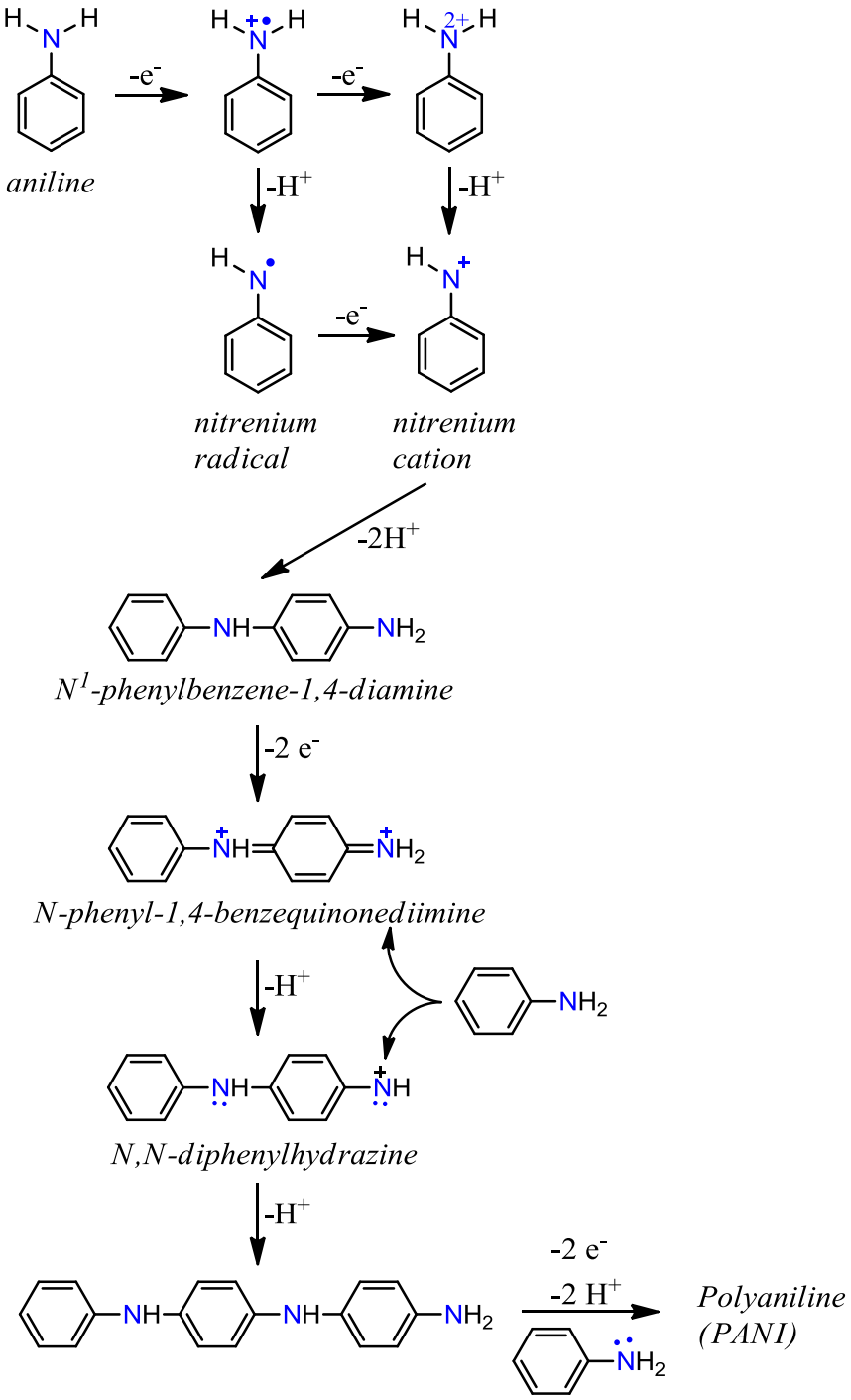

Scheme 3.2: Pathways for the initial steps of aniline oxidation and deprotonation and mechanism of aniline polymerisation, proposed by Wei *et al.* (**1990**).

The different ways of polymerisation give the opportunity for the deposition of PANI over plastic surfaces. Chemical polymerisation is an easy way of producing huge amounts of polymer which is in the form of a powder that is difficult to process. The

processability of PANI and its derivatives is still poorly developed. The design of new monomers as a means of introducing functional groups into conjugated polymers, has led to improvements in surface hydrophilicity, biocompatibility and adhesion properties. Improvements of this type allow the polymer films to be used in many potential applications such as transparent electrodes, chemical and biological sensors, organic electrical conductors, optically active materials and others by combining the appropriate functional groups with a conjugated polymer backbone.

Some reported attempts to improve the processability are based on alkyl-substituted polyanilines, the use of special counterions that are present in the conducting form of the polymer (Cao *et al.* **1992**), copolymerisation (Kim *et al.* **2002**). Approaches to soluble PANI also have been reported, using organic proton acids of a large molecular size as counterions (Lia *et al.* **1987**). Recently, one example was reported in which a conjugated polymer backbone was combined with the double bond functionality of a methacrylamide group in the form of the novel monomer *N*-phenylethylenediamine methacrylamide (NPEDMA) (Lakshmi *et al.* **2009**). NPEDMA undergoes chemical (oxidative) or electrochemical polymerisation to form PANI-based materials derivatised with double bonds. Furthermore the same material can be utilized as the basis for the construction of an electrochemical sensor (for catechol) by grafting a layer of a catalytically-active molecularly imprinted polymer (MIP) over an electropolymerised layer of poly (NPEDMA), deposited on a gold electrode (Lakshmi *et al.* **2009**) or prepared as nanotubes (Berti *et al.* **2010**). The sensors proved to be superior to electrodes prepared by immobilisation of MIP particles of essentially the same composition at the surface of a screen-printed electrode. This phenomenon was explained by the conjugated polymer acting as a "molecular wire" resulting in more intimate contact between the catalytically-active imprint sites and the conjugated polymer layer than was achievable by immobilisation of an electrically-insulating polymer onto an unmodified electrode. Grafting of the MIP layer was achieved by irradiating the double-bond bearing poly (NPEDMA) layer in the presence of *N,N*-diethyldithiocarbamic acid benzyl ester. This resulted in the partial conversion of the pendant double bonds into groups capable of initiating further polymerisation. It

would be desirable however to avoid the use of an additional activation step. This could be achieved if the conjugated polymer precursor was already derivatised with DTCE groups, rather than double bonds. Such a material would allow for the formation of conjugated PANIs, derivatised with DTCE groups and capable of direct UV-activated grafting of addition polymers.

In this work therefore the synthesis, characterisation and polymerisation behaviour of a new bifunctional monomer, *N*-(*N*΄,*N*΄-diethyldithiocarbamoyl ethyl amido ethyl) aniline (NDDEAEA) is described (Scheme 3.3). NDDEAEA can undergo electropolymerisation and chemical oxidative polymerisation in a similar manner to NPEDMA to give a conducting form of polyaniline, bearing a high density of DTCE pendant groups. Poly (NDDEAEA) can be formed as thick or thin films, powder, particles, microparticles or NPs, all of which can act as a *macroiniferter* in UV-activated graft polymerisation. In addition the use of polymers of NDDEAEA as a means of activating a range of surfaces towards grafting of polymer and block copolymers and their characterisation is reported as well.

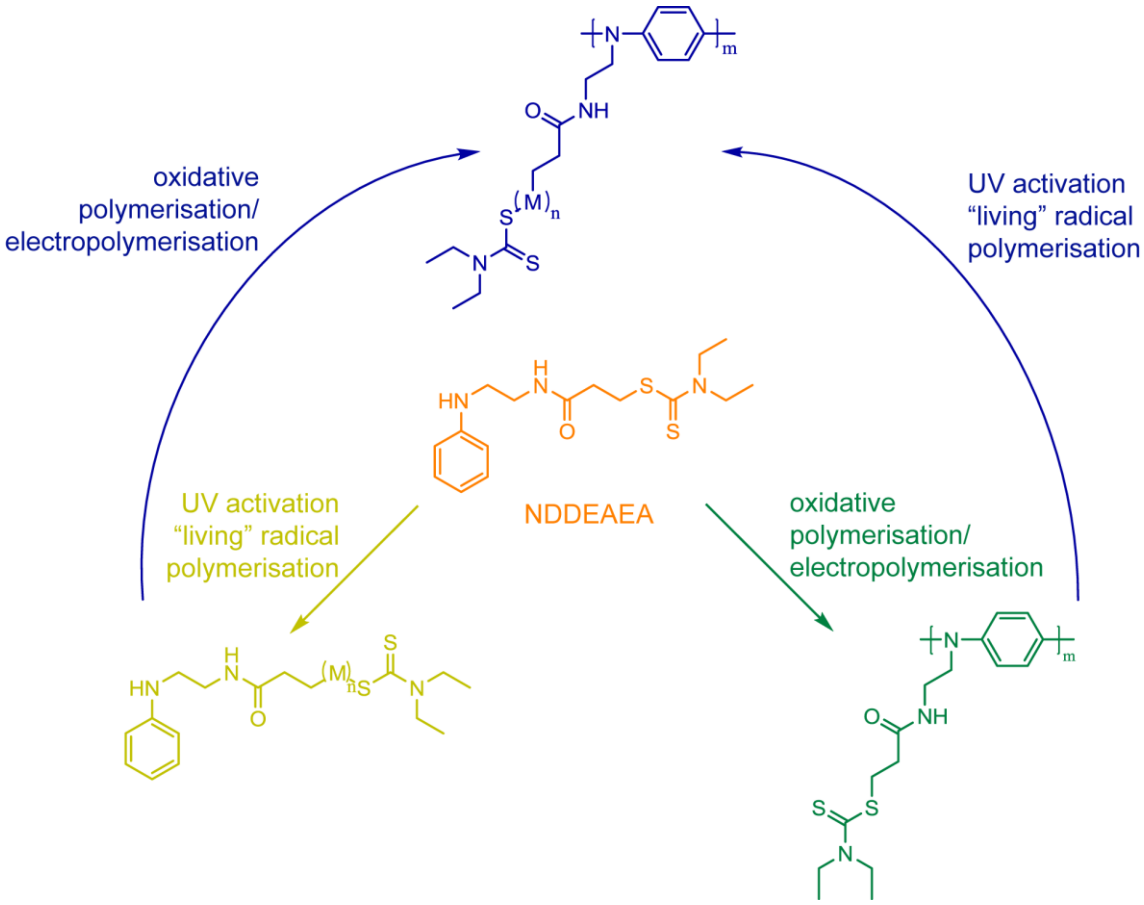

Scheme 3.3: Schematic representation of different polymerisation techniques and polymer structure of NDDEAEA monomer.

3.2 Results and Discussion

3.2.1 Synthesis of *N*-(*N´,N´*-diethyldithiocarbamoyl ethyl amido ethyl)-aniline (NDDEAEA)

A new monomer, *N*-(*N´,N´*-diethyldithiocarbamoyl ethyl amido ethyl)-aniline (NDDEAEA) (Scheme 3.4, **13**) was prepared by coupling *S*-(carboxypropyl)-*N,N*-diethyl-dithiocarbamic acid (CNDDA, **12**), prepared by reaction of acrylic acid, carbon disulfide and diethylamine in the presence of base (Hook *et al.* **1957**), with *N*-phenylethylene diamine.

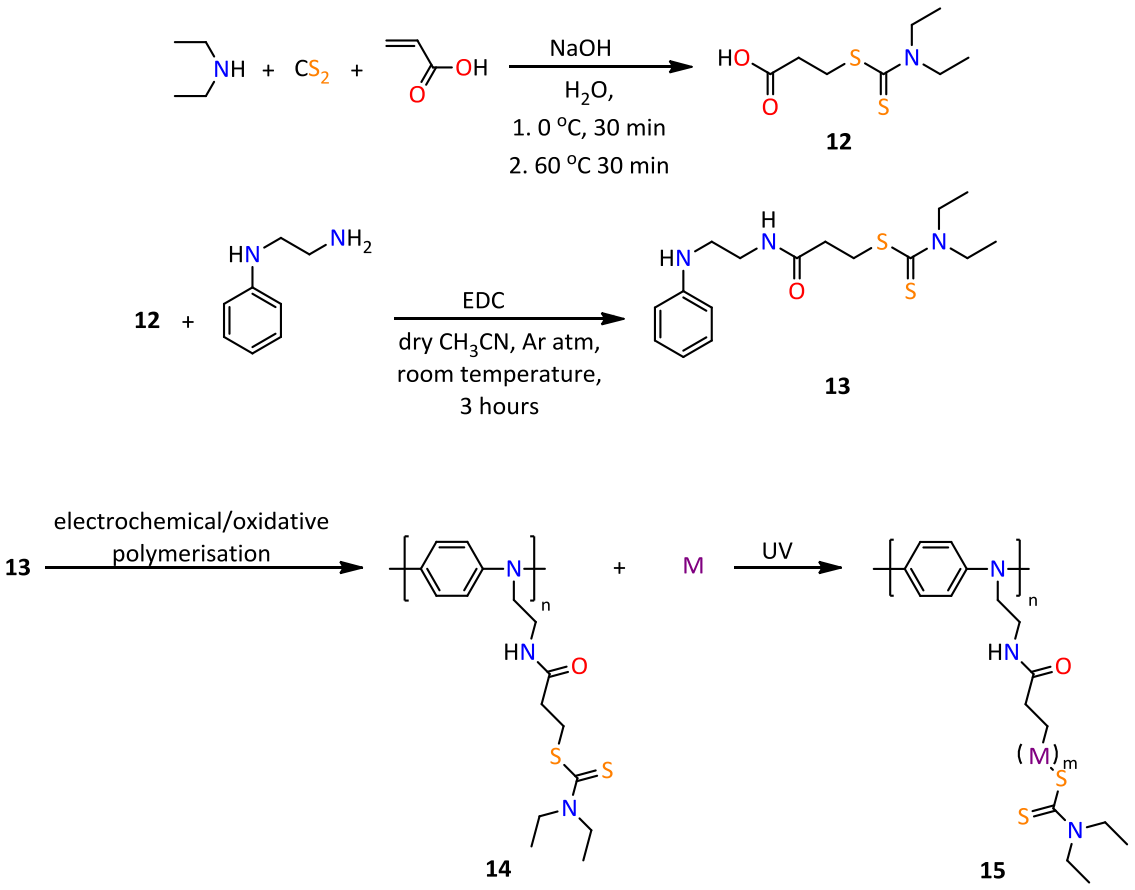

Scheme 3.4: Schematic representation of the synthesis of NDDEAEA (**13**) from CNDDA (**12**) and its polymers. Poly (NDDEAEA) (**14**) formed via electrochemical polymerisation or chemical oxidative polymerisation giving rise to polyaniline chains with pendant DTCE moieties. Addition of monomer (**M**), by UV grafting giving rise to poly (M)/poly (NDDEAEA) graft copolymers (**15**).

NDDEAEA was fully characterised via ^{1}H and ^{13}C NMR, IR spectrum (5B.1, page 219, Figure Apx B.1), mass spectroscopy (5B.1, page 219, Figure Apx B.2), and elemental

analysis (Experimental Details, 3.3.3). The ^{1}H NMR spectrum of NDDEAEA, recorded at room temperature (Figure 3.1) showed that some signals were split due to the existence of two conformers as a result of hindered rotation around the N-C(=S) single bond (Garcia-Con *et al.* **2010**). NMR spectra recorded at 100 °C and 130 °C (Figure 3.2 and Figure 3.3) showed coalescence of these signals to single peaks. This can be explained by overcoming the torsional barrier at higher thermal energy, resulting in rapid interconversion of the two forms on the NMR timescale (Garcia-Con *et al.* **2010**).

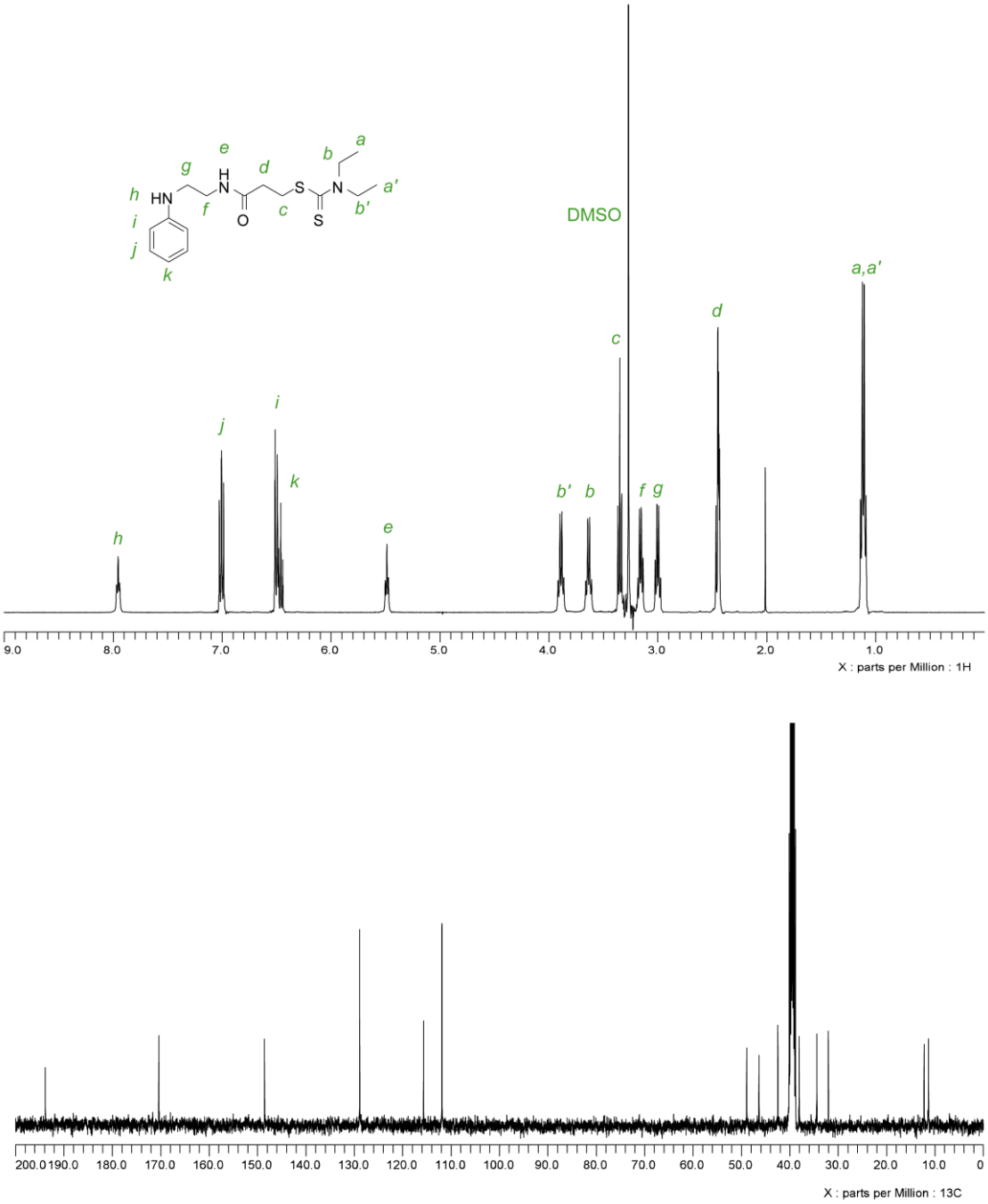

Figure 3.1: 400 MHz ^{1}H NMR spectrum of NDDEAEA **(2)** in DMSO-D_6 and 100 MHz ^{13}C NMR spectrum of NDDEAEA in DMSO-D_6 at 25 °C showing two peaks due to two conformations for the NDDEAEA around the N-C(=S) single bond.

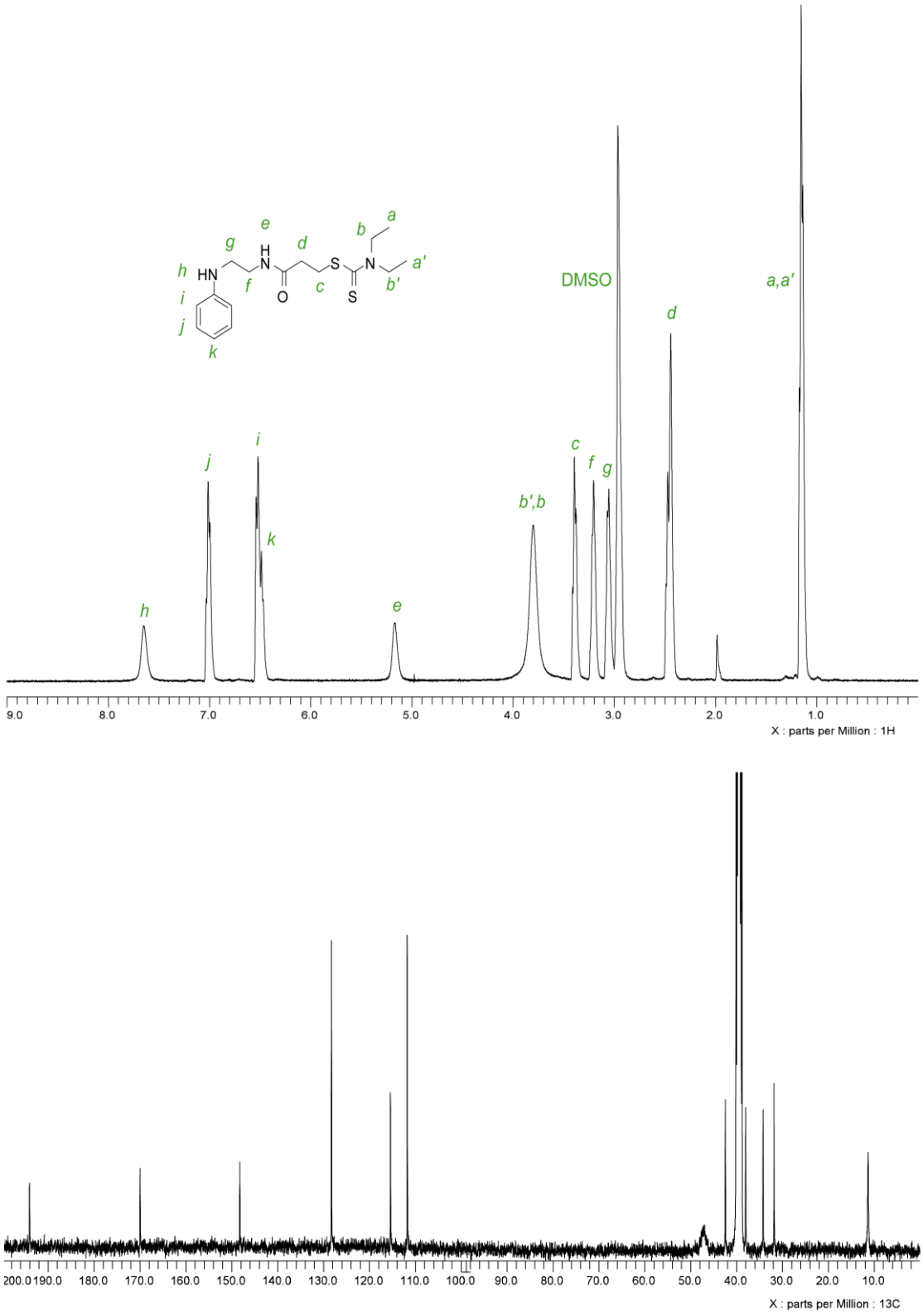

Figure 3.2: 400 MHz ^{1}H NMR spectrum of NDDEAEA **(2)** in DMSO-D6 and 100 MHz ^{13}C NMR spectrum of NDDEAEA in DMSO-D_6 at 100 °C showing single high resolution peaks.

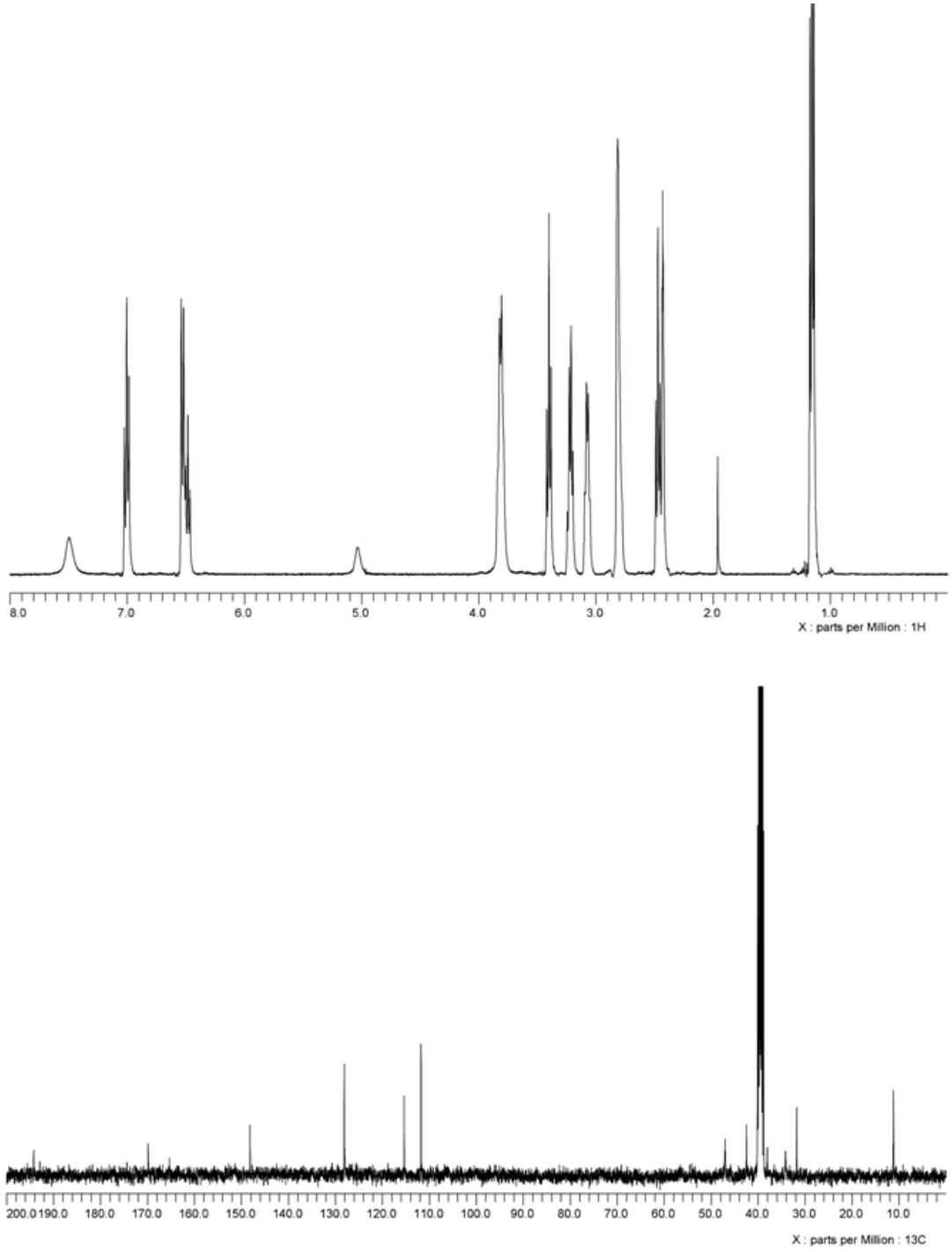

Figure 3.3: 400 MHz ^{1}H NMR spectrum of NDDEAEA (**2**) in DMSO-D_6 and 100 MHz ^{13}C NMR spectrum of NDDEAEA in DMSO-D_6 at 130 °C.

Polymerisation of the aniline functionality of NDDEAEA should result in the formation of a conjugated polymer bearing a high density of DTCE group (*iniferter*) as pendant side-chains. The ability of polyaniline to form stable coatings on both hydrophilic and

hydrophobic surfaces (Piletsky *et al.* **2003**; Bossi *et al.* **2000**; Piletsky *et al.* **2000**), suggests that this approach would allow a range of materials with different surface characteristics to be coated with *"living"* initiator species. The conjugated nature of the polymer may also have a number of advantages in the construction of electrochemical sensors (Lakshmi *et al.* **2009**) and other electronic devices. While there are examples of styrene- and methacrylate-based polymers bearing DTCE side chains, there are practically no examples of conjugated polymer backbones derivatized with *iniferter* groups. The polymeric macroinifeters of Lutsen *et al.* (**2006**), consisting of poly (vinylene phenylene) with pendant DTCE side groups, formed by the partial elimination of DTCE groups from a precursor polymer are a marked exception. However these polymers neither carry a high density of DTCE groups nor do they have a continuously conjugated structure since each remaining *iniferter* group is a result of incomplete elimination from the precursor.

The aniline functionality of NDDEAEA has the potential to be polymerised both electrochemically and using chemical oxidants such as ammonium persulfate. It was important to ascertain whether either route could be employed with this monomer and to show whether the integrity of the DTCE groups was compromised by either method of polymerisation.

3.2.2 Electropolymerisation of NDDEAEA

Electropolymerisation of NDDEAEA was carried out in cyclic voltammetry (CV) mode. Figure 3.4 shows the CV obtained during the electropolymerisation (twenty cycles) of a solution of NDDEAEA in a 3/1 v/v mixture of hydrochloric acid (0.75 M) and acetonitrile. The CV clearly shows oxidation and reduction peaks at +0.65 V and +0.52 V (vs. Ag/AgCl) respectively. The observed electrochemical behaviour is quite similar to that obtained during the polymerisation of aniline and ring-substituted anilines dissolved in acidic solutions (Lakshmi *et al.* **2009**; Bidan *et al.* **1989**; Diaz and Logan, **1980**; Schomburg and McCarley, **2001**; Hayes and Shannon, **1996**; Ulgut *et al.* **2006**). The large currents observed at the maximum positive potential are due to the

superposition of two distinct processes: one is electron transfer from poly (NDDEAEA), corresponding to the oxidation of the PANI film and the other is electron transfer from the monomer, NDDEAEA, to the electrode, corresponding to the oxidation of NDDEAEA to produce a precursor of polyaniline formation. In order to investigate the stability of poly (NDDEAEA) films, the electropolymerised electrodes were dipped into a solution of hydrochloric acid (0.75 M) and the CV measured. The CV showed quasi-reversible peaks: one at +0.12 V which corresponds to oxidation of the leucoemeraldine to protonated emeraldine form and also a peak at +0.65 V resulting from the oxidation of emeraldine and deprotonation of the polymer (Inzelt and Horanyi, **1990**). Both these peaks are quite stable. It has been reported that during the electropolymerisation of substituted anilines in acidic aqueous solutions an intermediate with high stability is formed (Malinauskas and Holze, **1997**; Malinauskas and Holze **1998**). It is therefore possible to perform both kinetic and mechanistic studies of the polymerisation reaction of poly (*N*-alkylaniline) derivatives.

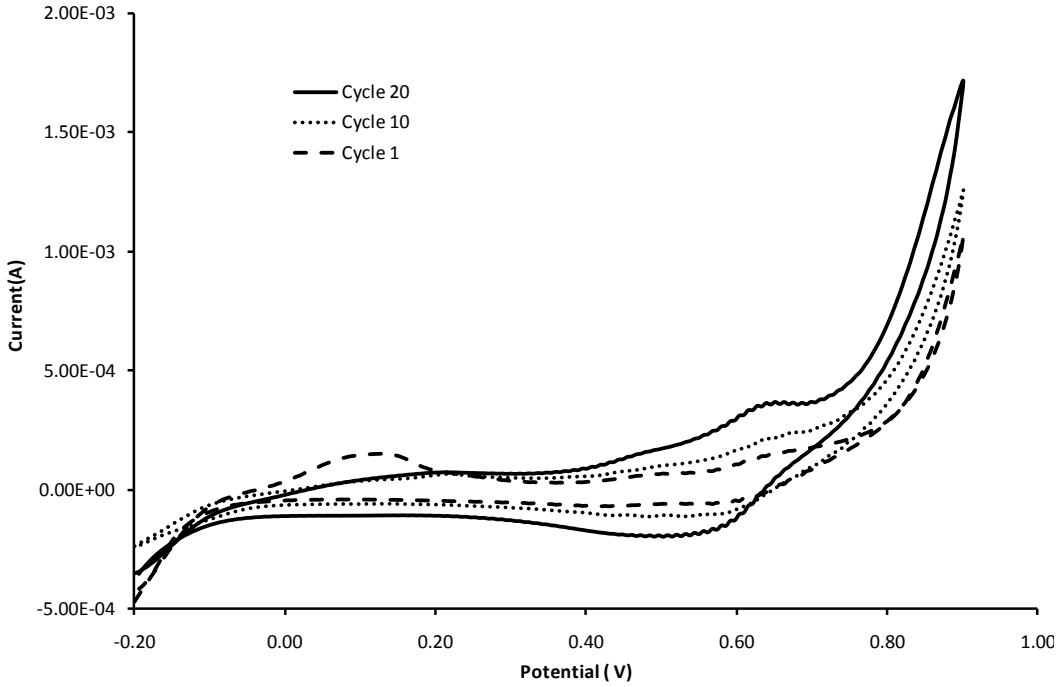

Figure 3.4: Cyclic voltammogram obtained during deposition of electropolymerised NDDEAEA films on gold screen-printed electrodes. Electropolymerisation of NDDEAEA (0.1 M in 0.75 M hydrochloric acid 25% acetonitrile in water) on a screen printed gold electrode by cyclic voltammetry (potential range: -0.2 V to 0.9 V versus Ag/AgCl, at 100 mV s^{-1} scan rate, 20 sweeps), under nitrogen atmosphere and in the dark, giving rise to poly (NDDEAEA).

The electrochemistry of poly (*N*-alkylanilines) is less complicated by comparison with PANI due to the absence of the pH-sensitive emeraldine base-emeraldine salt transition. Polymerisation of NDDEAEA, which contains both aniline and DTCE groups, may offer more advantages, provided the latter are stable under the conditions of polymerisation. Dithiocarbamate anions are unstable under aqueous acidic conditions (Ewing *et al.* **1980**), undergoing protonation and subsequent decomposition into carbon disulfide and amine, so there was some initial concern about the stability of the esters under the conditions necessary to polymerise NDDEAEA. It was also not clear whether the *iniferter* groups would be affected by the electrical potential needed for electropolymerisation of the monomer. It appears however that these fears were unfounded and suitable conditions were discovered for electropolymerisation of NDDEAEA, in which the integrity of the pendant groups were preserved (Figure 3.4). The existence of a high density of *iniferter* groups was confirmed by XPS analysis and

through grafting experiments. NMR measurements on NDDEAEA and its polymer also show no significant spectral changes with time under acidic conditions.

3.2.3 Molecular modeling of NDDEAEA and poly (NDDEAEA)

We utilised molecular modelling of NDDEAEA and poly (NDDEAEA) to investigate the structural changes before and after electropolymerisation in 0.75 M hydrochloric acid. The neutral and protonated forms of NDDEAEA monomer were modelled by calculating the charges for each atom on the template and the structures refined using molecular mechanical methods and Sybyl software. Figure 3.5 shows the energy minimized structure of neutral (left) and protonated (right) NDDEAEA. The oxygen atoms are shown in red and the nitrogen atoms are shown in dark blue. The white atoms are carbon and the light blue atoms are hydrogen. The energies of the neutral and protonated structures are -18.11 and -22.72 kcal/mol, respectively. The lower energy structure of the protonated NDDEAEA could be attributed to the additional intramolecular hydrogen bonding shown below (Figure 3.5) highlighted as a dotted blue line. When it is in its protonated form it was more stable and during electropolymerisation, the aniline group remains in protonated form.

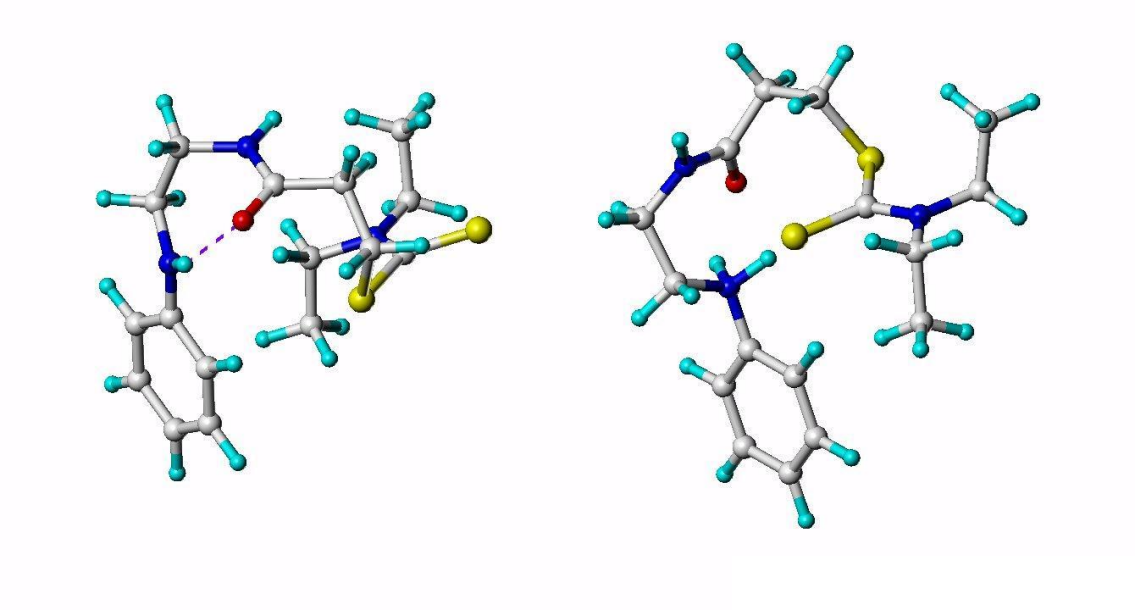

Figure 3.5: The energy minimized structure of neutral (left) and protonated (right) NDDEAEA showing intramolecular hydrogen bonding.

It was interesting to model the structure of the chain of poly (NDDEEA), doped with hydrochloric acid, therefore sixteen repeating units of aniline moieties of NDDEAEA in cationic form were modeled from quantum-mechanical point of view to determine their structure in the polymer matrix. For the purpose of predicting the possible configuration of poly (NDDEAEA), molecular modeling experiments were performed where the NDDEAEA monomer was used as an nitrogen substituted chain on aniline which was then used in the design of a conducting polyaniline structure of sixteen repeating aniline units with alternating positive charge (+1) on the nitrogen atoms of aniline (shown below in Figure 3.6 as blue balls). Molecular dynamics calculations were carried out on this structure (simulated annealing) at 300K and the resulting structure was then minimized to 0.05 kcal mol^{-1}. The molecular complex of poly (NDDEAEA) looked like a twisted stranded protein chain.

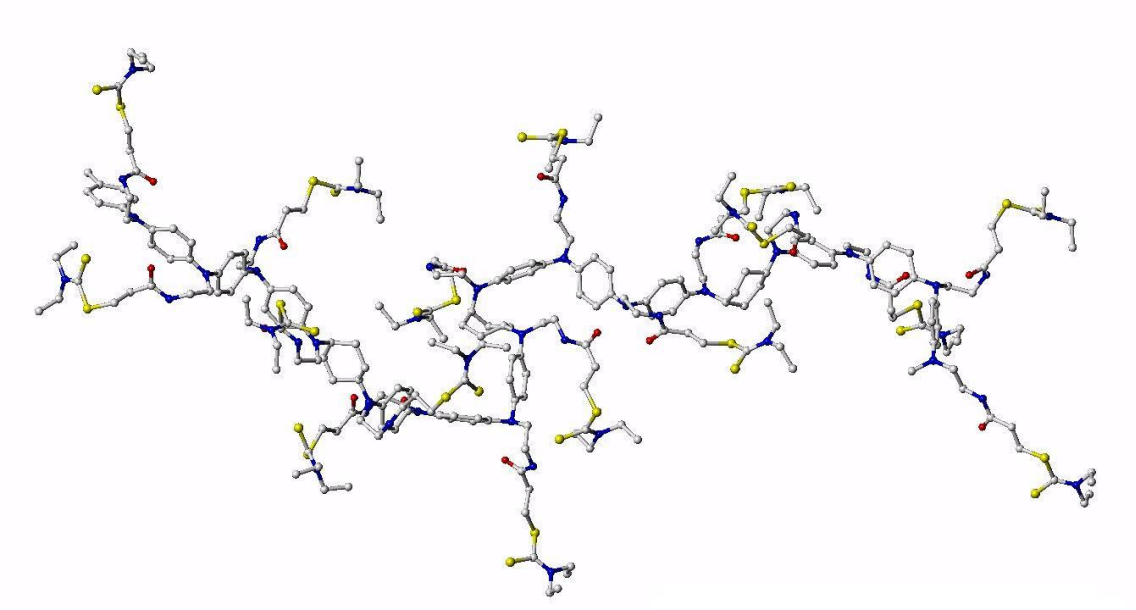

Figure 3.6: Postulated structure of poly (NDDEAEA) (n=16) which shows polyaniline chains with DTCE side groups.

Clearly, the chain structure of poly (NDDEAEA) is not linear but spiral and helical due to the presence of bulky DTCE side chains. The structure appears to form two strands which are likely to be in close contact in a side-by-side manner. There appears to be significant steric crowding especially around the central nitrogen atoms resulting in a *"ribbon like"* structure typically found in proteins.

3.2.4 Surface-confined photo grafting of various polymers

Surface-confined grafting of polymers was readily initiated upon UV irradiation of electropolymerised poly (NDDEAEA) layers in the presence of deoxygenated solutions of monomers such as acrylamido-2-methylpropane sulphonic acid (AMPSA), (Table 3.1) methacrylic acid (MAA) or styrene (Figure 3.7). This allowed precise control of the macromolecular architectures of the grafted surfaces (Figure 3.7). Grafting was readily achieved despite the highly-colored nature of the polyaniline backbone, presumably due to the high density of DTCE groups available at the surface. XPS analysis and water contact angle measurements (Table 3.1), performed before and after grafting provided evidence that polymerization proceeded at the surface only during photo-irradiation.

The results of XPS measurements (Figure 3.8 and Table 3.2), revealed an appreciable amount of sulfur in the electropolymerised poly (NDDEAEA) surfaces even after twenty minutes of UV irradiation and that irradiation in the presence of monomers can be used to graft any other layer onto the poly (NDDEAEA). SEM and AFM observations showed the surface morphology of grafted surfaces (5B.2, page 220, Figure Apx B.3; Figure Apx B.4 and Figure Apx B.5).

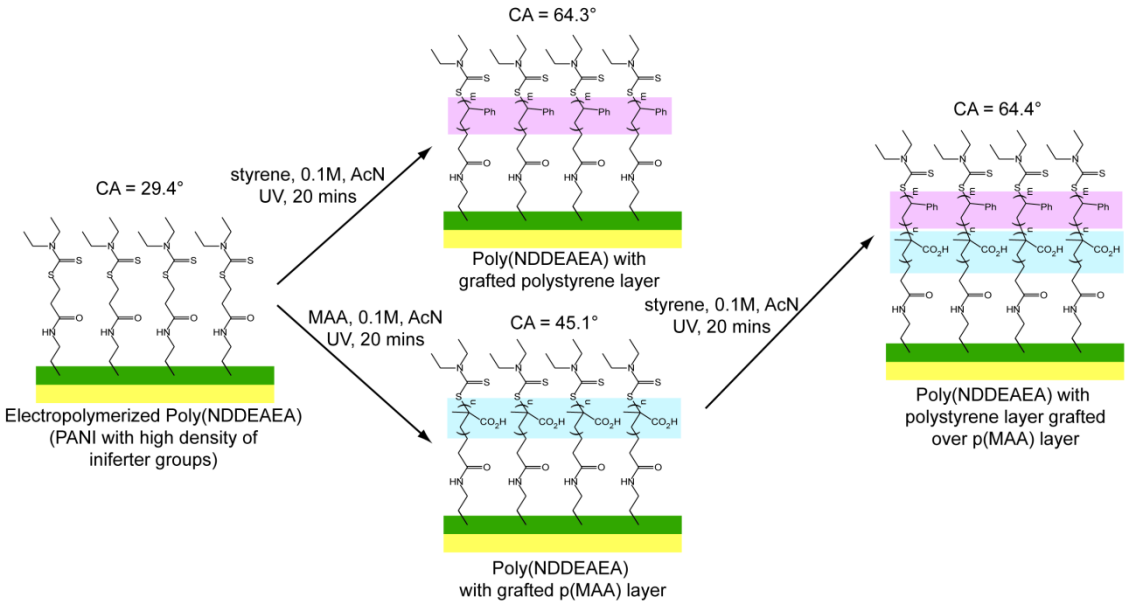

Figure 3.7: Electropolymerised poly (NDDEAEA) films UV irradiated for twenty minutes in the presence of styrene or methacrylic acid (0.1 M, acetonitrile), leading to surface-confined grafted polymer layers. Also the layer-by-layer (block copolymer) grafting of poly (styrene) over a grafted poly (methacrylic acid) layer is displayed. The static water contact angle shows changes consistent with the uppermost surface layer of the grafted polymer, such that polystyrene grafted over poly (MAA) shows the same contact angle as a single polystyrene grafted layer (Ivanova-Mitseva *et al.* **2010**).

Grafted polymeric surfaces were characterised by contact angle measurements. Table 3.1 shows the static water contact-angles for various grafted polymeric surfaces. Control of the surface contact angle through changes in the surface functionality, while retaining the bulk material properties, is useful for many applications, including sensors, flow control and cell patterning. Layer-by-layer grafting of polymers, as shown in Figure 3.7, provides evidence for *"living" iniferter-initiated* polymerisation at the

poly (NDDEAEA) surface. According to the literature, initiation with this type of *iniferter* can result in undesirable side reactions during photolysis of end groups on poly (methyl methacrylate) and low reactivity with acrylate ester monomers, potentially resulting in a less efficient grafting of a second layer (Manga *et al.* **1998**; Turner and Blevins, **1990**). However, in the reported experiments, two dimensional photopolymerisation processes, due to the presence of high density of DTCE groups; therefore the surface-growing polymer end explores only a two-dimensional space and grows in a uniform way for the first and second polymeric layer was confirmed. As expected, the contact angle (CA) measurements demonstrate that the electropolymerised poly (NDDEAEA) was quite hydrophilic, with CA of 29.4° (probably because it was deposited from an acidic solution and so exists in a protonated form). Considering these results together with those from XPS analysis, photoactivation of the DTCE unit was confirmed (Nakayama and Matsuda, **1996**). The poly (methacrylic acid) grafted layer was relatively more hydrophobic with a contact angle of 45.1°, while poly (AMPSA) was more hydrophilic (CA of 33.0°), due to the sulfonic acid moiety. On the other hand, polystyrene grafting led to increased hydrophobicity with a CA of 64.4°. A contact angle consistent with grafting of the second monomer (styrene, CA = 64.5°), on top of an initial methacrylic acid grafted layer (CA = 45.1°) was found, as expected (Table 3.1). The thickness of the poly (NDDEAEA) layer on the modified SPEs was measured as ~150 - 200 nm and the grafted polymethacrylic acid and poly (AMPSA) layers were ~50 nm as revealed by Dektek analysis.

Table 3.1: Static water contact angles in air for various substrates, substrates modified with poly (NDDEAEA) and after surface-grafting of polymers.

nature of the surface	water contact angle [deg]
pretreated screen-printed gold electrode (SPE)	66.0°
electropolymerised poly (NDDEAEA)	29.4°
poly (MAA) surface-grafted to electropolymerised poly (NDDEAEA) film	45.1°
poly (AMPSA) surface-grafted to electropolymerised poly (NDDEAEA) film	33.0°
polystyrene surface-grafted to electropolymerised poly (NDDEAEA) film	64.4°
polystyrene over poly (MAA) surface-grafted to electropolymerised poly (NDDEAEA) film (layer-by–layer grafting)	64.5°
bare polypropylene membranes	132.3°
poly (NDDEAEA) grafted layer over PP membrane by chemical oxidative polymerisation	85.2°
poly (MAA) surface-grafted to chemically polymerised poly (NDDEAEA) film onto PP membrane	57.6°
poly (AMPSA) surface-grafted to chemically polymerised poly (NDDEAEA) film onto PP membrane	37.2°
polystyrene surface-grafted to chemically polymerised poly (NDDEAEA) film onto PP membrane	72.8°
glass microscope slides	27.9°
poly (NDDEAEA) chemically polymerised over glass surface	55.6°
polystyrene surface-grafted to chemically polymerised poly (NDDEAEA) film onto glass slide	88.3°
poly (AMPSA) surface-grafted to chemically polymerised poly (NDDEAEA) film	35.3°

From SEM and AFM images it is possible to observe grafting of monomers onto electropolymerised poly (NDDEAEA) (5B.2, page 220, Figure Apx B.3; Figure Apx B.4 and Figure Apx B.5). In general, the uniformity of the grafted polymer on the modified electrode surface is usually crucial to control the grafting efficiency. SEM reveals a globular structure of the pre-treated SPE surface which displays an obvious change (some holes appear) associated with the electropolymerisation of NDDEAEA. After

grafting of hydrophilic monomers, MAA and AMPSA onto electropolymerised poly (NDDEAEA), the films show rather smooth surfaces and compact film structures compared to the surface with grafted styrene which displayed some uneven hollow structures. These results imply that the phase separation and structural heterogeneity are dependent on the monomer used. Surface characterisations of the grafted electrodes were also performed using XPS. Figure 3.8 shows the XPS spectra of electropolymerised poly (NDDEAEA) films before and after UV irradiation.

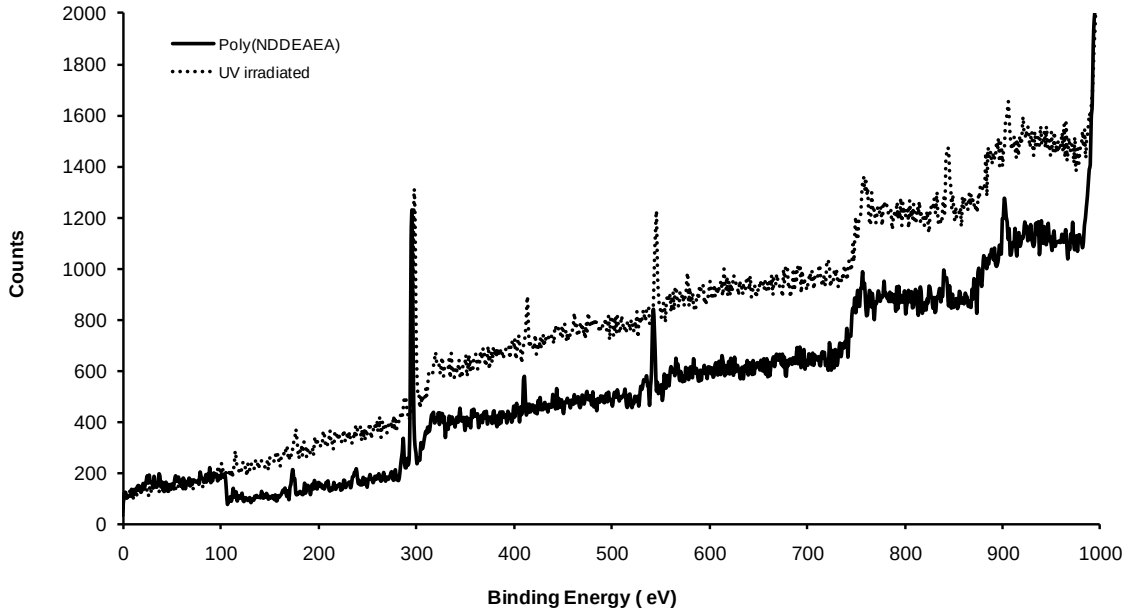

Figure 3.8: XPS spectra of electropolymerised film of poly (NDDEAEA) on a gold screen-printed electrode before UV irradiation (solid line) and after UV irradiation (dotted line).

The XPS spectra of NDDEAEA powder, and electropolymerised poly (NDDEAEA) films before and after UV irradiation exhibited N 1s and S 2p peaks due to the presence of the polyaniline and DTCE groups which were of comparable intensities. In addition, the S 2p (~174 eV) and N 1s (~411 eV) peaks were still observable after electropolymerisation and UV-irradiation. This indicates that a substantial amount of DTCE groups remained in the surface layer of poly (NDDEAEA) There was also no significant change in the elemental composition (wt %) which also provides evidence that the DTCE groups were still located at the surface.

XPS measurements allow the determination of elemental ratios within the films (Table 3.2). It was observed that the peak intensities of NDDEAEA corresponding to sulfur and carbon (296 eV) did not vary greatly before and after electropolymerisation. Upon twenty minutes UV irradiation of the poly (NDDEAEA)-coated electrode in 0.75 M hydrochloric acid solution and subsequent-washing with water, the S 2p peak was still observed, although the intensity is reduced by about 30% of the initial-value. No appreciable spectral change is observed after extensive washing with water.

Table 3.2: XPS element composition (wt %) of the NDDEAEA monomer and its polymers.

compound	S	N	O	C	Au	Bi	total	S 2p intensity	N 1s intensity	ratio S/N
NDDEAEA monomer	5	8	11	76			100	3.83	4.74	0.8
electropolymerised NDDEAEA	4	7	10	79			100	3.26	4.5	0.73
UV irradiated electropolymerised NDDEAEA	3	7	13	77			100	2.332	4.79	0.49
bare electrode			28	60	7	5	100			

3.2.5 Deposition of poly (NDDEAEA) films using chemical oxidation

Polymerisation of NDDEAEA can also be achieved using chemical oxidizing agents, such as persulfate, to deposit a layer of the conductive polymer onto a range of substrates, such as microtitre plates, cuvettes, membranes, glass, *etc.* This layer of DTCE-functionalised PANI can function as a vehicle to further coat the material with a layer of grafted addition polymer in a controlled manner (Lakshmi *et al.* **2009**). PANIs have previously been employed in the development of sensor devices by deposition as thin films over various surfaces followed by immobilisation of various species capable of sensing applications. It is a popular material due to its good optical properties, its pH and redox sensitivity, conducting nature and stability. To obtain poly (NDDEAEA) films by chemical oxidative polymerisation over hydrophobic polypropylene membranes and on glass surfaces (or any suitable substrate), the first step was to optimise the various deposition parameters within polystyrene cuvettes and microtitre plates by measuring

the optical densities after chemical oxidative polymerisation of NDDEAEA with varying concentrations of monomer, oxidant, pH, time of polymerisation *etc.* Two protocols were identified and optimised by variation in the concentrations of the reagents, according to whether thin transparent films for optical measurement were to be prepared or thicker coatings required. The details are presented in the (5B.3, page 227, Figure Apx B.6; Figure Apx B.7; Figure Apx B.8 and Figure Apx B.9). For thin films, a monomer concentration of 0.025 M in the presence of hydrochloric acid (0.225 M) and ammonium persulfate (0.0183 M) for two hours in 25% acetonitrile in water was judged to be optimum (5B.3.1, page 227, Figure Apx B.6). Similarly thicker films for grafting experiments were obtained at a monomer concentration of 0.08 M in the presence of hydrochloric acid (0.6 M) and ammonium persulfate (0.05 M) in 25% acetonitrile in water polymerised for one hour (5B.3.2, page 229, Figure Apx B.7; Figure Apx B.8 and Figure Apx B.9).

To determine the effect of pH on contact angles, microtitre plates coated with thin poly (NDDEAEA) films were treated with solutions of varying pH for one hour and their contact angle measured after drying. Contact angles decreased with decreasing pH; thus at pH 12.0 the films were relatively hydrophobic with a contact angle of 82.2° whereas at pH 1.0 the contact angle was 39.5°, behavior consistent with that reported in the literature for polyaniline (Blinova *et al.* **2008**).

It was shown that deposition of poly (NDDEAEA) onto solid surfaces is quite reproducible. IR spectra of the chemically oxidized poly (NDDEAEA) polymers which had been deposited onto microtitre plates, scraped off and redispersed in KBr discs, were obtained (5B.3.2, page 229. Figure Apx B.10) and showed two intense absorption bands at 1208 cm^{-1} and 1491 cm^{-1}, respectively which are assigned to stretching vibrations (N-C(S)). Other bands characteristic of *N*,*N*-diethyldithiocarbamate were also confirmed by the presence of absorption bands at: 2921 cm^{-1}, 1375 cm^{-1} and 1175 cm^{-1} (CH_3 stretching and bending vibrations and the C=S stretching vibration respectively). Also a peak at 1350 cm^{-1} was observed due to bending vibrations of CH_2. Other peaks at 1021 cm^{-1}, 910 cm^{-1} and 1452 cm^{-1} which are also characteristic of DTCE group were seen. There were peaks at 3430 cm^{-1} due to

N-H stretching vibrations, 700 cm^{-1}due to aromatic C-H bending, 1140 cm^{-1}due to C-N bending and at 1600 and 1480 cm^{-1} due to the presence of quinoid and benzenoid rings in the polyaniline backbone, respectively (Garcia-Con *et al.* **2010**; Williams and Fleming, **1995**; Kobayashi *et al.* **1992**).

The UV spectrum of a solution of poly (NDDEAEA) (1 mg mL^{-1} in methanol) showed absorption peaks at λ_{max} = 247 nm and 275 nm. These were attributed to the DTCE group (5B.3.2, page 229, Figure Apx B.11). The spectrum also showed three characteristic absorption bands due to PANI at around 320, 400 and 735 nm. The characteristic peaks of PANI appear at about 320 nm due to the π-π* transition of the benzenoid ring and at about 400-430 nm and 730-825 nm due to polaron-π* and π-polaron band transitions respectively, showing that PANI is present in the doped state (Abdiryim *et al.* **2005**).

A second substrate of choice was hydrophobic polypropylene microfiltration membranes onto which oxidative polymerisation of poly (NDDEAEA) was performed which resulted in the deposition of a thin, bluish-greenish layer of functionalized PANI coating across the membrane surfaces (see Experimental Details, Figure 3.9 and 5B.3.3, page 233, Figure Apx B.12). Contact angles were measured (Table 3.1) and the degree of grafting determined gravimetrically. PP membranes showed a 13.28% mass increase for thin films and up to 54.2% for thick film deposition (Figure 3.9a).

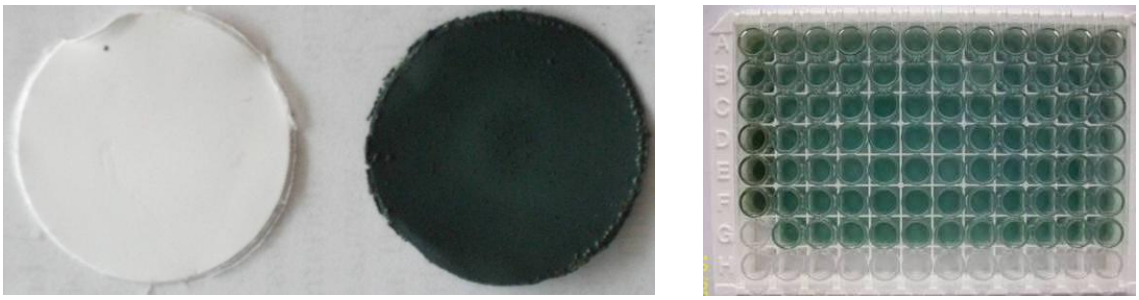

a. b.

Figure 3.9: a) polypropylene membrane (left) and poly (NDDEAEA)-coated membrane (right) and b) microtitre plate showing deposition of poly (NDDEAEA) in the wells.

Further grafting experiments with poly (NDDEAEA) chemically deposited onto microtitre plates (Figure 3.9b) showed that MAA, AMPSA and lauryl methacrylate could be successfully grafted (giving rise to contact angles of 52.2°, 30.6° and 102.5° respectively). Control experiments were performed using unfunctionalised polyaniline-coated microtitre plates which did not show any change in contact angle after irradiation in the presence of monomers, confirming the necessity of the DTCE functionality for photografting experiments. Similarly, photochemical polymerisation over poly (NDDEAEA)-modified PP membranes allowed the growth of various hydrophobic and hydrophilic polymers (AMPSA, MAA and styrene) as shown by changes in the contact angles (Table 3.1).

Glass slides were also coated with poly (NDDEAEA) using similar condition and the contact angle was measured to confirm successful polymerisation (Table 3.1). By successively masking two sides of a coated glass slide (aluminium foil) it was possible to graft poly (AMPSA) and polystyrene on adjacent areas of the glass, producing areas with very different contact angles on the same slide (Figure 3.10). The measured contact angles are reported in Table 3.1.

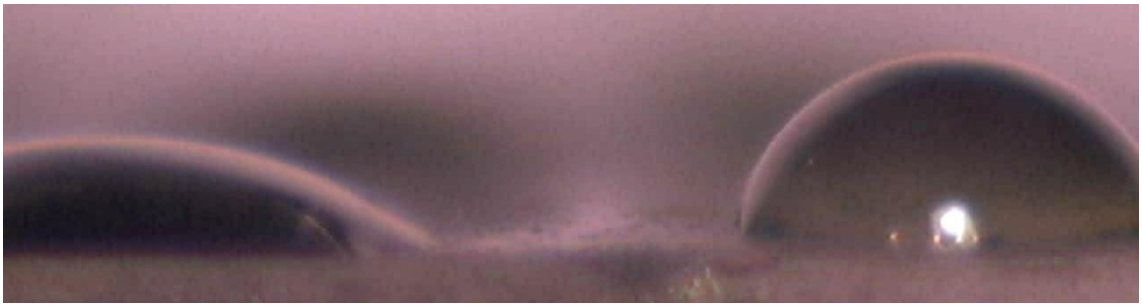

Figure 3.10: Water contact angle image of chemically polymerised poly (NDDEAEA) over glass slide after UV grafting of poly (acrylamido-2-methylpropane sulfonic acid) (left) and polystyrene (right).

3.2.6 Grafting of poly (*N*-(3-aminopropyl)-methacrylamide) over chemically polymerised poly (NDDEAEA) through a TEM grid

Poly (NDDEAEA), cast from solution in methanol onto a gold-sputtered glass slides was then grafted with poly (3-aminopropyl methacrylamide) from a solution of the monomer in 20% acetonitrile in water, via UV-initiation through a TEM grid. Confocal microscopy clearly confirms the growth of polymer in a pattern determined by the shape of the TEM grid (Figure 3.11).

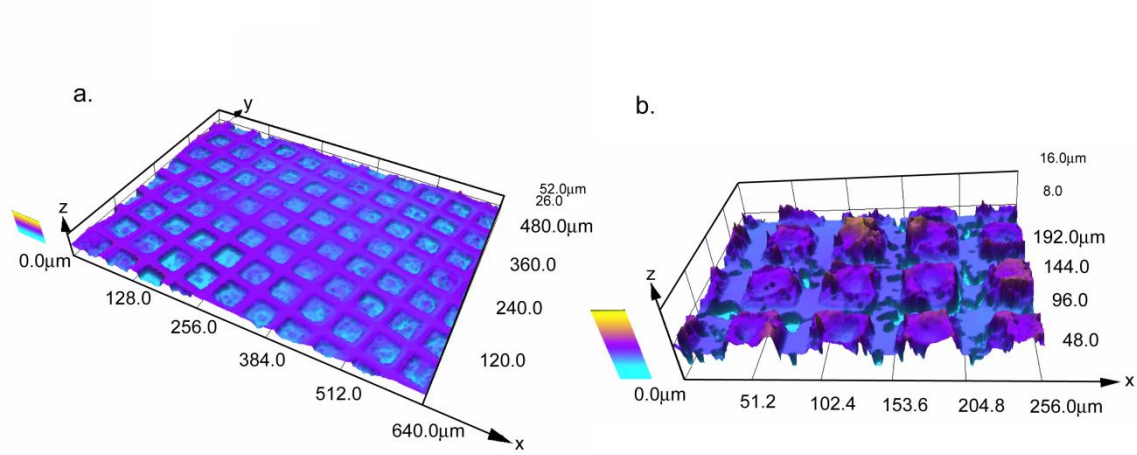

Figure 3.11: Confocal micrograph of poly (aminopropyl methacrylamide) grafted over poly (NDDEAEA) cast film over gold sputtered glass slide through chemical polymerisation. a) Before the removal of the TEM grid and b) after the removal of the TEM grid. Features are of the dimensions 200 µm × 200 µm.

3.3 Experimental Details

3.3.1 Materials

Carbon disulfide (99%) and sodium hydroxide (97%) were purchased from Acros Organics. 1-(3-Dimethylaminopropyl)-3-ethyl-carbodiimide hydrochloride (98%) was purchased from Alfa Aeser. Acrylic acid (99%) and *N*-phenylethylenediamine (98%) were purchased from Sigma Aldrich and diethylamine (98%) was obtained from Fisher Scientific. All other chemicals and solvents used within this work were purchased from Sigma-Aldrich and were of analytical grade and used as received unless stated otherwise. MilliQ distilled water was used in all experiments.

3.3.2 Apparatus

NMR measurements were made using a JEOL ECX 400 MHz NMR (Japan) and FT-IR spectra were recorded using KBr disks on a ThermoNicolet Avatar-370 spectrometer (Nicolet, US). For UV irradiation, CERMAX® Xenon Arc Lamp (Perkin-Elmer Optoelectronics, Inc., USA) fibre optic light source (300 W) or a Philips type HB 171/A self-tanning UV lamp, fitted with 4 CLEO 15W UVA fluorescent tubes (Philips, Germany) with continuous output in the region 300-400 nm, delivering 0.09 W cm^{-2} at a distance of 80 mm, were used. Sessile water contact angle (CA) measurements were made using a Cam 100 optical Angle Meter (KSV Instruments Ltd., Finland) along with the software provided. Elemental analyses were provided by Medac Ltd (Egham, UK). Optical densities were recorded using a micro plate reader (for microtitre plates) or a UV spectrophotometer (UV-1800 Schimadzu, Japan). An Autolab PSTAT-10 instrument (Eco-Chemie BV, Utrecht, Netherlands) was utilized for all electrochemical experiments. AFM experiments were performed using a DI3000 AFM (Digital Instruments, New York, USA) in tapping mode in air. SEM images were recorded with an FEI XL30 SFEG (Scanning Field Emission Gun) microscope. Mass spectra were obtained using a Waters LCT Premier XE mass spectrometer. X-Ray photoelectron spectroscopy (XPS) measurements were carried out using a VG ESCAlab (East Grinstead, UK) Mark-2 X-ray photoelectron spectrometer. The X-ray gun was operated

at 14kV and 20 mA. Spectra were collected at 20 eV pass energy with Mg Kα 1253.6 eV radiation at an analysis chamber pressure of 10^{-9} mBar. Elemental composition was calculated using peak areas and tabulated atomic sensitivity factors. A confocal Laser Scanning 3D colour microscope Olympus LEXT - Model OLS3000 was used for the imaged layers of chemically polymerised NDDEAEA and a Dektek 3 surface profiler (Veeco, New York, USA) was used for thickness measurements of grafted electrodes.

3.3.3 Synthesis of *N*-(*N´,N´*-Diethyldithiocarbamoyl ethyl amido ethyl)-aniline (NDDEAEA)

A solution of CNDDA (Scheme 3.4, **1**) (0.004 mol, 0.922 g, 1 equiv) in 20 mL of anhydrous acetonitrile was prepared in a dried 50 mL round bottomed flask, under argon atmosphere with exclusion of light. To this mixture, *N*-phenylethylenediamine (0.004 mol, 0.545 g, 1 equiv) and 1-(3-dimethylaminopropyl)-3-ethyl-carbodiimide hydrochloride (0.008 mol, 1.6 g, 2 equiv) were added in that order. After three hours of stirring, the solvent was removed *in vacuo*. The crude mixture was dissolved in 40 mL ethyl acetate and extracted five times with 40 mL distilled water, the organic layer dried with anhydrous sodium sulfate, filtered and the solvent evaporated *in vacuo* to obtain an oily product that solidified to a white waxy material in 50 % overall yield (98 % purity by NMR). The product *N*-(*N´,N´*-diethyldithiocarbamoyl ethyl amido ethyl)-aniline (NDDEAEA, Scheme 3.4, **2**) was used without further purification.

Spectroscopic data for NDDEAEA (Scheme 3.4, **2**): IR (KBr) 1647.26 (C=O), 1603.77 ((S)C-N), 1508.10 (N-C(O)), 1351.55 (C=S), 1268.93 (C-NC6H5), 981.92 (C-N), 755.80 ((S)C-S), 694.92 (S-CH3) cm^{-1} (5B.1, page 219, Figure Apx B.1).

^{1}H NMR (400 MHz, DMSO-D_6, 25 °C, Figure 3.1) δ 7.96 (1H, t, N**H**C_6H_5), 7.01 (2H, t, *J* = 7.68 Hz, C_6**H**$_5$), 6.51 (2H, d, *J* = 7.68 Hz, C_6**H**$_5$), 6.30 (1H, t, *J* = 7.34 Hz, C_6**H**$_5$), 5.49 (1H, t, *J* = 5.27, N**H**CO), 3.90-3.87 (2H, m, C**H**$_2$$CH_3$), 3.65-3.61 (2H, m, C**H**$_2$$CH_3$), 3.35 (2H, t, *J* = 6.99, C**H**$_2$S), 3.20-3.12 (2H, m, C**H**$_2$NHC(O)), 3.09-2.90 (2H, m, C_6H_5NHC**H**$_2$), 2.44 (2H, t, NHC(O)C**H**$_2$), 1.18-1.1 (6H, m, N(CH_2C**H**$_3$)$_2$) ppm.

^{1}H NMR (400 MHz, DMSO-D_6, 130 °C, Figure 3.3) δ 7.51 (1H, s, N**H**C_6H_5), 7.00 (2H, t, *J* = 7.68 Hz, C_6**H**$_5$), 6.52 (2H, d, *J* = 7.68 Hz, C_6**H**$_5$), 6.48 (1H, t, *J* = 7.34 Hz, C_6**H**$_5$), 5.04 (1H, s, N**H**CO), 3.88-3.74 (4H, m, N(C**H**$_2$CH$_3$)$_2$), 3.40 (2H, t, *J* = 6.99, C**H**$_2$S), 3.24-3.20 (2H, m, C**H**$_2$NHCO), 3.20-3.00 (2H, m, C**H**$_2$NHC(O)), 2.47 (2H, t, *J* = 6.99 Hz, NHC(O)C**H**$_2$), 1.18 (6H, t, N(CH$_2$C**H**$_3$)$_2$) ppm.

^{13}C NMR (100 MHz, DMSO-D_6, 25°C, Figure 3.1) δ 193.86 (**C**(S)S), 170.40 (**C**(O)), 148.57, 128.89, 115.69, 111.91 (**C**$_6$H$_5$), 49.60 (**C**H$_2$CH$_3$), 46.80 (**C**H$_2$CH$_3$), 42.10 (C_5H_6NH**C**H$_2$), 39.00 (**C**H$_2$NHC(O)), 34.30 (NHC(O)**C**H$_2$), 32.40 (**C**H$_2$SC(S)), 12.23 (CH$_2$**C**H$_3$), 11.36 (CH$_2$**C**H$_3$) ppm.

^{13}C NMR (100 MHz, DMSO-D_6, 130 °C, Figure 3.3) δ 194.33 (**C**(S)S), 169.75 (**C**(O)), 148.18, 128.11, 115.40, 111.77 (**C**$_6$H$_5$), 48.50 (**C**H$_2$CH$_3$), 42.10 (C_5H_6NH**C**H$_2$), 38.00 (**C**H$_2$NHC(O)), 34.00 (NHC(O)**C**H$_2$), 32.00 (**C**H$_2$SC(S)), 11.21 (N(CH$_2$**C**H$_3$)$_2$) ppm (The assignments were based on COSY, DEPT and HMQC experiments made in DMSO-D_6).

HRMS (ES) Calculated mass for $C_{16}H_{25}N_3NaOS_2$ $[M+Na]^+$: m/z: 362.13 found: 362.14; elemental analysis ($C_{16}H_{25}N_3OS_2$): C, 56.60; H 7.42; N 12.38, O 4.71, S 18.89; found 1: C 57.85, H 7.65, N 13.01, S 18.25; R_f = 0.24 (50 % ethyl acetate in hexane) (5B.1, page 219, Figure Apx B.2).

3.3.4 Electropolymerisation of the aniline group of NDDEAEA

Screen printed gold electrodes (SPE) (4.0 mm diameter, from Dropsens) were used, with gold working and counter electrode and Ag/AgCl reference electrode. Before polymerisation each new electrode was cleaned and pre-treated by cycling the potential between 0 to + 0.7 V, 50 mV s^{-1} scan rate in 1.5 M hydrochloric acid, 5 cycles. For the deposition step, electrodes were cycled (twenty times) between -0.2 V and + 0.9 V at a scan rate of 100 mV s^{-1}, (step potential 7 mV) in a 0.2 M solution of NDDEAEA in 0.56 M hydrochloric acid in a 25 % acetonitrile in water. Stock solution was prepared by adding 1.25 mL acetonitrile solution of 0.8 M NDDEAEA into a 5 mL beaker containing 1.87 mL of 1.5 M hydrochloric acid and 1.9 mL of water. Solutions were

mixed well and degassed for ten minutes by purging with argon or nitrogen and the solution kept covered with aluminium foil to protect from light before deposition. CV measurements were performed by placing 50 µL of the test solution of NDDEAEA onto the surface of the SPE for electropolymerisation. Electropolymerisation was carried out under argon and in the dark. Electropolymerised films were rinsed with deionized water (once), dried in a stream of nitrogen and stored dry and in the dark. A blue-green layer of poly (NDDEAEA) was observed to have formed on the working electrode (Figure 3.4).

3.3.5 Molecular Modeling of NDDEAEA and poly (NDDEAEA)

The neutral and protonated forms of NDDEAEA monomer and poly (NDDEAEA) were modelled by calculating the charges for each atom on the template and the structures refined using molecular mechanical methods. This was carried out on a PC using the Sybyl 7.3^{TM} software package (Tripos Inc., Missouri, 63144, USA) running under Linux. Energy minimization was performed to a value of 0.001 kcal/mol using Tripos force fields, Gasteiger-Huckel charges and refined by the molecular mechanics method applying an energy minimization using the MAXIMIN2 command.

3.3.6 Surface-confined photo grafting of various polymers onto electropolymerised films of NDDEAEA

An electropolymerised poly (NDDEAEA)-modified SPE was placed horizontally in a glass vial and the working electrode covered with 50 µL of a 0.1 M solution of unsaturated monomer in acetonitrile under dark conditions. The monomer solutions had been purged with nitrogen for ten minutes to remove oxygen prior to irradiation. The vial was sealed with Parafilm® and continuously purged with nitrogen to maintain an inert atmosphere over the solution during irradiation. The electrode surface was then UV-irradiated for twenty minutes with a fibre optic light source (CERMAX xenon arc lamp). The photografted electrodes were then rinsed in a mixture of 50 % methanol in

deionized water and dried in a stream of nitrogen. Contact angle measurements were used to characterise changes that had occurred in the functionality and hydrophobic/hydrophilic nature of the polymeric film after grafting.

Several polymers were grafted onto poly (NDDEAEA) following the protocol described above. Solutions (0.1 M) of MAA, AMPSA or styrene were utilized to produce grafted films of the respective polymers via UV-irradiation. As well as grafting single polymer onto poly (NDDEAEA), layered (block copolymer grafted) structures, MAA followed by styrene, could also be constructed. For the layer-by-layer grafting experiment, a poly (MAA) grafted SPE electrode, prepared as described in above, was treated with a solution of styrene (50 µL of 0.1 M in acetonitrile) and irradiated under the same conditions as described above for the grafting of polymer layers. The contact angles of the grafted films were measured and their thickness determined by Dektek analysis. All surfaces were characterised using SEM and AFM (5B.2, page 229, Figure_Apx B.4 and Figure_Apx B.5).

Polymerisation of NDDEAEA by chemical oxidation could also be used for the formation of thick or thin (transparent) coatings on a range of supports (polystyrene microtitre plates, cuvettes and polypropylene filtration membranes). Experimental parameters were optimised in order to obtain films of the desired thickness, which could then be used as substrates in a number of grafting procedures (5B.3.1, page 227, Figure_Apx B.6 and 5B.3.2, page 229, Figure_Apx B.7; Figure_Apx B.8 and Figure_Apx B.9) for the effect of varying the experimental parameter on film growth). Polymerisation resulted in the formation of green coatings of poly (NDDEAEA) on the surfaces of the microplate wells. The washed wells were filled with dilute acid (0.01 M hydrochloric acid, pH = 1) and the absorbance measured at 405 nm. Thin transparent layers (absorbance = 0.17, 5B.3.1, page 227, Figure_Apx B.6) were formed under the conditions: NDDEAEA (25 mM), hydrochloric acid (225 mM) and ammonium persulfate (18.3 mM), polymerised for two hours in 25 % acetonitrile in water. Similarly thicker films were obtained (absorbance (measured in water at 550 nm) = 3.5, 5B.3.2, page 229, Figure_Apx B.7; Figure_Apx B.8) under the conditions: NDDEAEA (80 mM),

hydrochloric acid (0.6 M) and ammonium persulfate (50 mM), polymerised for one hour in 25 % acetonitrile in water.

3.3.7 Chemical oxidative polymerisation of NDDEAEA on polypropylene (PP) ultra-filtration membranes (thinner films)

PP membranes (with a nominal cut-off pore diameter of 0.2 µm and thickness of 150 µm, PP 2E-HF, Membrana, Germany) were cut into small discs of 25 mm diameter. Membranes were pre-treated with methanol for one hour in a Petri dish. Oxidative polymerisation was performed using ammonium persulfate under the following conditions: 0.018 M ammonium persulfate, 0.025 M NDDEAEA, 0.225 M hydrochloric acid, 25% acetonitrile in water, 1.45 hours polymerisation in the dark at room temperature. The reaction mixture was prepared by combining 0.75 mL of NDDEAEA (0.1 M in acetonitrile) with 0.6 mL of an aqueous solution of ammonium persulfate (0.0915 M), 675 µL hydrochloric acid (0.1 M) and 0.98 mL of water. Polymerisation resulted in the deposition of a thin, green layer of functionalised PANI coating over the membrane surfaces. Poly (NDDEAEA) coated PP membranes were washed in three cycles of water, followed by 0.1 M hydrochloric acid. The degree of grafting was determined gravimetrically and expressed as a percentage change in mass. The following equation was used:

$$DG\ (\%) = (W_1 - W_0) / W_1 \times 100\ \%$$

Here W_0 and W_1 represent the weights of the membrane before and after grafting, respectively. Contact angles were also measured.

3.3.8 Photografting by UV polymerisation of monomers onto chemically oxidized poly (NDDEAEA)-modified PP membranes and glass slides

The pre-weighed poly (NDDEAEA)-coated membranes were immersed in a Petri dish containing 3 mL of 0.1 M monomer solution (methacrylic acid or AMPSA were dissolved in water and styrene in acetonitrile) which had been degassed by bubbling

with nitrogen for ten minutes (5Appendix B: Figure Apx B.12). The Petri dish was then placed inside a homemade box supplied with an inlet for continuous flow of nitrogen throughout the period of polymerisation and irradiated (Philips UV lamp) for forty five minutes. After drying at 45 °C overnight, the degree of grafting was calculated. Contact angles were measured before and after grafting. Similarly, chemical oxidative polymerisation of NDDEAEA was performed onto glass microscope slides to obtain thicker films. The slide was placed in a 500 mL glass beaker and 30 mL of a solution containing 0.08 M NDDEAEA, 0.6 M hydrochloric acid and 0.05 M ammonium persulfate in 25% acetonitrile in water was added. The polymerisation was allowed to proceed at ambient temperature for one hour. The glass slide was then rinsed with water and dried at ambient temperature for twelve hours. Half of the poly (NDDEAEA)-modified glass slide was then masked with aluminum foil and UV photografting of a hydrophobic monomer (styrene) was performed on the unmasked half. The sample was then rinsed, the styrene modified area masked and the other half was grafted with a hydrophilic monomer (AMPSA) as described above (Figure 3.10). Again contact angles were measured for the coatings.

3.3.9 Surface-confined photo grafting of various monomers on poly (NDDEAEA)-modified microtitre plates

Poly (NDDEAEA)-coated polystyrene microtitre plates were placed horizontally in a Petri dish. A solution of monomer (200 µL, 0.1 M, degassed with nitrogen for ten minutes) was placed in each of the wells in which grafting was to be carried out, in the dark. The Petri dish and microplate were placed inside a sealed homemade box purged with nitrogen. Monomer solutions were made up in water (methacrylic acid or AMPSA) or acetonitrile (lauryl methacrylate). The contents of the box were irradiated for forty five minutes using a Philips UV lamp, mounted at a distance of 8 cm from the well bottoms. The photografted surfaces were rinsed with deionized water and dried in a stream of nitrogen. Contact angle measurements were performed on the grafted films.

Control experiments were performed in the same manner using unsubstituted PANI in place of the poly (NDDEAEA) films.

3.3.10 Spatially-confined grafting of poly (*N*-(3-aminopropyl)-methacrylamide) over chemically polymerised poly (NDDEEA) using a TEM grid as a photomask

A solution comprising NDDEAEA (0.08 M), hydrochloric acid (0.6 M) and ammonium persulfate (0.05 M) in 8 mL 25% acetonitrile in water was allowed to react for one hour in the dark. The resultant polymer formed as a precipitate at the bottom of the vial was washed several times by the addition and decantation of water. The washed residue was dissolved in 1 mL of methanol. One drop of this solution was placed on a pre-cleaned gold coated glass slide (2 × 2 cm) and the solvent allowed to evaporate to deposit a cast film of poly (NDDEAEA). A TEM grid (G213, Bal-Tec, 200 mesh copper with 100 μm × 100 μm square holes) was placed on the surface of the polymeric film and then a drop of a previously degassed solution of *N*-(3-aminopropyl)-methacrylamide (0.43 M in 20% acetonitrile in water mixture) was placed onto the grid. The grid was covered with a standard microscope cover glass slide and the assembly then placed in a plastic bag with nitrogen atmosphere. After five minutes purging with nitrogen, the assembly was UV irradiated for twenty minutes with the Philips UV lamp. The slide was rinsed with water and left to dry for twelve hours at room temperature. Confocal microscopy (10 × magnification) was used to record 3D images of grafted poly-*N*-(3-aminopropyl)-methacrylamide structures, before and after removal of the TEM grid (Figure 3.11).

3.4 Conclusions

A new bi-functional monomer, *N*-(*N´,N´*-Diethyldithiocarbamoyl ethyl amidoethyl)-aniline (NDDEAEA), incorporating both aniline and dithiocarbamate ester (DTCE) groups, was synthesised and fully characterised. Conjugated poly (NDDEAEA), consisting of *N*-substituted PANI backbones bearing a high density of DTCE groups (*iniferter*) was produced, either by electrochemical polymerisation or chemical oxidation using ammonium persulfate. Polymerisation of the aniline functionality of NDDEAEA was performed on a number of substrates, namely: polystyrene (cuvettes and microtitre plates), polypropylene filtration membranes, screen-printed gold electrodes and glass. UV-activation of the DTCE-based *iniferter* groups of these polymeric materials, deposited on solid surfaces allowed grafting of further addition polymers, or block copolymers. Monomers utilized for grafting were: methacrylic acid, styrene, acrylamido-2-methylpropane sulfonic acid, lauryl methacrylate and 3-aminopropyl methacrylamide. That these polymers were also capable of re-initiating polymerisation upon reapplication of UV light was confirmed by the grafting of polystyrene over a poly (MMA) grafted film. UV-initiated surface graft polymerisation was also shown to be capable of producing fine surface designs via a masking process.

Photochemical grating of various monomers and XPS studies (before and after polymerisation) clearly indicated that the DTCE groups survived oxidative polymerisation and retain their *"living"* behaviour. This versatile new material has the potential for the creation of materials with integrated functionalities (*e.g.* conductivity and molecular recognition, catalysis, controlled transport properties *etc.*) for application in sensors, microfluidic devices, and in surface patterning. Our results suggest that NDDEAEA is a versatile monomer for use within the fabrication of sensors and optoelectronic devices and in polymer and material chemistry applications.

4 Enhancement of Conductivity by UV Irradiation in Polyanilines *N*-Substituted with *Dormant* or Active Radical Species

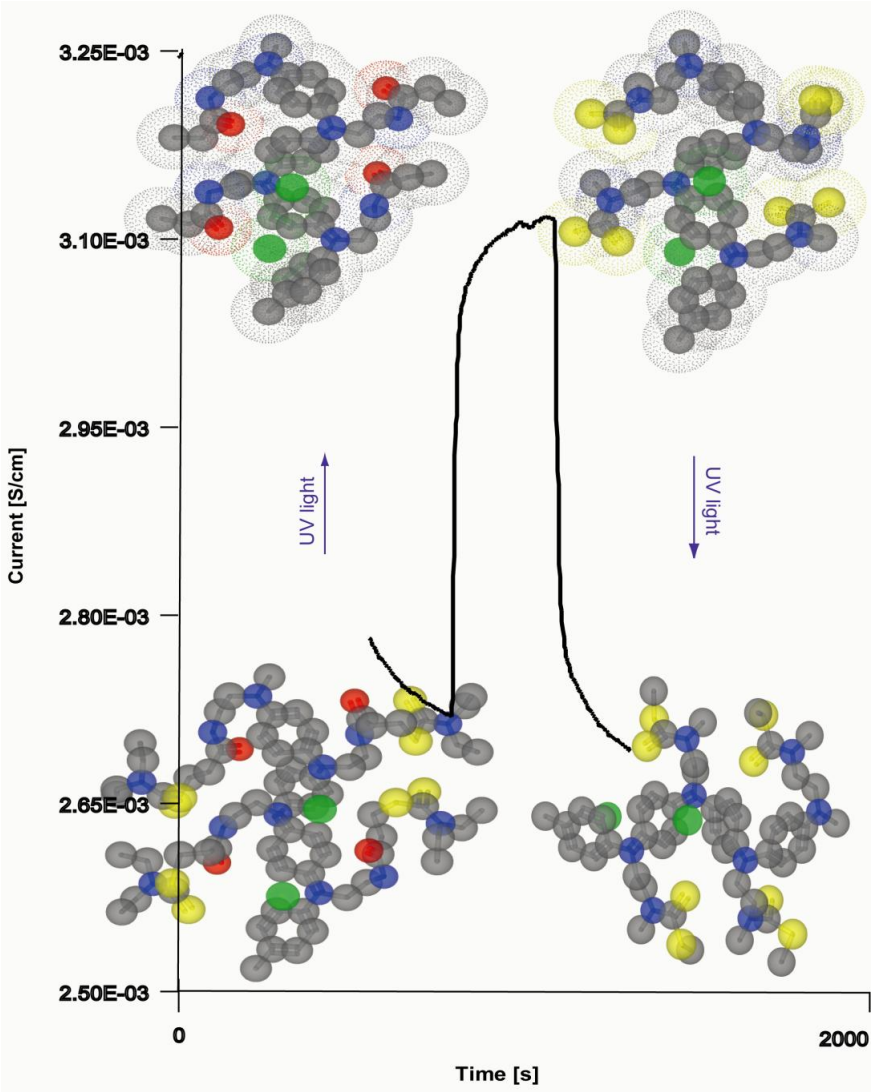

4.1 Introduction

The interaction of mater with energy is a basic phenomenon which sits behind most of the modern analytical devices and all physical events in general. Creating photoresponsive materials with well-defined molecular structures in nanoscale is one of the main challenges in the field of optoelectronic devices and molecular electronics (Cho *et al.* **2010**). Converting optical irradiation into electrical signals in a well-controlled manner is a state-of-the-art ongoing task (Hayden *et al.* **2006**, Ahn *et al.* **2005**; Freitag *et al.* **2003**).

Electrically conducting organic polymers are a class of *''synthetic metals''* that combine the chemical and mechanical properties of polymers with the electronic properties of metals and semiconductors. These polymers become conductive on partial oxidation or reduction, a process commonly referred as doping. With the doping process a polymer with insulator properties is reversibly converted to its *"metallic"* conductive form. It has been demonstrated that the electrical properties of conductive polymers can be reversibly changed over the full range from an insulator to a *"metallic"* conductor (MacDiarmid **1997**).

Polyaniline (PANI) is one of the conductive polymers that receive most attention due to the relatively cheap price of the monomer used (aniline/aniline hydrochloride), the polymerisation reaction can be well controlled for higher yields and the polymer shows high thermal and chemical stability (Salaneck *et al.* **1985**). One of the unique features of PANI is that its nonconductive form can be converted to the conductive state by proton doping or oxidation–reduction reactions (Heeger, **2002**). Reversible charge injection by 'doping' can be accomplished in a number of ways: chemical doping by charge transfer, electrochemical doping, photo-doping or charge injection at a metal–semiconducting polymer interface (Heeger, **2002**).

Studies of the interaction of PANIs with different sources of energy have been conducted. Energy sources used include electromagnetic radiation (Molina *et al.* **2011**), gamma radiation (Bodugoz-Senturk and Guven, **2011**; Araujo *et al.* **2011**; Guven, **2007**), beta radiation (Kane *et al.* **2010**), ultrasound irradiation (Bardavid *et al.* **2011**;

Xia and Wang, **2002**) and ultraviolet (UV) irradiation (Yow-Jon *et al.* **2007**). It is well known that PANI strongly absorbs electromagnetic radiation, particularly in the microwave range which leads to heating of the polymer (Molina *et al.* **2011**). The authors showed that PANI nanoparticles (NPs) synthesised via precipitation polymerisation could be absorbed in a macroporous thermosensitive hydrogel (poly (*N*-isopropylacrylamide-*co*-(2-acrylamido-2-methyl propane sulfonic acid)). When this composite was subject to microwaves or irradiated by laser light the encapsulate PANI NPs increased in temperature and induced the phase transition in the thermosensitive hydrogel matrix, resulting in release of the internal solution.

It has been shown that ionising gamma radiation is an effective tool to induce and control conductivity in PANI blends with poly (vinylidene chloride-co-vinyl acetate) (Guven, **2007**; Bodugoz-Senturk and Guven, **2011**; Araujo *et al.* **2011**). The conductivity of the cast films was measured as a function of polymer composition, film thickness, irradiation dose and the temperature (Guven, **2007**; Bodugoz-Senturk and Guven, **2011**). It was shown that the conductivity increases with increasing dose up to certain level but dropped rapidly with continued irradiation. It is well known that the conductivity increases with increasing polymer thickness. The conductivity also increases with increases in temperatures, up to about 200 °C the conductivity was increasing. This is a very common observation for semi-conductor materials. In general, when the temperature of a semiconductor is raised, intrinsic conductivity increases because more free electrons cross the band-gap and holes are produced in the valance band. For temperatures about ~200 °C a decrease in conductivity can be observed due to decomposition.

After beta-irradiation PANI showed decreased conductivity by several orders of magnitude (Kane *et al.* **2010**). This fact was attributed to the extensive chain scission that occurs, leading predominantly to chain recombination (cross-linking). The conductivity changes were speculated to be limited to physical changes in the polymer structure. PANI was shown to be very sensitive to oxidative degradation.

Xia and Wang (**2002**) showed that ultrasound can enhance the doping level in PANI. When PANI was deposited on the surface of nano-TiO_2, the crystalline behaviour of PANI is hampered and the degree of crystallinity decreases, leading to an increase in conductivity. An increase in the conductivity of PANI on exposure to ultrasound was reported by De Azevedo *et al.* (**2006**). This was explained in terms of redox and doping transition in the polymer. The experiments were conducted in DMSO as solvent in the presence of water. The ultrasonic waves interacted with the water molecules which induced homolytic dissociation of the water molecules producing radical species. These radicals interacted with the dissolved PANI modifying its oxidation and doped state.

Yow-Jon *et al.* (**2007**) found that the UV irradiation could lead to a decrease in the electrical conductivity of PANI as a result of an increase in the surface band bending and a reduction in the work function (Figure 4.1).

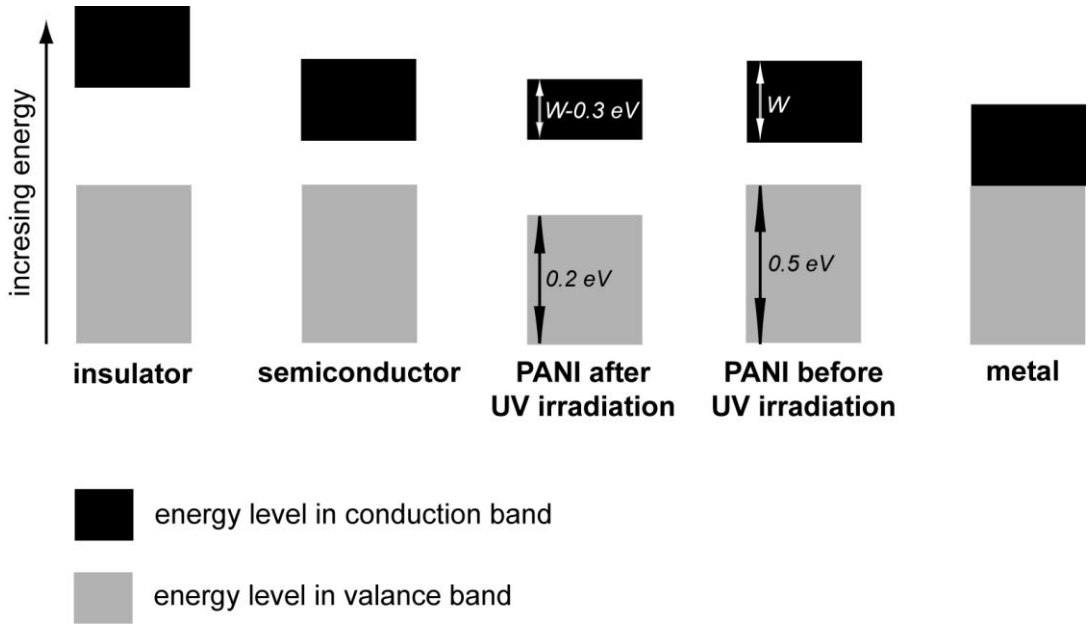

Figure 4.1: Simple band energy dsiagram, showing the difference between insulator, semiconductor, PANI after UV irradiation, PANI before UV irradiation and metal (W: work function).

Bardavid *et al.* (**2011**) investigated the effect of UV irradiation on the conductivity of PANI covalently grafted with photo-reactive molecules of spiropyran. Upon irradiation

with UV light spiropyran was transformed to its merocyanine form, which is a molecule containing a large dipole. The authors observed reversible increases in conductivity of two others of magnitude that was explained by an increase in the hole mobility which lead to an increase in the hopping probability from one conducting system to the other. It was also shown that there was a decrease in the band gap energy.

An interesting question arises from the above. Would the conductivity of PANI be influenced by an increase in the density of unpaired electrons attached to the polymer chain and would differences in the lifetime of the radicals influence the conductivity in a different way? The reaction between *dormant* radical and conductive PANI in methanol has been reported in the literature (Gizdavic-Nikolaidis *et al.* **2004**). The authors explained that *dormant* radicals extracted protons and oxidised each reduced PANI unit. This mechanism would give rise to a doping effect on the PANI chain and a consequent increase in conductivity.

The electron spin resonance (ESR) signal of the *N*-substituted PANI, poly (*N*,*N*-dimethylaniline) increased when placed in ethanol solution with the stable radical 1,1-diphenyl-2-picrylhydrazyl (Zheng *et al.* **1997**). The authors explained this effect as being due to an electron transfer process from nitrogen atoms of the polymer to those of the radical, which eliminated the radical and formed more stable radical cations on the polymer. The magnitude of this effect was dependent on the concentration of the *free* radicals used.

Within this work *N*-substituted anilines with an *iniferter* group attached to the substituent were synthesised (Scheme 4.1). As the *iniferter*, dithiocarbamate ester (DTCE) group was chosen due to its UV activity (Otsu, **2000**). When irradiated with UV light a homolitic cleavage of the C-S bond occurs. This process leads to the formation of two new species: a relatively stable *dormant* radical on sulfur and a short living/unstable active radical on carbon. The design of the *N*-substituted PANI was arranged in this way that the DTCE part would be attached to the aniline part either with its *N*-end or with its *S*-end. *N*-substituted PANIs were prepared by oxidative polymerisation, as described in Chapter 3 and in the related publication (Ivanova-

Mitseva *et al.* **2010**). During irradiation in a dry state one of the polymers would bear a *dormant* radical on each of its side-chain units while the other would bear a short-lived active radical on the PANI backbone. This difference would be explored in connection with the change of the conductivity of these PANIs in the dry state during UV irradiation. As a control PANI was used. Conductivity measurements, UV spectroscopy, electron spin resonance (ESR) spectroscopy, cyclic voltammetry (CV) and confocal microscopy were engaged to follow the process.

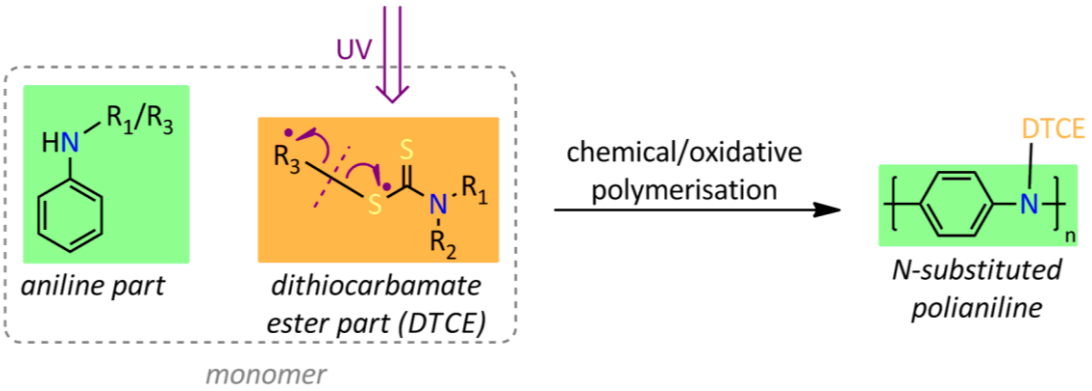

Scheme 4.1: Schematic representation of the designed structures of monomers in terms of the structures of their individual sub-units and their polymerisation to *N*-substituted PANIs.

4.2 Results and Discussion

Two monomers were designed and synthesised that comprised an aniline and a dithiocarbamate ester (DTCE) part. *N*-(*N´,N´*-diethyldithiocarbamoyl ethyl amido ethyl)-aniline (NDDEAEA, Scheme 4.2, **13**) and *S*-methyl-*N*-methyl-*N*-ethyl (2-(phenylamino)) dithiocarbamate ester (MEPDTC, **16**) were synthesised. NDDEAEA was synthesised as described in Sections 3.2.1 and 3.3.3 (page 116). The synthesis of MMDTCE is discussed below.

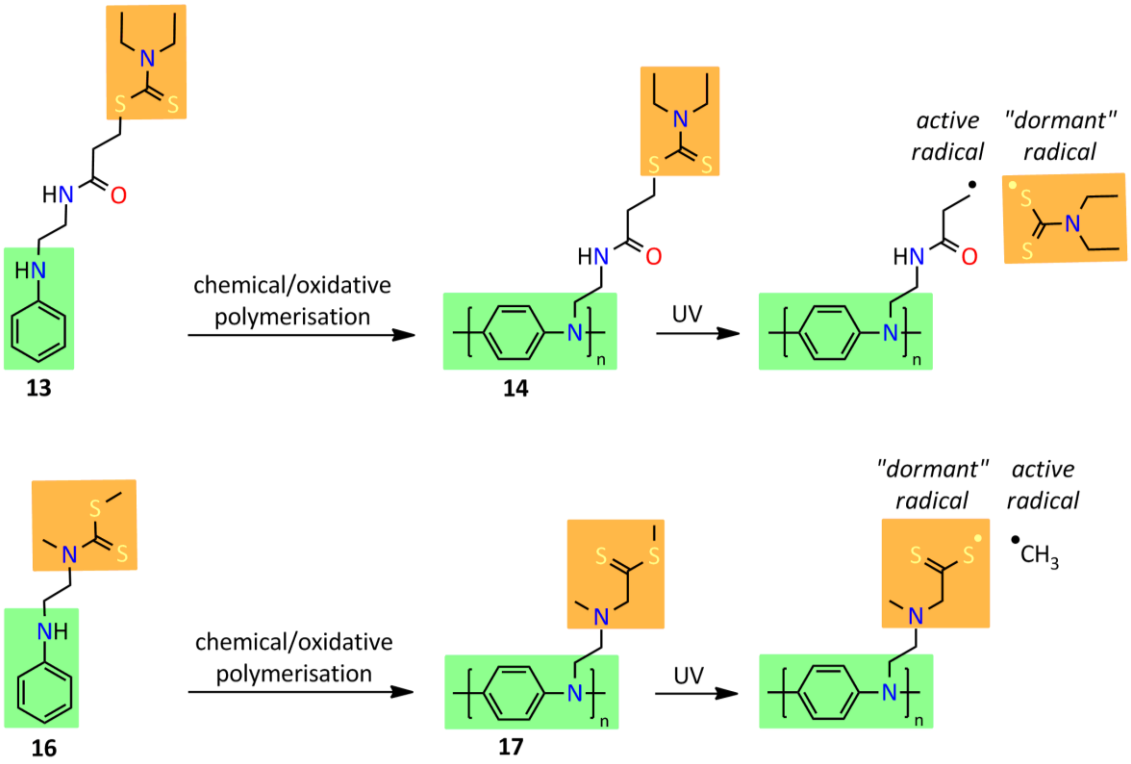

Scheme 4.2: Schematic representation of the structures of the monomers NDDEAEA (**13**) and MMDTCE (**16**) and their oxidative polymerisation leading to the formation of the corresponding *N*-substituted PANIs (**14** and **17**). During UV irradiation the polymers will form active and *dormant* radicals, respectively along the PANI chain.

4.2.1 Synthesis of *S*-methyl-*N*-methyl-*N*-ethyl (2-(phenylamino)) dithiocarbamate ester (MMDTCE)

A highly efficient and simple synthesis of dithiocarbamates based on the one-pot reaction of aliphatic amines, carbon disulphide, and alkyl halides without the use of any catalyst, under solvent-free conditions and at *ambient temperature* has been adopted for the synthesis of *S*-methyl-*N*-methyl-*N*-ethyl (2-(phenylamino)) dithiocarbamate ester (MMDTCE). Generally, the solvent-free reactions are experimentally simple. However, due to the immediate solidification of the reaction mixture, efficient stirring was prevented, leaded to a low yield. For this reason experiments with tetrahydrofuran and methanol as solvents were performed. The best results and most homogeneous reaction mixtures were achieved in tetrahydrofuran. Therefore all the experiments for the synthesis for this compound were conducted in tetrahydrofuran as solvent. MMDTCE (Scheme 4.3, **16**) was synthesised via simple electrophilic substitution of *N*-methyl-*N'*-phenyl-1,2-ethylenediamine (MPEDA, **18**) with carbon disulphide, in the presence of sodium hydroxide as base. Methyl iodide was added to the resultant dithiocarbamate salt to form the ester.

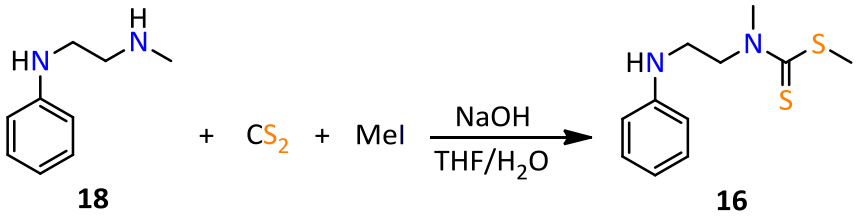

Scheme 4.3: Schematic representation of the synthesis of MMDTCE (**16**) via electrophilic substitution of MPEDA (**18**) with carbon disulfide. Methyl iodide was added to the dithiocarbamate salt to form the ester.

The obtained product was isolated as yellow oil and characterised by ^{1}H, ^{13}C and DEPT NMR, MS and EA (4.3.4, page 161 and 5C.1, page 234: from Figure Apx C.4 to Figure Apx C.11).

MPEDA (**18**), that is a precursor in the above reaction, was synthesised in house as well. The 1,2-ethanediamines are an important class of materials which are useful for various applications such as intermediates in the synthesis of pharmaceuticals and for

use in photographic applications. This is why their synthesis has been well explored, and ways for use of environmentally friendly reagents were investigated (Taniguchi *et al.* **2009**; Azizi *et al.* **2006**; Altman *et al.* **2002**; Heinrich *et al.* **2001**; Salerno *et al.* **1997**; Poindexter *et al.* **1992**; Poindexter, **1981**). For the synthesis of MPEDA a synthetic method that was adopted from Poindexter (**1981**) was applied. The process involved the aminoethylation of aniline hydrochloride with one equivalent of *N*-methyl-2-oxazolidinone at 140 °C. Under these conditions, the *N*-methyl-2-oxazolidinone is ring-opened at the fifth position and decomposes to form carbon dioxide as a by-product and the desired aminoethylated aromatic amine hydrochloride. Neutralisation of the hydrochloride salt with base affords the free aminoethylated aromatic amine.

The ability of aromatic amine salts and of aliphatic amine salts to promote ring-opening, could be explained as a function of the relative acidities of their corresponding conjugate acids. Aromatic amine salts have a pK_a around 5, whereas in contrast aliphatic amine salts have a pK_a of around 10. That is why aliphatic amines are not strong enough acids to initiate this reaction.

The mechanism of the reaction is illustrated in Scheme 4.4. Protonation of **19** by the amine salt at high temperatures could lead directly to intermediate **20**, followed by ring-opening by nucleophilic attack at C-5 with aniline, leading to intermediate **22**. Loss of carbon dioxide leads to the product **23**. Alternatively, ring-opening could also occur through an aziridinium species, such as **21**. Nucleophilic attack at the C-2 position of **21**, would result the intermediate **22**, and the product **23**.

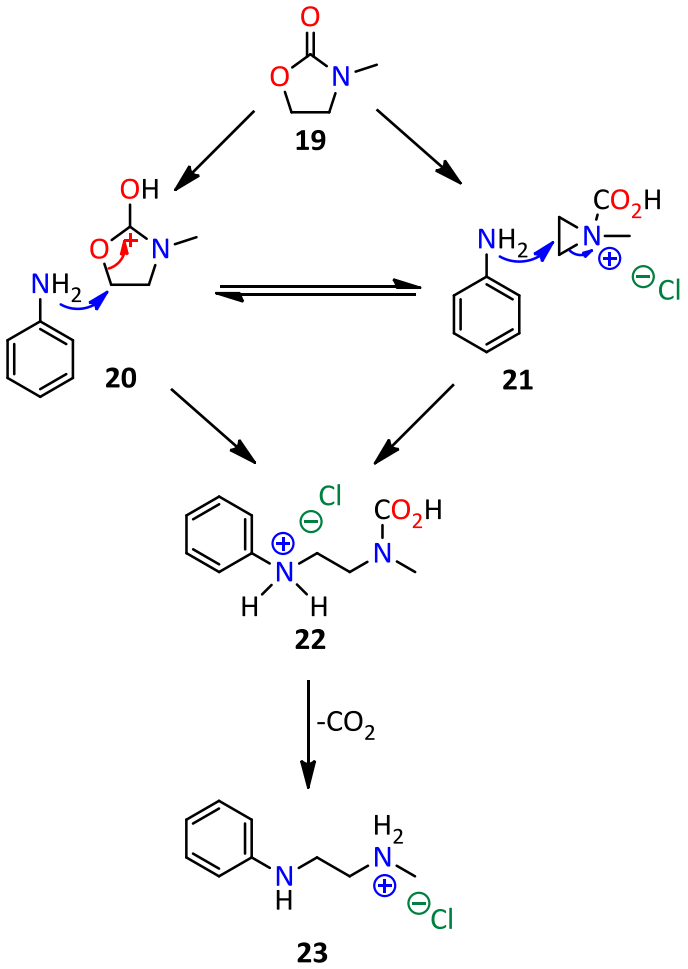

Scheme 4.4: Schematic representation of the mechanism for the synthesis of MPEDA hydrochloride (**23**). The mechanism is adapted from Poindexter *et al.* (**1992**).

MPEDA was successfully synthesised and characterised by ^{1}H, ^{13}C and DEPT NMR (4.3.3, page 160 and 5C.1, page 234: Figure Apx C.1,Figure Apx C.2 and Figure Apx C.3).

4.2.2 Conductivity enhancement of chemically polymerised poly (NDDEAEA) and poly (MMDTCE) during UV irradiation

NDDEAEA, MMDTCE and aniline hydrochloride were chemically polymerised and deposited over interdigitated microsensor electrodes (IMEs) (Figure 4.2). Thick layers were formed on the surface of the electrodes as the polymer thickness is in important characteristic in sensors (Bodugoz-Senturk and Guven, **2011**) (5B.3.2, page 229:

Figure Apx B.7 and Figure Apx B.8 and 5C.2, page 243: Figure Apx C.12 and Figure Apx C.13). For all three different materials similar conditions of polymerisation were applied in order to achieve comparable results. The potential of poly (NDDEAEA), poly (MMDTCE) and PANI (control) deposited over IMEs was monitored during UV irradiation, using a lock-in-amplifier. The current was calculated from Ohm's law. *N*-alkyl substituted PANIs have conductivities in the range of 10^{-2}-10^{-7} S cm^{-1} (Long *et al.* **2004**) as was observed in this case as well. The different materials were compared in their doped and dedoped states. When the doped state was used, a reversible increase in the current with application of UV light was observed. This increase was dependent on the intensity of the light and showed saturation behaviour at 50 % lamp intensity. The response was immediate with starting or stopping the UV light source and was constant over the whole irradiation period. The increase in current was greater with poly (NDDEAEA) and poly (MMDTCE) than with PANI (Figure 4.3, Figure 4.4 and Figure 4.5). All the materials showed unstable baselines. When the dedoped state was used the polymers did not show any response in their conductivity during UV irradiation.

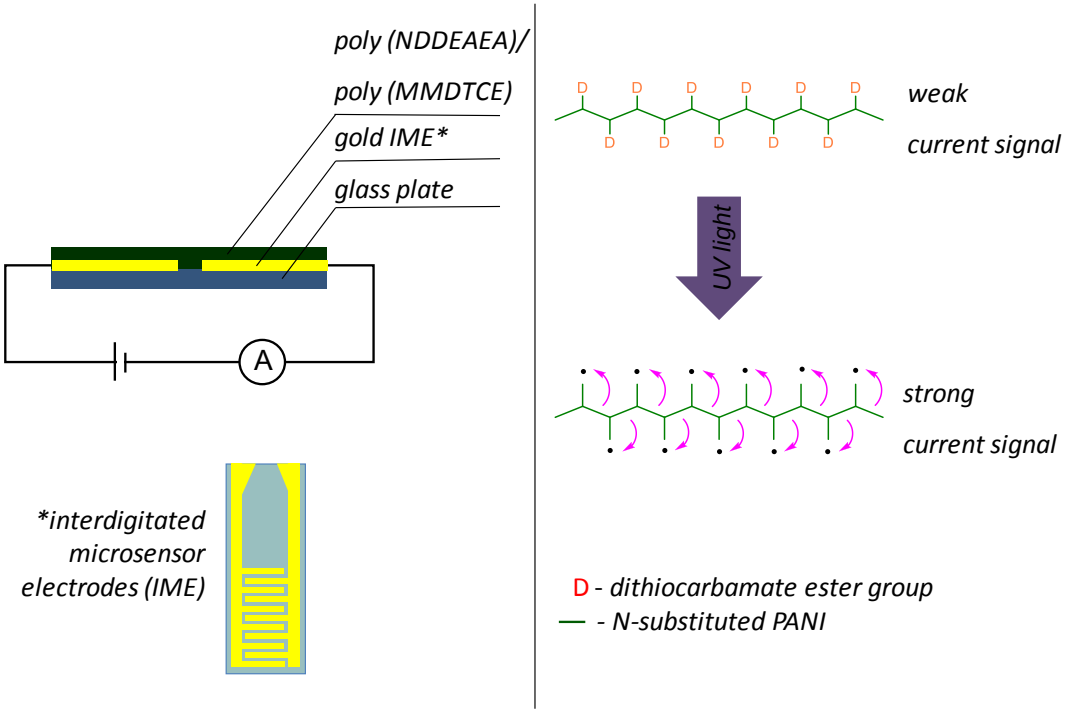

Figure 4.2: Conductivity measurements experimental set up diagram and principal idea behind the expected result.

For poly (NDDEAEA) the baseline at the beginning of the experiment was at 1.46 × 10^{-3} S cm^{-1} which showed a constant slow increase up to 1.465 × 10^{-3} S cm^{-1} (Figure 4.3). This increase could be due to a decrease in the band gap energy (Bardavid *et al.* **2011**). Also cross-linking could occur, predominantly due to chain scission, which leads to increase in the conductivity after UV irradiation. After applying 50 % light intensity the current jumped rapidly to 1.49 × 10^{-3} S cm^{-1} from 1.463 × 10^{-3} S cm^{-1}. This could be explained by an increase in the hole mobility, leading to an increase in the hopping probability from one conducting system to the other (Bardavid *et al.* **2011**). With UV irradiation more polymer bonds break and intrinsic conduction increases because more *free* electrons and holes are produced, thus resistance of the polymer decreases, resulting in increasing conductivity. This behaviour was observed for all the three tested materials. During irradiation poly (NDDEAEA) forms short lived active radicals on each one of the polymer units. These could recombine with other active radicals from the neighbouring chains faster than they can participate in the hopping mechanism. This leads to the increase in the conductivity after each step of irradiation.

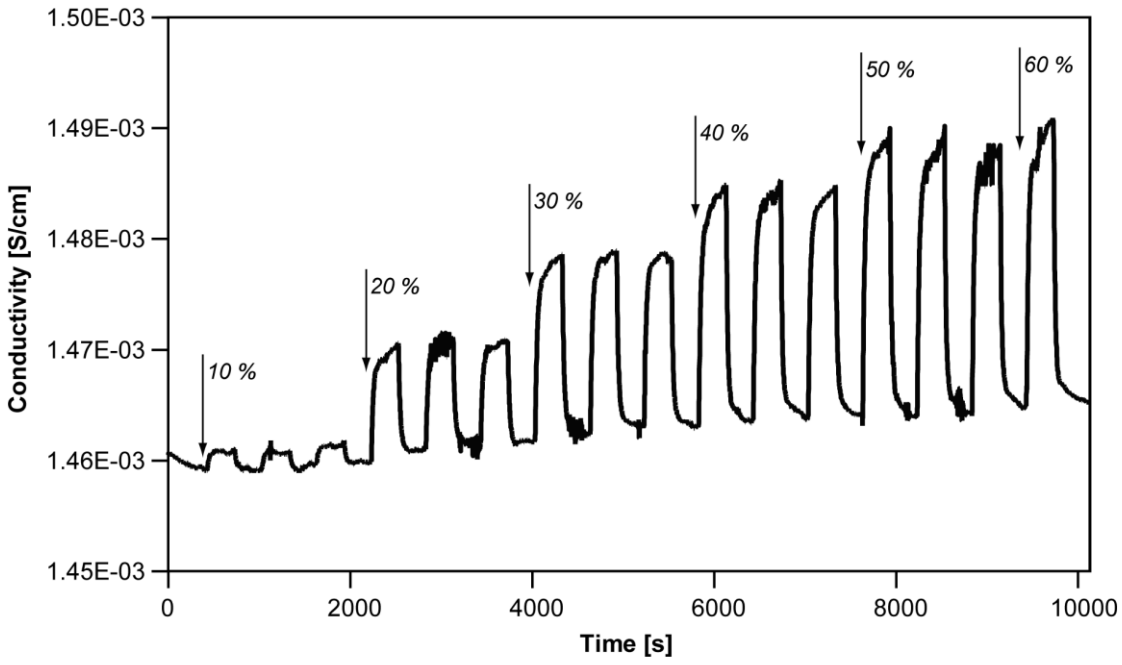

Figure 4.3: Change in conductivity observed for poly (NDDEAEA), doped with 1 M hydrochloric acid, coated onto IMEs during UV irradiation. The intensity of the UV source was varied from 10 to 50 %. Each intensity level was repeated three times per electrode.

With poly (MMDTCE) the baseline settled down to 3.25×10^{-3} S cm^{-1} in the beginning of the experiment which dropped to 2.65×10^{-3} S cm^{-1} during the course of the experiment (Figure 4.4). This phenomenon could be due to decreasing electrical conductivity of the polymer as a result of an increase in the surface band bending and a reduction in the work function (Yow-Jon *et al.* **2007**). Also this fact could be attributed to the chain scission after UV irradiation that could occur predominantly to chain recombination (Kane *et al.* **2010**). The baseline conductivities changes were limited to the physical changes in the polymer structure. When 50 % intensity was applied, there was an immediate response of 3.20×10^{-3} S cm^{-1} from 2.65×10^{-3} S cm^{-1} baseline. The last peak at 60 % was much higher than the rest but this result was not a reproducible event. The response with poly (MMDTCE) was higher than with poly (NDDEAEA). This could be due to the formation of longer lived *dormant* radicals along the polymer chain. They are able to live long enough to participate in the hopping mechanism and to increase the doping level of the polymer (Gizdavic-Nikolaidis *et al.* **2004**).

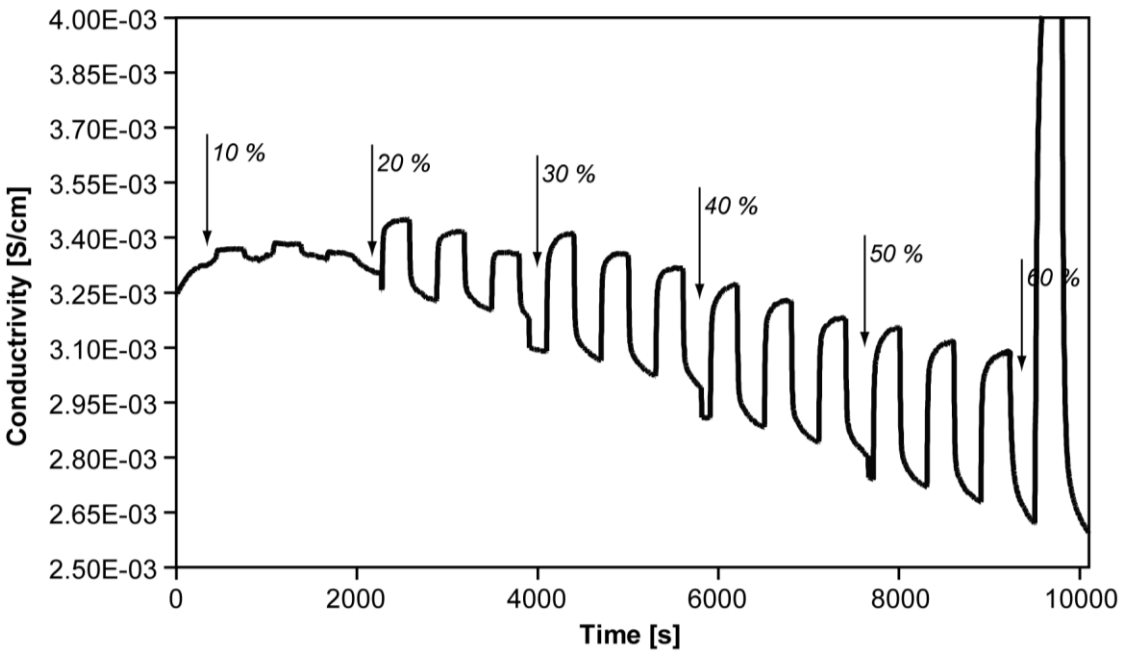

Figure 4.4: Change in conductivity observed for poly (MMDTCE) coated IMEs doped with 1M hydrochloric acid, during UV irradiation. The intensity of the UV source was varied from 10 to 50 %. Each intensity level was repeated three times per electrode.

In the case of PANI the initial baseline signal was at 1.43 × 10^{-3} S cm^{-1}, which value was increasing constantly during the whole experiment up to 1.82 × 10^{-3} S cm^{-1} (Figure 4.5). This event was analogous to the one observed with poly (NDDEAEA). Here also a cross-linking could occur predominantly to chain scission, which leads to increase in the conductivity (Bardavid *et al.* **2011**). The material showed a jump in the current from 1.79 × 10^{-3} Scm^{-1} to 1.96 × 10^{-3} Scm^{-1} with 50 % intensity. The UV initiated response was weaker than the one registered for poly (MMDTCE).

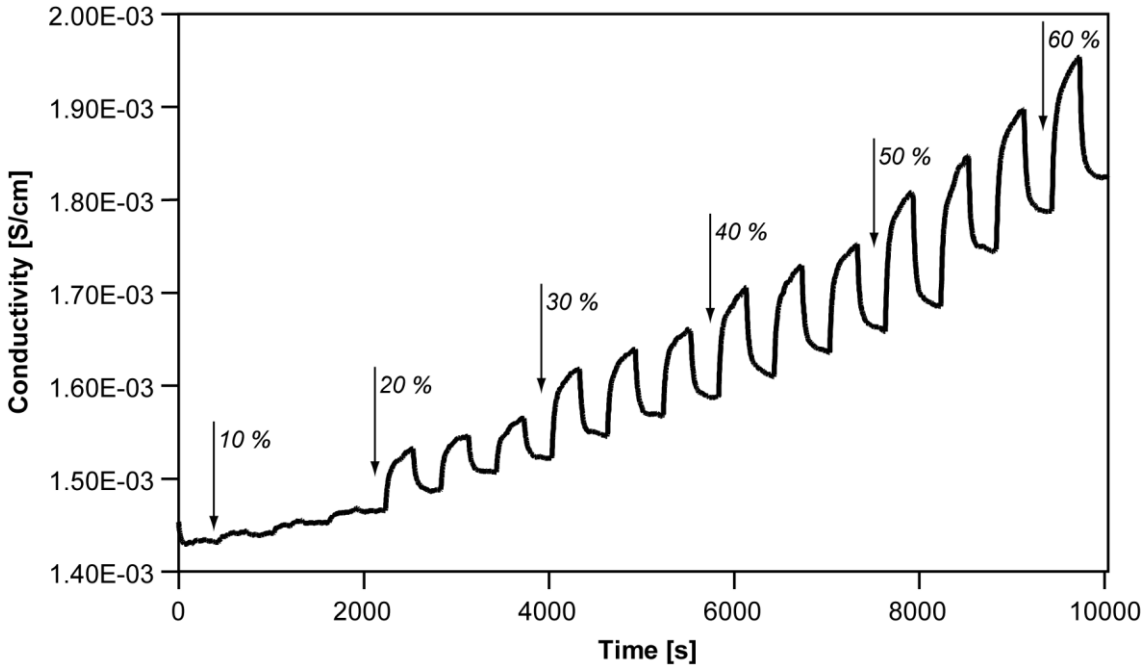

Figure 4.5: Change in conductivity observed for PANI, doped with 1 M hydrochloric acid, coated IMEs during UV irradiation. The intensity of the UV source was varied from 10 to 50 %. Each intensity level was repeated three times per electrode.

The baseline instability was higher for PANI - an increase of around 0.39 × 10^{-3} S cm^{-1}, than for poly (MMDTCE) - a decrease of around 0.6 × 10^{-3} S cm^{-1}, and the lowest change was seen with poly (NDDEAEA) – an increase of around 0.01 × 10^{-3} S cm^{-1}. The observed baseline instability can be attributed to physical and/or structural changes that may have occurred in the polymer, such as cross-linking (increase in conductivity) or scission of the polymer chain (decrease in conductivity). The *N*-substituted PANI used showed greater stability during UV irradiation than its unsubstituted structural analogue due to the showed higer stability of the baceline. The difference in the

behaviour of the three materials is due to the different oxidation potential needed for redox process or for destruction of the chain. Poly (MMDTCE) is less stable under UV irradiation and decomposes faster (decrease in the baseline after UV irradiation) than poly (NDDEAEA). In the case of poly (NDDEAEA) the increase in the baseline conductivity is clear evidence for cross-linking (active radical recombination) having occurred in the course of UV irradiation.

The highest change of conductivity was calculated to be with poly (MMDTCE): 0.6×10^{-3} S cm^{-1}, than with PANI: 0.17×10^{-3} S cm^{-1}, and the lowest was with poly (NDDEAEA), 0.03×10^{-3} S cm^{-1}. Poly (MMDTCE) forms *dormant* radicals along the polymer chain during UV irradiation. These radicals could live long enough that instead of recombining instantly, they may participate in the hopping mechanism (Gizdavic-Nikolaidis *et al.* **2004**). This hopping leads to an increase in the doping state of the polymer.

Due to the fact that PANIs are very sensitive to oxidation, all the experiments were conducted under a flow of nitrogen. The temperature on the surface of the electrode during irradiation was measured with a thermocouple in order to determine if the effect observed upon irradiation was due to increases in temperature (Table 4.1). The response to UV irradiation of the working surface of the electrode was immediate. It did not following the pattern of temperature change which was very slow.

Table 4.1: Measurement of the electrode surface temperature with thermocouple with nitrogen gas flow and in air. The readings were taken at the end of a five minutes irradiation period.

light intensity [%]	Temperature, N_2 flow [°C]	Temperature, air [°C]
0	24.4	24.1
10	25.5	24.6
20	25.0	26.5
30	25.4	27.2
40	25.5	28.6
50	25.9	29.5

In order to investigate the influence of the method by which the monomers were polymerised on the enhancement of the current during UV irradiation, different polymerisation methods were compared. Conductivity measurements were also performed with doped electropolymerised materials on the surface of the IME. Via electropolymerisation higher order polymers are created which should lead to higher enhancement in the conductivity. Changes in the conductivity dependent upon the UV irradiation with the electopolymerised materials were not monitored. The reason behind this result is that the polymers on the surface of gold electrodes could not form as thick layer as the chemically deposited materials. For the conventional film sensors, the current response is strongly affected by the film thickness (Guven, O. **2007** and Bodugoz-Senturk, H. *et al.* **2011**).

4.2.3 UV spectroscopy of chemically polymerised poly (NDDEAEA) and poly (MMDTCE) before and after UV irradiation

Poly (NDDEAEA), poly (MMDTCE) and PANI were deposited on the walls of cuvettes as films during chemical polymerisation using the same conditions as those used for the conductivity measurements (5B.3.2, page 229: Figure Apx B.7 and Figure Apx B.8 and

5C.2, page 243: Figure Apx C.12 and Figure Apx C.13). The materials were dried and in the quvettes nitrogen atmosphere was established. UV measurements before and after UV irradiation were taken (Figure 4.6). Samples in the doped and dedoped state were compared. Spectra were taken every five minutes for twenty minutes total irradiation time per sample. There was no change in the spectra of poly (NDDEAEA) and PANI after irradiation neither in the doped nor in the dedoped state. Poly (NDDEAEA) and poly (MMDTCE) showed absorption peaks at λ_{max} = 247 and 275 nm which are attributed to the –S-C=S and S=C-N groups of DTCE groups respectively.

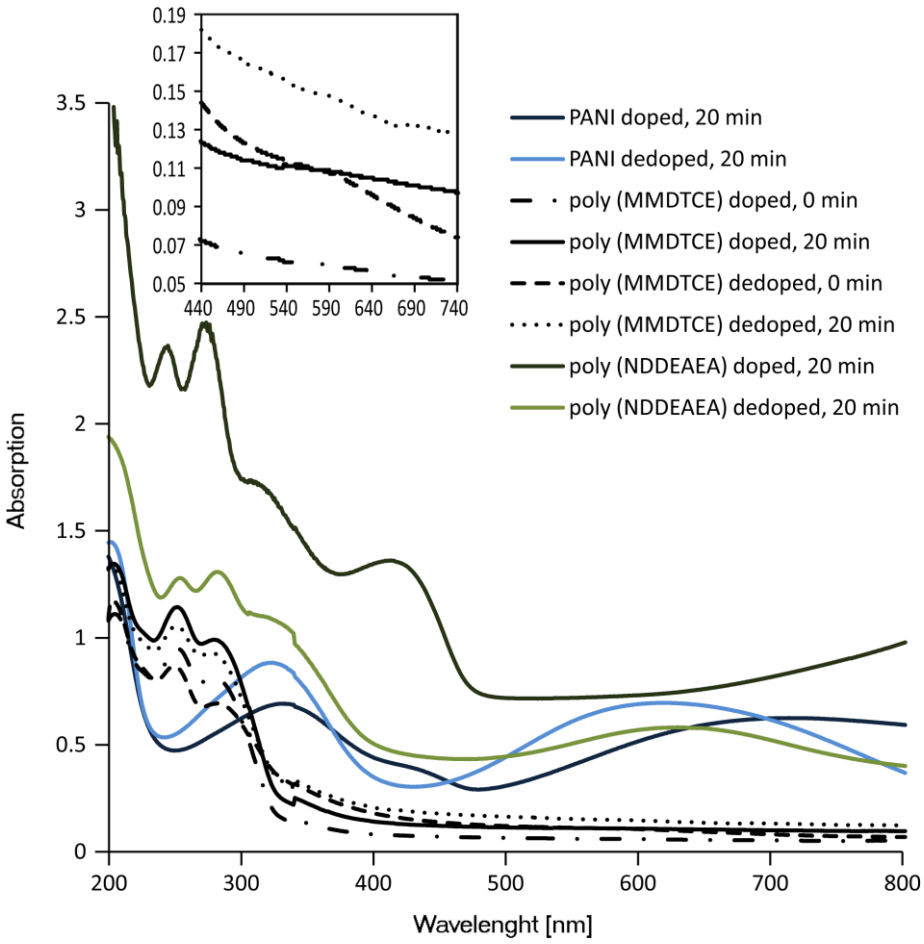

Figure 4.6: UV spectra of chemically polymerised PANI, poly (NDDEAEA) and poly (MMDTCE) deposited on the walls of quarts cuvettes. For reference nitrogen gas was used.

The spectrum of doped poly (NDDEAEA) showed three characteristic absorption bands due to PANI at around 300, 400 and 600 nm. The characteristic peaks of doped PANI appear at about 320 nm due to the π–π^* transition of the benzenoid ring and at about

400-430 nm and 730–825 nm due to polaron-π^* and π-polaron band transitions respectively, showing that PANI is present in the doped state (Abdiryim *et al.* **2005**; Stafstrom *et al.* **1987**). When the dedoped state of poly (NDDEAEA) and PANI was analysed the characteristic peaks of the PANI chain showed the expected shift to 300 nm and 600 nm, respectively (Ivanova-Mitseva *et al.* **2010**; Stafstrom *et al.* **1987**).

The characteristic peaks for the DTCE group in the spectra of poly (MMDTCE) were present, analogously to the case with poly (NDDEAEA) but they were increasing by intensity with the irradiation time. This phenomenon could be due to the fact that when irradiated this material frees a *dormant* radical that is attached to the PANI chain and an active methyl radical that could be volatile. The possible recombination of the *dormant* radicals formed in this way should be with another *dormant* radical from the nearest neighbour chain. This event would lead to small increasing in the concentration of the dithiocarbamete moeities. The formation of an even end optically transparent layer with this material was extremely hard, although many attempts were made to create a better layer, but all proved unsuccessful. The material deposited on the walls did not forme an even layer. This was due to the fact that the polymer was precipitating at the bottom of the cuvette faster than the other materials and the absorption to the cuvette walls was hampered. The characteristic peaks for PANI backbone were with very low intensity at around 550 nm for the doped state and at around 600 nm for the dedoped state (Stafstrom *et al.* **1987**).

These results were in correspondence with the results from the conductivity measurements and with the proposed mechanism as there were no DTCE structural changes in the polymers after UV irradiation. In the case of poly (NDDEAEA) the DTCE groups were predominantly recombining after irradiation in dry state and that is why no change in their concentration was observed by UV spectroscopy. With poly (MMDTCE) the recorded slight increase in the concentration of the DTCE group was a logical representation of the fact that thiuram disuflfides were formed after the removal of the highly volatile active methyl radical after irradiation. This cross-linking would lead to increased polymer density and to higher conductivity enhancement.

4.2.4 Electron spin resonance (ESR) of chemically polymerised poly (NDDEAEA), poly (MMDTCE) and PANI

Chemically polymerised poly (NDDEAEA), poly (MMDTCE) and PANI (5B.3.2, page 229: Figure Apx B.7 and Figure Apx B.8 and 5C.2, page 243: Figure Apx C.12 and Figure Apx C.13) were analysed with ESR spectroscopy in dry state, in nitrogen atmosphere, before and during UV irradiation (Figure 4.7, Figure 4.8 and Figure 4.9) at 120 K temperature. In all the samples very strong signals were observed, corresponding to the delocalised conducting electrons of the PANI chain (Langer, J. J. *et al.* **2001**). All anilines were strongly paramagnetic materials with EPR spectral characteristics dependant on the electrical conductivity (Langer, J. J. *et al.* **2001**).

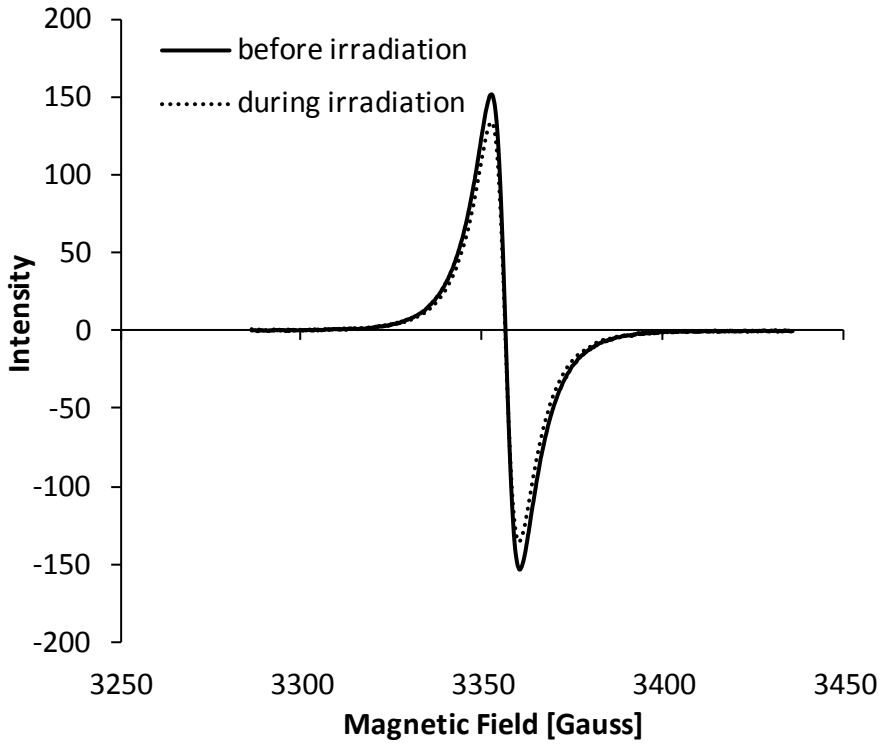

Figure 4.7: ESR spectrum of poly (NDDEAEA) before (solid line) and after (dotted line) UV irradiation at 120 K.

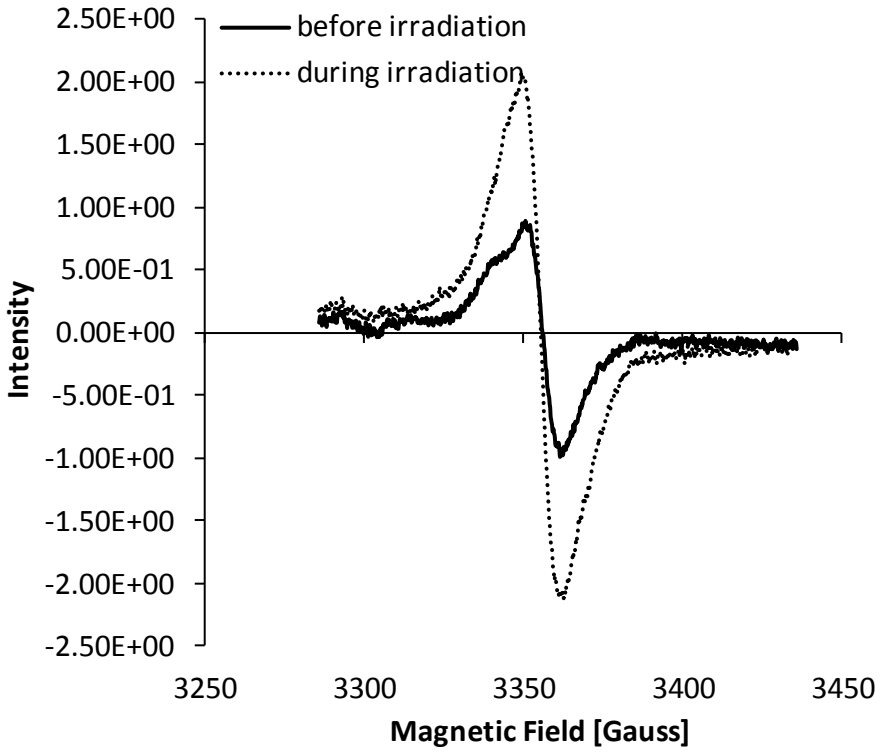

Figure 4.8: ESR spectrum of poly (MMDTCE) before (solid line) and after (dotted line) UV irradiation at 120 K.

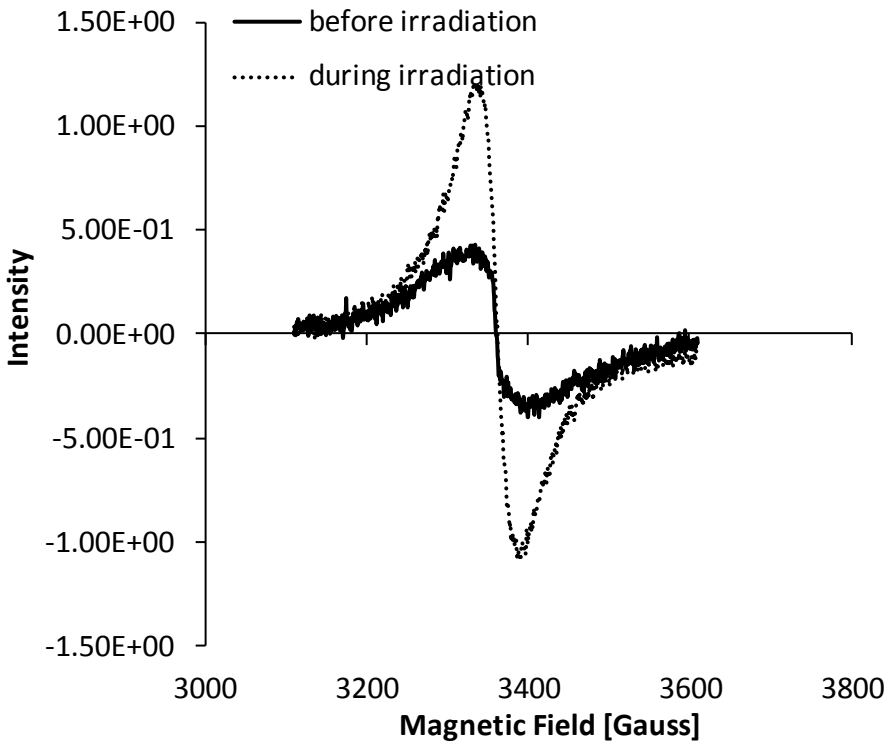

Figure 4.9: ESR spectrum of PANI before (solid line) and after (dotted line) UV irradiation at 120K.

EPR is a sensitive tool to detect the electron transfer processes. During irradiation increase of the conductive band of PANI was observed with PANI and with poly (MMDTCE). With PANI the signal increased from around 0.4 to 1.0 in intensity (Langer *et al.* **2001**). This increase as well as the initial value was higher with poly (MMDTC) – from 0.9 to 2.2 (3356). The increase in the signal of poly (MMDTCE) is due to electron transfer from nitrogen atoms of PANI backbone chain of poly (MMDTCE) to the dithiocarbamate stable radicals, which makes PANI backbone chain form more radical cations than before and reduces the dithiocarbamate *free* radicals (Zheng *et al.* **1997**). This result is in correspondence with the increase of conductivity and the hopping mechanism discussed previously.

With poly (NDDEAEA) the intensity changes were from 153 before irradiation to 127 during irradiation (3356). This slight decrease in the signal intensity could not be explained by the same mechanism. On the other hand the intensity of the signal was the highest with poly (NDDEAEA) even before irradiation. The difference in the

intensity of poly (NDDEAEA) and poly (MMDTCE) was significant, almost 150 times higher. The possible reason behind this result could be due to the presence of the active instead of *dormant* radicals on each building block of the polymer which can lead to predominantly recombination with *dormant* or active radicals.

4.2.5 Confocal laser scanning microscopy of chemically polymerised poly (NDDEAEA), poly (MMDTCE) and PANI

For a better understanding of the properties of the three materials used in this work, confocal laser scanning microscopy was used to analyse the surface of the materials (from Figure 4.10 to Figure 4.15). All three materials were chemically polymerised (5B.3.2, page 229: Figure Apx B.7 and Figure Apx B.8 and 5C.2, page 243: Figure Apx C.12 and Figure Apx C.13) over 96 % Al_20_3 supports.

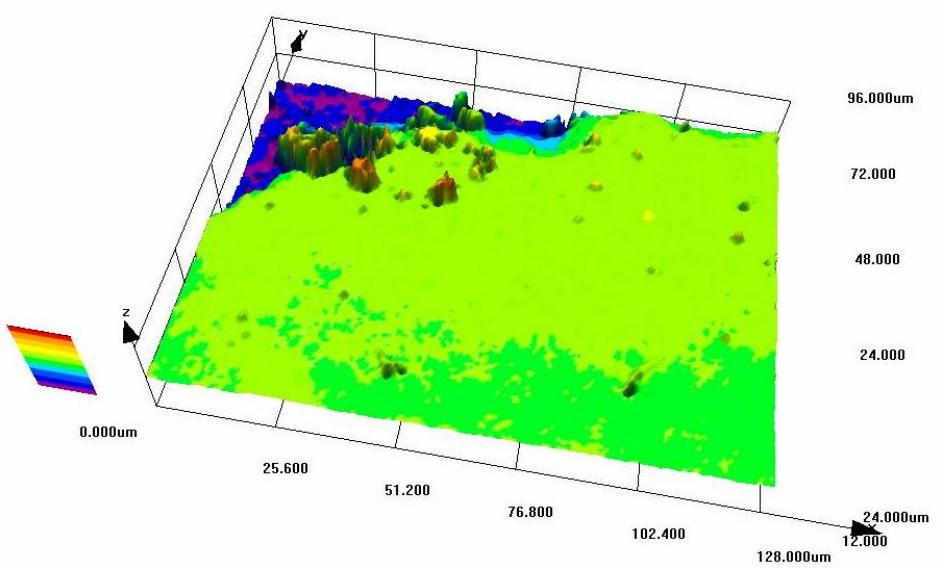

Figure 4.10: Confocal 3D laser topography of PANI layer deposited over 96 % Al_20_3 support (blue top corner).

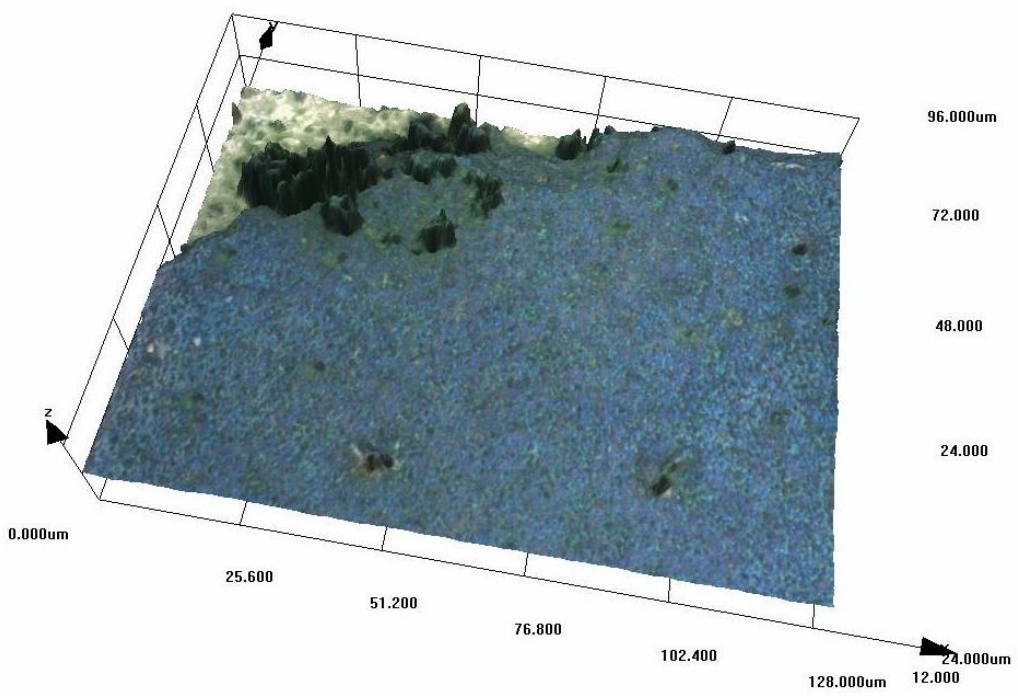

Figure 4.11: Confocal 3D laser colour model of PANI showing a blue, fine structure continuous organic layer over 96 % Al_20_3 support (the white top corner).

The image above depicts a 3D laser colour model of PANI, showing a blue-light green, finely porous structure of an uninterrupted continuous PANI layer over 96 % Al_20_3 support (Figure 4.11, white area, top left). The black top left spikes are artificial of analytical method and indicate light absorbing areas. The PANI layer is horizontal to the mineral substrate surface and adheres sufficiently to it.

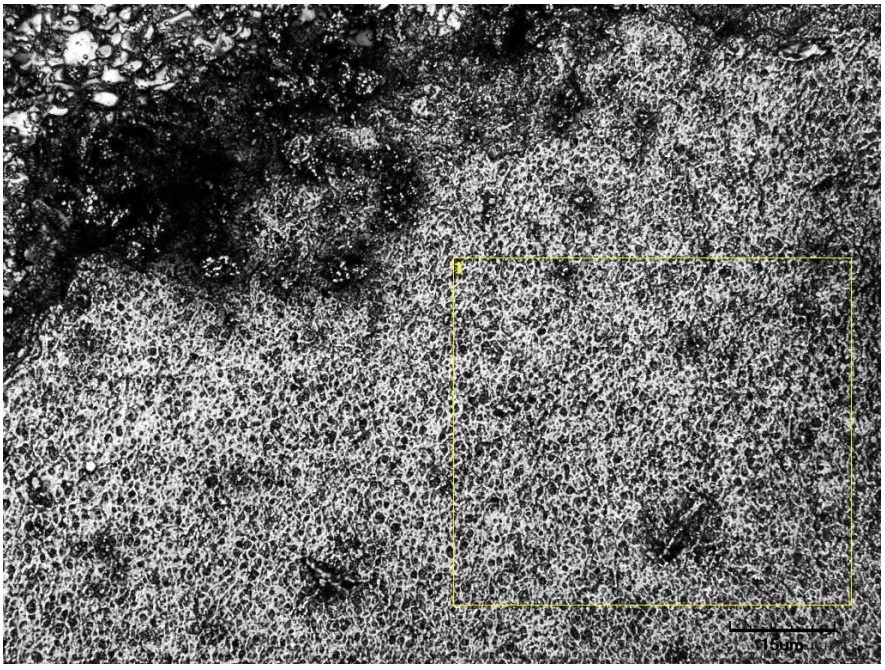

Figure 4.12: 2D laser monochromatic con-focal surface reproduction of PANI at a 2300 times magnification (scale bar 15 µm).

The PANI, analysed at this higher resolution (approximately 2300 times, Figure 4.12), exhibits clearly a fine porous structure (including sub-micron nonporous). The statistically analysed area of the picture (1, yellow rectangle, right bottom) shows a 3021 sq. µm surface versus a 3240 sq. µm area, indicative of mild texture unevenness and, again, porosity. Further statistical analysis reveals an average surface roughness of SRa 310nm, which is homogeneously distributed.

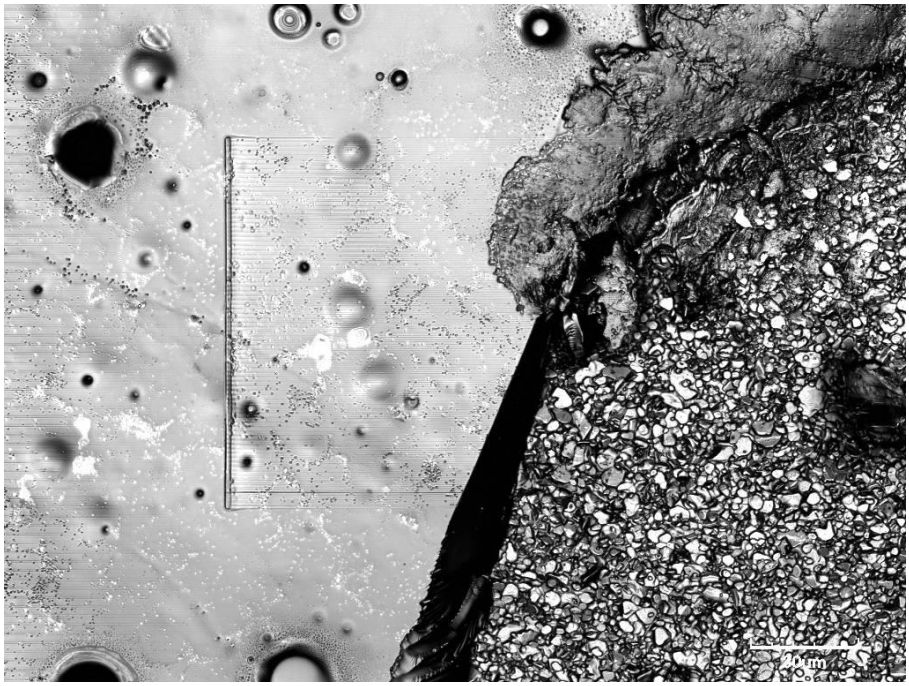

Figure 4.13: 2D laser monochromatic con-focal image of poly (NDDEAEA) (left) over an Al_2O_3 96% substrate support (right) (scale bar 20 µm).

The poly (NDDEAEA) layer is continuous, smooth, however, deep circular opening are observed on the surface, which could be a result of an outgassing process, or fast drying (Figure 4.13). The microstructure of poly (NDDEAEA) (left) is much finer and smoother than that of the alumina crystalline substrate (right) and to that of PANI. Poly (NDDEAEA) has a surface of 10187 sq. µm and an area of 10320 sq. µm, allowing for the much coarser openings. Poly (NDDEAEA) measured surface roughness, analysed using the SRa methodology, is 130 nm.

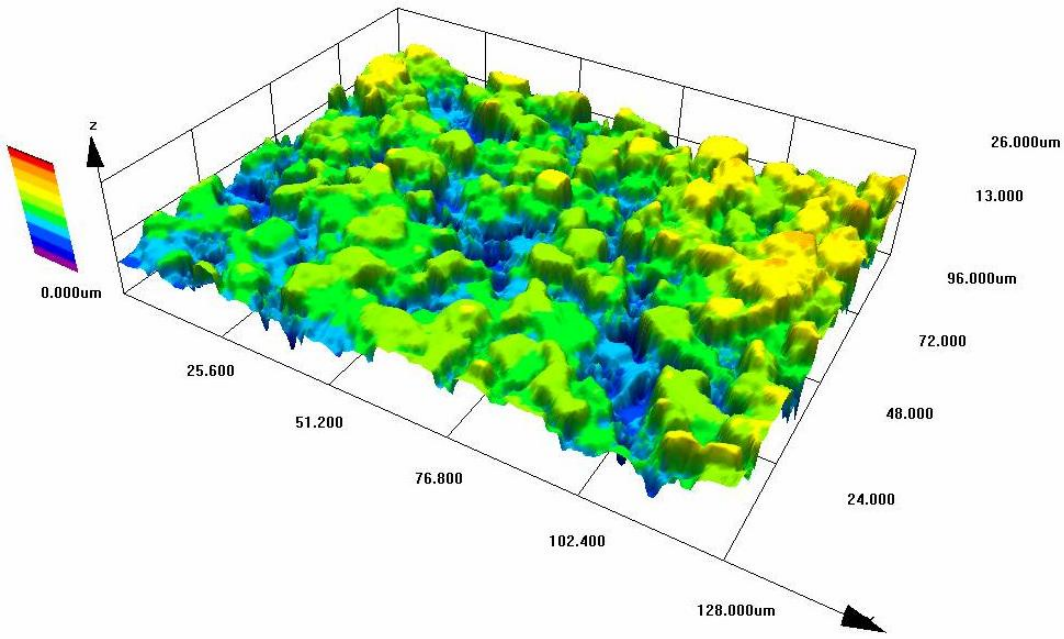

Figure 4.14: 3D laser con-focal surface topography model of poly (MMDTCE).

The topography demonstrates a much coarser surface structure, as compared to PANI and poly (NDDEAEA), consisting of approximately evenly distributed peaks and valleys (Figure 4.14).

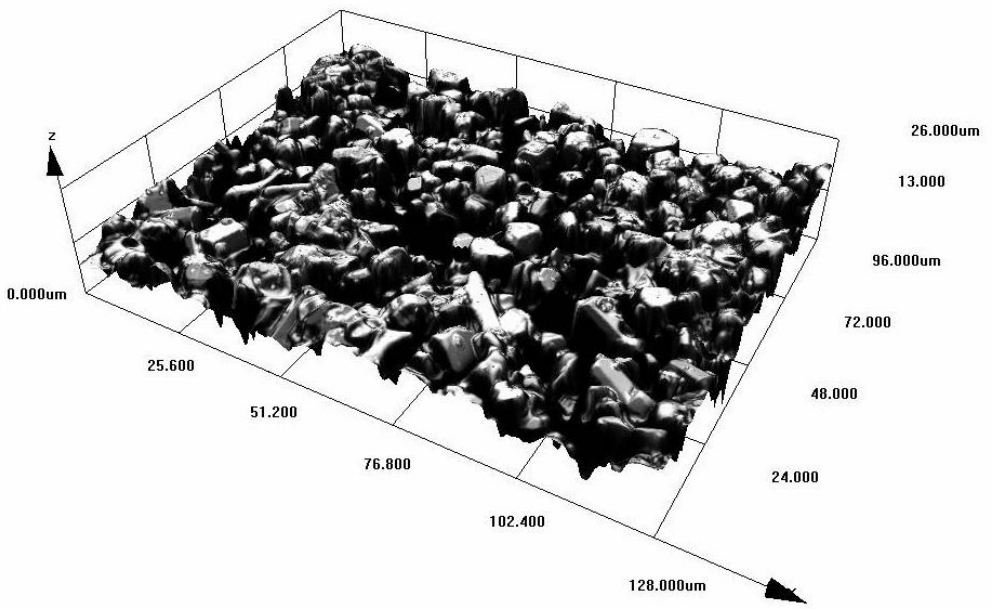

Figure 4.15: 3D laser con-focal surface texture model of poly (MMDTCE).

The texture of poly (MMDTCE), as imaged above consists of agglomerate-like particle clusters of even shapes, resembling crystal agglomerations (Figure 4.15). Poly (MMDTCE) possesses a surface of 7906 sq. µm versus a surface area of 16597 sq. µm reflecting the much greater surface roughness and inhomogeneity. The SRa equals 1670 µm, which is significantly greater than the other two analysed samples: PANI and poly (NDDEAEA), respectively.

Compound roughness coefficients of the analyzed materials in increasing order were: poly (NDDEAEA) 1.013, PANI 1.072 and poly (MMDTCE) 2.099.

4.2.6 Conductivity measurements of electrochemically polymerised poly (NDDEAEA), poly (MMDTCE) and PANI during UV irradiation

The three materials of interest were polymerised not only chemically but also electrochemically on the surface of screen-printed electrodes, in order to compare their CV behaviour during UV irradiation this time in electrolyte solution. Figure 4.16 shows the CV obtained during the electropolymerisation (20 cycles) of NDDEAEA in a 3:1 mixture of hydrochloric acid (0.75 M) and acetonitrile solution, clearly displaying oxidation and reduction peaks at +0.57 V and +0.47 V (versus Ag/AgCl) respectively (Ivanova-Mitseva *et al.* **2010**; and 3.2.2, page 100). The obtained electrochemical behaviour is quite similar to that obtained during the polymerization of aniline and ring-substituted anilines dissolved in acidic solutions (Lakshmi *et al.* **2009**; Ulgut *et al.* **2006**; Schomburg and McCarley, **2001**; Bidan *et al.* **1989**; Hayes and Shannon, **1996**; Diaz and Logan, **1980**). The large currents observed at the positive end of the CV are due to the superposition of two distinct processes: one is the electron transfer from the poly (NDDEAEA) film corresponding to the oxidation of the PANI film and the other is the electron transfer from the NDDEAEA monomer to the electrode corresponding to the oxidation of the NDDEAEA monomer to produce a precursor for the PANI film.

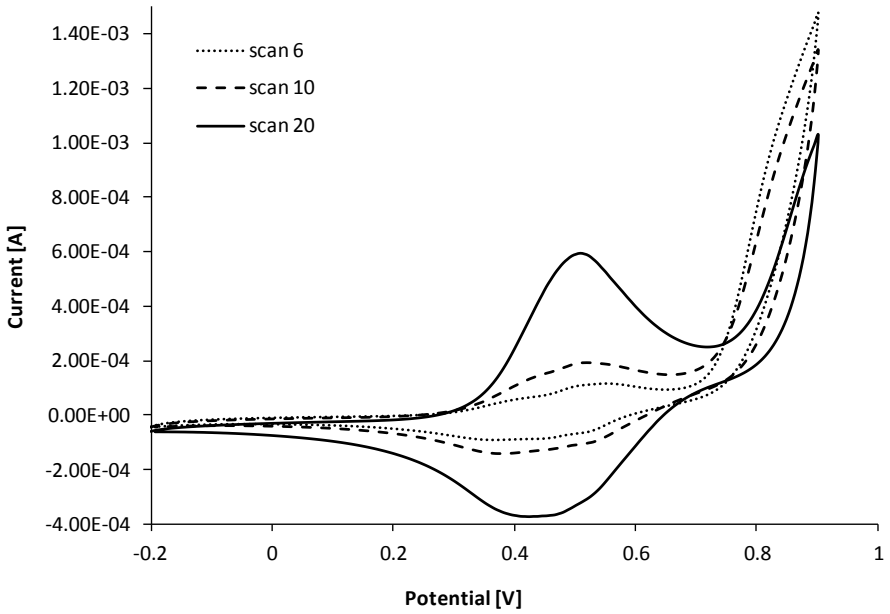

Figure 4.16: Cyclic voltammogram obtained during deposition of electropolymerised poly (NDDEAEA) films on gold screen-printed electrodes. The electropolymerisation of NDDEAEA (0.1 M in 0.75 M hydrochloric acid 25% acetonitrile in water) was obtained by cyclic voltammetry (potential range: -0.2 V to 0.9 V versus Ag/AgCl, at 100 mV s^{-1} scan rate, 20 sweeps), under nitrogen atmosphere and in the dark which afforded the generation poly (NDDEAEA).

In order to investigate the CV behaviour during UV irradiation of poly (NDDEAEA) films in electrolyte solution, the electropolymerised electrodes were dipped in hydrochloric acid (0.1 M) and the CV measured. The CV of poly(NDDEAEA), (Figure 4.17) showed quasi reversible peaks at +0.25 V which indicates the oxidation of leucoemeraldine to protonated emeraldine and also the peak at +0.50 V resulting from the oxidation of emeraldine and deprotonation of the polymer (Ivanova-Mitseva *et al.* **2010** and Inzelt and Horanyi, **1990**). During irradiation, a decrease of the current was observed. This decrease could be due to a loss of material due to increased solubility during UV irradiation. It could not be attributed to the stability of the polymer in electrolyte on its own as discussed by Ivanova-Mitseva *et al.* (**2010**) and in 3.2.2, page 100. CV is giving different type of information than the recorded current increase during irradiation. It is showing the stability of the formed layer in electrolyte solution under UV irradiation and the transformation between the different oxidative states of the polymer.

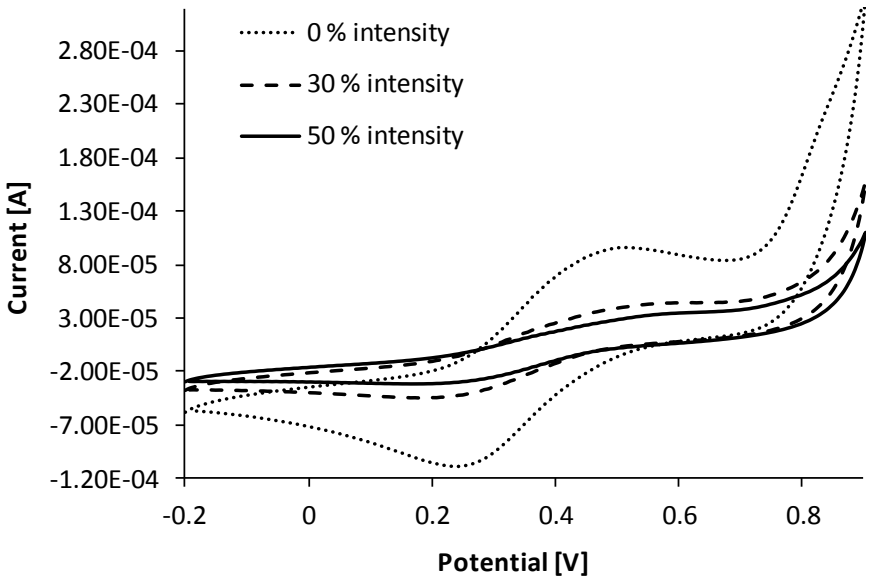

Figure 4.17: Cyclic voltammogram of electropolymerised poly (NDDEAEA) films obtained during UV irradiation (light intensity 0%, 10% and 50 %) in hydrochloric acid (0.1 M, 5 mL solution) on gold screen-printed electrodes by cyclic voltammetry (potential range: -0.2 V to 0.9 V versus Ag/AgCl, at 100 mV s^{-1} scan rate), under nitrogen atmosphere and in the dark.

For comparison reasons the same experimental conditions were applied to the other two materials. MMDTCE showed similar behaviour to that of NDDEAEA (Figure 4.18). The peaks are with lower height and shifted to smaller potentials when compared to the ones observed with NDDEAEA.

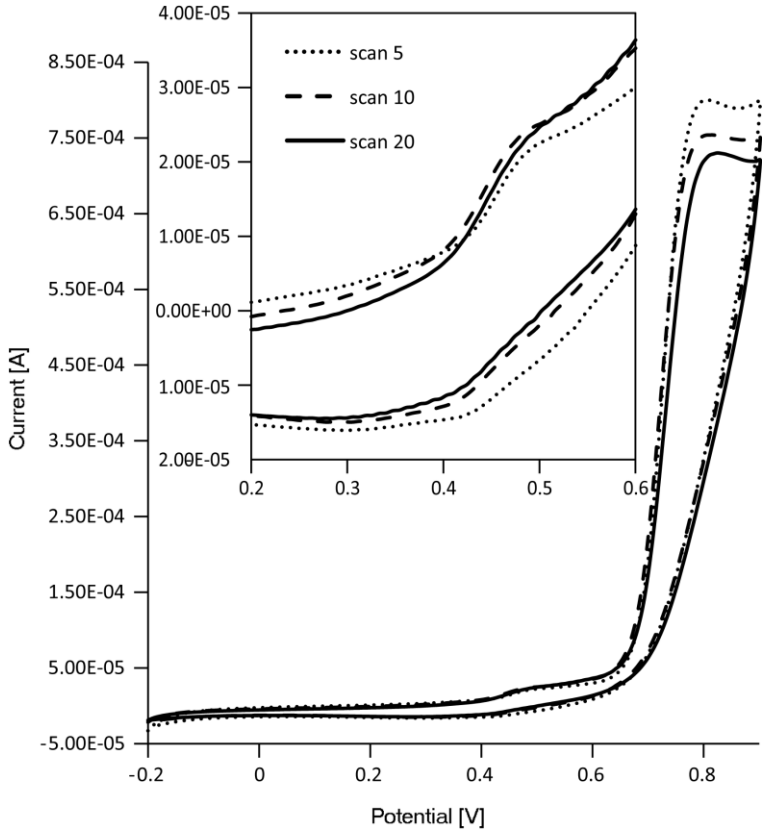

Figure 4.18: Cyclic voltammogram obtained during deposition of electropolymerised poly (MMDTCE) films on gold screen-printed electrodes. The electropolymerisation of MMDTCE (0.1 M in 0.75 M hydrochloric acid 25% acetonitrile in water) was obtained by cyclic voltammetry (potential range: -0.2 V to 0.9 V versus Ag/AgCl, at 100 mV s^{-1} scan rate, 20 sweeps), under nitrogen atmosphere and in the dark which afforded the generation poly (MMDTCE).

When the electropolymerised poly (MMDTCE) on screen-printed electrodes was inserted in electrolyte bath and irradiated the same behaviour typical for the previous analysed material was observed (Figure 4.19).

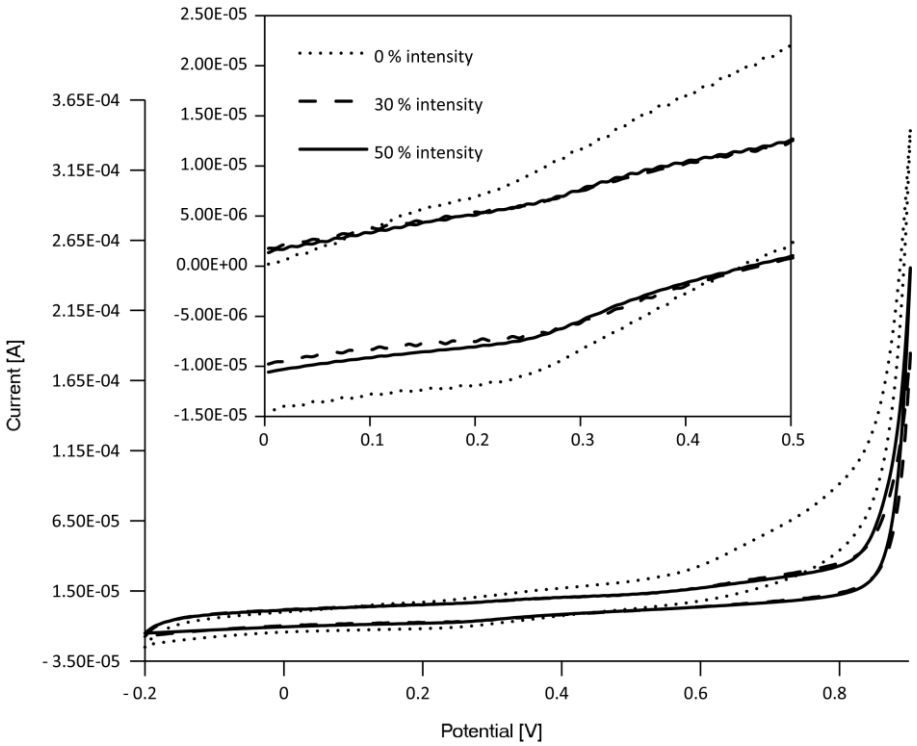

Figure 4.19: Cyclic voltammogram of electropolymerised poly (MMDTCE) films obtained during UV irradiation (light intensity 0%, 10% and 50 %) in hydrochloric acid (0.1 M, 5 mL solution) on gold screen-printed electrodes by cyclic voltammetry (potential range: -0.2 V to 0.9 V versus Ag/AgCl, at 100 mV s^{-1} scan rate), under nitrogen atmosphere and in the dark.

Aniline was elecropolymerised under the same conditions used for NDDEAEA and MMDTCE (Figure 4.20).

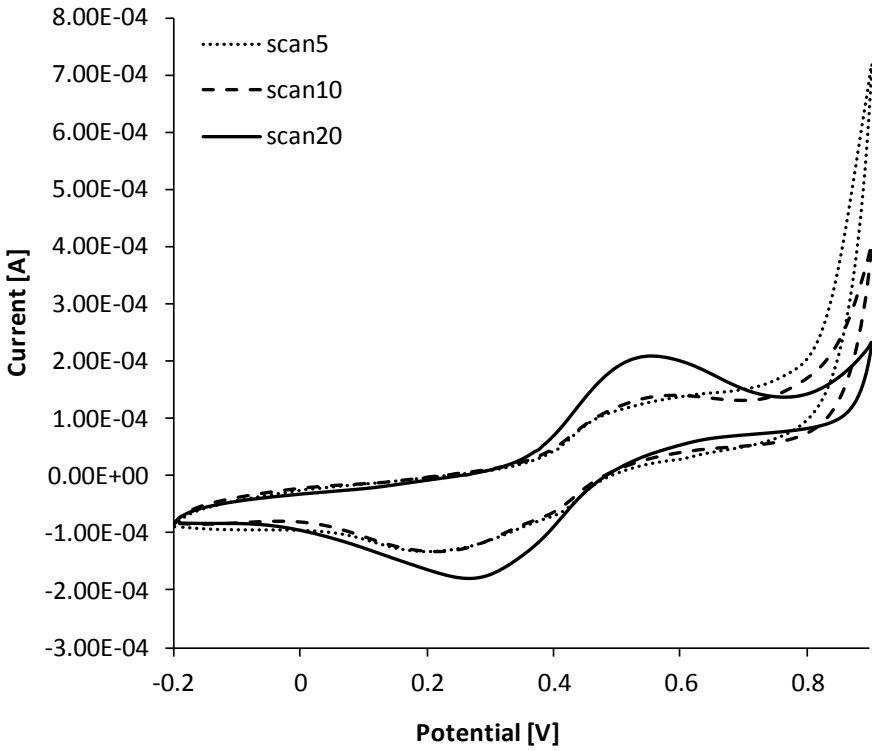

Figure 4.20: Cyclic voltammogram obtained during deposition of electropolymerised PANI films on gold screen-printed electrodes. The electropolymerisation of PANI (0.1 M in 0.75 M hydrochloric acid 25% acetonitrile in water) was obtained by cyclic voltammetry (potential range: -0.2 V to 0.9 V versus Ag/AgCl, at 100 mV s^{-1} scan rate, 20 sweeps), under nitrogen atmosphere and in the dark which afforded the generation poly (PANI).

The same behaviour was observed with PANI (Figure 4.21). This reproducible result with PANI and its *N*-substituted derivatives can be attributed to the redox processes involving the PANI backbone on the electrode surface, and to the loss of material during irradiation in solution.

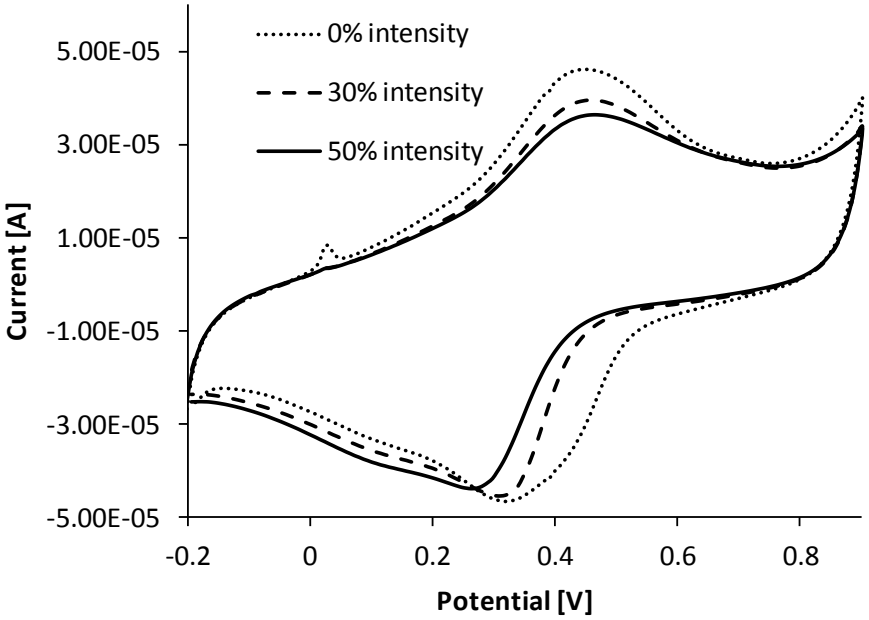

Figure 4.21: Cyclic voltammogram of electropolymerised PANI films obtained during UV irradiation (light intensity 0 %, 10 % and 50 %) in hydrochloric acid (0.1 M, 5 mL solution) on gold screen-printed electrodes by cyclic voltammetry (potential range: -0.2 V to 0.9 V versus Ag/AgCl, at 100 mV s^{-1} scan rate), under nitrogen atmosphere and in the dark.

These polymers, apart from the expected electrochemical activity due to the cation transportation, seem to be potentially attractive for optoelectronic devices, storage devices and sensor fabrication.

4.3 Experimental Details

4.3.1 Materials

N-Phenylethylene diamine (98 %), ammonium persulfate (98 %), methyl iodide (99 %), butyl lithium 2.5 M in hexane, ethylene dimethacrylate (98 %), acrylic acid (99 %), 1-(3-dimethylaminopropyl)-3-ethyl-carbodiimide hydrochloride (98 %), silica gel 60 (particle size 0.063-0.2 mm), 3-methyl-2-oxazolidinone (99.5 %), 2-(2-methoxyethoxy)ethanol (> 99 %), aniline (99.5 %), aniline hydrochloride (99%), and sodium hydroxide (100 %) were purchased from Sigma Aldrich (US). Carbon disulfide (99 %), diethyl amine (> 99 %), triethylamine (> 99 %), sodium hydrogen carbonate (99 %), sodium sulfate anhydrous (100 %), hydrochloric acid (36 %) were purchased from Fisher Scientific (UK). Tetrahydrofuran (99,85 %, extra dry) was purchased from Acros Organics. NMR solvents were obtained from Gross Scientific (UK). Ultra pure water (Millipore) was used for all analysis. All chemicals and solvents were analytical or HPLC grade and were used without further purification unless specified otherwise. Interdigitated monolitic gold microsensor electrodes (IME 1525.3-M-Au-U) were purchased from Abtech Scientific, Inc. (USA).

4.3.2 Apparatus

NMR measurements were made using a Jeol ECX 400 MHz NMR (Japan). Mass spectra and elemental analysis were provided by Medac Ltd (UK). The change in alternating current potential and phase was monitored using a lock-in-amplifier (Stanford instruments, SR830 DSP, USA). With the use of a reference resistor and custom software the resistance and the conductivity were calculated and monitored over time (frequency - 1000 Hz; amplitude - 100 mV; phase - 0 degrees; harmonics – 1; time constant - 1 x1 s, 12 dB; sensitivity - 5 x10 mV; signal output - A, AC, float; reserve - low noise; filters – none; resistor box - was adjusted to measure about 50 % of the amplitude, so about 50 mV). The irradiation was performed using Xenon Fibre-Optic Light Source (PerkinElmer Optoelectronics, XL3000, USA). An Autolab PSTAT-10 (Eco-Chemie BV, Utrecht, Netherland) was utilized for all electrochemical experiments.

Conventional screen printed platinum electrodes (4 mm diameter) from Dropsens were used with platinum working and counter electrodes and an Ag/AgCl reference electrode. Bruker ESP-300E EPR spectrometer (Japan) operating at X band was used for the electron spin resonance measurements. Confocal laser scanning 3D colour microscope Olympus LEXT - Model OLS3000 was used for the imaging. The polymer films were deposited over polycrystalline, 96 % Al_20_3 substrates with thickness 635µm. Optical densities were recorded using a micro plate reader (for microtitre plates) or a UV spectrophotometer (UV-1800 Schimadzu, Japan).

4.3.3 Synthesis of *N*-methyl-*N'*-phenyl-1,2-ethylenediamine (MPEDA)

A mixture of aniline hydrochloride (13. 00 g, 0.10 mol, 1 equiv), 3-methyl-2-oxazolidinone (11.00 g, 0.109 mol, 1.1 equiv) and 35 ml of 2-(2-metoxyethoxy) ethanol were placed in a 100 mL three-necked round-bottomed flask, equipped with magnetic stirring bar, condenser and thermometer, and heated to 170 °C in an oil bath (Scheme 4.4). The reaction mixture became yellow homogenous liquid and carbon dioxide evolution occurred on heating. After seventeen hours, the reaction was allowed to cool to ambient temperature. Most of the solvent was removed *in vacuo* to give a dark oily residue. This residue was taken up in 100 mL of aqueous sodium hydroxide (10 %) and extracted with three portions of 40 mL chloroform. The combined chloroform extractions were then dried over anhydrous sodium sulphate. After filtration, the chloroform was removed *in vacuo* to afford 20.4 g of the crude diamine as a brown liquid. Distillation at 105 °C to 110 °C (0.4 mm Hg), afforded isolation of 81 % distilled yield of the product as a clear liquid.

*Spectroscopic data for MPEDA (Scheme 4.3, **18**):*

^{1}H NMR (400 MHz, MeOH-D_3, 25 °C): δ 7.84 (2H, t, *J* = 8.37 Hz, $C_6\mathbf{H_5}$), 7.34 (2H, d, *J* = 7.68 Hz, $C_6\mathbf{H_5}$), 7.29 (1H, t, *J* = 6.53 Hz, $C_6\mathbf{H_5}$), 3.86-3.82 (2H, q, *J* = 6.08 Hz, $C\mathbf{H_2}NHC_6H_5$), 3.43 (2H, t, J = 6.30 Hz, $C\mathbf{H_2}NHCH_3$), 3.08 (3H, s, $C\mathbf{H_3}$), 2.37 (1H, s, $N\mathbf{H}CH_3$) ppm (5C.1, page 234: Figure Apx C.1);

^{13}C NMR (100 MHz, MeOH-D_3, 25 °C): δ 146.23(**C**$_6$H$_5$), 126.07 (**C**$_6$H$_5$), 112.73 (**C**$_6$H$_5$), 109.21 (**C**$_6$H$_5$), 47.67 (**C**H$_2$C$_6$H$_5$), 39.73 (**C**H$_2$NHCH$_3$), 33.20 (**C**H$_3$) ppm (5C.1, page 234: Figure Apx C.2);

DEPT 135 NMR (100 MHz, MeOH-D_3, 25 °C): δ 130.19 (up, **C**$_6$H$_5$), 116.85 (up, **C**$_6$H$_5$), 113.33 (up, **C**$_6$H$_5$), 51.79 (down, **C**H$_2$NHC$_6$H$_5$), 43.84 (down, **C**H$_2$NHCH$_3$), 37.32 (up, **C**H$_3$) ppm (5C.1, page 234: Figure Apx C.3).

4.3.4 Synthesis of *S*-methyl-*N*-methyl-*N*-ethyl (2-(phenylamino)) dithiocarbamate ester (MMDTCE)

A mixture of sodium hydroxide (1.59 g, 39.9 mmol, 3 equiv) in 10 mL water, MPEDA (2.00 g, 0.0133 mol) and carbon disulfide (1.22 g, 15.98 mmol, 1.1 equiv) were placed in a 50 mL one-necked round-bottomed flask equipped with magnetic stirring bar and argon atmosphere, at 0 °C bath temperature (Scheme 4.3). After thirty minutes stirring, iodomethane (1.89 g, 13.3 mmol, 1 equiv), in 20 mL tetrahydrofuran was added at 0 °C bath temperature. After thirty minutes stirring, the mixture was allowed to warm up to ambient temperature, and left to stir for two hours. After that, the solvent was removed *in vacuo*. The mixture was dissolved in 30 mL ethyl acetate and extracted three times with 30 mL water. The ethyl acetate layer was collected, dried over anhydrous sodium sulphate, filtered and the solvent was evaporated *in vacuo*. This procedure afforded 81 % purity of the product, as yellow oil. Purification of the residue by column chromatography over silica gel (25% ethyl acetate/hexane) afforded pale yellow oil (Yield 55 %).

*Spectroscopic data for MMDTCE (Scheme 4.3, **16**):*

^{1}H NMR (400 MHz, DMSO-D_6, 25 °C): δ 7.03 (2H, t, J = 7.34 Hz, C$_6$**H$_5$**), 6.60-6.58 (2H, d, J = 7.79 Hz, C$_6$**H$_5$**), 6.49 (1H, t, J = 7.34 Hz, C$_6$**H$_5$**), 5.78 (0.33H, t, J = 6.19 Hz, N**H**C$_6$H$_5$), 5.71 (0.67H, t, J = 6.19 Hz, N**H** C$_6$H$_5$), 4.12 (1.35H, t, J = 6.99 Hz, C**H$_2$**NHC$_6$H$_5$), 3.88 (0.65H, t, J = 6.99 Hz, C**H$_2$**NHC$_6$H$_5$), 3.42 (1.07H, s, C(S)SC**H$_3$**) 3.34-3.23 (2H, m, C**H$_2$**N(CH$_3$)C(S)S),

3.29 (1.8H, s, C(S)SC**H$_3$**), 2.53 (3H, s, C**H$_3$**NC(S)S) ppm (5C.1, page 234: Figure Apx C.4Figure Apx C.1);

^{1}H NMR (400 MHz, DMSO-D$_6$, 130 °C): δ 6.96 (2H, s, C$_6$**H$_5$**), 6.52 (2H, s, C$_6$**H$_5$**), 6.41 (1H, s, C$_6$**H$_5$**), 5.18 (1H, s, N**H**C$_6$H$_5$), 3.99 (2H, s, C**H$_2$**NHC$_6$H$_5$), 3.29 (3H, s, C(S)SC**H$_3$**) 2.75 (2H, s, C**H$_2$**N(CH$_3$)C(S)S), 2.49 (3H, s, N(C**H$_3$**)C(S)S) ppm (5C.1, page 234: Figure Apx C.5);

^{13}C NMR (100 MHz, DMSO-D$_3$, 130 °C): δ 198.52 (**C**(S)S), 147.79 (**C$_6$**H$_5$), 128.28 (**C$_6$**H$_5$), 115.00 (**C$_6$**H$_5$), 111.89 (**C$_6$**H$_5$), 55.61 (**C**H$_2$NHC6H5), 40.80 (**C**H$_2$N(CH$_3$)C(S)S), 39.63 (**C**H$_3$SC(S)) 19.81 (N(**C**H$_3$)C(S)S) ppm (5C.1, page 234: Figure Apx C.7);

DEPT 45 NMR (100 MHz, DMSO-D$_3$, 25 °C): δ 129.52 (**C$_6$**H$_5$), 116.89 (**C$_6$**H$_5$), 112.49 (**C$_6$**H$_5$), 56.23 (**C**H$_2$NHC$_6$H$_5$), 41.21 (**C**H$_2$N(CH$_3$)C(S)S), 39.63 (**C**H$_3$SC(S)), 20.39 (N(**C**H$_3$)C(S)S) ppm (5C.1, page 234: Figure Apx C.8);

DEPT 90 NMR (100 MHz, DMSO-D$_3$, 25 °C): δ 129.52 (**C$_6$**H$_5$), 116.39 (**C$_6$**H$_5$), 112.49 (**C$_6$**H$_5$) ppm (5C.1, page 234: Figure Apx C.9);

DEPT 135 NMR (100 MHz, DMSO-D$_3$, 25 °C): δ 129.52 (up, **C$_6$**H$_5$), 116.39 (up, **C$_6$**H$_5$), 112.49 (up, **C$_6$**H$_5$), 56.23 (down, **C**H$_2$NHC$_6$H$_5$), 41.21 (down, **C**H$_2$N(CH$_3$)C(S)S), 39.63 (up, **C**H$_3$SC(S)), 20.39 (up, N(**C**H$_3$)C(S)S) ppm (5C.1, page 234: Figure Apx C.10).

HRMS (ES) Exact mass calculated for C$_{11}$H$_{16}$N$_2$S$_2$ [M+H]+: m/z: 240.08 (100.0 %), 241.08 (12.1 %), 242.07 (9.1 %), 241.07 (2.3 %), 243.07 (1.2 %), found: 241.08 (60 %), 210.15 (100 %) (5C.1, page 234: Figure Apx C.11);

Elemental analysis (C$_{11}$H$_{16}$N$_2$S$_2$): C, 54.96; H 6.71; N 11.65, S 26.68; found 1: C 54.07, H 7.51, N 11.63, S 24.50; found 2: C 53.88, H 7.68, N 11.60, S 24.66;

R_f = 0.3 (25 % ethyl acetate/hexane).

4.3.5 Polymer deposition over interdigitated microsensor electrodes (IMEs)

Interdigitated microsensor electrodes were used for detection of the current change upon UV irradiation of poly (NDDEAEA), poly (MMDTCE) and PANI. The materials were

deposited on the electrodes during chemical polymerisation the conditions of which were previously optimised (5B.3.2, page 229: Figure_Apx B.7 and Figure_Apx B.8 and 5C.2, page 243: Figure_Apx C.12 and Figure_Apx C.13). The reaction conditions chosen as optimum were as follows:

NDDEAEA: 8 mL solution of 0.08 M NDDEAEA, 0.6 M hydrochloric acid and 0.05 M ammonium persulfate in 25 % acetonitrile in water were placed in a 10 mL glass bottle (height 70 mm, diameter 15 mm).

MMDTCE: 8 mL solution of 0.08 M MMDTCE hydrochloride and 0.05 M ammonium persulfate in 25% ethanol in water was placed in a 10 mL bottle (height 70 mm, diameter 15 mm).

PANI: 8 mL solution of 0.5 M aniline, 0.1 M hydrochloric acid and 0.05 M ammonium persulfate in 25 % acetonitrile in water were placed in a 10 mL bottle (height 70 mm, diameter 15 mm).

The polymerisation was performed at ambient temperature for one hour. The electrodes were rinsed first with water and then with hydrochloric acid (1 M) or sodium hydroxide (1 M), to give fully doped or fully dedoped materials respectively. The electrodes were dried at ambient temperature in the dark for twelve hours. poly (NDDEAEA) (0.7 mg), PANI (0.7 mg) and poly (MMDTCE) (8.3 mg) were deposited on the surface of the electrodes.

4.3.6 Measuring the electrical properties of poly (NDDEAEA), poly (MMDTCE) and PANI during UV irradiation

The change in alternating current potential and phase was monitored using a lock-in-amplifier. With the use of a reference resistor and custom software the resistance and the conductivity were calculated and monitored over time (frequency - 1000 Hz; amplitude - 100 mV; phase - 0 degrees; harmonics – 1; time constant - 1 x1 s, 12 dB; sensitivity - 5 x10 mV; signal output - A, AC, float; reserve - low noise; filters – none; resistor box - should be adjusted to measure about 50% of the amplitude, about 50

mV). The irradiation was performed using Xenon Fibre-Optic Light Source. The irradiation distance was 100 mm. The light intensity was varied from 10 to 50 % in 10 % interval. Each irradiation interval was five minutes with five minutes break between the intervals. The measurements were performed while nitrogen gas was purged in a plastic bag with the connected electrode in it. Each single change of the light intensity was performed in triplicates per one electrode. This experiment was repeated three times with each polymer. The temperature was monitored with a thermocouple and a multimeter over period of five minutes with the different intensities of the light. The temperature was read at the end of the fifth minute.

4.3.7 UV spectroscopy of chemically polymerised poly (NDDEAEA), poly (MMDTCE) and PANI before and after UV irradiation

Layers of poly (NDDEAEA), poly (MMDTCE) and PANI were deposited over quarts cuvettes (Hellma® absorption cuvettes, standard cells, Macro Herasil quartz, limit 200-2,500 nm spectral range, path-length 10 mm, chamber volume 3,500 µL) during chemical polymerisation. The protocol for the polymerisation was as described in 4.3.5 (page 162). The polymerisation volume was decreased to 4 mL. The polymerisation time was one hour in the dark. After the polymerisation was completed the cuvettes were rinsed with water and dried at ambient temperature, in the dark for twelve hours. Prior to analysis nitrogen atmosphere was established. UV measurements were performed before and after irradiation every five minutes in twenty minutes total irradiation interval. The irradiation was performed using Xenon Fibre-Optic Light Source (50 % intensity of the light). The irradiation distance was 100 mm.

4.3.8 Cyclic voltamometry of electrochemically polymerised poly (NDDEAEA), poly (MMDTCE) and PANI during UV irradiation

The screen printed platinum electrodes, prepared as described in previous section (3.3.4, page 117) with all three different materials (in triplicates), were tested for

conductivity changes during UV irradiation with cyclic voltammetry in electrolyte solution. All voltammograms were obtained using AutoLab between -0.2 V to 0.9 V at a scan rate of 100 mV s^{-1} in hydrochloric acid (0.1 M). The irradiation was performed using Xenon Fibre-Optic light source. The irradiation distance was 100 mm. The light intensity was varied from 10 % to 50 % in 10 % interval. Five cycles were performed per light intensity and five cycles in between without irradiation. Measurements were performed under nitrogen atmosphere. The electrolyte solution was degassed with nitrogen gas for two minutes prior to use.

4.4 Conclusions

The newly synthesised *N*-(*N´,N´*-diethyldithiocarbamoyl ethyl amido ethyl)-aniline (NDDEAEA, Scheme 4.2, **13**) and *S*-methyl-*N*-methyl-*N*-ethyl (2-(phenylamino)) dithiocarbamate ester (MEPDTC, **16**) that incorporate both aniline and dithiocarbamate ester (DTCE) parts were chemically polymerised from their aniline part to form the *N*-substituted polyanilines (PANIs) poly (NDDEAEA) and poly (MMDTCE), respectively. The so-prepared materials were deposited on the surface of interdigitated microsensor electrodes (IMEs) and their conductivity measured as a function of time during ultraviolet (UV) irradiation. As a reference PANI was used. All three materials, when in their doped state exhibited reproducible and reversible enhancement of the conductivity during UV irradiation. This increase in the conductivity was proportional to the intensity of the light. The biggest increase was with poly (MMDTCE) at 50 % intensity of the light (0.6×10^{-3} Scm^{-1}). This was attributed to the fact that during irradiation this material forms *dormant free* radical on each of the aniline unit from the polymer that indulged hopping effect from the PANI chain and leads to a doping effect. In the case of the other analysed polymer poly (NDDEAEA), this showed similar behaviour but the increase in the conductivity during irradiation was less than that observed with PANI (0.03×10^{-3} Scm^{-1}). This was attributed to the fact that during irradiation this material forms active *free* radicals on each one of the aniline units from the polymer that could lead to predominantly recombination with a *dormant* or with another active *free* radical. The increase of the current baseline after irradiation suggests that the cross-linking process dominates. When the dedoped state of the materials was used for analysis no change in the conductivity was observed. The UV spectra of the materials in the dry state after irradiation show that there are no changes in the oxidation state of the DTCE group. Electron spin resonance (ESR) spectroscopy was used to detect the electron transfer processes. Confocal laser scanning microscopy was applied to analyse the surface of the materials. Compound roughness coefficients in increasing order were: poly (NDDEAEA) 1.013, PANI 1.072 and poly (MMDTCE) 2.099, which is in correspondence with the observed increases in conductivity. When the materials were

electropolymerised no increase in the current was observed even in their doped state. This was related to the fact the polymer film thickness when electropolymerised was much less that when chemically polymerised. This new materials could be potentially attractive for optoelectronic devices, storage devices and sensor fabrication.

5 General Conclusions and Future Work

A close look at the current literature on molecularly imprinted polymers (MIP) synthesised via *"living"* or *controlled* radical polymerisations (CRP) techniques was presented in Chapter 1. Different CRP techniques such as surface-initiated nitroxide-mediated *free-radical* polymerisation (SI-NMP), surface-initiated atom transfer radical polymerisation (SI-ATRP), surface-initiated reversible addition-fragmentation chain-transfer (SI-RAFT) polymerisation, and surface-initiated *photo-iniferter* (initiator, transfer agent and terminator) mediated polymerisation (SI-PIMP) were introduced. Their application in MIP synthesis has recently received a lot of attention due to the possibility of a better control over the polymerisation process. This has enabled precise tuning of the thickness of the polymer layer and led to facile routes to the development of a variety of MIP formats, such as nano-scaled objects with improved imprinted properties. These nano-MIP composites should find future applications in the development of more sensitive biosensors with faster analysis times.

Among the presented SI-CRP techniques, SI-PIMP has proven to be the most promising. It has demonstrated the fastest polymerisation times even at sub-zero temperatures, the biggest choice of monomer-template compositions that could be used and the simplest preparation procedures. SI-PIMP does not require the use of additives, such as surfactants, initiators or metal ions, that are not incorporated in the polymer structure, and that would require additional and long washes of the resultant polymer. This is why this technique was chosen in the present work to be further explored in respect to the synthesis of different MIPs formats, as a grafting technique form different surfaces and as a source of new sensing materials and techniques.

In Chapter 2 the synthesis of MIP nanoparticles (NPs) via *"grafting from"* approach was described and discussed. As a graftable core, dendrimers were used. On their periphery dithiocarbamate ester (DTCE) groups (*iniferter*) were covalently attached to form a soluble *macroiniferter*. Photo-initiated *living* polymerisation was initiated spontaneously from 48 points per dendrimer to form a MIP shell imprinted with the herbicide acetoguanamine in just two minutes irradiation time. For this time around

200 nm particles were synthesised. Surprisingly the shape of the particles proved to be cubic. All different techniques employed: scanning electron microscopy (SEM), transmission electron microscopy (TEM), electron diffraction, and chemical analysis using electron-dispersive X-ray (EDX), unambiguously confirmed the shape of the NPs and their organic nature. This result was attributed to be a property of the dendrimer core, as the result was reproducible, as shown by a decreased irradiation time giving rise to smaller particles but still exhibiting the cubic shape.

The particles showed very good affinity to the analyte compound. For this purpose, surface plasmon resonance (SPR) was used as an analytical technique. Biacore chips were surface covalently modified with the target analyte and samples of MIP NPs were injected at a range of concentration. The dissociation constant, K_d calculated via Biaevaluation software, provided by Biacore, was calculated to be 1.76×10^{-10} M for MIP, and 1.11×10^{-8} M for Blank (control) NPs. Their selectivity was demonstrated by injecting samples on a Biacore chip modified with close analogue to the template: atrazine desisopropyl. The apparent K_d calculated for MIP NPs was 3×10^{-8} M and 3.2×10^{-5} M for Blank on the non specific surface.

In order for fluorescent sensing to be exploited with these particles, ~50 % of the available amine groups at the periphery of a PAMAM dendrimer core was modified with a fluorescent label (dansyl chloride), the remainder being modified with the iniferter group. The MIP shell was formed afterwards, forming fluorescent core MIP NPs. This is a novel technique for the preparation of fluorescent MIP NPs that provides two important advantages: precise control over the quantity of the fluorescent label per each particle, and shielding of the fluorescent label from the environment. These NPs have demonstrated very good affinity to the template analyte and excellent selectivity over close structural analogues (atrazine desisopropyl and simazine) of the template. When placed in a solution of the template, the particles showed fluorescence emission maxima enhancement after just ten minutes incubation time. Almost no response was observed in the case of the Blank polymer or of the MIP or Blank in the presence of the analogues. The limit of detection was calculated to be 3×10^{-8} M. Enhancement of the fluorescent emission is another event that has rarely been

reported. Usually the detection of the fluorescent MIP sensors is based on reduction of the intensity with the binding events. This discovery would lead to improved sensitivity of the devices for small concentrations and rapid detection.

These NPs could be used in biosensors for fast and sensitive detection of target compounds. Their shape could be advantageous for applications were close packing is required. This aspect of the discovery should be further investigated. For example dendrons could be used as a graftable core instead of dendrimers. This would most probably provide nanoparticles with pyramidal shape. The application of these nano-MIP shapes should further be investigated in respect of improved qualities of biosensors and in nanomedicine as drug delivery systems. Future studies could also be aimed at providing a deeper understanding of the mechanism involved behind the core fluorescent sensing. Another future development of the florescent core MIP NPs could be the synthesis of MIPs imprinted with different targets. For each one of the targets used different a fluorescent label could be attached to the core, each having a narrow emission band centred on a unique wavelength. A mixture of this nanoparticles could provide fast and quantative analysis of mixtures of their respective analytes. Another possible future work involving fluorescent sensing could be a comparison of surface-modified fluorescent NPs with these in which fluorescent groups are attached to the core.

Within this work new *N*-substituted polyaniline (PANI) bearing a DTCE group on each one of the monomer units was prepared and presented in details in Chapter 3. This new material was fully characterised and used in a *"grafting from"* technique to deposit, layer-by-layer, different polymer layers in a controlled and well defined way. For the purpose, a new monomer *N*-(*N'*,*N'*-diethyldithiocarbamoyl ethyl amido ethyl)-aniline (NDDEAEA), incorporating both DTCE and aniline groups was synthesised and fully characterised. This monomer has demonstrated the ability to polymerise its aniline part via both electropolymerisation and chemical polymerisation. As a result PANI bearing DTCE pendant units was synthesised. Surface-confined photo-grafting of various polymers was conducted, from both electropolymerised and chemically polymerised material, deposited on different surfaces such as glass, gold,

polypropylene and polystyrene substrates. The monomers grafted were: methacrylic acid, styrene, acrylamido-2-methylpropane sulfonic acid, lauryl methacrylate and 3-aminopropyl methacrylamide.

This new material has the potential for creating materials with different integrated functionalities, such as conductivity, MIPs, and materials with changed surface polarity. This material could have application in biosensors and surface patterning in microelectronic devices. Future development could include grafting of MIP layer from the conductive surface in analogy to Lakshmi *et al.* (**2009**) but without one of the modification steps. Another possible future development of the polymer could be its preparation in the form of NPs. This would provide conducting core surface graftable material.

Investigation on the conductivity enhancement in *N*-substituted PANIs with DTCE groups upon UV irradiation was investigated in Chapter 4. Two different materials were synthesised: one with *dormant* radicals on the PANI chain (S-methyl-N-methyl-N-ethyl-(2-(phenylamino) dithiocarbamate ester), MEPDTC), and a second with active radicals on the PANI chain during UV irradiation (poly (NDDEAEA)). Reproducible enhancement of the conductivity during irradiation in the dry state was observed in both cases. The enhancement was greater with poly (MEPDTC), which was attributed to the longer living *dormant* radicals introduced along the polymer chain. The formed radicals participated in hopping mechanism than leads to doping effect in the polymer. In the case of poly (NDDEAEA), smaller enhancement than that seen with PANI (used as a control) was observed. This was attributed to the fact that the introduced active radicals along the polymer chain were too short lived to participate in hoping mechanism. The events were proven to be not arising from changes in temperature.

MEPDTC could be applied in UV sensors. A suggestion for future work would be to conduct theoretical calculations of the electrons energy level in order to obtain a better understanding of the mechanism behind these events to be elucidated.

In conclusion different new materials were synthesised using *iniferters* and SI-PIMP. Their properties were investigated and obvious improvements in their qualities were

observed. This has contributed to development of new horizons of future applications in the field of biosensors.

REFERENCES

A

1. Abdiryim, T.; Zhang, X. G.; Jamal, R. **2005**. Comparative studies of solid-state synthesized polyaniline doped with inorganic acids. *Material Chemistry Physics*, **90** (2-3), 367-372.

2. Ahn, Y.; Dunning, J.; Park, J. **2005**. Scanning photocurrent imaging and electronic band studies in SiNW field effect transistors. *Nano Letters*, **5**, 1367-1370.

3. Alemdar, N.; Erciyes, A. T.; Yagci, Y. **2010**. Styrenation of air-blown linseed oil by nitroxide-mediated radical polymerization. *Progress in Organic Coatings*, **61** (1), 55-59.

4. Alexander, C.; Andersson, H. S.; Andersson, L. I.; Ansell, R. J.; Kirsch, N.; Nicholls, I. A.; O'Mahony, J.; Whitcombe, M. J. **2006**. Molecular imprinting science and technology: A survey of the literature for the years up to and including 2003. *Journal* of *Molecular Recognition*, **19** (2), 106-180.

5. Al-Kindy, S.; Badoia, R.; Suarez-Rodriguez, J. L.; Diaz-Garcia, M. E. **2000**. Molecularly imprinted polymers and optical sensing applications. *Critical Reviews in Analytical Chemistry*, **30** (4), 291-309.

6. Altman, E.; Renaud, J.; Green, J.; Farley, D.; Cutting, B.; Jahnke, W. **2002**, Arylaminoethylamides as novel non-covalent Cathepsin K inhibitors. *Journal of Medicinal Chemistry*, **45**, 2352-2354.

7. Ancher, M.; Vofsi, D. **1963**. Chlorine-activation by redox-transfer. Part III. The abnormal addition of chloroform to olefins. *Journal of the Chemical Society*, 3921-3927.

8. Andruzzi, L.; Senaratne, W.; Hexemer, A.; Sheets, E. D.; Ilic, B.; Kramer, E. J.; Barid, B.; Ober, C. K. **2005**. Oligo (ethylene glycol) containing polymer brushes as bioselective surfaces. *Langmuir*, **21**, 2495-2504.

9. Araujo, P. L. B.; Ferreira, C. R. P. C.; Araujo, F. S. **2011**. Biodegradable conductive composites of poly (3-hydroxybutyrate) and polyaniline nanofibers: Preparation, characterization and radiolytic effects. *Express Polymer Letters*, **5** (1), 12-22.

10. Arshady, R.; Mosbach, K. **1981**. Synthesis of substrate-selective polymers by host-guest polymerization. *Macromolecular Chemistry*, **182**, 687-692.

11. Ayres, N. **2011**. Atom transfer radical polymerisation: A robust and versatile route for polymer synthesis. *Polymer Reviews*, **51** (2), 138-162.

12. Azizi, N.; Aryanasab, F.; Saidi, M. R. **2006**, Straightforward and highly efficient catalyst-free one-pot synthesis of dithiocarbamates under solvent-free conditions. *Organic Letters,* **8** (23), 5275–5277.

B

13. Barahona, F.; Turiel, E.; Cormack, P. A. G.; Martín-Esteban, A. **2010**. Chromatographic performance of molecularly imprinted polymers: Core-shell microspheres by precipitation polymerization and grafted MIP films via iniferter-modified silica beads. *Journal of Polymer Science Part A: Polymer Chemistry*, **48**, 1058-1066.

14. Barbey, R.; Lavanant, L.; Paripovic, D.; Schüwer, N.; Sugnaux, C.; Tugulu, S.; Klok, H. A. **2009**. Polymer brushes via surface-initiated controlled radical polymerization: synthesis, characterization, properties, and applications. *Chemical Reviews*, **109**, 5437-5527.

15. Bardavid, Y.; Goykhman, I.; Nozaki, D.; Cuniberti, G.; Yitzchaik, S. **2011**. Dipole assisted photogated switch in spiropyran grafted polyaniline nanowires. *The Journal of Physical Chemistry. C*, **115** (7), 3123-3128.

16. Barner-Kowollic, C.; Buback, M.; Charleux, B.; Coote, M. L.; Drache, M.; Fucuda, T.; Goto, A.; Klumperman, B.; Lowe, A. B.; Mcleary, J. B.; Moad, G.; Monteiro, M. J.; Sanderson, R. D.; Tonge, M. P.; Vana, P. **2006**. Mechanism and kinetics of

dithiobenzoates-mediated RAFT polymerisation. I. The current situation. *Journal of Polymer Science: Part A: Polymer Chemistry*, **44**, 5809-5831.

17. Bartholome, C.; Beyou, E.; Bourgeat-Lami, E.; Chaumont, P.; Zydowicz, N. **2003**. Nitroxide-mediated polymerisations from silica nanoparticle surfaces: "Graft from" polymerisation of styrene using a triethoxysilyl-terminated alkoxyamine initiator. *Macromolecules*, **36**, 7946-7952.

18. Barz, M.; Luxenhofer, R.; Zentel, R.; Vicent, M. J. **2011**. Overcoming the PEG-addiction: Well-defined alternatives to PEG, from structure-property relationships to better defined therapeutics. *Polymer Chemistry*, **2** (9), 1900-1918.

19. Basable-Desmonts, L.; Reinhoudt, D. N.; Crego-Calama, M. **2007.** Design of fluorescent materials for chemical sensing. *Chemical Society Review*, **36**, 993-1017.

20. Baum, M.; Brittain, W. J. **2002**. Synthesis of polymer brushes on silicate substrates via reversible addition fragmentation chain transfer technique. *Macromolecules*, **35**, 610-615.

21. Bellus, D. **1985**. Copper-catalyzed additions of organic polyhalides to olefins: A versatile synthetic tool. *Pure and Applied Chemistry*, **57** (12), 1827.

22. Beltran, A.; Borrull, F.; Marce, R. M.; Cormack, P. A. G. **2010**. Molecularly-imprinted polymers: useful sorbents for selective extractions. *Trends in Analytical Chemistry*, **29** (11), 1363-1375.

23. Benoit, D.; Chaplinski, V.; Braslau, R.; Hawker, C. J. **1999**. Development of a universal alkoxyamine for "living" free radical polymerisations. *Journal of the American Chemical Society*, **121**, 3904-3920.

24. Benoit, D.; Grimaldi, S.; Robin, S.; Finet, J.-P.; Tordo, P.; Gnanou, Y. **2000**. Kinetics and mechanism of controlled free-radical polymerisation of styrene and n-butyl

acrylate in the presence of an acyclic β-phosphonylated nitroxide. *Journal of the American Chemical Society*, **122** (25), 5929-5939.

25. Berti, F.; Todros, S.; Lakshmi, D.; Whitcombe, M. J.; Chianella, I.; Ferroni, M.; Piletsky, S. A.; Turner, A. P. F.; Marrazza, G. **2010**. Quasi-monodimensional polyaniline nanostructures for enhanced molecularly imprinted polymer-based sensing. *Biosensors and Bioelectronics*, **26** (2), 497-503.

26. Bertin, D.; Gigmes, D.; Marque, S. R. A.; Tordo, P. **2011**. Kinetic subtleties of nitroxide mediated polymerization. *Chemical Society Reviews*, **40** (5), 2189-2198.

27. Bian, K.; Cunningham, M. F. **2006**. Surface-initiated nitroxide-mediated radical polymerisation of 2-(dimethylamino)ethyl acrylate on polymeric microspheres. *Polymer*, **47** (16), 5744-5753.

28. Bidan, G.; Genies, E. M.; Penneau, J. F. **1989**. Poly (2-propylaniline): An electroactive polymer, soluble in organic medium in the reduced state. *Journal of Electroanalytical Chemistry and Interfacial Electrochemistry*, **271** (1-2), 59-68.

29. Blas, H.; Save, M.; Boissiere, C.; Sanchez, C.; Charleux, B. **2011**. Surface-initiated nitroxide-mediated polymerization from ordered mesoporous silica. *Macromolecules*, **44** (8), 2577-2588.

30. Blencowe, A.; Tan, J. F.; Goh, T. K.; Qiao, G. G. **2009**. Core cross-linked star polymers via controlled radical polymerisation. *Polymer*, **50**, 5-32.

31. Blinova, N. V.; Stejskal, J.; Trchová, M.; Prokes, J. **2008**. Control of polyaniline conductivity and contact angles by partial protonation. *Polymer International*, **57** (1), 66-69.

32. Bodugoz-Senturk, H.; Guven, O. **2011**. Enhancement of conductivity in polyaniline-[poly (vinylidene chloride)-co- (vinyl acetate)] blends by irradiation, *Radiation Physics and Chemistry*, **80**, 153–158.

33. Boonpangrak, S.; Whitcombe, M. J.; Prachayasittikul, V.; Mosbach, K.; Ye, L. **2006**. Preparation of molecularly imprinted polymers using nitroxide-mediated living radical polymerization. *Biosensors and Bioelectronics*, **22**, 349-354.

34. Borner, H. G.; Beers, K.; Matyjaszewski, K.; Sheiko, S. S.; Moller, M. **2001**. Synthesis of molecular brushes with block copolymer side chains using atom transfer radical polymerization. *Macromolecules*, **34**, 4375-4383.

35. Bossi, A.; Piletsky, S. A.; Piletska, E. V.; Righetti, P. G.; Turner, A. P. F. **2000**. An assay for ascorbic acid based on polyaniline-coated microplates. *Analytical Chemistry*, **72** (18), 4296-4300.

36. Bossi, A.; Whitcombe, M. J.; Uludag, Y.; Fowler, S.; Chianella, I.; Subrahmanyam, S.; Sanchez, I.; Piletsky, S. A. **2010**. Synthesis of controlled polymeric cross-linked coatings via iniferter polymerisation in the presence of tetraethyl thiuram disulphide chain terminator. *Biosensors and Bioelectronics*, **25**, 2149-2155.

37. Braunecker, W. A.; Matyjaszewski, K. **2007**. Controlled/living radical polymerization: Features, developments, and perspectives. *Progress in Polymer Science*, **32**, 93-146.

38. Brinks, M. K.; Studer, A. **2009**. Polymer brushes by nitroxide-mediated polymerization. *Macromolecular Rapid Communications*, **30**, 1043-1057.

C

39. Carter, S. R.; Rimmer, S. **2005**. Aqueous compatible polymers in bionanotechnology. *IEE Proceedings – Nanobiotechnology*, **152** (5), 169-176.

40. Callejas-Fernandez, J.; Martinez-Garcia, R.; Hidalgo-Alvarez, R.; de las Nieves, F.J. **1993.** Effect of some inhibitors on the zeta-potential of calcium oxalate monohydrate particles. *Progress in Colloid & Polymer Science*, 210-215.

41. Cao, Y.; Smith, P.; Heeger, A. J. **1992**. Counter-ion induced processibility of conducting polyaniline and of conducting polyblends of polyaniline in bulk polymers. *Synthetic Metals*, **48** (1), 91-97.

42. Chaitidou, S.; Kotrotsiou, O.; Kotti, K.; Kammona, O.; Bukhari, M.; Kiparissides, C. **2008**. Precipitation polymerization for the synthesis of nanostructured particles. *Material Science Engineering: B*, **152** (1-3), 55-59.

43. Chang, L.; Li, Y.; Chu, J.; Qi, J. Li, X. **2010**. Preparation of core-shell molecularly imprinted polymer via the combination of reversible addition-fragmentation chain transfer polymerization and click chemistry. *Analytica Chimica Acta*, **680**, 65-71.

44. Chen, L.; Xu, S.; Li, J. **2011**. Recent advances in molecular imprinting technology: current status, challenges and highlighted applications. *Chemical Society Reviews*, **40**, 2922-2942.

45. Chen, R. R.; Qin, L.; Jia, M.; He, X. W.; Li, W. Y. **2010**. Novel surface-modified molecularly imprinted membrane prepared with iniferter for permselective separation of lysozyme. *Journal of Membrane Science*, **363**, 212-220.

46. Chen, X. W.; Gholamkhass, B.; Han, X.; Vamvounis, G.; Holdcroft, S. **2007**. Polythiophene-graft-styrene and polythiophene-graft-(styrene-graft-C_{60}) copolymers. *Macromolecular Rapid Communications*, **28** (17), 1792-1797.

47. Chen, Z.; Nagaoka, T. **2000**, Recognition of vitamin K_1 with a molecularly imprinted self-assembled monolayer film. *Bunseki Kagaku*, **49**, 543-545.

48. Chen, Z. J.; Yang, Q. X.; Peng, K.; Guo, Y. B. **2011**. Surface-initiated nitroxide-mediated radical polymerization of 4-vinylpyridine on magnetite nanoparticles. *Journal of Applied Polymer Science*, **119** (6), 3582-3590.

49. Chiefari, J.; Chong, Y. K.; Ercole, F.; Krstina, J.; Jeffery, J.; Le, T. P. T.; Mayadunne, R. T. A.; Meijs, G. F.; Moad, C. L.; Moad, G.; Rizzardo, E.; Thang, S. H.**1998**. Living

free-radical polymerization by reversible addition−fragmentation chain transfer: The RAFT process. *Macromolecules*, **31**, 5559-5562.

50. Chiefari, J; Mayadunne, R. T. A.; Moad, C. L.; Moad, G.; Rizzardo, E.; Postma, A.; Skidmore, M. S.; Thang, S. T. **2003**. Thiocarbonylthio compounds (SC(Z)S-R) in free radical polymerisation with reversible addition-fragmentation chain transfer (RAFT polymerisation). Effect of the activating group Z. *Macromolecules*, **36** (7), 2273-2283.

51. Cho, J.; Shin, K. H.; Jang, J. **2010**. Polyaniline micropattern onto flexible substrate by vapor deposition polymerization-mediated inkjet printing. *Thin Solid Films*, **518**, 5066-5070.

52. Chong, B. Y. K.; Krstina, J.; Le, T. P. T.; Moad, G.; Postma, A.; Rizzardo, E.; Thang, S. H. **2003**. Thiocarbonylthio compounds (SC(Z)S-R) in free radical polymerisation with reversible addition-fragmentation chain transfer (RAFT polymerisation). Role of the free-radical leaving group (R). *Macromolecules*, **36** (7), 2256-2272.

53. Christropher Barner-Kowollik, **2008**. Handbook of RAFT polymerization. *Whiley-VHS Verlag GmbH and Co. KGaA. Weinkeim*, pages 222-223.

54. Coessens, V.; Pintauer, T.; Matyjaszewski, K. **2001**. Functional polymers by atom transfer radical polymerization. *Progress in Polymer Science*, **26**, 337-377.

55. Cucio, P.; Zandanel, C.; Wagner, A.; Mioskowski, C. **2009**. Semi-covalent surface molecular imrinting of polymers by one-stage mini-emulsion polymerisatio: glucopyranoside as a model analyte. *Macromolecular Bioscience*, **9**, 596-604.

56. Cunliffe, D.; Kirby, A.; Alexander, C. **2005**. Molecularly imprinted drug delivery systems. *Advanced Drug Delivery Reviews*, **57** (12), 1836-1853.

57. Curcio, P.; Zandanel, C.; Wagner, A.; Mioskowski, C.; Baati, R. **2009**. Semi-covalent surface molecular imprinting of polymers by one-stage mini-emulsion polymerisation: Glucopyranoside as a model analyte. *Macromolecular Bioscience*, **9**, 596-604.

58. Czaun, M.; Rahman, M.; Takafuji, M.; Ihara, H. **2008**. Moleculer shape recognition-structure correlation in a phenylalanine-based polymer-silica composite by surface-initiated atom transfer radical polymerisation. *Polymer*, **49**, 5410-5416.

D

59. De Azevedo, W. M.; De Oliveira Luna, A. J. H.; Silva, E. F. V. B. N.; Silva, R. O. **2006**. The effect of ultrasonic waves in conducting polymer solution. *Ultrasonics Sonochemistry*, **13** (5), 433-437.

60. De Boer, B.; Simon, H. K.; Werts, M. P. L.; Van Der Vegte, E. W.; Hadziioannou, G. **2000**. "Living" free radical photopolymerization initiated from surface-grafted iniferter monolayers. *Macromolecules*, **33**, 349-356.

61. De Clercq, R.; Verpoort, F. **2003**. Synthesis and evaluation of a new class of ruthenium-based catalytic systems for atom transfer radical addition and enol ester synthesis. *Journal of Organometalyc Chemistry*, **672** (1-2), 11-16.

62. Dehonor, M.; Masenelli-Varlot, K.; González-montiel, A.; Gauthier, C.; Cavaillé, J. Y.; Terrones, M. **2007**. Grafting of polystyrene on nitrogen-doped multi-walled carbon nanotubes. *Journal of Nanoscience and Nanotechnology*, **7** (10), 3450-3457.

63. Deng, J.; Wang, L.; Liu, L.; Yang, W. **2009**. Development and new applications of UV-induced surface graft polymerisations. *Progress in Polymer Science*, **34**, 156-193.

64. Destaras, M. **2011**. On the critical role of RAFT agent design in reversible addition-fragmentation chain transfer (RAFT) polymerization. *Polymer Reviews*, **51** (2), 163-187.

65. Diaz, A. F.; Logan, J. A. **1980**. Electroactive polyaniline films. *Journal of Electroanalytical Chemistry and Interfacial Electrochemistry*, **111** (1), 111-114.

66. Dongjun, W. D.; Imae, T. **2004**. Fluorescence emission from dendrimers and its pH dependence. *Journal of the American Chemical Society*, **126**, 13204-13205.

67. Dyer, D. **2006**. Photoinitiated synthesis of grafted polymers. *Advances of Polymer Science*, **197**, 47-65.

E

68. Edmondson, S.; Armes, S. A. **2008**. Synthesis of surface-initiated polymer brushes using macro-initiators. *Polymer International*, **58**, 307-316.

69. Ejaz, M; Yamamoto, S.; Ohno, K.; Tsujii, Y.; Fukuda, T. **1998**. Controlled graft polymerisation of methyl methacrylate on silicon substrate by the combined use of the langmuir−blodgett and atom transfer radical polymerisation techniques. *Macromolecules*, **31**, 5934-5936.

70. Ewing, S. P.; Lockshon, D.; Jencks, W. P. **1980**. Mechanism of cleavage of carbamate anions. *Journal of the American Chemical Society*, **102** (9), 3072-3084.

F

71. Frasconi, M.; Tel-Vered, R.; Riskin, M.; Willner, I. **2010**. Electrified selective “sponges” made of Au nanoparticles. *Journal of the American Chemical Society*, **132**, 9373-9382.

72. Freitag, M.; Martin, Y.; Misewich, J. A.; Martel, R.; Avouris, P **2003**. Photoconductivity of single carbon nanotubes. *Nano Letters*, **3** (8), 1067–1071.

G

73. Gai, Q. Q.; Liu, Q. Y.; Li, W. Y.; He, X. W.; Chen, L. X.; Zhang, Y. U. **2008**. Preparation of bovine hemoglobin-imprinted polymer beads via the photografting surface-modified method. *Chemical Journal of Chinese Universities*, **29** (1), 64-70.

74. Gai, Q. Q.; Qu, F.; Liu, Z. J.; Dai, R. J.; Zhang, Y. K. **2010**. Supermagnetic lyzozyme surface-imprinted polymer prepared by atom transfer radical polymerisation and its application for protein separation. *Journal of Chromatography A*, **1217** (13), 5035-5042.

75. Gam-Derouich, S.; Nguyen, M. N.; Madani, A.; Maouche, N.; Lang, P.; Perruchot, C.; Chehimi, M. M. **2010**. Aryl diazonium salt surface chemistry and ATRP for the preparation of molecularly imprinted polymer grafts on gold substrates. *Surface and Interface Analysis*, **42**, 1050-1056.

76. Gao, D. M.; Wang, Z. Y.; Liu, B. H.; Ni, L.; Wu, M. H.; Zhang, Z. P. **2008**. Resonance energy transfer-amplifying fluorescence quenching at the surface of silica nanoparticles toward ultrasensitive detection of TNT. *Analytical Chemistry*, **80** (22), 8545-8553.

77. Gao, D. M.; Zhang, Z. P.; Wu, M. H.; Xie, C. G.; Guan, D. J..; Wang, D. P. **2007**. A surface functional monomer-directing strategy for highly dense imprinting of TNT at surface of silica nanoparticles. *Journal of the American Chemical Society*, **129**, 7859-7866.

78. Gao, H.; Matyjaszewski, K. **2009.** Synthesis of functional polymers with controlled architecture by CRP of monomers in the presence of cross-linkers: From stars to gels. *Progress in Polymer Science*, **34**, 317-350.

79. García-Con, L. M.; Whitcombe, M. J.; Piletska, E. V.; Piletsky, S. P. **2010**. A sulfur-sulfur cross-linked polymer synthesized from a polymerizable dithiocarbamate as a source of dormant radicals. *Angewandte Chemie, International Edition*, **49**, 4075-4078.

80. Ge, Y.; Turner, A. P. F. **2008**. Too large to fit? Recent developments in macromolecular imprinting. *Trends in Biotechnology*, **26**, 218-224.

81. Georgiev, N. I.; Bojinov, V. B. **2010**. The design and synthesis of a novel 1,8-naphthalimide PAMAM light-harvesting dendron with fluorescence “off-on” switching core. *Dyes and Pigments*, **84**, 249-256.

82. Ghannam, L.; Parvole, J.; Laruelle, G.; Francois, J.; Billon, L. **2006**. Surface-initiated nitroxide-mediated polymerisation: A tool for hybrid inorganic/organic nanocomposites 'in situ' synthesis. *Polymer International*, **55** (10), 1199-1207.

83. Gizdavic-Nikolaidis, M.; Travas-Sejdic, J.; Bowmaker, G. A.; Cooney, R. P.; Kilmartin, P. A. **2004**. Conducting polymers as free radical scavengers. *Synthetic Metals*, **140**, 225-232.

84. Gonzato, C.; Courty, M. Pasetto, P. Haupt, K. **2011**. Magnetic molecularly imprinted polymer nanocomposites via surface-initiated RAFT polymerization. *Advanced Functional Materials*, **21** (20), 3947-3953.

85. Gospogova, N.; Terlemezyan, L. **1998**. Conducting polymers prepared by oxidative polymerization: Polyaniline. *Progress in Polymer Science*, **23**, 1443–1484.

86. Goto, A.; Kwak, Y.; Yoshikawa, C.; Tsujii, Y.; Sugiura, Y.; Fukuda, T. **2002**. Comparative study on decomposition rate constants for some alkoxyamines. *Macromolecules*, **35**, 3520-3525.

87. Grabchev, I.; Staneva, D.; Chovelon, J.-M. **2010**. Photophysical investigations on the sensor potential of novel, poly (propyleneamine) dendrimers modified with 1,8-naphthalimide units. *Dyes and Pigments*, **85**, 189-193.

88. Gregory, A.; Stenzel, M. H. **2011**. The use of reversible addition fragmentation chain transfer polymerization for drug delivery systems. *Expert Opinion on Drug Delivery*, **8** (2), 237-269.

89. Grubbs, R. B. **2011**. Nitroxide-mediated radical polymerization: Limitations and versatility. *Polymer Reviews*, **51** (2), 104-137.

90. Guan, G.; Liu, B.; Wang, Z.; Zhang, Z. **2008**. Imprinting of molecular recognition sites on nanostuctures and its application in chemosensors. *Sensors*, **8**, 8291-8320.

91. Guerreiro, A. R.; Chianella, I.; Piletska, E.; Whitcombe, W. J.; Piletsky, S. A. **2009**. Selection of imprinted nanoparticles by affinity chromatography. *Biosensors and Bioelectronics*, **24**, 2740-2743.

92. Gultekin, A.; Ersoz, A.; Hur, D.; Sariozlu, N. Y.; Denizli, A.; Say, R. **2009**. Gold nanoparticles having dipicolinic acid imprinted nanoshell for *Bacillus cereus* spores recognition. *Applied Surface Science*, **256**, 142-148.

93. Guven, O. **2007**. Radiation-induced conductivity control in polyaniline blends/composites. *Radiation Physics and Chemistry*, **76**, 1302–1307.

H

94. Hagashi, J.; Nakajama, Y.; Marchant, R. E.; Matsuda, T. **1999**. High-spatioresolved microarchitectural surface prepared by photograft copolymerization using dithiocarbamate: Surface preparation and cellular responses. *Langmuir*, **15**, 2080-2088.

95. Haris, P. B.; Metters, A. T. **2006**. Generation and characterization of photopolymerized polymer brush gradients. *Macromolecules*, **39**, 2764-2772.

96. Harz, S.; Schimmelpfennig, M.; Bui, B. T. S; Marchyk, N.; Haupt, K.; Feller, K. H. **2011**. Fluorescence optical spectrally resolved sensor based on molecularly imprinted polymers and microfuidics. *Engineering in Live Science*, **11** (6), 559-565.

97. Haupt, K.; Mosbach, K. **1998**. Plastic antibodies: Developments and applications. *Trends in Biotechnology*, **16** (11), 468-475.

98. Hawker, C. J.; Barclay, G. G.; Orellana, A.; Dao, J.; Devonport, W. **1996**. Initiating systems for nitroxide-mediated "living" free radical polymerisations: Synthesis and evaluation. *Macromolecules*, **29**, 5245-5254.

99. Hawker, C. J.; Bosman, A. W.; Harth, E. **2001**. New polymer synthesis by nitroxide mediated living radical polymerisations. *Chemical Reviews*, **101**, 3661-3688.

100. Hayden, O.; Agarwal, R.; Lieber, C. M. **2006**. Nanoscale avalanche photodiodes for highly sensitive and spatially resolved photon detection. *Nature Materials*, **5** (5), 352-356.

101. Hayes, W. A.; Shannon, C. **1996**. Electrochemistry of surface-confined mixed monolayers of 4-aminothiophenol and thiophenol on Au. *Langmuir*, **12** (15), 3688-3694.

102. Heeger, A. J. **2002**. Semi-conducting and metallic polymers: the fourth generation of polymeric materials. *Synthetic Metals*, **125**, 23–42.

103. Heinrich, M. R.; Kashman, Y.; Priller, P.; Steglich, W. **2001**, Revision of the structure of haliclorensin to (S)-7-methyl-1,5-diazacyclotetradecane and confirmation of the new structure by synthesis. *Tetrahedron Letters*, **57**, 9973-9978.

104. Helene, B.; Maud, S.; Cerdic, B. **2011**. Surface-initiated nitroxide-mediated polymerization from ordered mesoporous silica. *Macromolecules*, **44** (8), 2577-2588.

105. Hook, E. O.; Beegle, L. C.; Wystrach, D. P.; Wystrach, V. P. **1952**. Esters of dithiocarbamic acid and a method for their preparation. *US Patent No. 292972*.

106. Hoshino, Y.; Haberaecker, W. W.; Kodama, T.; Zeng, Z.; Okahata, Y.; Shea, K. J. **2010**. Affinity purification of multifunctional polymer nanoparticles. *Journal of the American Chemical Society*, **132** (39), 13648–13650.

107. Hoshino, Y.; Koide, H.; Urakami, T.; Kanazawa, H.; Kodama, T.; Oku, N.; Shea, K. J. **2010**. Recognition, neutralization and clearance of target peptides in the target peptides in the bloodstream of living mice by molecularly imprinted polymer nanoparticles: A plastic antibody. . *Journal of the American Chemical Society*, **132** (39), 6644-6645.

108. Husseman, M.; Malmström, E. E.; McNamara, M.; Mate, M.; Mecerreyes, D.; Benoit, D. G.; Hedrick, J. L.; Mansky,P.; Huang, E.; Russell, T. P.; Hawker, C. J. **1999**. Controlled synthesis of polymer brushes by "living" free radical polymerisation techniques. *Macromolecules*, **32**, 1424-1432.

109. Husemann, M.; Morrison, M; Benoit, D.; Frommer, J.; Mate, C. M.; Hinsberg, W. D.; Hedrick, J. L.; Hawker, J. C. **2000**. Manipulation of surface properties by patterning of covalently bound polymer brushes. *Jorunal of the American Chemical Society*, **122**, 1844-1845.

I

110. Ignatova, M.; Voccia, S.; Gilbert, B.; Markova, N.; Sandra, P.; Galleni, M.; Sciannamea, V.; Lenoir, S.; Cossement, D.; Gouttebaron, R.; Jèrôme, R.; Jèrôme, C. **2004**. Synthesis of copolymer brushes endowed with adhesion to stainless steel surfaces and antibacterial properties by controlled nitroxide-mediated radical polymerization. *Langmuir*, **20**, 10718-10726.

111. Inzelt, G.; Horányi, G. **1990**. Some problems connected with the study and evaluation of the effect of pH and electrolyte concentration on the behaviour of polyaniline film electrodes. *Electrochimica Acta*, **35** (1), 27-34.

112. Isarankura-Na-Ayudhya, C.; Boonpangrak, S.; Prachayasittikul, V.; Bülow, L.; Ye, L. **2005**. Construction of molecularly imprinted polymers for cholesterol by semi-covalent imprinting approach and nitroxide mediated radical polymerization. *Thammasat International Journal of Science and Technology*, **10** (4), 1-6.

113. Ishizu, K.; Katsuhara, H. **2006**. Diethyldithiocarbamate-mediated living radical polymerization and vevelopment for architechture of nanostuctured polymers. *Designed Monomers and Polymers*, **9** (2), 99-115.

114. Ivanova-Mitseva, P. K.; Fragkou, V.; Lakshmi, D.; Whitcombe, M. J.; Davis, F.; Guerreiro, A.; Grayston, J. A.; Ivanova, D. K.; Mitsev, P. A.; Piletska, E. V.; Piletsky, S. A. **2011**. Conjugated Polymers with pendant iniferter units: Versatile materials for grafting. *Macromolecules*, **44** (7), 1856-1865.

J

115. Jiang, D.; Tang, J.; Liu, B.; Yang, P.; Shen, X.; Kong, J. **2003**. Covalently coupling the antibody on an amine-self-assembled gold surface to probe hyaluronan-binding protein with capacitance measurement. *Biosensors and Bioelectronics*, **18**, 1183-1191.

K

116. Kane, M. C.; Lascola, R. J.; Clark, E. A. **2010**. Investigation on the effects of beta and gamma irradiation on conducting polymers for sensor applications. *Radiation Physics and Chemistry*, **79**, 1189–1195.

117. Kamigaito, M.; Ando T.; Sawamoto, M. **2001**. Metal-catalyzed living radical polymerisation. *Chemical Reviews*, **101**, (12), 3689-3746.

118. Kato, M.; Kamigaito, M.; Sawamoto, M.; Higashimura, T. **1995**. Polymerisation of methyl methacrylate with the carbon tetrachloride/dichlorotris - (triphenylphosphine) ruthenium (II)/methylaluminum bis (2,6-di-tert-butylphenoxide) initiating system: Possibility of living radical polymerisation. *Macromolecules*, **28**, 1721-1723.

119. Kim, B. J.; Oh, S. G.; Han, M. G.; Im, S. S. **2002**. Preparation of PANI-coated poly (styrene-co-styrene sulfonate) nanoparticles. *Polymer*, **43** (1), 111-116.

120. Kim, H. N.; Guo, Z.; Zhu, W.; Yoon, J.; Tian, H. **2011**. Recent progress on polymer-based fluorescent and colorimetric chemosensors. *Chemical Society Review*, **40**, 79-93.

121. Kim, J. B.; Bruening, M. L.; Backer, G. L. **2000**. Surface-initiated atom transfer radical polymerisation on gold at ambient temperature. *Journal of the American Chemical Society,* **122**, 7616-7617.

122. Klajnert, B.; Bryszewska, M. **2007**. Interactions between PAMAM dendrimers and gallic acid studied by spectroflurimetric methods. *Bioelectrochemistry*, **70**, 50-52.

123. Kloskowski, A.; Pilarczyk, M.; Przyjazny, A.; Namièsnik, J. **2009**. Progress in development of molecularly imprinted polymers as sorbents for sample preparation. *Critical Reviews in Analytical Chemistry*, **39**, 43-58.

124. Kobayashi, T.; Takahashi, S.; Nosaka, Y.; Fujii, N. **1992**. Silane coupling agents for photografting of vinyl monomer. Preparation and properties of (*N*,*N*-diethylamino) dithiocarbamoylpropyl (trimethoxy) silane. *Chemistry Letters*, **21** (7), 1321-1324.

125. Konn, C.; Morel, F; Beyou, E.; Chaumont, P.; Bourgeat-Lami, E. **2007**. Nitroxide-mediated polymerisation of styrene initiated from the surface of laponite clay platelets. *Macromolecules*, **40**, 7464-7472.

L

126. Ladmiral, V.; Morinaga, T.; Ohno, K.; Tsujii, Y.; Fukuda, T. **2006**. Synthesis of monodisperse zinc sulfide particles grafted with concentrated polymer brush. Surface-initiated living radical polymerisation on high refractive index particles. *Polymer Preprints, Japan*, **55** (2), 3424.

127. Lakshmi, D.; Bossi, A.; Whitcombe, M. J.; Chianella, I.; Fowler, S. A.; Subrahmanyam, S.; Piletska, E. V.; Piletsky, S. A. **2009**. Electrochemical sensor for catechol and dopamine based on a catalytic molecularly imprinted polymer-conducting polymer hybrid recognition element. *Analitical Chemistry*, **81** (9), 3576-3584.

128. Lakshmi, D.; Whitcombe, M. J.; Davis, F.; Chianella, I.; Piletska, E. V.; Guerreiro, A.; Subrahmanyam, S.; Brito, P. S.; Fowler, S. A.; Piletsky, S. A. **2009**. Chimeric polymers formed from a monomer capable of free radical, oxidative and electrochemical polymerization. *Chemical Communications*, 2759-2761.

129. Lalo, H.; Ayela, C.; Dague, E.; Vieu, C.; Haupt, K. **2010**. Nanopatterning molecularly imprinted polymers by soft lithography: A hierarchical approach. *Lab on a chip*, **10**, 1316-1318.

130. Langer, J. J.; Krzyminiewski, R.; Kruczynski, Z.; Gibinski, T.; Czajkowski, I.; Framski, G. **2001.** EPR and electrical conductivity in microporous polyaniline. *Synthetic Materials*, **122**, 359-362.

131. Lasàkovà, M.; Jandera, P. **2009**. Review: Molecularly imprinted polymer and their application in solid phase extraction. *Journal of Separation Science* , **32**, 799-812.

132. Lautner, G.; Kaev, J.; Reut, J.; Opik, A.; Rappich, J.; Syritski, V.; Robert E. Gyurcsanyi, R. E. **2011**. Selective artificial receptors based on micropatterned surface-imprinted polymers for label-free detection of proteins by SPR imaging. *Advanced Functional Materials*, **21** (3), 591–597.

133. Le, T. P.; Moad, G.; Rizzardo, S. H. **1998**. Polymerization with living characteristics. *Canadian Application Publication*, Publication No. CA **2259559 A1**.

134. Lee, E.; Park, D.-W.; Lee, J.-O; Kim, D. S.; Lee, B. H.; Kim, B. S. **2008**. Molecularly imprinted polymers immobilised on carbon nanotube. *Colloids and Surfaces A: Physicochemical Engineering Aspects*, **313-314**, 202-206.

135. Lee, H. Y.; Kim, B. S. **2009**. Grafting of molecularly imprinted polymers on iniferter-modified carbon nanotube. *Biosensors and Bioelectronics*. **25**, 587-591.

136. Lee, W. I.; Bae, Y.; Bard, A. J. **2004.** Strong blue photoluminescence and ESL from OH-terminated PAMAM dendrimers in the absence of gold nanoparticles. *Journal of the American Chemical Society*, **126**, 8358-8359.

137. Li, C.; Han, J.; Ryu, C. Y.; Beniczewicz, B. C. **2006**. A versatile method to prepare RAFT agent anchored substrates and the preparation of PMMA grafted nanoparticles. *Macromolecules*, **39**, 3175-3183.

138. Li, J.; Chen, X.; Chang, Y. C. **2005**. Preparation of end-grafted polymer brushes by nitroxide-mediated free radical polymerization of vaporized vinyl monomers. *Langmuir*, **21**, 9562-9567.

139. Li, J. Y.; Zu, B. Y.; Zhang, Y.; Guo, X. Z.; Zhang, H. Q. **2010**. One-pot synthesis of surface-functionalized molecularly imprinted polymer microspheres by iniferter-indulced *„living“* radical precipitation polymerization. *Journal of Polymer Science: Part A: Polymer Chemistry*, **48**, 3217-3228.

140. Li, X.; Husson S. M. **2006**. Adsorbtion of dansylated amino acids on molecularly imprinted surfaces: A surface plasmon resonance study. *Biosensors and Bioelectronics*, **22**, 336-348.

141. Li, Y.; Dong, C.K.; Chu, J.; Qi, J.Y.; Li, X. **2011**. Surface molecular imprinting onto fluorescein-coated magnetic nanoparticles via reversible addition fragmentation chain transfer polymerization: A facile three-in-one system for recognition and separation of endocrine disrupting chemicals. *Nanoscale*, **3** (1), 280-287.

142. Li, Y.; Yin, X. F.; Chen, F. R.; Yang, H. H.; Zhuang, Z. X.; Wang, X. R. **2006**. Synthesis of magnetic molecularly imprinted polymer nanowires using a nanoporous alumina template. *Macromolecules*, **39**, 4497-4499.

143. Li, Y.; Zhou, W. H.; Yang, H. H.; Wang, X. R. **2009**. Grafting of molecularly imprinted polymers from the surface of silica gel particles via reversible addition-

fragmentation chain transfer polymerization: A selective sorbent for theophylline. *Talanta*, **79**, 141-145.

144. Lia, S.; Caoa, Y.; Xuea, Z. **1987**. Soluble Polyaniline. *Synthetic Metals*, **20** (2), 141-149.

145. Listigovers, N. A.; Georges, M. K.; Odell, P. G.; Keoshkerian, B. **1996**. Narrow-polydispersity diblock and triblock copolymers of alkyl acrylates by a "living" stable free radical polymerisation. *Macromolecules*, **29**, 8992-8993.

146. Liu, G.; Wu, H. X.; Zheng, H. R.; Tang, L. H.; Hu, H.; Yang, H.; Yang, S. P. **2011**. Synthesis and application of fluorescent-magnetic-bifunctional dansylated Fe_3O_4@SiO_2. *Journal of Material Science*, **46**, 5959-5968.

147. Liu, H.; Zhuang, X.; Turson, M.; Zhang, M.; Dong, X. **2008**. Enrofloxacin-imprinted monolitic columns synthesized using reversible adittion-fragmentation chain transfer polymerisation. *Journal of Separation Science*, **31**, 1694-1701.

148. Liu, J. B.; Yang, X. H.; He, X. X.; Wang, K. M.; Wang, Q.; Guo, Q. P.; Shi, H.; Huang, J.; Huo, X. Q. **2011**. Fluorescent nanoparticles for chemical and biological sensing. *Science China Chemistry*, **54**, 1157-1176.

149. Liu, R. Y.; Guan, G. J.; Wang, S. H.; Zhang, Z. P. **2011**. Core-shell nanostructured molecular imprinting fluorescent chemosensor for selective detection of atrazine herbicide. *Analyst*, **136**, 184-190.

150. Long, Y. Z.; Chen, Z. J.; Huang, K.; Wan, M. **2004**. Synthesis and electrical properties of freestanding film of azobenzene side-chain polyaniline. *Applied Physics Letters*, **84** (11), 1898-1900.

151. Lu, C. H.; Zhou, W. H.; Han, B.; Yang, H. H.; Chen, X.; Wang, X. R. **2007**. Surface-imprinted core-shell nanoparticles for sorbent assays. *Analytycal Chemistry*, **79** (14), 5457-5461.

152. Lui, P.; Su, Z. **2006**. Surface-initiated atom transfer radical polymerisation (SI-ATRP) of styrene from chitosan particles. *Materials Letters*, **60**, 1137-1139.

153. Luo, N.; Hutchison, J. B.; Anseth, K. S.; Bowman, C. N. **2002**. Synthesis of a novel methacrylic monomer iniferter and its application in surface photografting on crosslinked polymer substrates. *Journal of Polymer Science, Part A: Polymer Chemistry*, **40**, 1885-1891.

154. Lutsen, L.; Vanderzande, D. **2010**. Conjugated polymers provided with at least one molecular imprinted polymer and a method for their preparation via conjugated macro-iniferters. *US Patent 7649048*.

M

155. MacDiarmid, A. G. **1997**. Polyaniline and polypyrrole: Where are we headed? *Synthetic Metals*, **84** (1-3), 27-34.

156. MacDiarmid, A. G.; Chiang, J. C.; Halpern, M.; Huang, W. S.; Mu, S. L.; Somasiri, N. L. D.; Wu, W. Q.; Yaniger, S. I. **1985**. "Polyaniline": Interconversion of metallic and insulating forms. *Molecular Crystals and Liquid Crystals*, **121**, 173–180.

157. Maddock, S. C.; Pasetto, P.; Resmini, M. **2004**. Novel imprinted soluble microgels with hydrolytic catalytic activity. *Chemical Communications*, 536-537.

158. Malinauskas, A.; Holze, R. **1997**. In situ UV-Vis spectroelectrochemical evidence of an EC mechanism in the electrooxidation of *N*-methylaniline. *Berichte der Bunsen-Gesellschaft für Physikalische Chemie*, **101**, 1859-1864.

159. Malinauskas, A.; Holze, R. **1998**. UV-VIS spectroelectrochemical detection of intermediate species in the electropolymerization of an aniline derivative. *Electrochimica Acta*, **43** (16-17), 2413-2422.

160. Malkaj, P.; Dalas, E.; Vitoratos, E.; Sakkopoulos, S. **2006**. pH electrodes constructed from polyaniline/zeolite and polypyrrole/zeolite conductive blends. *Journal of the Applied Polymer Science*, **101** (3), 1853-1856.

161. Manga, J. D.; Polton, A.; Tardi, M.; Sigwalt, P. **1998**. Mechanism of the polymerization of n-butyl acrylate initiated by *N*,*N*-diethyldithiocarbamate derivatives. Part 1. Photolysis of butyl-2-(*N*,*N*-diethyldithiocarbamyl)propionate and oligomerization of butyl acrylate. *Polymer International*, **45** (1), 14-21.

162. Mansky, P.; Liu, Y.; Huang, E.; Russell, T. P.; Hawker, C. **1997**. Controlling polymer-surface interactions with random copolymer brushes. *Science*, **275**, 1458-1460.

163. Matsuda, T.; Otsu, S. **2005**. Photoiniferter-based thermoresponsive graft architecture with albumin covalently fixed at growing graft chain end. *Langmuir*, **21**, 9660-9665.

164. Matsuno, R.; Otsuka, H.; Takahara, A. **2006**. Polystyrene-grafted titanium oxide nanoparticles prepared through surface-initiated nitroxide-mediated radical polymerisation and their application to polymer hybrid thin films. *Soft Materials*, **2** (5), 415-421.

165. Matyjaszewski, K.; Shigemoto, T.; Frechet, J. M.; Leduc, M. **1996**. Controlled/"living" radical polymerization with dendrimers containing stable radicals. *Macromolecules*, **29**, 4167-4171.

166. Mayes, A. G.; Whitcombe, M. J. **2005**. Synthetic strategies for the generation of molecularly imprinted organic polymers. *Advanced Drug Delivery Review*, **57**, 1742-1778.

167. McCormic, C. L.; Lowe, A. B. **2004**. Aqueous RAFT polymerisation: Recent developments in synthesis of functional water-soluble (co) polymers with controlled structures. *Accounts in Chemical Research*, **37** (5), 312-325.

168. Merion, K. B.; Armodo, S. **2009**. Polymer brushes by nitroxide-mediated polymerization. *Macromolecular Rapid Communications*, **30** (13), 1043-1057.

169. Min, K.; Matyjaszewski, K. **2009**. Atom transfer radical polymerization in aqueous media. *Central European Journal of Chemistry*, **7** (4), 657-674.

170. Mirsky, M. V.; Hirsch, T.; Piletsky, S. A.; Wolfberies, O. S. **1999**. A spreader-bar approach to molecular architecture: Formation of stable artificial chemoreceptors. *Angewandte Chemie International Edition,* **38** (18), 1108-1110.

171. Mijangos, I.; Guerreiro, A.; Piletska, E.; Whitcombe, M. J.; Karim, K.; Chianella, I.; Piletsky, S. **2009**. Macroradical initiated polymerisation of acrylic and methacrylic monomers. *Journal of Separation Science, Special Issue: Molecular Imprinting*, **32**, 3340-3346.

172. Moad, G.; Rizzardo, E.; Thang, S. H. **2008**. Toward living radical polymerization. *Accounts of Chemical Research*, **41**, 1133-1142.

173. Moad, G.; Rizzardo, E.; Thang, S. H. **2008**. Radical addition-fragmentation chemistry in polymer synthesis. *Polymer*, **49**, 1079-1131.

174. Moad, G.; Rizzardo, E.; Thang, S. H. **2011**. End-functionalpolymers, thiocarbonylthio group removal/transformation and reversible addition-fragmentation-chain transfer (RAFT) polymerization. *Polymer International*, **60** (1), 9-25.

175. Molina, M. A.; Rivarola, C. R.; Miras, M. C.; Lescano, D.; Barbero, C. A. **2011**. Nanocomposite synthesis by absorption of nanoparticles into macroporous hydrogels. Building a chemomechanical actuator driven by electromagnetic radiation. *Nanotechnology*, **22**, 1-8.

176. Mu, S. L.; Chen, C. X.; Wang, J. M. **1997**. The kinetic behavior for the electrochemical polymerization of aniline in aqueous solution. *Synthetic Metals*, **88** (3), 249-254.

177. Muldoon, M. T.; Stanker, L. H. **1997**. Molecularly imprinted solid phase extraction of atrazine from beef liver extracts. *Analytical Chemistry*, **69** (5), 803-808.

N

178. Nalwa, H. S. **2001**, Handbook of advanced electronic and photonic materials and divices. Volume 8: Conducting polymers, Holze, R. Spectroelectrochemistry of conducting polymers, pages 218-231.

179. Nakayama, Y.; Matsuda, T. **1996**. Surface macromolecular architectural designs using photo-graft copolymerization based on photochemistry of benzyl *N*,*N*-diethyldithiocarbamate. *Macromolecules*, **29** (27), 8622-8630.

180. Nakayama, Y.; Matsuda, T. **1999**. In situ observation of dithiocarbamate-based surface photograft copolymerization using quartz crystal microbalance. *Macromolecules*, **32**, 5405-5410.

181. Nakayama, Y; Matsuda, T; Irie, M. **1993**. A novel surface photograft polymerisation method for fabricated devices. *American Society for Artificial Internal Organs transactions*, **39**, M545-M549.

182. Neslihan, A.; Tuncer, E. A.; Yusuf, Y. **2009**. Styrenation of triglyceride oil by nitroxide mediated radical polymerisation. *Progress in Organic Coationgs*, **66** (2), 99-106.

183. Norrlöw, O.; Glad, M.; Mosbach, K. **1984**. Acrylic polymer preparations containing recognition sites obtained by imprinting with substrates. *Journal fo Chromatography*, **299**, 29-41.

184. Novak, P.; Muller, K.; Santhanam, K. S. V.; Haas, O. **1997**. Electrochemically active polymers for rechargeable batteries. *Chemical Reviews*, **97** (1), 207-282.

O

185. Ogawa, M.; Nitahara, S.; Aoki, H.; Ito, S.; Narazaki, M.; Matsuda, T. **2010**. Fluorinated Polymer Nanoparticles as a Novel 19F MRI Contrast Agent Prepared by Dendrimer-Initiated Living Radical Polymerization. *Macromolecular Chemical Physics*, **211**, 1369-1376.

186. O'Reilly, R. K. **2010**. Using controlled radical polymerisation techniques for the synthesis of functional polymers containing amino acidmoieties. *Polymer International*, **59** (5), 568-573.

187. Otsu, T. **2000**. Iniferter concept and living radical polymerization. *Journal of Polymer Science: Part A: Polymer Chem*istry, **38**, 2121-2136.

188. Otsu, T.; Yamashita, K.; Tsuda, K. **1986**. Synthesis, reactivity, and role of 4-vinylbenzyl *N*,*N*-diethyldithiocarbamate as a monomer-iniferter in radical polymerization. *Macromolecules*, **19**, 287-290.

189. Otsu, T.; Yoshida, M. **1982**. Role of initiator-transfer agent-terminator (iniferter) in radical polymerisations: Polymer design by organic disulfides as iniferters. *Makromolekulaare Chemie Rapid Communications*, **3**, 127-132.

190. Oxelbark, J.; Legido-Quigley, C.; Aureliano, C. S. A.; Titirici, M. M.; Schillinger, E.; Sellergren, B.; Courtois, J.; Irgum, K.; Dambies, L.; Cormack, P. A. G.; Sherrington, D. C.; Lorenzi, E. D. **2007**. Chromatographic comparison of bupivacaine imprinted polymers prepared in crushed monolith, microsphere, silica-based composite and capillary monolith formats. *Journal of Chromatography A*, **1160**, 215-226.

191. Ozin, G. A.; Arsenault, A. C. **2005**, Nanochemistry: A chemical approach to nanomaterials, RSC publishing, Cambridge.

P

192. Pan, G. Q.; Zhang, Y.; Guo, X. Z.; Li, C. X.; Zhang, H. Q. **2010**. An efficient approach to obtaining water-compatible and stimuli-responsive molecularly imprinted polymers by the facile surface-grafting of functional polymer brushes via RAFT polymerization. *Biosensors and Bioelectronics*, **26** (3), 976-982.

193. Pan, G.; Zu, B.; Guo, X.; Zhang, Y.; Li, C.; Zhang, H. **2009**. Preparation of molecularly imprinted polymer microspheres via reversible addition-

fragmentation chain transfer precipitation polymerisation. *Polymer*, **50**, 2819-2825.

194. Pan, G. Q.; Zhang, Y.; Ma, Y.; Li, C. X.; Zhang, H. Q. **2011**. Efficient one-potsynthesis of water-compatible molecularly imprinted polymer microspheres by facile RAFT precipitation polymerization. *Angewandte Chimie International Edittion*, **50** (49), 11731-11734.

195. Patten, T. E.; Matyjaszewski, K. **1998**. Atom transfer radical polymerisation and the synthesis of polymeric materials. *Advanced Materials*, **10**, (12), 901-915.

196. Pearson, S.; Allen, N.; Stenzel, M. H. **2009**. Core-shell particles with glucopolymer shell and polynucleoside core via RAFT: From micelles to rods. *Journal of Polymer Sciense: Part A: Polymer Chemistry*, **47**, 1706-1723.

197. Pérez-Moral, N.; Mayes, A. G. **2007**. Molecularly imprinted multi-layer core-shell nanoparticles – a surface grafting approach. *Macromolecular Rapid Communications*, **28**, 2170-2175.

198. Piletska, E. V.; Piletsky, S. A.; Subrahmanyam, S.; Karim, K.; Turner, A. P. F. **2000**. A new reactive polymer suitable for covalent immobilization and monitoring of primary amines. *Polymer*, **42**, 3603-3608.

199. Piletsky, S. A.; Matuschewski, H.; Schedler, U.; Wilper, A.; Piletska, E. V.; Thiele, T. A.; *et al.*. **2000**. Surface functionalisation of porous polypropylene membranes with molecularly imprinted polymers by photograft copolymerisation in water. *Macromolecules*, **33**, 3092-3098.

200. Piletsky, S. A.; Panasyuk, T. L.; Piletskaya, E. V.; Sergeeva, T. A.; El'skaya, A. V.; Pringsheim, E.; Wolfbeis, O. S. **2000**. Polyaniline-coated microtiter plates for use in longwave optical bioassays. *Fresenius' Journal of Analytical Chemistry*, **366** (8), 807-810.

201. Piletsky, S. A.; Piletska, E. V.; Karim, K.; Freebairn, K. W.; Legge, C. H.; Turner, A. P. F. **2002**. Polymer cookery: influence of polymerization conditions on the

performance of molecularly imprinted polymers. *Macromolecules*, **35**, 7499-7504.

202. Piletsky, S.; Piletska, E.; Bossi, A.; Turner, N.; Turner, A. **2003**. Surface functionalization of porous polypropylene membranes with polyaniline for protein immobilization. *Biotechnology and Bioengineering*, **82** (1), 86-92.

203. Poindexter, G. S. **1981**, Aminoethylation process. *United States Patent,* № **4,381,401.**

204. Poindexter, S. G.; Owens, D.A.; Dolan, P. L., Woo, E. **1992**, The use of 2-oxazolidinones as latent aziridine equivalents. 2. Aminoethylation of aromatic amines, phenols and thiophenols. *Journal of Organic Chemistry*, **57**, 6257-6265.

205. Poma, A.; Turner, A. P. T.; Piletsky, S. A. **2010**. Advances in the manufacture of MIP nanoparticles. *Trends in Biotechnology*, **28** (12), 629-637.

206. Polyakov M. V. **1931**. Adsorption properties and structure of silica gel. *Zhur. Fiz. Khim.*, **2**, 799-805.

207. Prasad, B. B.; Kumar, D.; Madhuri, R.; Tiwari, M. P. **2011**. Metal ion mediated imprinting for electrochemical enantioselective sensing of L-histidine at trace level. *Biosensors and Bioelectronics*, **28**, 117-126.

Q

208. Qin, L.; He, X. W.; Zhang, W.; Li, W. Y.; Zhang, Y. K. **2009**. Surface-modified polystyrene beads as photografting imprinted polymer matrix for chromatographic separation of proteins. *Journal of Chromatography A*, **1216**, 809-814.

209. Qin, S. H.; Qiu, K. Y. **2001**. A new polymerizable photoiniferter for preparing poly (methyl methacrylate) macromonomer. *European Polymer Journal*, **37**, 711-717.

R

210. Rahane, S. B.; Kilbey II, S. M.; Metters, A. T. **2005**. Kinetics of surface-initiated photoiniferter-mediated photopolymerization. *Macromolecules*, **38**, 8202-8210.

211. Rosen, B. M.; Percec, V. **2007**. A density functional theory computational study of the role of ligand on the stability of Cu^{I} and Cu^{II} species associated with ATRP and SET-LRP. *Journal of Polymer Science: Part A: Polymer Chemistry*, **45**, 4950-4964.

S

212. Saito, R. **2008**. Combination of template polymerisation and atom transfer radical polymerisation: Strategy for synthesis of specifically structural polymers. *Polymer*, **49**, 2625-2631.

213. Salaneck, W. R.; Liedberg, B.; Inganaes, O.; Erlandsson, R.; Lundstroem, I.; MacDiarmid, A. G.; Halpern, M.; Somasiri, N. L. D. **1985**. Physical characterization of some polyaniline. *Molecular Crystals and Liquid Crystals*, **121** (1-4), 191-194.

214. Salerno, A.; Ceriani, V.; Perillo, I. A. **1997**, Nucleophilic addition to substituted 1H-4,5-Dihydroimidazolium salts. *Journal of Heterocyclic Chemistry*, **34**, 709-716.

215. Saridakis, E.; Khurshid, S.; Govada, L.; Phan, Q.; Hawkins, D.; Crichlow, G. V.; Lolis, E.; Reddy, S. M.; Chayen, N. E. **2011**. Protein crystallization facilitated by molecularly imprinted polymers. *PNAS*, Published online before print June 20, 2011, doi: 10.1073/pnas.1016539108.

216. Schomburg, K. C.; McCarley, R. L. **2001**. Surface-confined monomers on electrode surfaces. 11. Electrochemical and infrared spectroscopic characteristics of aniline-terminated alkanethiol monolayers on Au electrochemically treated in nonaqueous media. *Langmuir*, **17** (6), 1993-1998.

217. Sellergren, B.; Rückert, B. J.; Hall, A. **2002**. Layer-by-layer grafting of molecularly imprinted polymers via iniferter modified supports. *Advanced Materials*, **14**, 1204-1208.

218. Sergeyeva, T. A.; Matuschewski, H.; Pletsky, S. A.; Bendig, J.; Schedler, U.; Ulbricht, M. **2001**. Molecularly imprinted polymer membranes for substance-selective solid-phase extraction from water by surface photo-grafting polymerisation. *Journal of Chromatografy A*, **907**, 89-99.

219. Sergeyeva, T. A.; Piletsky, S. A.; Brovko; A. A.; Slinchenko; E. A.; Sergeeva; L. M.; El'skaya, A. V. **1999**. Selective recognition of atrazine by molecularly imprinted polymer membranes. Development of conductometric sensor for herbicides detection. *Analytical Chimica Acta*, **392** (2-3), 105-111.

220. Shen, S.; Wu, W.; Guo, K.; Chen, J. **2005**. In situ preparation of nano-silica/polymethylmethacrylate composite particles by two-step inverse microemulsion method. *Journal of the Chinese Ceramic Society*, **33** (3), 304-308.

221. Shen, Y.; Wang, Y.; Chen, J.; Li, H.; Li, Z.; Li, C. **2010**. Nitroxide-mediated polymerisation of styrene initiated from the surface of montmorillonite clay plates. *Journal of Applied Polymer Science*, **118**, 1198-1203.

222. Singha, N.; Wang, J.; Ulbricht, M.; Wickramasinghe, S. R.; Husson, S. M. **2008**. Surface-initiated atom transfer radical polymerization: A new method for preparation of polymeric membrane adsorbers. *Journal of Membrane Science*, 309 (1-2), 64-72.

223. Siwy, Z.; Trofin, L.; Kohli, P.; Backer, L. A.; Trautmann, C.; Martin, C. R. **2005**. Protein biosensors based on biofunctionalized conical gold nanotubes. *Journal of the American Chemical Society*, **127**, 5000-5001.

224. Skrabania, K.; Li, W.; Laschewsky, A. **2008**. Synthesis of double-hydrophilic BAB triblock copolymers via RAFT polymerisation and their thermoresponsive self-assembly in water. *Macromolecular Chemistry and Physics*, **209**, 1389-1403.

225. Smith, A. E.; Xu, X. W.; McCormick, C. L. **2010**. Stimuli-responsive amphiphilic (co)polymers via RAFT polymerization. *Progress in Polymer Science*, **35**, 45-93.

226. Smith, N. K. R. **1979.** A review of sources of spurious silicon peaks in electron microprobe X-ray spectra of biological specimens. *Analytical Biochemistry*, **94** (1), 100-104.

227. Southard, G. E.; Van Houten, K. A.; Ott, E. W.; Murray, G. M. **2007**. Luminescent sensing of organophosphates using europium (III) containing imprinted polymers prepared by RAFT polymerization. *Analytica Chimica Acta*, **581**, 202-207.

228. Southard, G. E.; Van Houten, K. A.; Murray, G. M. **2007**. Soluble and processable phosphonate sensing star molecularly imprinted polymers. *Macromolecules*, **40**, 1395-1400.

229. Srivastava, P.; Shahid, M.; Misra, A. **2011**. Protein assisted fluorescence enhancement of a dansyl containing fluorescent reagent: Detection of Hg^{+} ion in aqueous medium. *Organic and Biomolecular Chemistry*, **9**, 5051-5051.

230. Stafstrom, S.; Breadas, J. L.; Epstein, A. J.; Woo, H. S.; Tenner, D. B.; W.S. Huang, W. S. **1987**. Polaron lattice in highly conducting polyaniline: Theoretical and optical studies. *Physical Review Letters,* **59** (13), 1464–1467.

231. Studer, A.; Schulte, T. **2005**. Nitroxide-mediated radical processes. *The Chemical Record*, **5**, 27-35.

232. Su, S. F.; Zhang, M.; Li, B. L.; Zhang, H. Y.; Dong, X. C. **2008**. HPLC determination of sulfamethazine in milk using surface-imprinted silica synthesized with iniferter technique. *Talanta*, **76**, 1141-1146.

233. Suarez, I. J.; Rosal, R.; Rodriguez,A.; Ucles, A.; Fernandez-Alba, A. R.; Hernando, M.D.; Garcia-Calvo, E. **2011**. Chemical and ecotoxicological assessment of poly (amidoamine) dendrimers in the aquatic environment. *Trends in Analytical Chemistry*, **30** (3), 492-506.

234. Suryanarayanan, V.; Wu, C. T.; Ho, K. C. **2010**. Molecularly imprinted electrochemical sensors. *Electroanalysis*, **22**, 1795-1811.

235. Szwarc, M. **1956**. “Living” polymers. *Nature*, **178**, 1168-1169.

236. Szwarc, M.; Levy, R.; Mitkovich, J. **1956**. Polymerization initiated by electron transfer to monomer. A new method of formation of block polymers. *Journal of the American Chemical Society*, **78** (11), 2656-2657.

T

237. Tabushi, I.; Kurihara, K.; Naka, K.; Yamamura, K.; Hatakeyama, H. **1987**. Supramolecular sensor based on SnO2 electrode modified withoctadecylsilyl monolayer having molecular binding sites. *Tetrahedron Letters*, **28** (47), 4299-4302.

238. Tamayo, F. G.; Turiel, E.; and Martín-Esteban, A. **2007**. Molecularly imprinted polymers for solid-phase extraction and solid-phase microextraction: recent developments and future trends. *Journal of Chromatography A*, *1152* (1-2), 32-40.

239. Tanaka, M.; Tanaka, H.; Pelton, R. **2007.** Amine-derivatized poly (diallyldimethylammonium chloride) from *N*-vinylformamide copolymerization. *Journal of Applied Polymer Science*, **104**, 1068-1075.

240. Taniguchi, T.; Goto, N.; Ishibashi, H. **2009**. Novel synthesis of 3-aminopropionitriles by ring opening of 2-oxazolidinones with cyanide ion. *Tetrahedron Letters*, **50** (34), 4857-4858.

241. Titirici, M.-M.; Sellergren, B. **2006**. Thin molecularly imprinted polymer films via reversible addition-fragmentation chain transfer polymerisation. *Chemistry of Materials*, **18**, 1773-1779.

242. Tokonami, S.; Shiigi, H.; Nagaoka, T. **2009**. Review: Micro- and nanosized molecularly imprinted polymers for high-throughput analytical application. *Analytica Chimica Acta*, **641**, 7-13.

243. Turner, S. R.; Blevins, R. W. **1990**. Photoinitiated block copolymer formation using dithiocarbamate free radical chemistry. *Macromolecules*, **23** (6), 1856-1859.

U

244. Ulgut, B.; Zhao, Y.; Grose, J. E.; Ralph, D. C.; Abruña, H. D. **2006**. Electrochemical properties of self-assembled monolayers of polyaniline: Effects of the thiol substituent and reduced dimensionality. *Langmuir*, **22** (9), 4433-4437.

V

245. Vaihinger, D.; Landfester, K.; Kräuter, I.; Brunner, H.; Tovar, G. E. M. **2002**. Molecularly imprinted polymer nanospheres as synthetic affinity receptors obtained by miniemulsion polymerisation. *Macromolecular Chemical Physics*, **203** (13), 1965-1973.

246. Vandevelde, F.; Belmont, A. S.; Pantigny, J.; Haupt, K. **2007**. Hierarchically nanostructured polymer films based on molecularly imprinted surface-bound nanofilaments. *Advanced Materials*, **19** (21), 3717-3720.

247. Vaughan, A. D.; Zhang, J. B.; Byrne, M. E. **2010**. Enhancing therapeutic loading and delaying transport via molecular imprinting and living/controlled polymerization. *American Institute of Chemical Engineers Journal*. **56** (1), 268-279.

248. Wang, H. Y.; Kobayashi, T.; Fujii, N. **1997**. Surface molecular imprinting on photosensitive dithiocarbamoil polyacrilonitrile membranes using photograft polymerisation. *Journal of Chemical Technology and Biotechnology*, **70**, 355-362.

249. Wang, H. J.; Zhou, W. H.; Yin, X. F.; Zhuang, Z.-X.; Yang, H. H.; Wang, X. R. **2006**. Template synthesized molecularly imprinted polymer nanotube membranes for chemical separations. *Journal of the American Chemical Society,* **128**, 15954-15955.

250. Wang, J. S.; Matyjaszewski, K. J. **1995**. Controlled/"living" radical polymerisation. Atom transfer radical polymerisation in the presence of transition-metal complexes. *Journal of the American Chemical Society*, **117**, 5614-5615.

251. Wang, L.; Zhang, Z.; Huang, L. **2008**. Molecularly imprinted polymer based on chemiluminescence imaging for the chiral recognition of dansyl-phenylalanine. *Analytical and Bioanalitical Chemistry*, **390**, 1431-1436.

252. Wang S. S.; Li, D. M.; Hua, Z. D.; Zhao, M. P. **2011**. Molecularly imprinted monolith coupled on-line with high performance liquid chromatography for simultaneous quantitative determination of cyromazine and melamine. *Analyst*, **136** (6), 3672-3679.

253. Wang, Y.; Shen, Y.; Pei, X.; Zhang, S.; Liu, H.; Ren, J. **2008**. In situ synthesis of poly (srtrene-co-maleic anhydride)/SiO_2 hybrid composites via „grafting onto“ strategy based on nitroxide-mediated radical polymerisation, *Reactive and Functional Polymers*, **68**, 1225-1230.

254. Webster, O. W. **1991**. Living polymerization methods. *Science*, **251**, 887-893.

255. Wei, S.; Molinelli, A.; Mizaikoff, B. **2006**. Molecularly imprinted micro- and nanospheres for the selectively recognition of 17β-estradiol. *Biosensors Bioelectronics*, **21** (10), 1943-1951.

256. Wei, X.; Husson, S. M. **2007**. Surface-grafted, molecularly imprinted polymers grown from silica gel for chromatographic separations. *Industrial Engineering Chemical Research*, **46**, 2117-2124.

257. Wei, X.; Li, X.; Husson, S. M. **2005**. Surface molecular imprinting by atom transfer radical polymerisation. *Biomacromolecules*, **6**, 1113-1121.

258. Wei, Y.; Jang, G. W.; Chan, C. C., Hsueh, K. F.; Hariharan, R. H.; Patel, S. A.; Whitecar, C. K. **1990**. Polymerization of aniline and alkyl ring-substituted anilines in the presence of aromatic additives. *Journal of Physical Chemistry*, **94** (19), 7716-7721.

259. Weimer, M. W.; Chen, H.; Giannelis, E. P.; Sogah, D. Y. **1999**. Direct synthesis of dispersed nanocomposites by in situ living free radical polymerisation using a silicate-anchored initiator. *Journal of the American Chemical Society*, **121**, 1615-1616.

260. Whitcombe, M. J. **2011.** Smart hydrogel crystal gardens. *Nature Chemistry*, **3** (9), 657-658.

261. Whitcombe, M. J.; Chianella, I.; Larcombe, L.; Piletsky, S. A.; Noble, J.; Porter, R.; Horgan, A. **2011**. The rational development of molecularly imprinted polymer-based sensors for protein detection. *Chemical Society Review*, **40**, 1547-1571.

262. Williams, D.H.; Fleming, I. **1995**. *Spectroscopic Methods in Organic Chemistry*, 5th Edition, McGraw-Hill, Maidenhead.

263. Wu, Z.; Chen, H.; Lui, X.; Zhang, Y.; Li, D.; Huang, H. **2009**. Protein adsorption on poly (*N*-vinylpyrrolidone)-modified silicon surfaces prepared by surface initiated atom transfer radical polymerisation. *Langmuir*, **25**, 2900-2906.

264. Wulff, G. **1995**. Molecular imprinting in cross-linked materials with the aid of molecular templates - A way towards artificial antibodies. *Angewandte Chemie International Edition*, **34** (17), 1812-1832.

265. Wulff, G.; Chong, B. O.; Kolb, U. **2006**. Soluble single-molecule nanogels of controlled structure as a matrix for efficient artificial enzymes. *Angewandte Chemie International Edition*, **45** (18), 2955–2958.

X

266. Xia, H. S.; Wang, Q. **2002**. Ultrasonic irradiation: A novel approach to prepare conductive polyaniline/nanocrystalline titanium oxide composites. *Chemistry of Materials*, **14** (5), 2158-2165.

267. Xie, C.; Zhang, Z.; Wang, D; Guan, G.; Gao, D.; Lui, J. **2006**. Surface molecular self-assembly strategy for TNT imprinting of polymer nanowire-nanotube arrays. *Analytical Chemistry*, **78** (24), 8339-8346.

268. Xu, J. X.; Gao, Y.; Li, H. M. **2011**. Controlled fabrication of theophyline imprinted polymers on multiwalled carbon nanotubes via atom transfer radical polymerization. *Journal of Nanoscience and Nanotechnology*, **11** (2), 1217-1224.

269. Xu, S. F.; Chen, L. G.; Li, J. H.; Qin, W.; Ma, J. P. **2011**. Preparation of hollow porous molecularly imprinted polymers and their applications to solid-phase extraction of triazines in soil samples. *Journal of Materials Chemistry*, **21**, 12047-12053.

270. Xu, W. J.; Su, S. F.; Jiang, P.; Wang, H. S.; Dong, X. C.; Zhang, M. **2010**. Determination of sulfonamides in bovine milk with column-switching high performance liquid chromatography using surface imprinted silica with hydrophilic external layer as restricted access and selective extraction material. *Journal of Chromatography A*, **1217**, 7198-7207.

Y

271. Yang, K.; Berg, M. M.; Zhao, C.; Ye, L. **2009**. One-pot synthesis of hydrophilic molecularly imprinted nanoparticles. *Macromolecules*, **42**, 8739-8746.

272. Ye, L.; Cormack, P. A. G.; Mosbach, K. **2001**, Molecular imprinting on microgel spheres. *Analytical Chimica Acta*, **435** (1), 187-196.

273. Ye, L.; Mosbach, K. **2008**. Molecular imprinting: Synthetic materials as substitutes for biological antibodies and receptors. *Chemical Materials*, **20**, 859-868.

274. Ye, T.; Lu, S. Y.; Hu, Q. Q.; Jiang, X.; Wei, G. F.; Wang, J. J.; Lu, J. Q. **2011**. One-bath synthesis of hydrophilic molecularly imprinted quantum dots for selective recognition of chlorophenol. *Chinese Chemical Letters*, **22** (11), 1253-1256.

275. Yi, C.; Xu, Z.; Ford, W. T. **2004**. Nano-sized dendrimer PAMAM/polystyrene composite polymer emulsion. *Colloid Polymer Science*, **282**, 1054-1058.

276. Yoshimatsu, K.; Reimhult, K.; Krozer, A.; Mosbach, K.; Sode, K.; Ye, L. **2007**. Uniform molecularly imprinted microspheres and nanoparticles prepared by precipitation polymerization: The control of particle size suitable for different analytical applications. *Analytical Chimica Acta*, **584** (1), 112-121.

277. Yoshikawa, C.; Goto, A.; Tsujii, Y.; Fukuda, T.; Yamamoto, K.; Kishida, A. **2005**. Fabrication of high-density polymer brush on polymer substrate by surface-initiated living radical polymerisation. *Macromolecules*, **38** (11), 4604-4610.

278. Yow-Jon, L.; Fu-Ming, Y.; Lin Chi-Shin, L. **2007**. Effects of ultraviolet irradiation on energy band structure and conductivity of polyaniline. *Journal of Applied Physics*, **102** (10), 102-104.

Z

279. Zaucha, M.; Adamczyk, Z.; Barbasz, J. **2011**. Zeta potential of particle bilayers on mica: A streaming potential study. *Journal of Colloid and Interface Science*, **360** (1), 195-203.

280. Zeng, Z.; Hoshino, Y.; Rodrigues, A.; Yoo, H.; Shea, K. **2010**. Synthetic polymer nanoparticles with antibody-like affinity for a hydrophilic peptide. *American Chemical Society Nano*, **4** (1), 199-204.

281. Zhai, G; Yu, W. H.; Kang, E. T.; Neoh, K. G.; Huang, C. C.; Liaw, D. J. **2004**. Functionalization of hydrogen-terminated silicon with polybetaine brushes via surface-initiated reversible addition-fragmentation chain-transfer (RAFT). *Industrial and Engineering Chemistry Research*, **43**, 1673-1680.

282. Zhang, H.; Deng, J.; Lu, L.; Cai, Y. **2007**. Ambient-temperature RAFT polymerisation of styrene and its functional derivatives under mild long-wave UV-Vis radiation. *Macromolecules*, **40** (26), 9252-9261.

283. Zhang, W.; He, X.W.; Chen, Y.; Li, W.Y.; Zhang, Y.K. **2011**. Composite of CdTe quantum dots and molecularly imprinted polymer as a sensing material for cytochrome C. *Biosensors and Bioelectronics*, **26** (5), 2553-2558.

284. Zhao, X. D. Fan, X. H.; Chen, X. F.; Chai, C. P.; Zhou, Q. F. **2006**. Surface modification of multiwalled carbon nanotubes via nitroxide-mediated radical polymerization. *Journal of Polymer Science: Part A: Polymer Chemistry*, **44** (15), 4656-4667.

285. Zheng, H.; Zhang, R.; Dong, F.; Zheng, Y.; Shen, J. **1997**. Electron transfer between two stable radicals. *Macromolecular Rapid Communications*, **18**, 379-383.

286. Zhu, Q. J.; Tang, J.; Dai, J.; Gu, S. W.; Chen, S. W. **2007**. Synthesis and characteristics of imprinted 17-estradiol microparticle and nanoparticle with TFMAA as functional monomer. *Journal of Applied Polymer Science*, **104** (3), 1551-1558.

287. Zimmerman, S. C.; Wendland, M. S.; Rakow, N. A.; Zharov, I.; Suslick, K. S. **2002**. Synthetic host by molecular imprinting inside dendrimers. *Nature*, **418**, 399-403.

288. Zu, B. Y.; Pan, G.; Guo, X.; Zhang, Y.; Zhang, H. **2009**. Preparation of molecularly imprinted polymer microspheres via atom transfer radical precipitation

plymerisation. *Journal of Polymer Science: Part A: Polymer Chemistry*, **47**, 3257-3270.

289. Zu, B. Y.; Zhang, Y.; Guo, X. Z.; Zhang, H. Q. **2010**. Preparation of molecularly imprinted polymers via atom transfer radical “bulk” polymerisation. *Journal of Polymer Science, Part A: Polymer Chemistry*, **48** (3), 532-541.

APPENDICES

Appendix A Cubic MIP Nanoparticles – Building Blocks for a Bright Future

A.1 Characterisation of PAMAM dendrimers

Table Apx A.1: Calculated values based on theoretical prediction of the perfect structure of dendrimer PAMAM 25 % C_{12}, generations from 0 to 5, of the molecular weight, molecular formula, and number of different groups, including number of different non-equivalent protons from the different methylene groups presented.

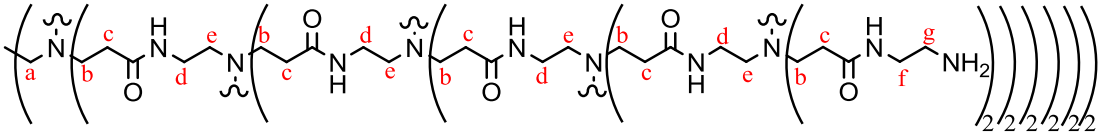

PAMAM G4

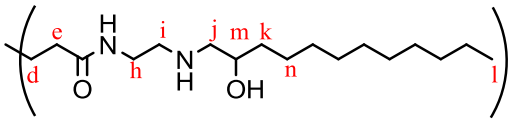

25% of PAMAM surface C_{12} groups

Polyamidoamine (PAMAM) 25% C_{12} (N-(2-hydroxydodecyl) groups)						
Generation №	0	1	2	3	4	5
Molecular weight	700	1786	3988	8372	17140	33876
Molecular formula	$C_{34}H_{72}N_{10}O_5$	$C_{86}H_{176}N_{26}O_{14}$	$C_{190}H_{384}N_{58}O_{32}$	$C_{398}H_{800}N_{122}O_{68}$	$C_{814}H_{1632}N_{250}O_{140}$	$C_{1646}H_{3296}N_{506}O_{284}$
Total № $-CH_2-$ groups	28	70	154	322	658	1330
№ terminal groups	4	8	16	32	64	128
№ $-NH_2$ groups	3	6	12	24	48	96
№ C_{12} groups	1	2	4	8	16	32
№ terminal $-CH_2-$ groups	8	16	32	64	128	256
№ -OH groups	1	2	4	8	16	32

Polyamidoamine (PAMAM) 25% C_{12} (N-(2-hydroxydodecyl) groups)						
Generation №	0	1	2	3	4	5
Molecular weight	700	1786	3988	8372	17140	33876
Molecular formula	$C_{34}H_{72}N_{10}O_5$	$C_{86}H_{176}N_{26}O_{14}$	$C_{190}H_{384}N_{58}O_{32}$	$C_{398}H_{800}N_{122}O_{68}$	$C_{814}H_{1632}N_{250}O_{140}$	$C_{1646}H_{3296}N_{506}O_{284}$
№ $-CH_2-$ (core & branches)	18	50	114	242	498	1010
№ $-CH_2-$ (a) groups	2	2	2	2	2	2
№ $-CH_2-$ (b) groups	4	12	28	60	124	252
№ $-CH_2-$ (c) groups	4	12	28	60	124	252
№ $-CH_2-$ (d) groups	0	4	12	28	60	124
№ $-CH_2-$ (e) groups	0	4	12	28	60	124
№ $-CH_2-$ (f) groups	3	6	12	24	48	96
№ $-CH_2-$ (g) groups	3	6	12	24	48	96
№ $-CH_2-$ (h) groups	1	2	4	8	16	32
№ $-CH_2-$ (i) groups	1	2	4	8	16	32
№ $-CH_2-$ (j) groups	1	2	4	8	16	32
№ $-CH_2-$ (k) groups	1	2	4	8	16	32
№ $-CH_3$ groups (l)	1	2	4	8	16	32
№ >CH- groups (m)	1	2	4	8	16	32
№ >C=O groups	4	12	28	60	124	252
№ -NH- amido-groups	5	14	32	68	140	284
№ >N- tertiary amino-groups	2	6	14	30	62	126

Table Apx A.2: Calculated values based on theoretical prediction of the perfect structure of dendrimer PAMAM 25 % C_{12} – modified (*macroiniferter*), generations from 0 to 5, of the molecular weight, molecular formula, and number of different groups, including number of different non-equivalent protons from the different methylene groups presented.

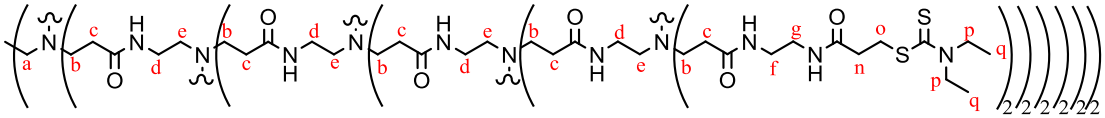

PAMAM G4 -modified

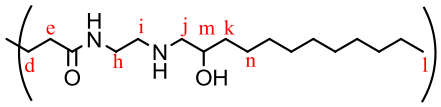

25% of PAMAM - modified surface C_{12} groups

Polyamidoamine (PAMAM) 25% C_{12} (N-(2-hydroxydodecyl) groups) - modified						
Gene-ration №	0	1	2	3	4	5
Molecular weight	1279	2990	6376	13196	26888	55172
Molecular formula	$C_{58}H_{105}N_{13}O_8S_6$	$C_{134}H_{230}N_{32}O_{20}S_{12}$	$C_{286}H_{492}N_{70}O_{44}S_{24}$	$C_{590}H_{1064}N_{146}O_{92}S_{48}$	$C_{1198}H_{2260}N_{298}O_{188}S_{96}$	$C_{2514}H_{4352}N_{602}O_{380}S_{192}$
Total № $-CH_2-$ groups	46	106	226	466	946	1906
№ terminal groups	4	8	16	32	64	128
№ $-NH_2$ groups	0	0	0	0	0	0
№ -C(=S)-S -groups	3	6	12	24	48	96
№ C_{12} groups	1	2	4	8	16	32
№ terminal $-CH_2-$ groups	8	16	32	64	128	256
№ -OH groups	1	2	4	8	16	32
№ $-CH_2-$ (core & branches)	10	34	82	150	370	754
№ $-CH_2-$ (a) groups	2	2	2	2	2	2
№ $-CH_2-$ (b) groups	4	12	28	60	124	252
№ $-CH_2-$ (c) groups	4	12	28	60	124	252

Polyamidoamine (PAMAM) 25% C_{12} (N-(2-hydroxydodecyl) groups) - modified						
Gene-ration №	0	1	2	3	4	5
Molecular weight	1279	2990	6376	13196	26888	55172
Molecular formula	$C_{58}H_{105}N_{13}O_8S_6$	$C_{134}H_{230}N_{32}O_{20}S_{12}$	$C_{286}H_{492}N_{70}O_{44}S_{24}$	$C_{590}H_{1064}N_{146}O_{92}S_{48}$	$C_{1198}H_{2260}N_{298}O_{188}S_{96}$	$C_{2514}H_{4352}N_{602}O_{380}S_{192}$
№ $-CH_2-$ (d) groups	0	4	12	28	60	124
№ $-CH_2-$ (e) groups	0	4	12	28	60	124
№ $-CH_2-$ (f) groups	3	6	12	24	48	96
№ $-CH_2-$ (g) groups	3	6	12	24	48	96
№ $-CH_2-$ (h) groups	1	2	4	8	16	32
№ $-CH_2-$ (i) groups	1	2	4	8	16	32
№ $-CH_2-$ (j) groups	1	2	4	8	16	32
№ $-CH_2-$ (k) groups	1	2	4	8	16	32
№ $-CH_2-$ (n) groups	3	6	12	24	48	96
№ $-CH_2-$ (o) groups	3	6	12	24	48	96
№ $-CH_2-$ (p) groups	6	12	24	48	96	192
№ $-CH_2-$ (q) groups	6	12	24	48	96	192
№ $-CH_3$ groups (l)	1	2	4	8	16	32
№ >CH- groups (m)	1	2	4	8	16	32
№ >C=O groups	7	18	40	84	172	348
№ -NH- amido-groups	8	20	44	92	188	380
№ >N- tertiary amino-groups	5	12	26	54	110	222

A.2 Determining the concentration of the nanoparticles

Concentration (mg/ml)	Absorbance
0.164	1.184
0.082	0.609
0.041	0.316
0.021	0.173
0.01	0.09
0.005	0.046

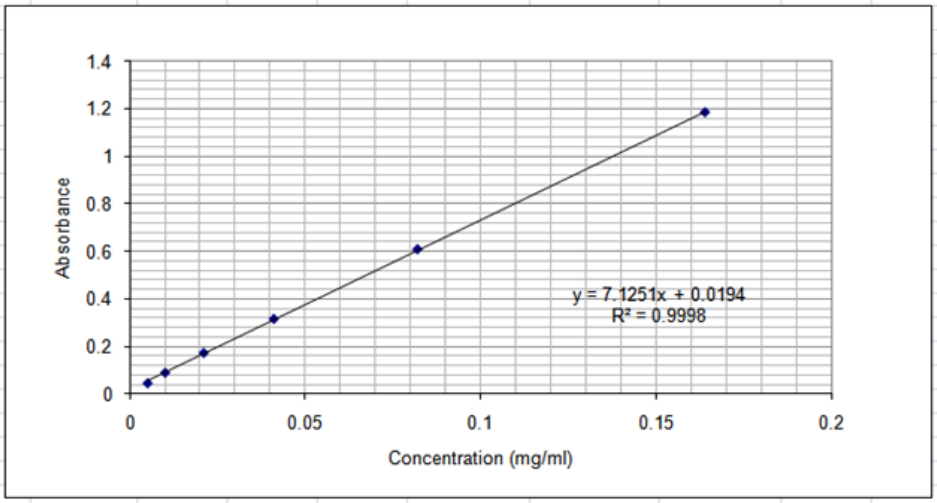

Figure_Apx A.1: Calibration curve obtained from gravimetric analysis of dried samples.

						Y, adsorbance	Calculations (mg/ml)				
Blank polymer, non-affinity (λ=197.4 nm)- 0.180				x=(y-0.0194)/7.1251		0.18	0.022540035				
Particle diameter =		278	nm	radius =	0.0000139	cm	pi =	3.141593			
Assume spherical particles		Volume of 1 particle =			1.12495E-14	cm3					
Density of particle	assume	1	g/ml								
mass of 1 particle					1.12495E-14	g					
therefore 1 ml of suspension contains					2.00365E+15	particles					
1 ml contains					3.32721E-09	moles					
molar concentration of particles =					3.32721E-06	M	0.003327215	mM	3.327215	μM	3327.215 nM
Assume 1 binding site per X Å^2		(square Angstrom)			X =	100	Å^2	per binding site			
Surface area of a sphere = 4 pi r^2			radius (Å) =		1390	Ångstrom					
			Area of particle =		24279484.66	sq. Å					
		binding sites per particle =			242794.8466						
Concentration of *binding sites* therefore =					0.807830563	M	807.8305634	mM	807830.6	μM	8.08E+08 nM

Figure Apx A.2: Copy of spreadsheet calculation used to estimate concentration of *binding sites* (in mol L^{-1}) from concentration of *nanoparticles* (in mg mL^{-1}, obtained from the calibration plot shown in **Figure Apx A.1**). In the worked example, an absorbance of 0.18 at λ = 197.4 nm gives a particle concentration of 0.023 mg mL^{-1}. From the measured diameter (Nanosizer) of 278 nm, the volume of an individual particle (assuming a sphere) is 1.12×10^{-14} cm^3. Assuming a density of 1 g mL^{-1}, the mass of one particle is calculated to be 1.12×10^{-14} g. This gives a figure of 2.0×10^{15} particles in 1 mL or 3.33×10^{-9} moles of particles per mL, from which a molar concentration of particles: 3.33 μM can be estimated. A further assumption is that there will be one binding site per 100 Å^2 of particle surface. Calculation of the surface area, gave a figure of 2.4×10^7 Å^2 per particle or 2.4×10^5 binding sites per particle. Multiplying this figure by the molar particle concentration gives a binding site concentration of 0.8 M. This figure was used in the Biacore software to provide the estimates of K_d for the imprinted nanoparticles.

Appendix B Conjugated Polymers with Pendant Iniferter Units – Versatile Materials for Grafting

B.1 Characterisation of NDDEAEA

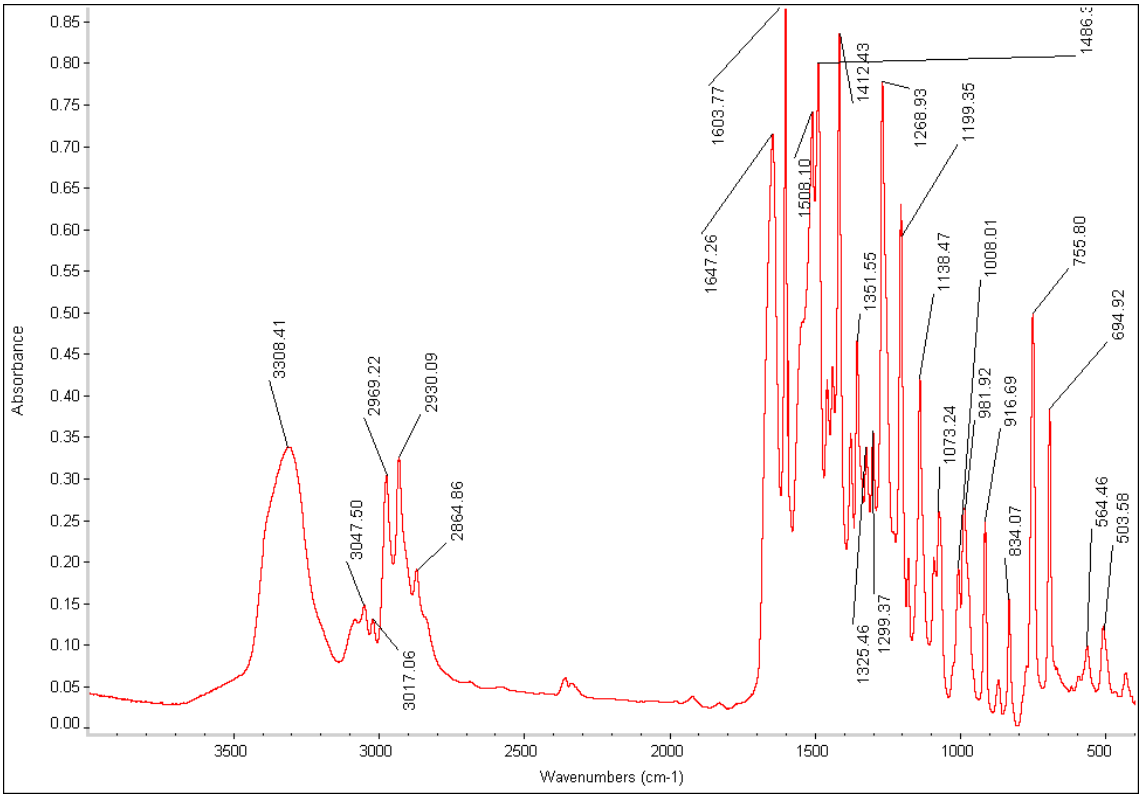

Figure Apx B.1: Infra-red spectra of NDDEAEA monomer (**Scheme 3.4**, **2**).

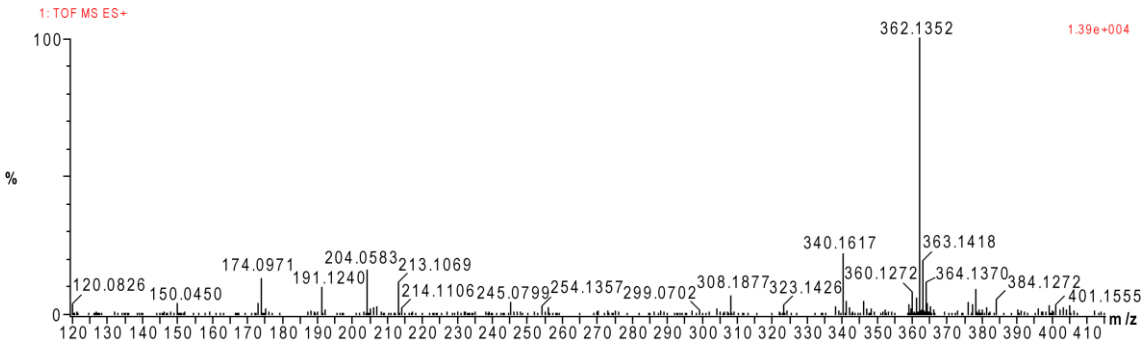

Figure Apx B.2: MS spectrum of NDDEAEA (**Scheme 3.4**, **2**), actual mass: 362. 1352; calculated mass: 362.1337.

B.2 Surface-confined photo grafting of various polymers

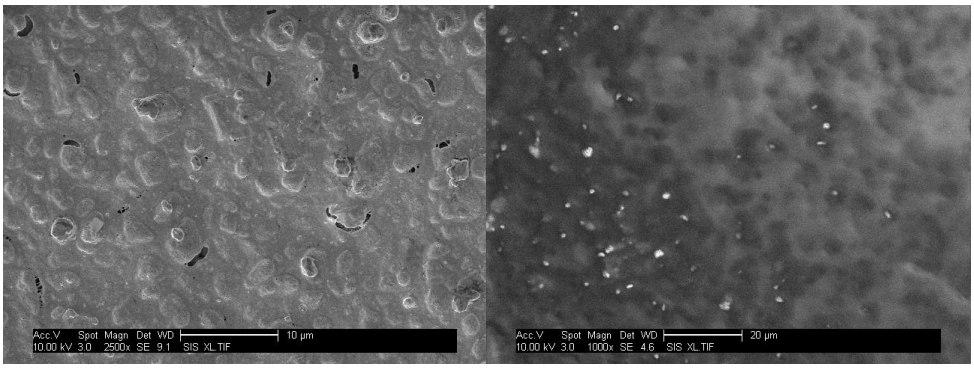

Figure Apx B.3: SEM images of surface morphology of (left) pre-treated gold screen-printed electrode and (right) electropolymerised NDDEAEA electrode (0.2 M NDDEAEA and 0.75 M hydrochloric acid in 25% acetonitrile).

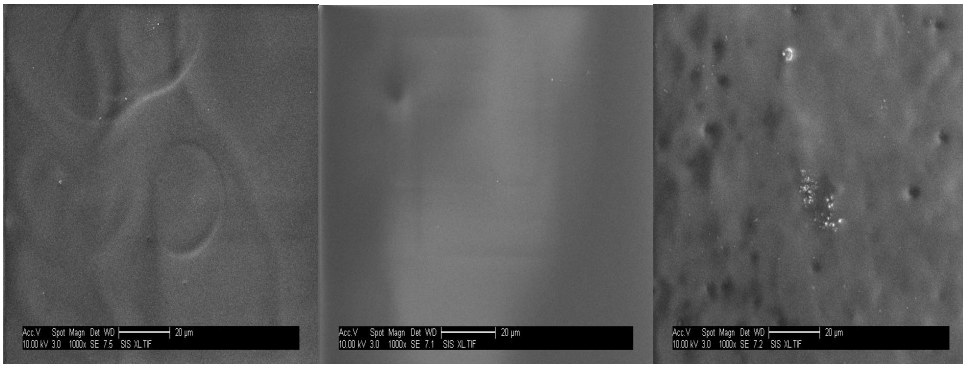

Figure Apx B.4: SEM images of surface morphology of electropolymerised NDDEAEA grafted with (left) MAA, (centre) AMPSA and (right) styrene.

AFM images of grafted polymers over poly (NDDEAEA) modified electrodes

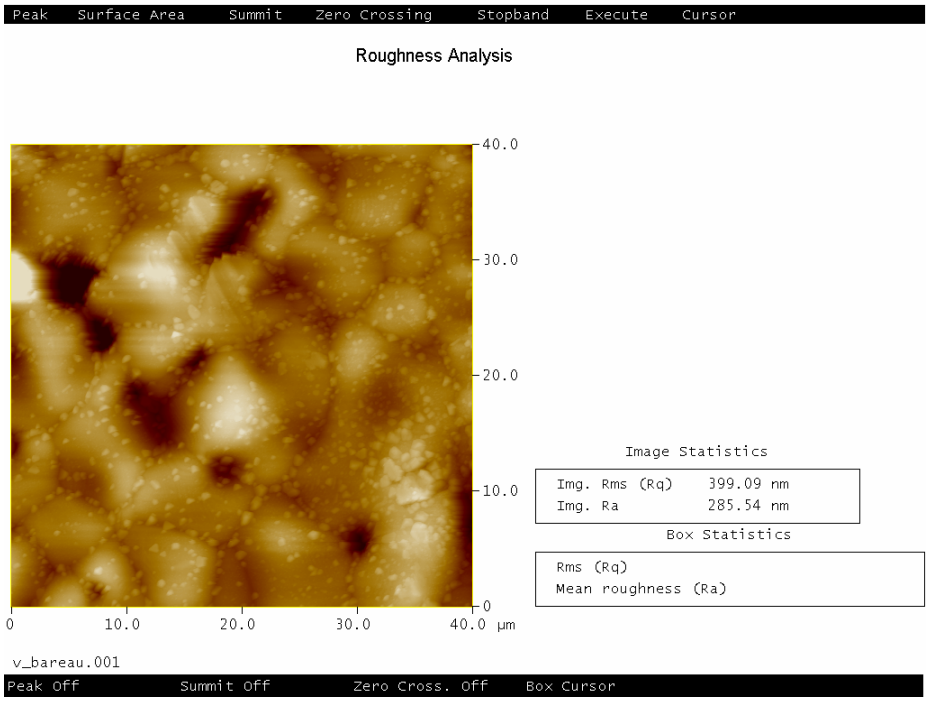

A.

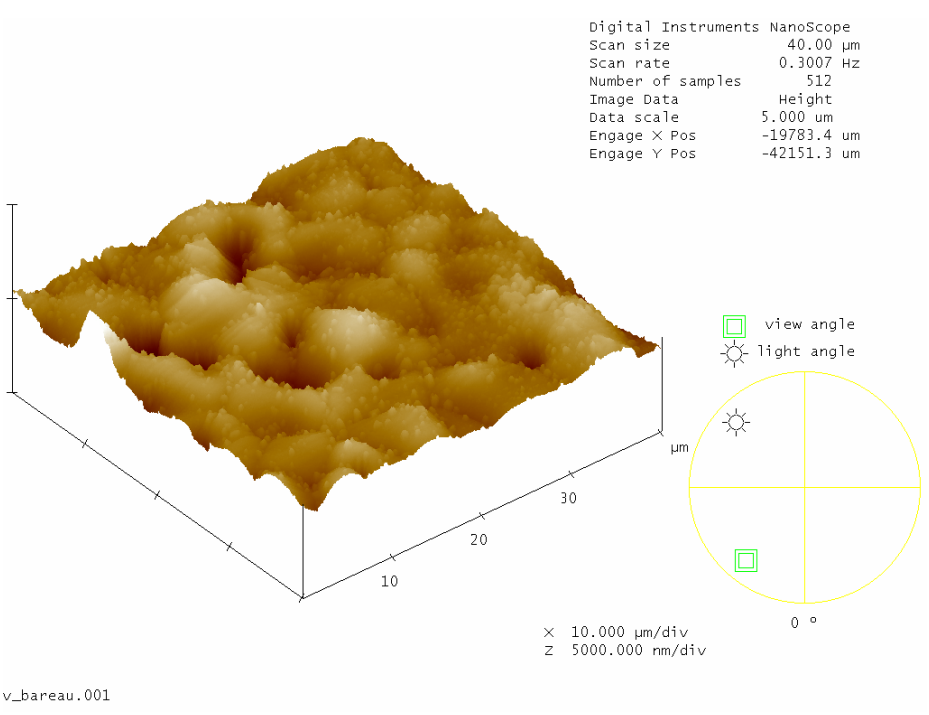

B.

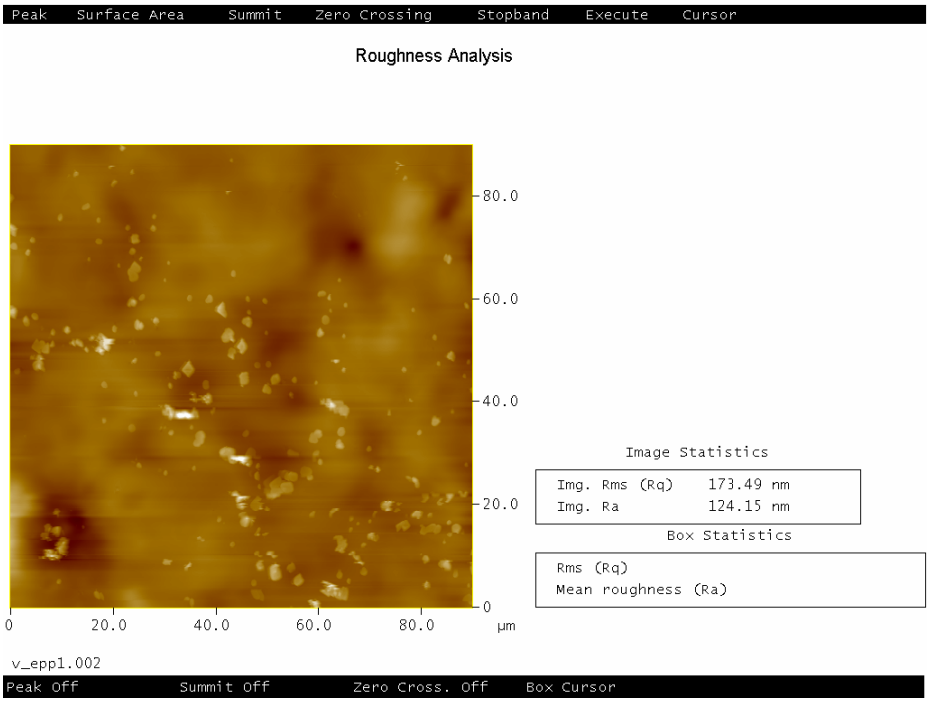
Peak Surface Area Summit Zero Crossing Stopband Execute Cursor
Roughness Analysis
80.0
60.0
40.0
20.0
0
0 20.0 40.0 60.0 80.0 µm
Image Statistics
Img. Rms (Rq) 173.49 nm
Img. Ra 124.15 nm
Box Statistics
Rms (Rq)
Mean roughness (Ra)
v_epp1.002
Peak Off Summit Off Zero Cross. Off Box Cursor

C.

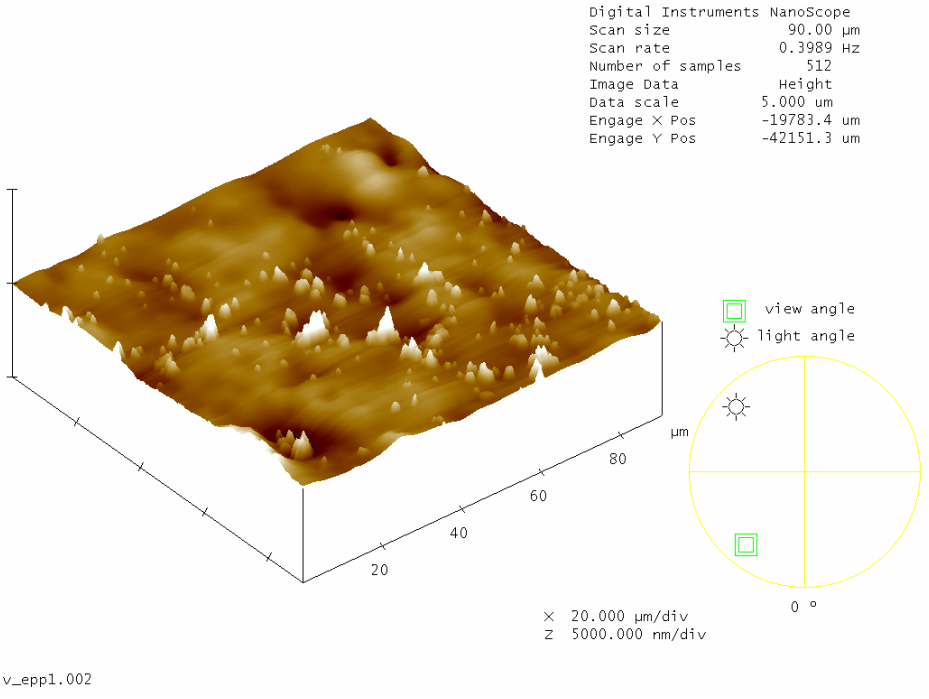
Digital Instruments NanoScope
Scan size 90.00 µm
Scan rate 0.3989 Hz
Number of samples 512
Image Data Height
Data scale 5.000 um
Engage X Pos -19783.4 um
Engage Y Pos -42151.3 um
view angle
light angle
µm
20
40
60
80
0 °
X 20.000 µm/div
Z 5000.000 nm/div
v_epp1.002

D.

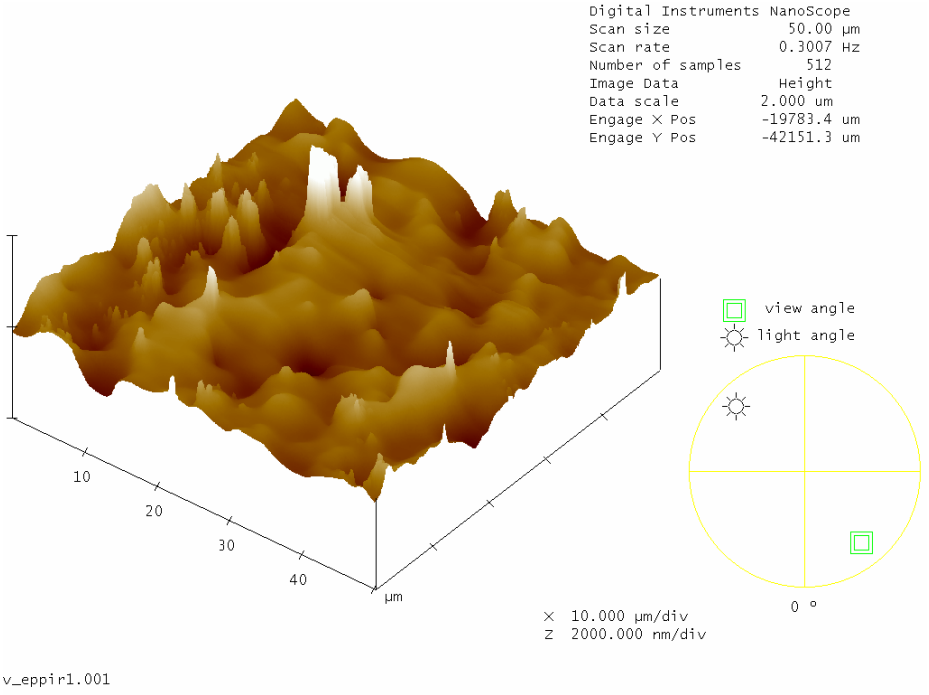
Digital Instruments NanoScope
Scan size 50.00 µm
Scan rate 0.3007 Hz
Number of samples 512
Image Data Height
Data scale 2.000 um
Engage X Pos -19783.4 um
Engage Y Pos -42151.3 um
view angle
light angle
10
20
30
40
µm
0 °
X 10.000 µm/div
Z 2000.000 nm/div
v_eppir1.001

E.

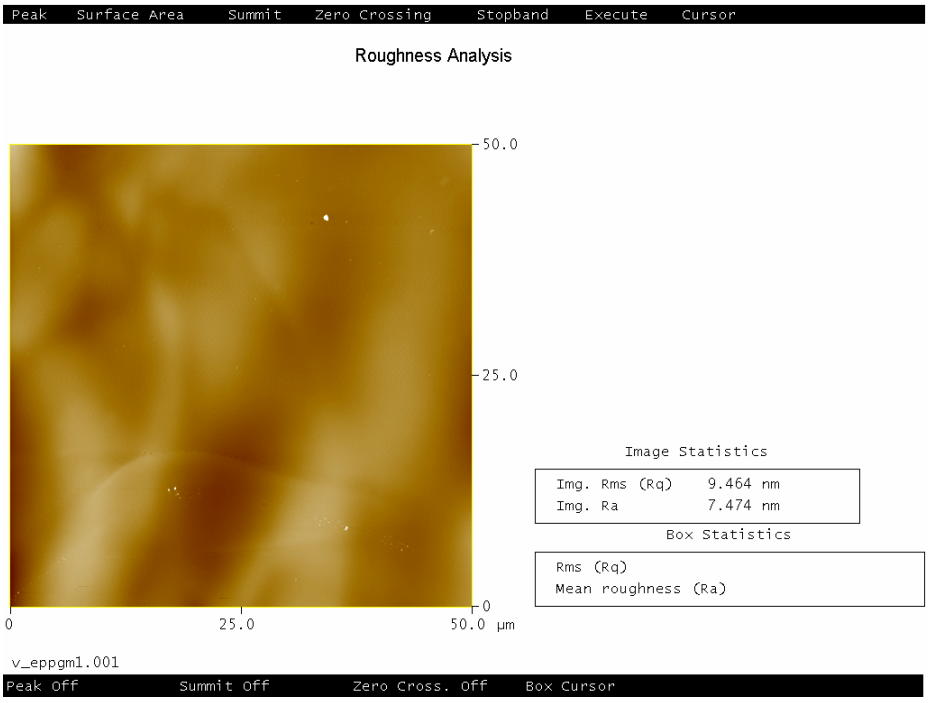
Peak Surface Area Summit Zero Crossing Stopband Execute Cursor
Roughness Analysis
50.0
25.0
0
0
25.0
50.0 µm
Image Statistics
Img. Rms (Rq) 9.464 nm
Img. Ra 7.474 nm
Box Statistics
Rms (Rq)
Mean roughness (Ra)
v_eppgm1.001
Peak Off Summit Off Zero Cross. Off Box Cursor

F.

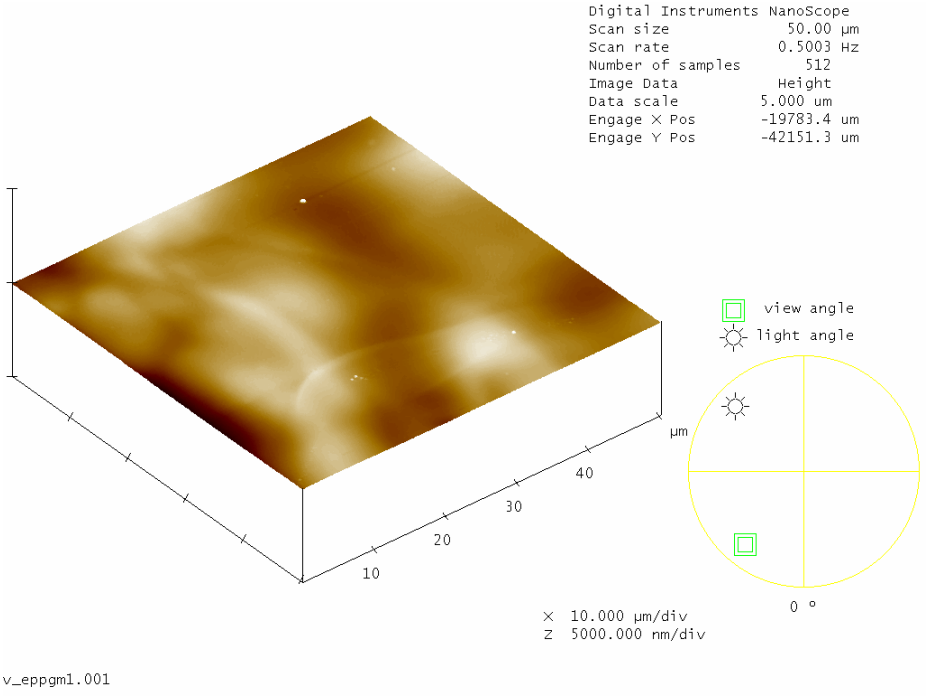
Digital Instruments NanoScope
Scan size 50.00 µm
Scan rate 0.5003 Hz
Number of samples 512
Image Data Height
Data scale 5.000 um
Engage X Pos -19783.4 um
Engage Y Pos -42151.3 um
view angle
light angle
µm
10
20
30
40
0 °
X 10.000 µm/div
Z 5000.000 nm/div
v_eppgm1.001

G.

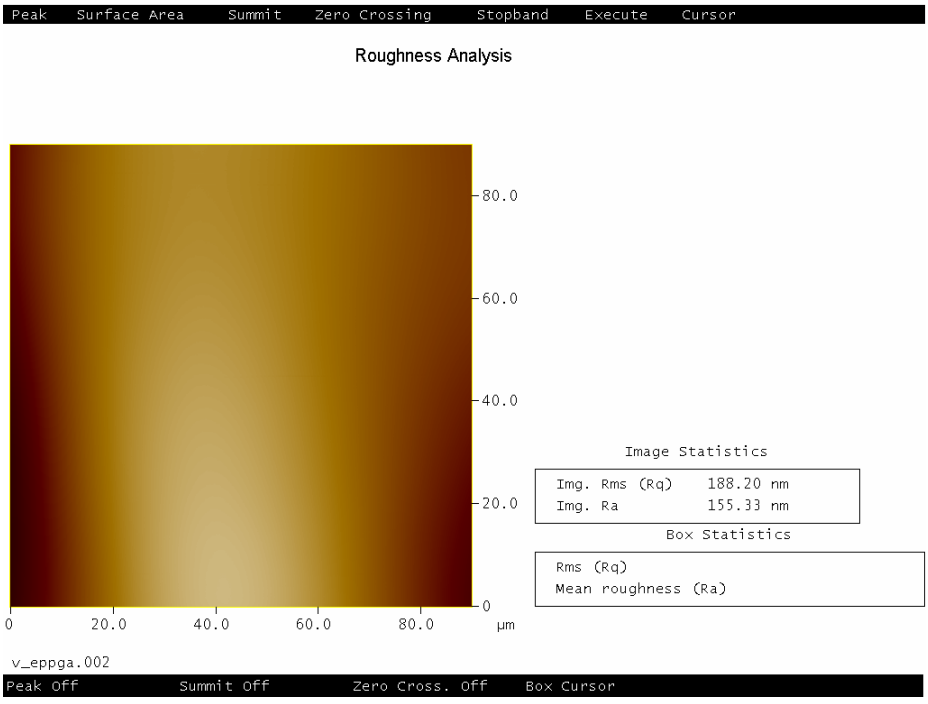
Peak Surface Area Summit Zero Crossing Stopband Execute Cursor
Roughness Analysis
80.0
60.0
40.0
20.0
0
0 20.0 40.0 60.0 80.0 µm
Image Statistics
Img. Rms (Rq) 188.20 nm
Img. Ra 155.33 nm
Box Statistics
Rms (Rq)
Mean roughness (Ra)
v_eppga.002
Peak Off Summit Off Zero Cross. Off Box Cursor

H.

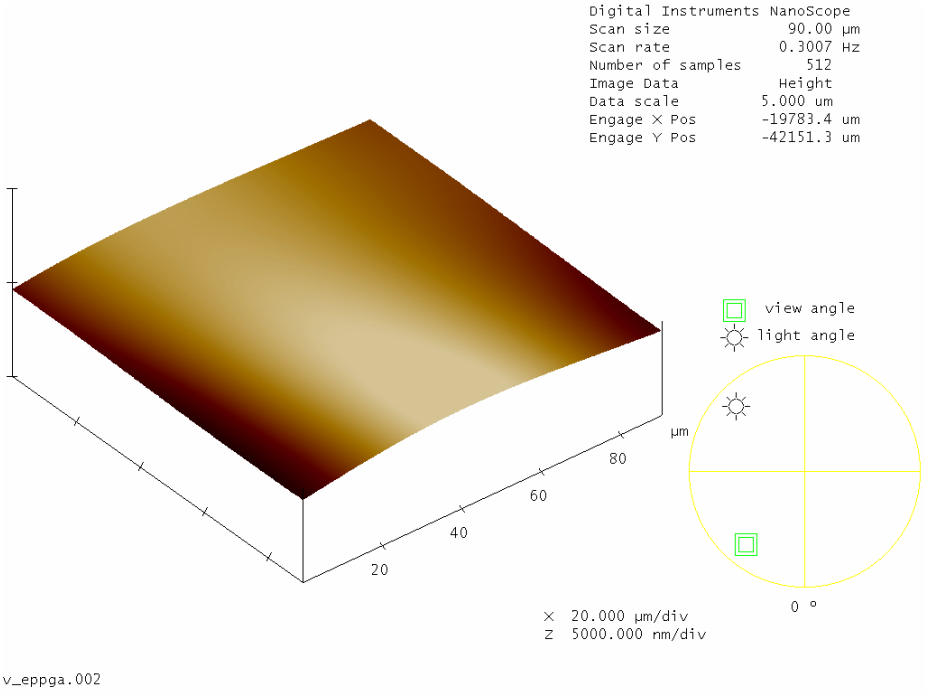
Digital Instruments NanoScope
Scan size 90.00 µm
Scan rate 0.3007 Hz
Number of samples 512
Image Data Height
Data scale 5.000 um
Engage X Pos -19783.4 um
Engage Y Pos -42151.3 um
view angle
light angle
µm
20
40
60
80
0 °
X 20.000 µm/div
Z 5000.000 nm/div
v_eppga.002

I.

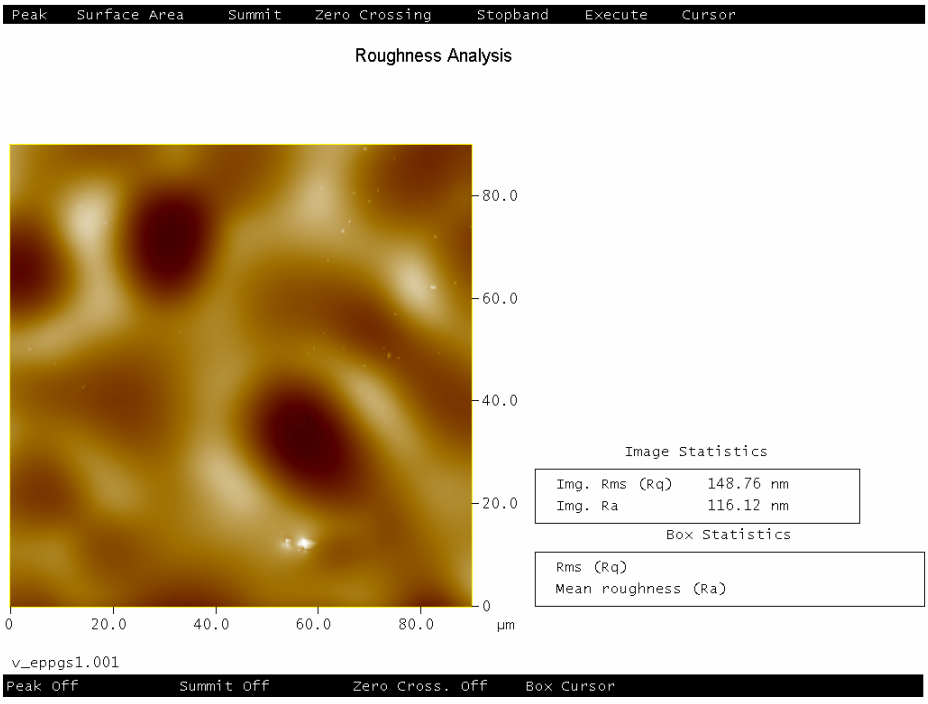
Peak Surface Area Summit Zero Crossing Stopband Execute Cursor
Roughness Analysis
80.0
60.0
40.0
20.0
0
0 20.0 40.0 60.0 80.0 µm
Image Statistics
Img. Rms (Rq) 148.76 nm
Img. Ra 116.12 nm
Box Statistics
Rms (Rq)
Mean roughness (Ra)
v_eppgs1.001
Peak Off Summit Off Zero Cross. Off Box Cursor

J.

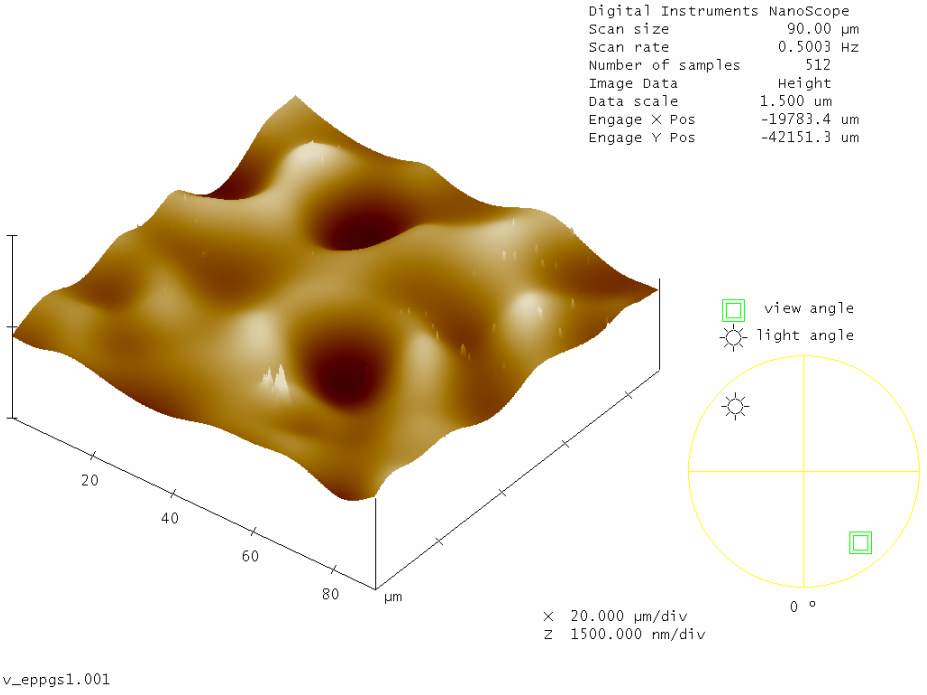

K.

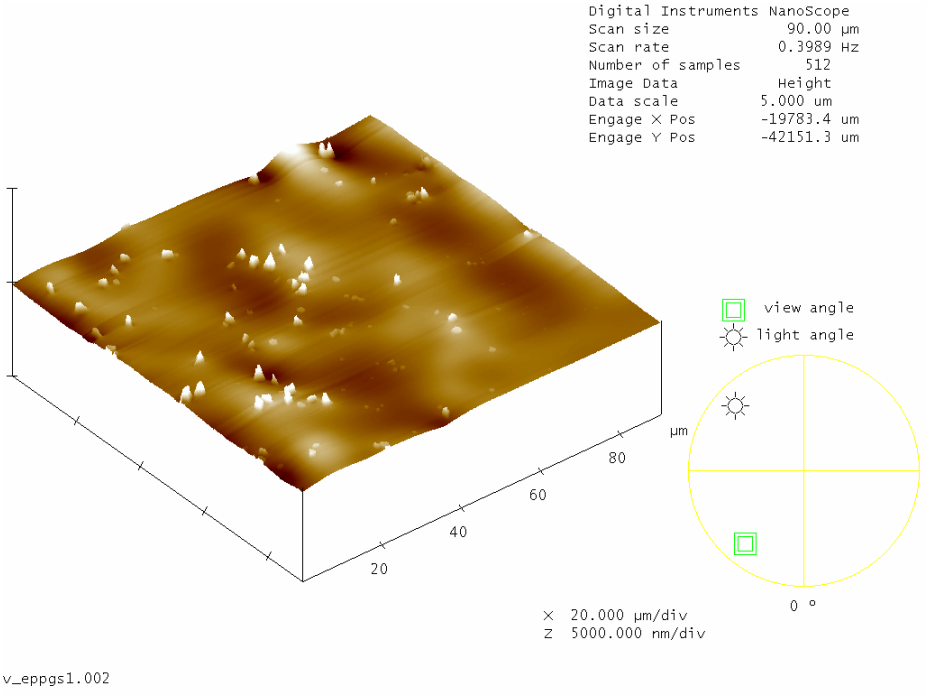

L.

Figure Apx B.5: AFM of (**A** and **B**) bare pre-treated gold SPE, mean roughness 285.54 nm; (**C** and **D**) electropolymerised NDDEAEA film on pre-treated gold SPE, mean roughness 124.15nm;

(**E**) electropolymerised NDDEAEA, after fifteen minutes of UV-irradiation, mean roughness 164.26 nm; (**F** and **G**), poly (methacrylic acid) film grafted over electropolymerised NDDEAEA by *iniferter* activation using UV irradiation mean roughness 7.474 nm; (**H** and **I**), poly (AMPSA) film grafted over electropolymerised NDDEAEA by *iniferter* activation using UV irradiation, mean roughness 155.33 nm; (**J** and **K**), poly (styrene) film grafted over electropolymerised NDDEAEA by *iniferter* activation using UV irradiation, mean roughness 116.12nm; (**L**), layer by layer grafting of poly (styrene) film over poly (methacrylic acid) over electropolymerised NDDEAEA by *iniferter* activation using UV irradiation, mean roughness 65.097nm.

B.3 Optimisation of conditions for chemical oxidative polymerisation of NDDEAEA

B.3.1 Optimisation of condition A for chemical oxidative polymerisation of NDDEAEA to obtain optically transparent layers over microtitre plates, cuvettes, and polypropylene membranes

The effect of monomer (NDDEAEA) concentration and hydrochloric acid concentration on the polymerisation of NDDEAEA by oxidation with ammonium persulphate (0.0183 M) was assessed by preparing solutions in which the concentration of NDDEAEA was varied between 0.01 M and 0.025 M and the concentration of hydrochloric acid was varied between 0.225 M and 0.45 M in a 4 × 4 grid. Polymerisation was conducted in 25% acetonitrile in water for two hours in the dark at room temperature. Bluish-green films of poly (NDDEAEA) were seen to form on the inner surfaces of the cuvettes or microtitre plate wells or on the surface of polypropylene ultra filtration membranes. Poly (NDDEAEA) films were washed with water and 1 M hydrochloric acid. Optical densities were recorded under various pH conditions. Similarly the effect of varying the ammonium persulphate concentration between 0.001 M and 0.03 M and NDDEAEA concentration, varied between 0.025 M and 0.045 M, was assessed at a concentration of 0.225 M, also in a 4 × 4 grid (Figure Apx B.6).

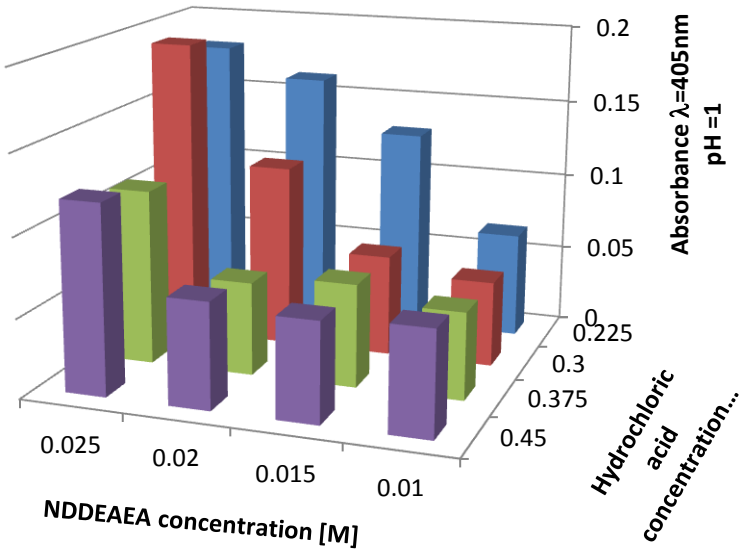

A.

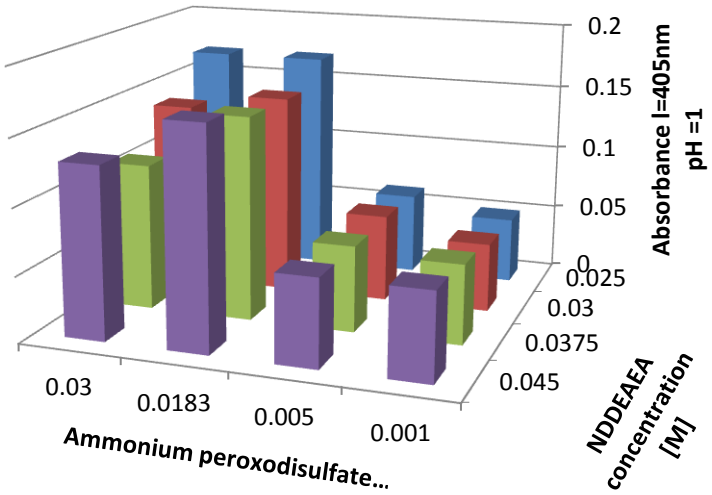

B.

Figure Apx B.6: Chemical polymerisation conditions (condition A): (**A**) The effect of monomer concentration and hydrochloric acid concentration on the optical density of chemically polymerised films of poly (NDDEAEA) at constant (0.0183 M) ammonium persulphate concentration (measured at pH 1) and (**B**) the effect of monomer concentration and ammonium persulphate concentration on the optical density of chemically polymerised films of poly (NDDEAEA) at constant (0.225 M) hydrochloric acid concentration (measured at pH 1).

B.3.2 Optimisation of conditions B for chemical oxidative polymerisation of NDDEAEA to obtain thicker, even layers: Microtitre plates were used for optimisation of the chemical polymerisation

The concentration of hydrochloric acid was kept constant at 0.6 M. The concentration of ammonium persulfate was varied between 0.001 M and 0.05 M, and the concentration of the monomer was varied between 0.01 M and 0.5 M, and 0.01 M and 0.08 M in 8×8 grids.

The concentration of ammonium persulfate was varied on the vertical site of the matrix of 8×8 grids on microtitre plate as given here:

0.001 M, 0.008 M, 0.015 M, 0.022 M, 0.029 M, 0.036 M, 0.043 M, 0.05 M.

The concentrations of the monomers were varied on the horizontal site of the matrix as given here:

A. 0.01 M, 0.08 M, 0.15 M, 0.22 M, 0.29 M, 0.36 M, 0.43 M, 0.5 M;

B. 0.01 M, 0.02 M, 0.03 M, 0.04 M, 0.05 M, 0.06 M, 0.07 M, 0.08 M.

The solvent used was 25% acetonitrile in water. The polymerisation time was one hour in the dark. The microtitre wells were then rinsed with water, and left to dry at ambient temperature, in the dark for twelve hours. The optical density was measured for each well. These experiments were repeated twice for each monomer (Figure_Apx B.7; Figure_Apx B.8 and Figure_Apx B.9).

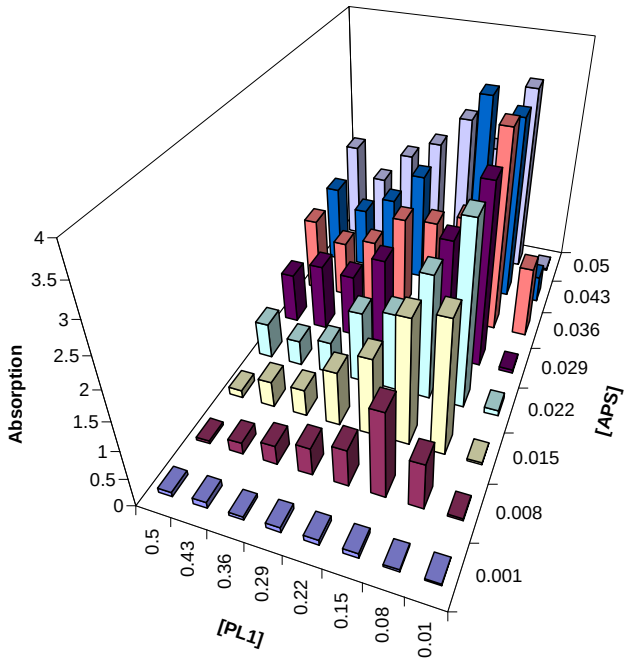

Figure Apx B.7: Absorption (at 550 nm) of chemically polymerised poly (NDDEAEA) films deposited on a microtitre plate with variation of the concentration of the monomer (0.5 M, 0.43 M, 0.36 M, 0.29 M, 0.22 M, 0.15 M, 0.08 M, 0.01 M) and of the ammonium persulfate (0.05, 0.043, 0.036, 0.029, 0.022, 0.015, 0.008, 0.001). The concentration of the hydrochloric acid was kept constant at 0.6 M in 25% acetonitrile in water.

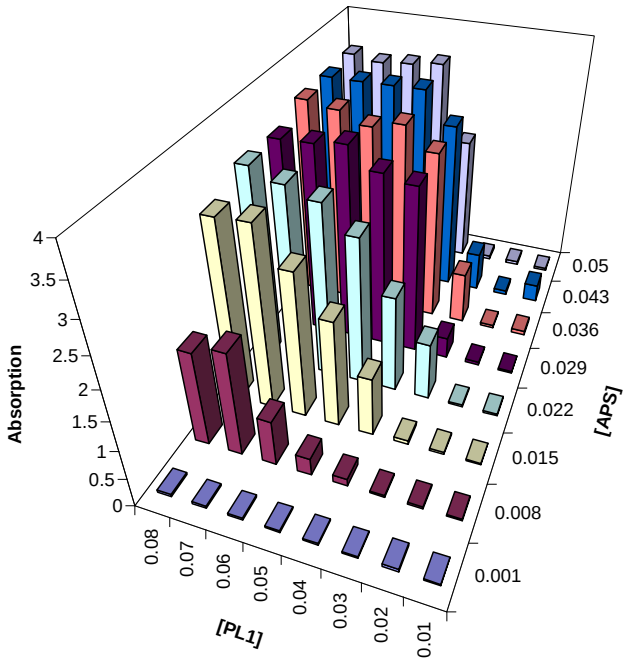

Figure Apx B.8: Absorption of chemically polymerised poly (NDDEAEA) films deposited on a microtitre plate (condition B) with variation of the concentration of the monomer (0.08 M, 0.07 M, 0.06 M, 0.05 M, 0.04 M, 0.03 M, 0.02 M, 0.01 M) and of the ammonium persulfate (0.05, 0.043, 0.036, 0.029, 0.022, 0.015, 0.008, 0.001). The concentration of the hydrochloric acid was kept constant at 0.6 M in 25% acetonitrile in water.

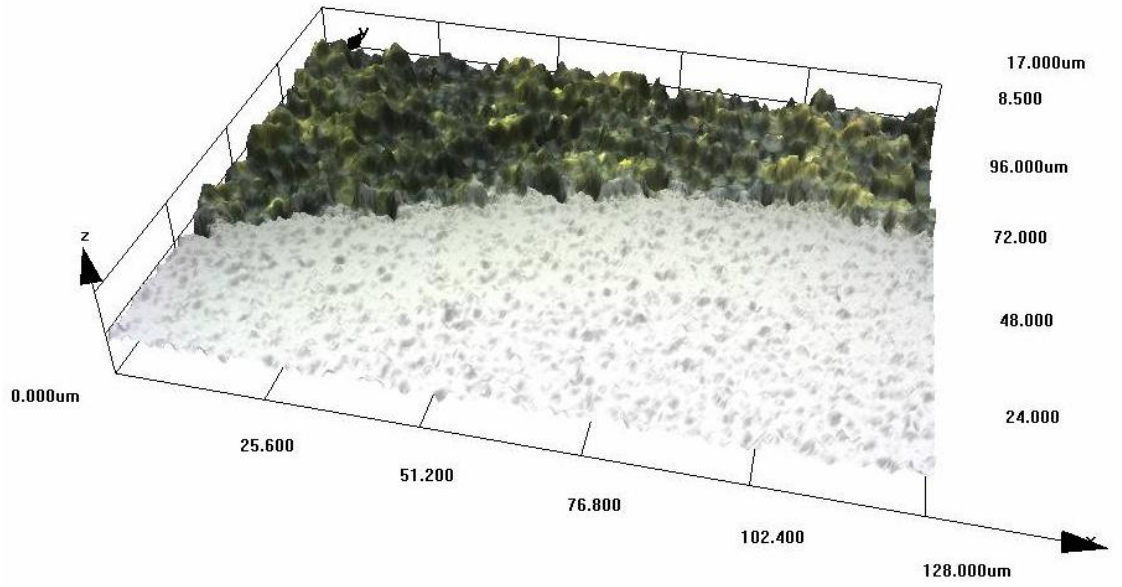

Figure Apx B.9: Confocal microscopic images of chemically polymerised poly (NDDEAEA) (the green material) using condition B on microtitre plate (the white part of the image).

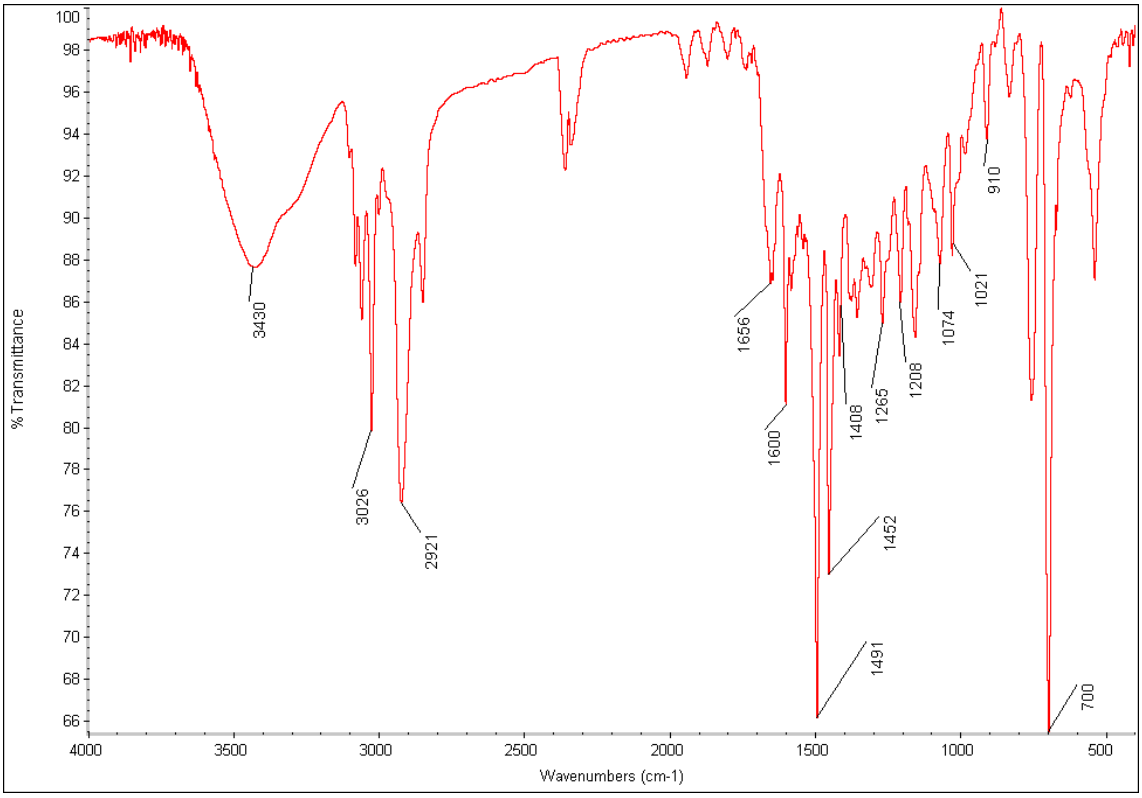

Figure_Apx_B.10: IR spectra of chemically polymerised poly (NDDEAEA) scraped off a microtitre plate and redispersed in KBr.

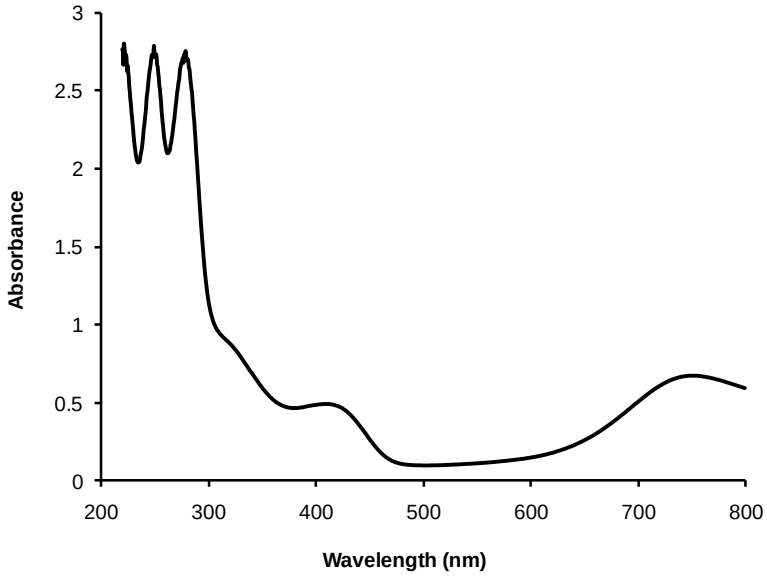

Figure_Apx B.11: UV spectrum of poly (NDDEAEA) solution 1 mg mL^{-1} in methanol in a quartz cuvette.

B.3.3 Chemical oxidative polymerisation of NDDEAEA on polypropylene (PP) ultrafiltration membranes (thicker films)

NDDEAEA was deposited onto polypropylene (PP) membranes (25 mm diameter) using chemical polymerisation. The reaction conditions were as follows: 8 ml solution of 0.08 M NDDEAEA, 0.6 M hydrochloric acid and 0.05 M ammonium persulfate in 25% acetonitrile in water was placed in a 20 mL glass beaker. The polymerisation was performed at ambient temperature for one hour. The membranes were washed in water for thirty minutes three times and then with 20% acetonitrile in water for thirty minutes. After washing they were dried at ambient temperature for twelve hours. Weights of the membranes were 13.7 mg before polymerisation, 29.9 mg after polymerisation (16.2 mg poly (NDDEAEA) deposited, degree of grafting 54.2 %).

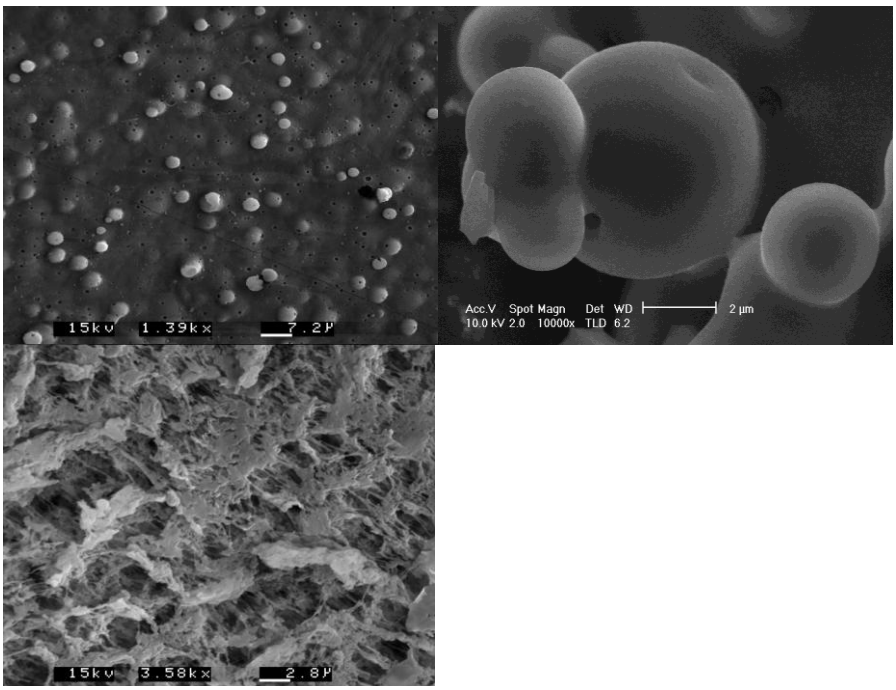

Figure Apx B.12: SEM images of chemically polymerised poly (NDDEAEA) on (top left) microtitre plates, (top right) as bulk polymer (showing bead type structure of the polymer) and (below) over PP membranes.

Appendix C Enhancement of Conductivity by Ultraviolet Irradiation in Polyanilines *N*-substituted with *Dormant* or Active Radical

C.1 NMR spectroscopic characterisation of MPEDA and MMDTCE

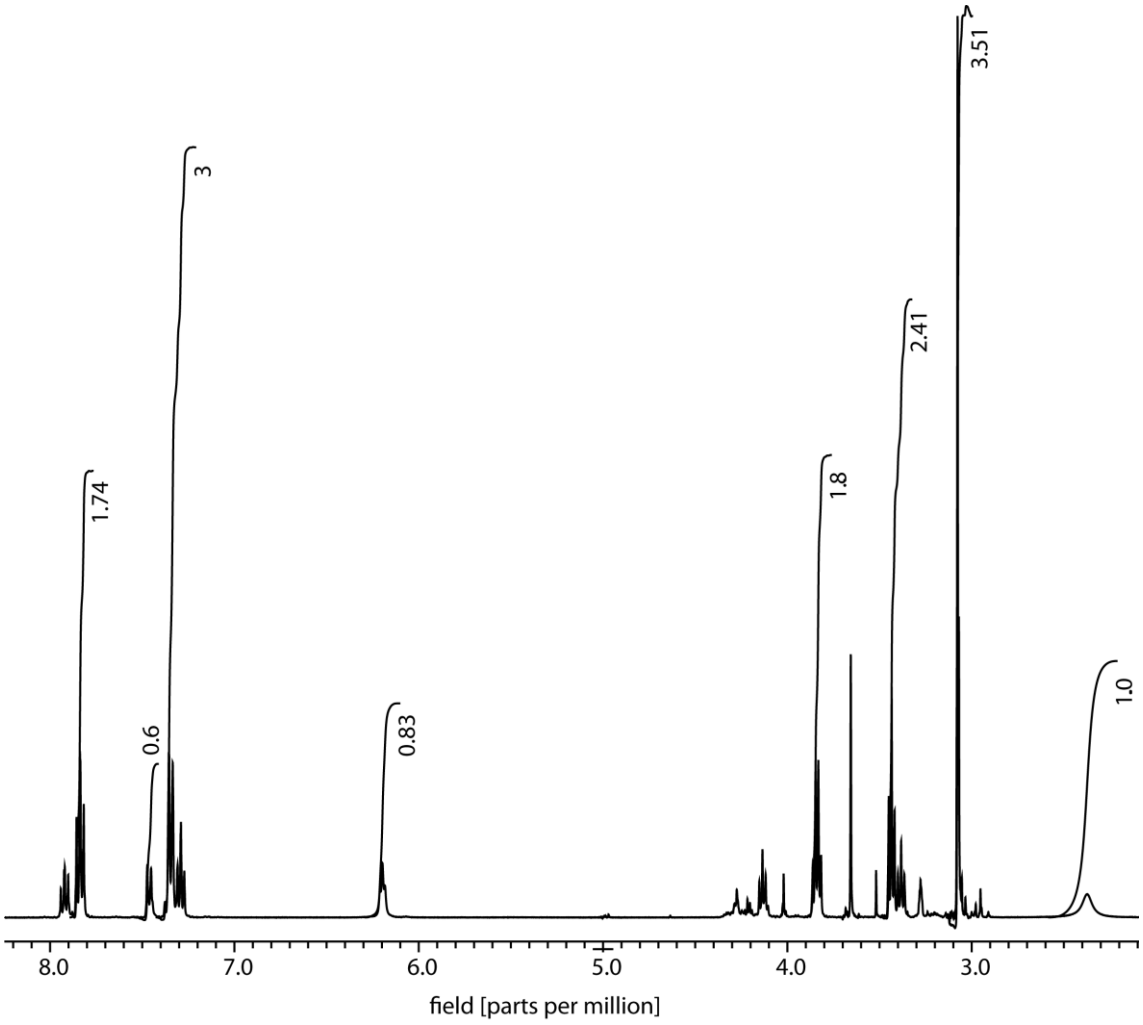

Figure Apx C.1: ^{1}H NMR (400 MHz, MeOH-D_3, 25 °C) of MPEDA.

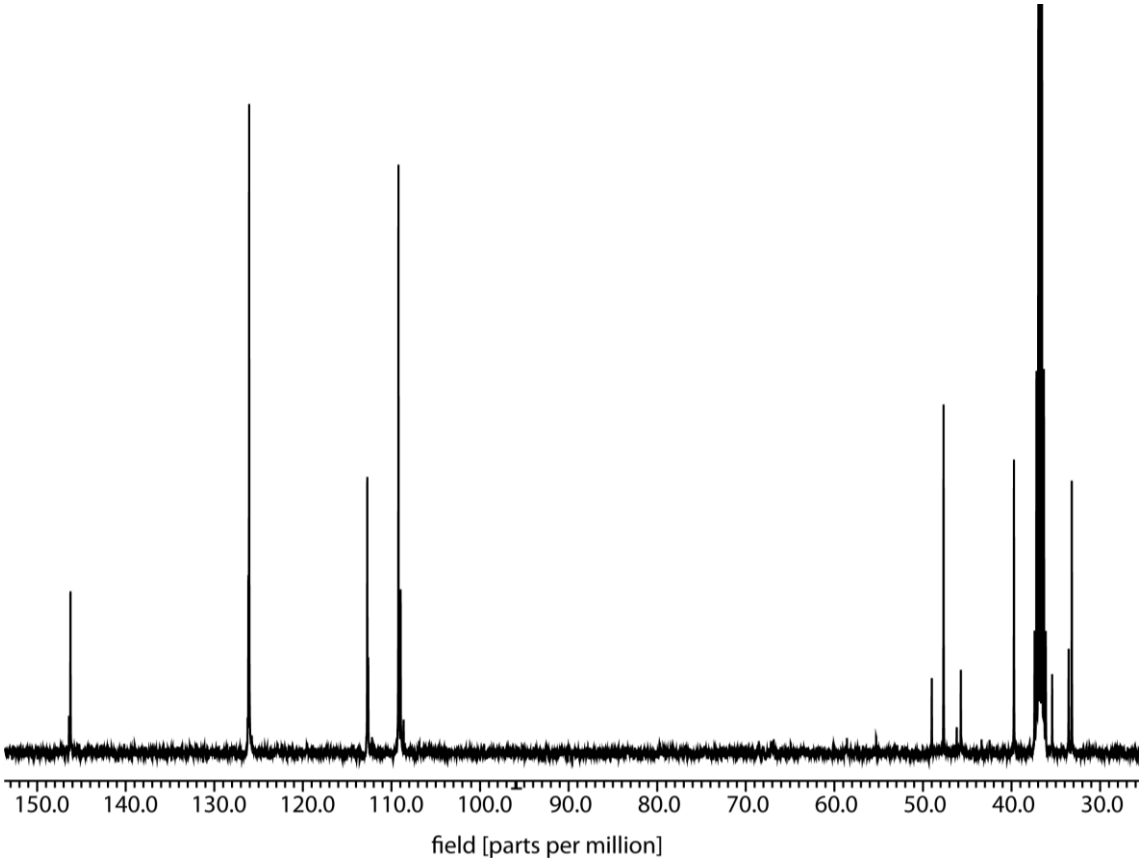

Figure Apx C.2: ^{13}C NMR (100 MHz, MeOH-D_3, 25 °C) of MPEDA.

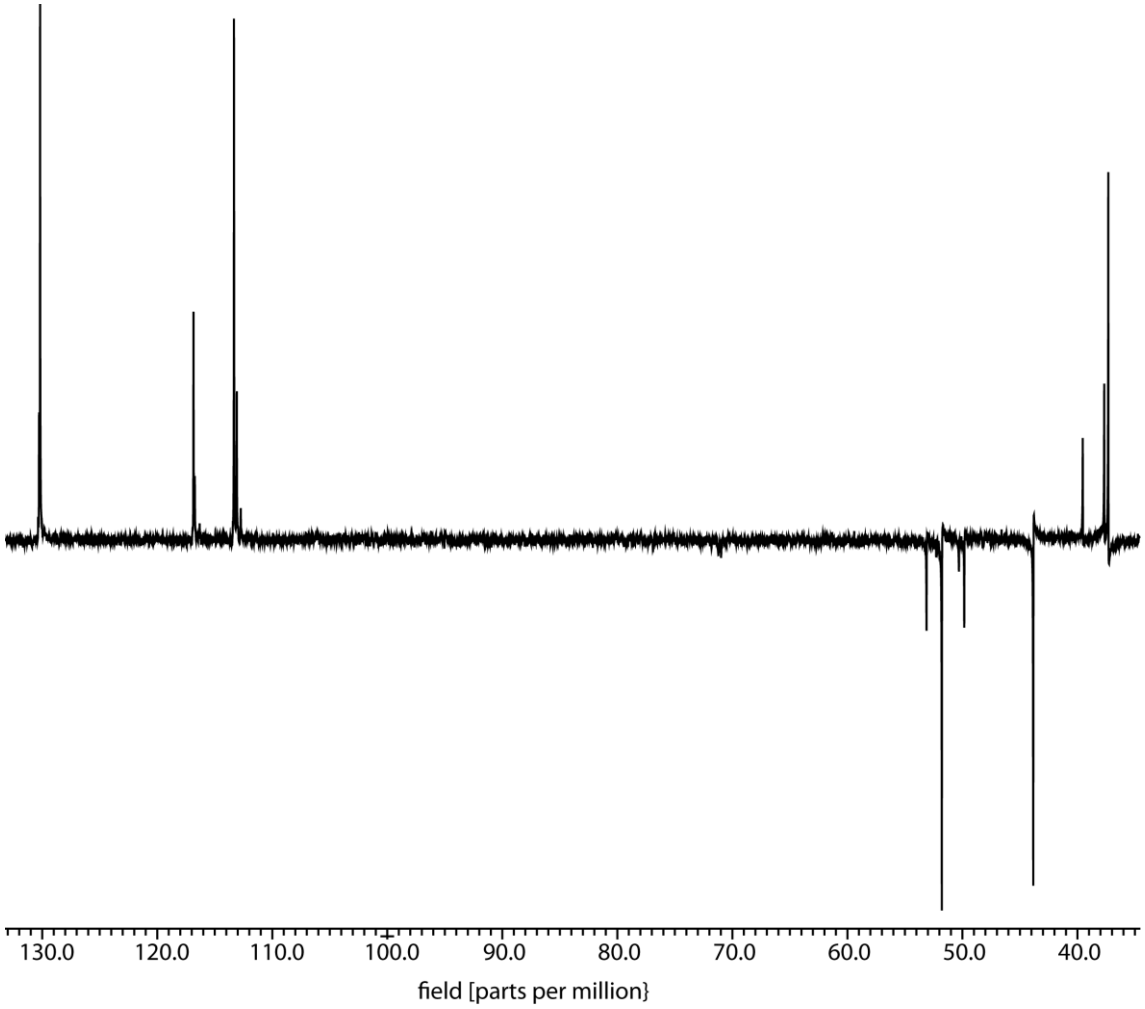

Figure Apx C.3: DEPT 135 NMR (100 MHz, MeOH-D_3, 25 °C) of MPEDA.

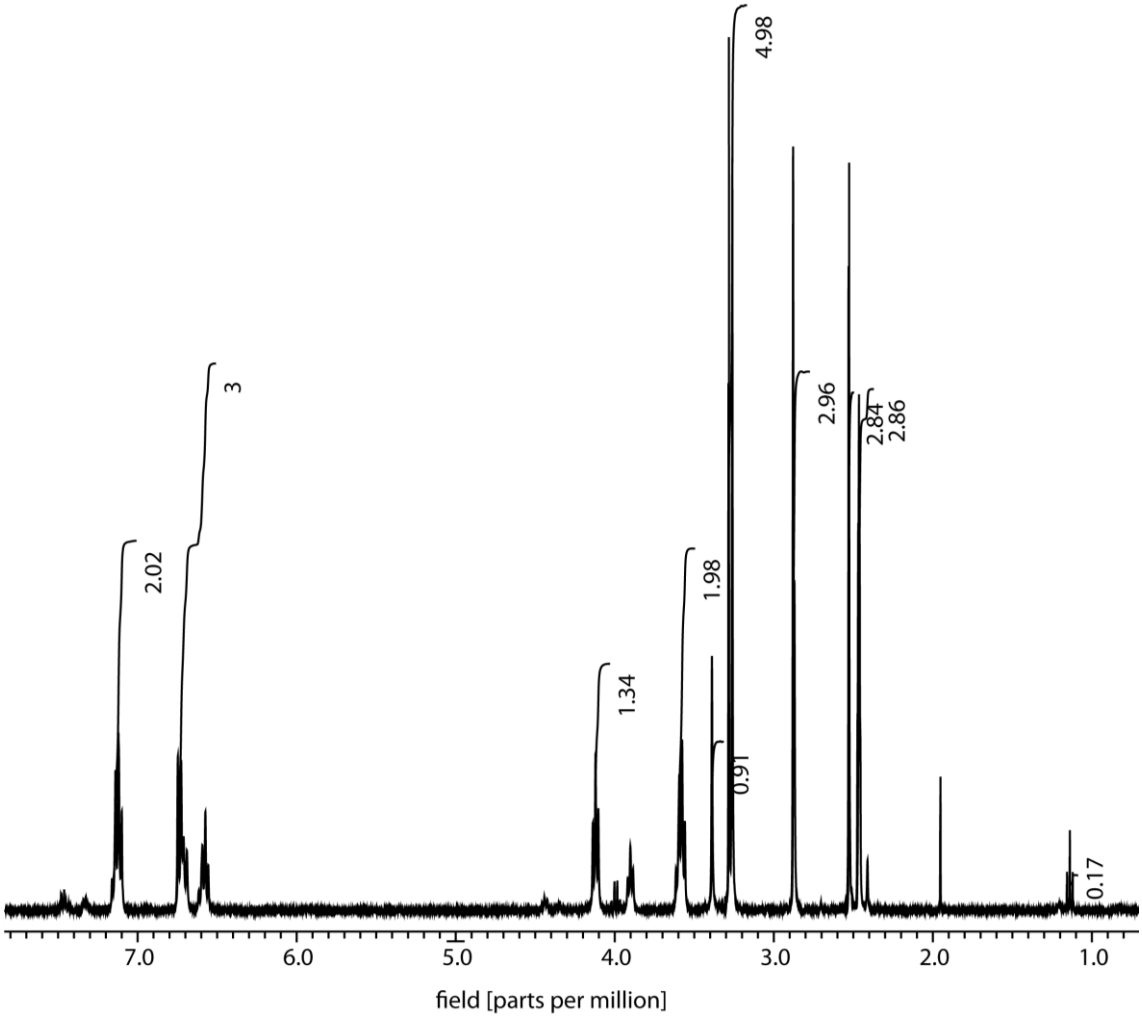

Figure Apx C.4: ^{1}H NMR (400 MHz, DMSO-D_6, 25°C) of MMDTCE.

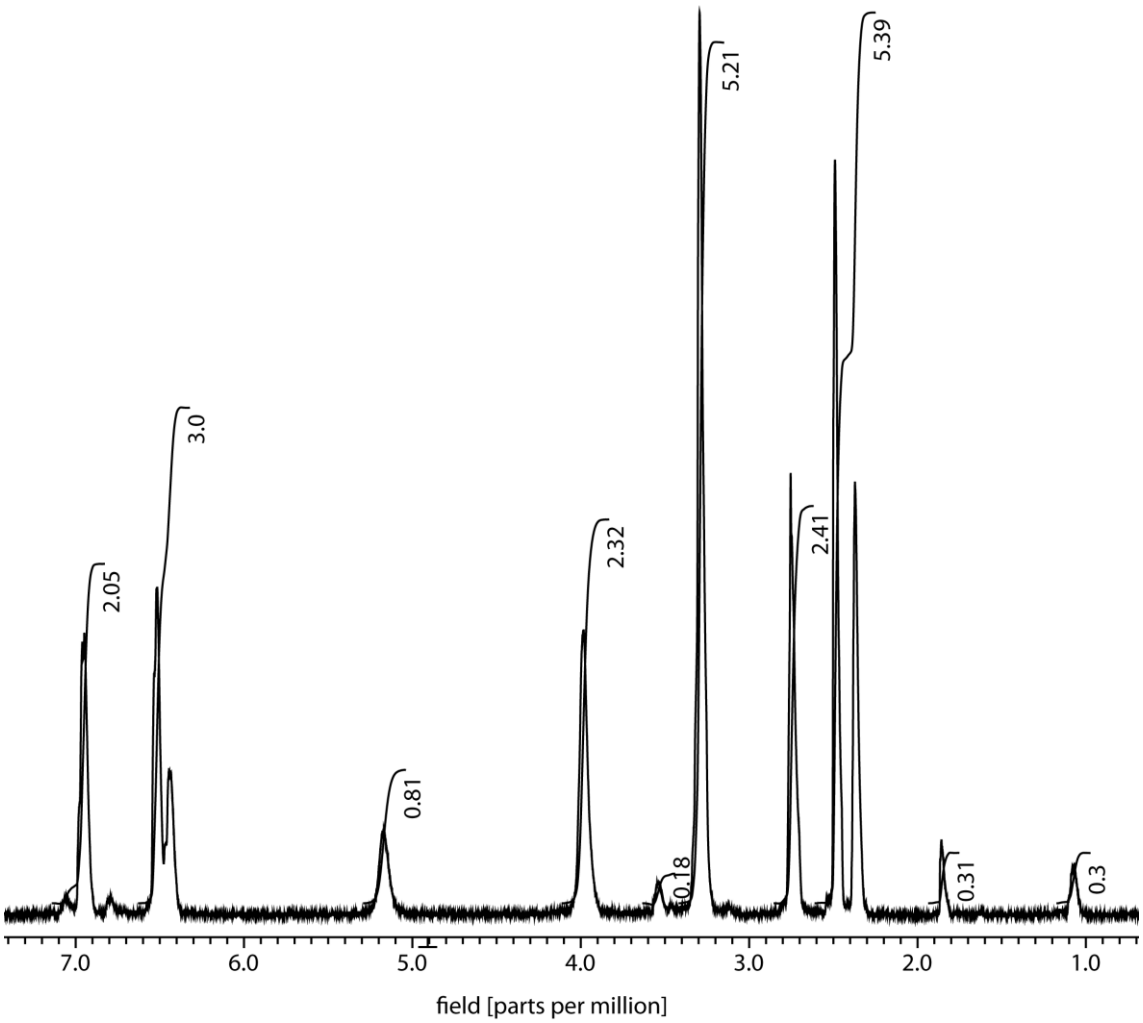

Figure_Apx C.5: ^{1}H NMR (400 MHz, DMSO-D_6, 130 °C) of MMDTCE.

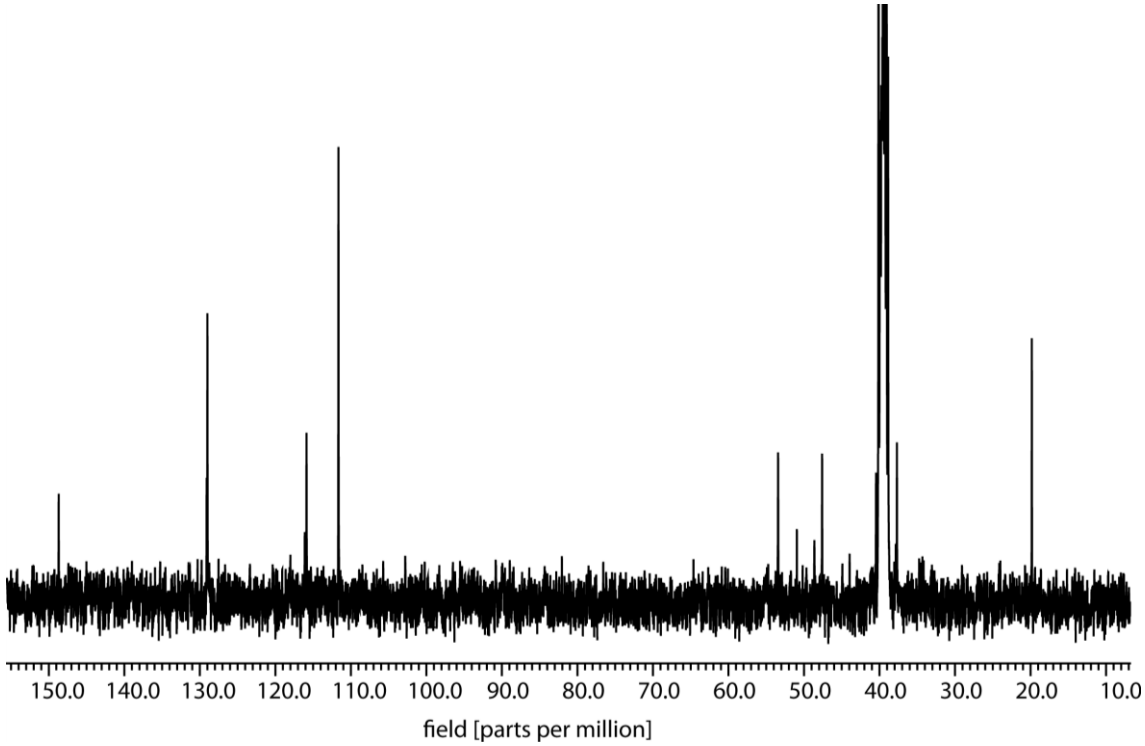

Figure_Apx C.6: ^{13}C NMR (100 MHz, DMSO-D_6, 25 °C) of MMDTCE.

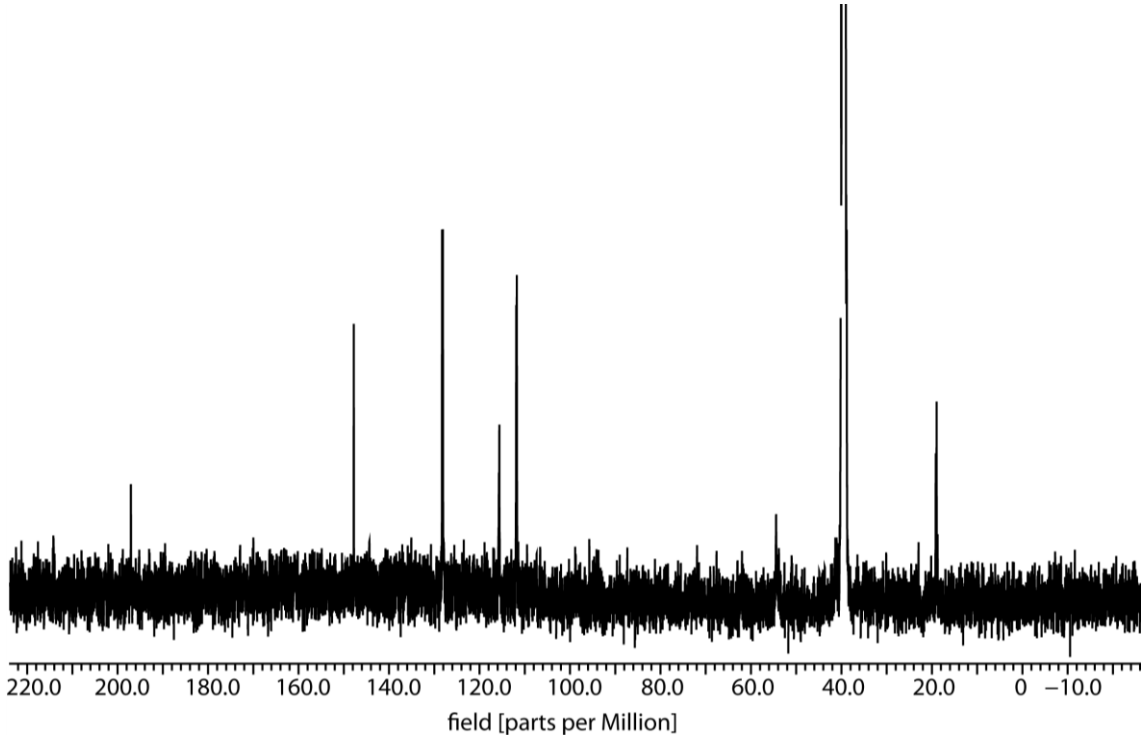

Figure_Apx C.7: ^{13}C NMR (100 MHz, DMSO-D_6, 130 °C) of MMDTCE.

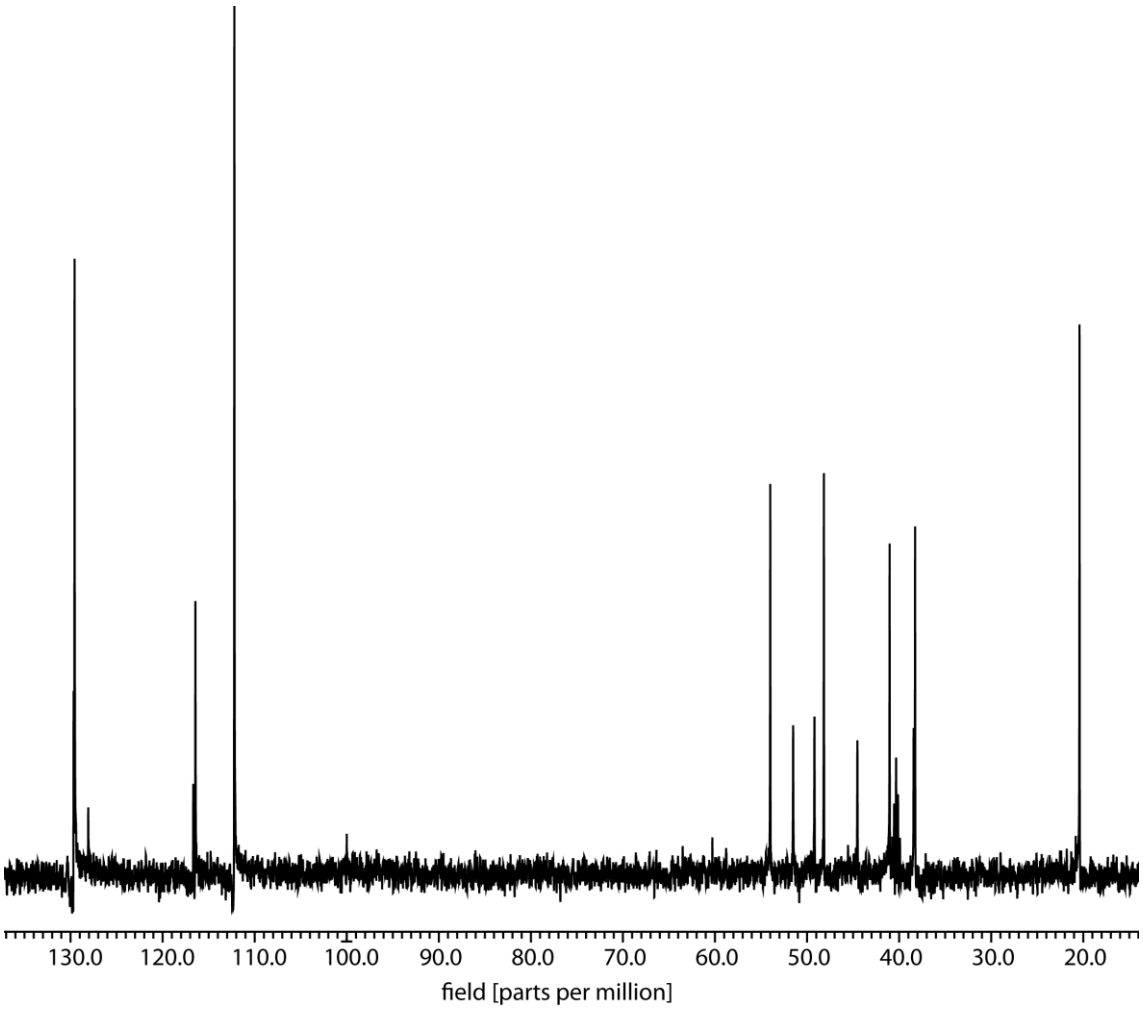

Figure_Apx C.8: DEPT 45 NMR (100 MHz, DMSO-D_6, 25 °C) of MMDTCE.

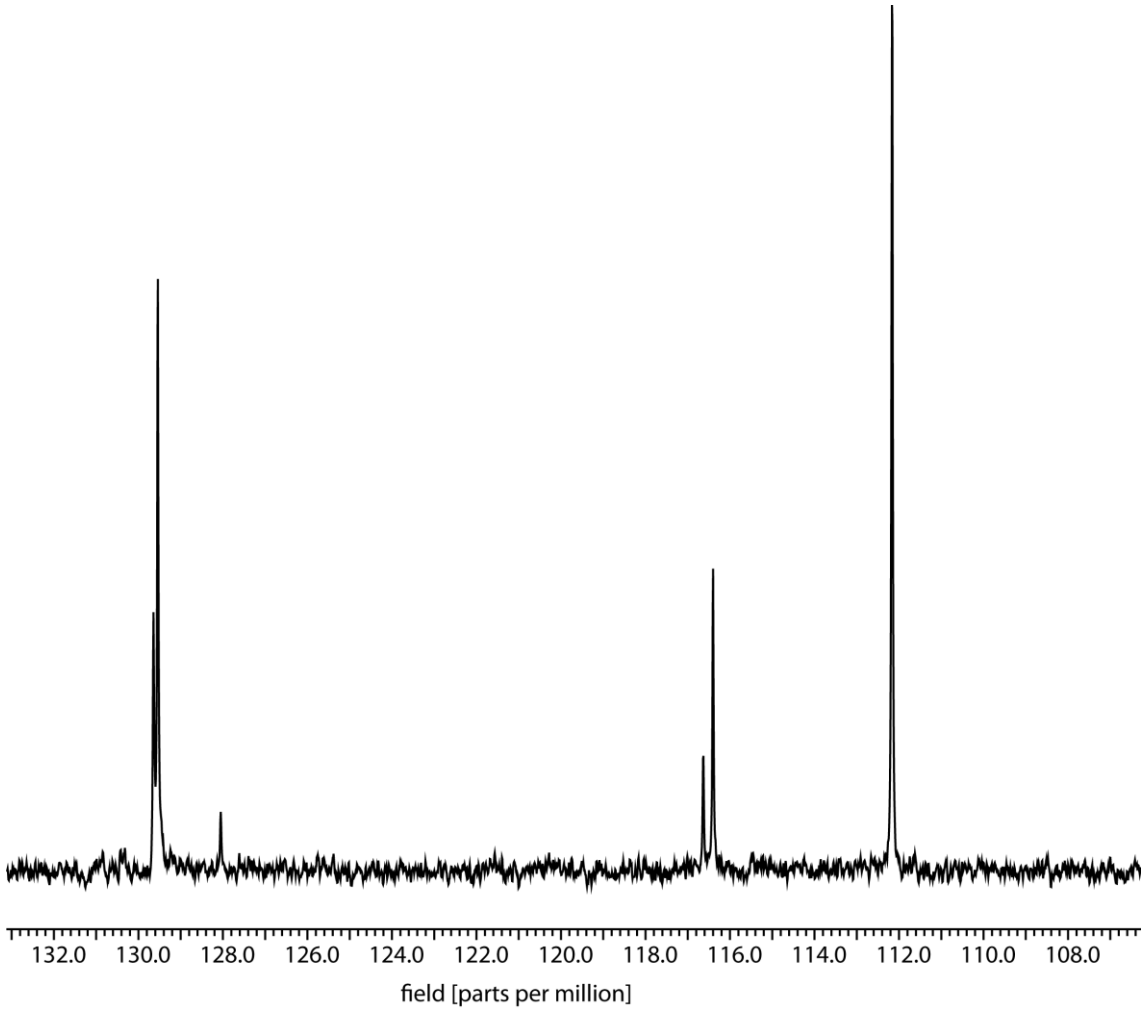

Figure Apx C.9: DEPT 90 NMR (100 MHz, DMSO-D_6, 25 °C) of MMDTCE.

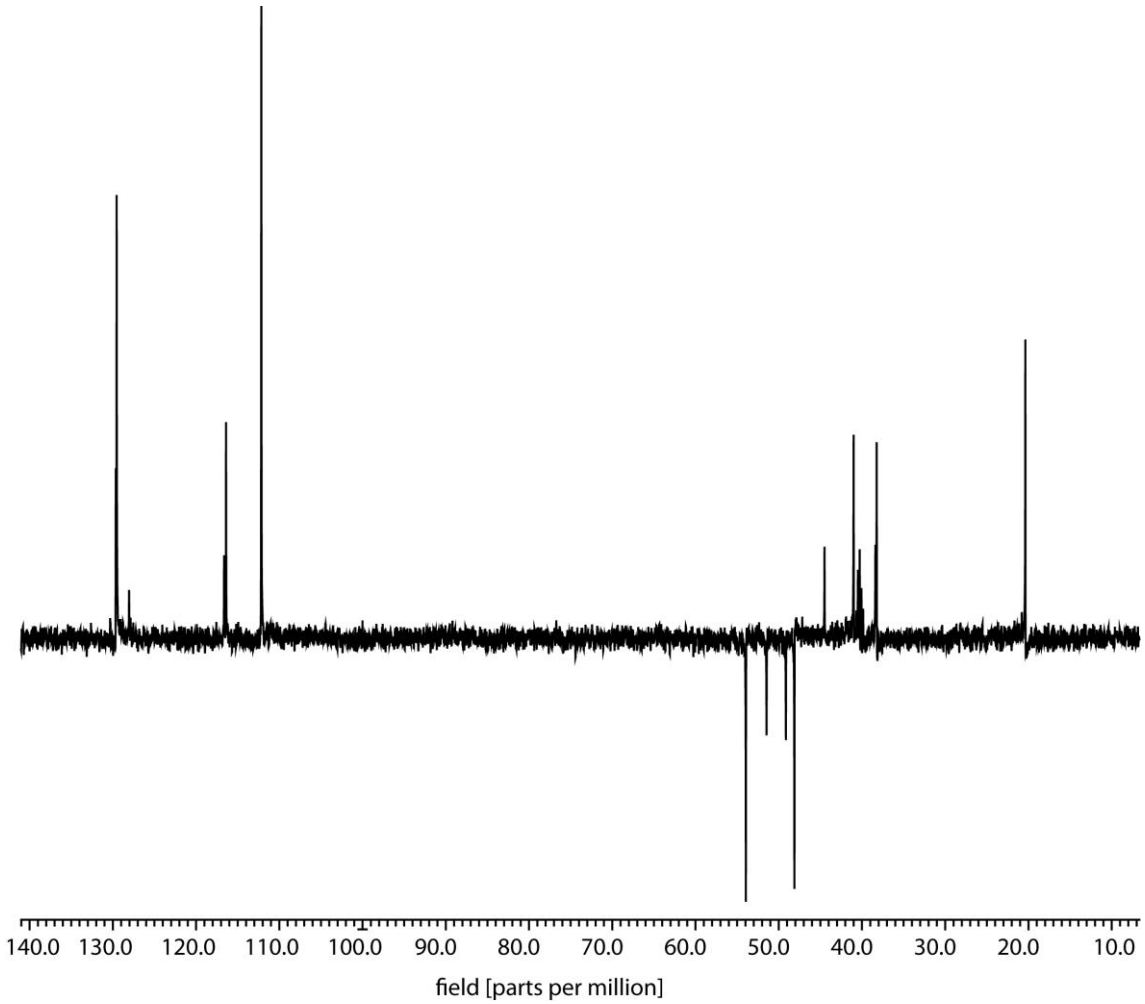

Figure Apx C.10: DEPT 135 NMR (100 MHz, DMSO-D_6, 25 °C) of MMDTCE.

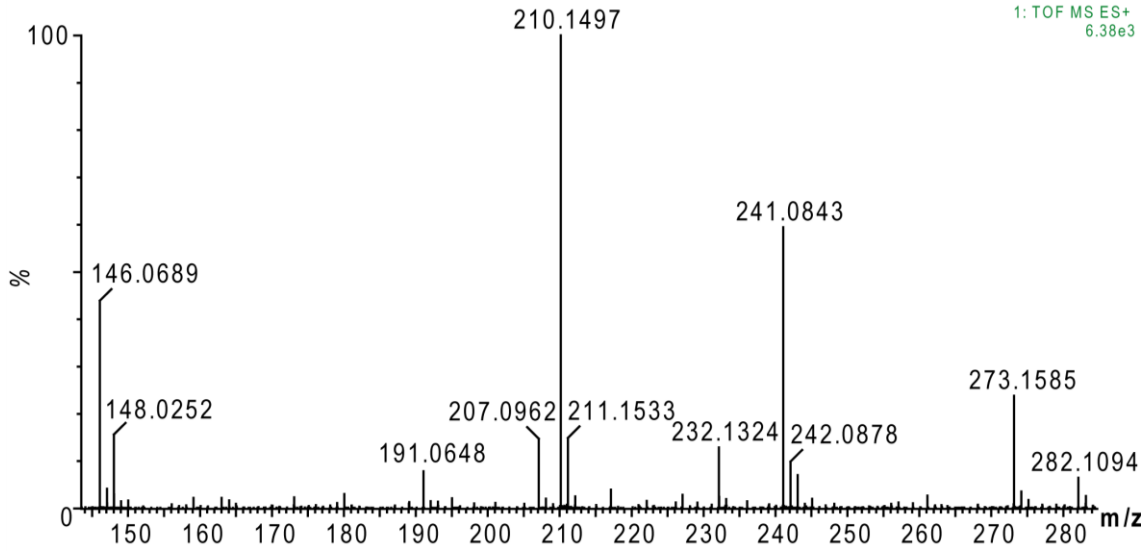

Figure Apx C.11: Mass spectrum of MMDTCE.

C.2 Optimisation of the conditions for chemical oxidative polymerization of MMDTCE and aniline

The chemical polymerisation of the synthesised monomers was investigated in order to achieve the optimum conditions that would be suitable for a particular application like deposition of a polymer layer on an electrode. For the purpose, the concentration of the ammonium persulfate and of the monomers used was varied to achieve optimum ratio between them in respect to the intensity of the layer formed at absorption at 550 nm and to the thickness and smoothness of the layer (Figure 4.5). For this reason a protocol for the polymerisation of PANI was adopted from Bossi *et al.* (**2000**) and was used as a base for the further optimisation. The protocol for the optimisation procedure of NDDEAEA was described earlier (B.3.2, page 229). The same protocol was applied to the other two materials (MMDTCE and aniline). In order to improve the solubility of MMDTCE in the proposed conditions that were proved efficient for NDDEAEA, hydrochloride of the monomer was used for the polymerisation. In each case an immediate pink coloration was observed the intensity of which increased in the following order: aniline<NDDEAEA<MMDTCE. This coloration persisted for approximately one minute for aniline and five minutes for NDDEAEA and MMDTCE. After this the mixtures changed colour to dark blue for aniline and to dark green for NDDEAEA and MMDTCE, which at the end of the polymerisation time (one hour) changed to brownish green for MMDTCE. This difference in the polymerisation behaviour could be attributed to the different oxidation energy required for the initiation and the propagation of the redox process (Gospodova *et al.* **1998**).

The first set of experiments for optimisation of the concentration ratio of ammonium persulfate and the monomer resulted in formation of a thick uneven layer of polymer on the bottom of the wells for concentrations of the monomer between 0.5 and 0.15 (Figure Apx B.7). This is why varying of the monomer concentration between 0.08 M and 0.01 M was required.

Figure Apx B.8 shows the absorption maximums of the poly (NDDEAEA) film formed with varying the monomer concentration between 0.08 M and 0.01 M. For formation

of an even thin film of polymer the ratio ammonium persulfate/NDDEAEA of 0.625 (0.05 M ammonium persulfate and 0.08 M NDDEAEA) was chosen as optimal with an absorption of 3.452.

When polymerisation of MMDTCE under the same conditions was performed, a yellow rather than green layer was formed. This was attributed to the decreased solubility of the monomer in these conditions. Preparation of hydrochloric salt of the monomer improved the solubility and resulted in brownish-green layers. For the preparation of the layer of polymer over electrode, the same ratio ammonium persulfate/MMDTCE was chosen as for NDDEAEA 0.625 with absorption 1.432 (Figure Apx C.12).

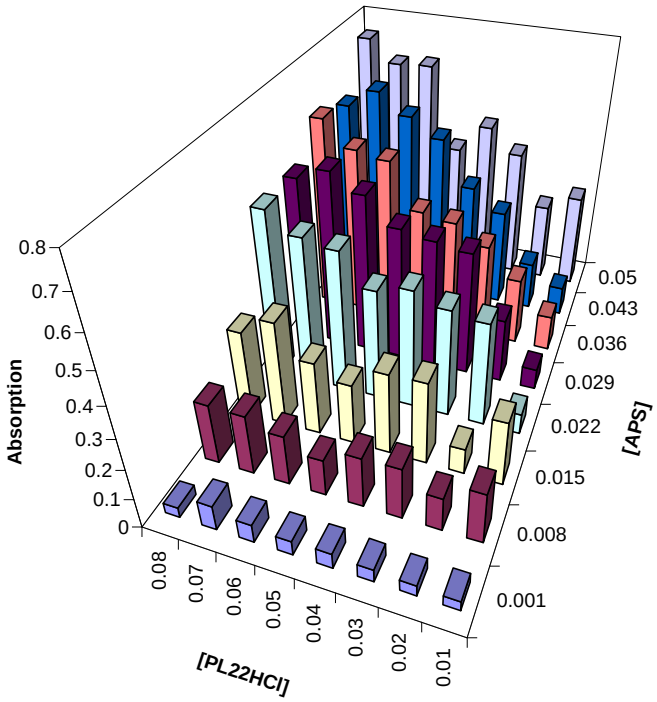

Figure Apx C.12: Absorption (at 550 nm) of chemically polymerised poly (MMDTCE) films deposited on a microtitre plate with variation of the concentration of the monomer (0.08 M, 0.07 M, 0.06 M, 0.05 M, 0.04 M, 0.03 M, 0.02 M, 0.01 M) and of the ammonium persulfate (0.05, 0.043, 0.036, 0.029, 0.022, 0.015, 0.008, 0.001). The concentration of the hydrochloric acid was kept constant at 0.6 M in 25% acetonitrile in water.

The same experiment was performed with aniline. It resulted in optically transparent layers on the microtiter plates. This is why the monomer concentration was increased and varied from 0.5 M to 0.01 M. The thickest layers were formed with ratio

ammonium persulfate/aniline 0.1 (0.05 M ammonium persulfate, 0.5 M aniline) with absorption 0.201, and this were the conditions of the formation of a polymer layer over electrode that were chosen (Figure Apx C.13).

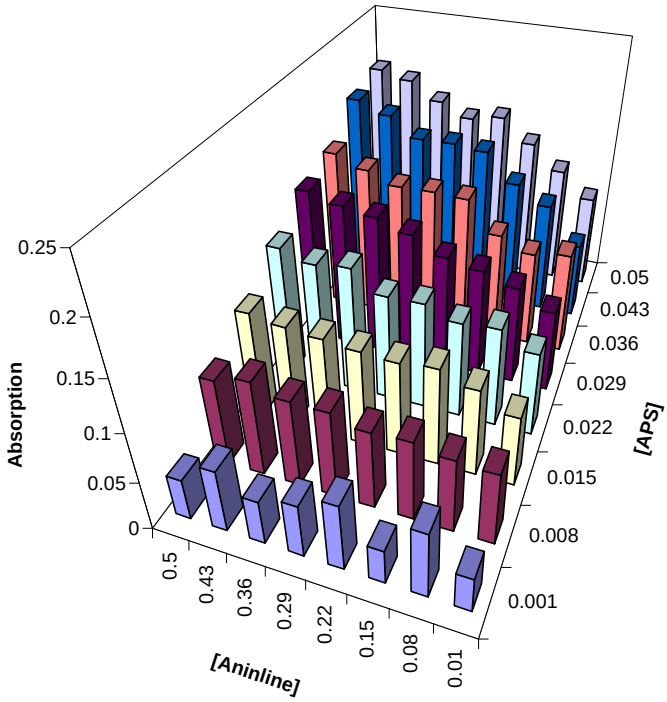

Figure Apx C.13: Absorption (at 550 nm) of chemically polymerised PANI films deposited on a microtitre plate with variation of the concentration of the monomer (0.5 M, 0.43 M, 0.36 M, 0.29 M, 0.22 M, 0.15 M, 0.08 M, 0.01 M) and of the ammonium persulfate (0.05, 0.043, 0.036, 0.029, 0.022, 0.015, 0.008, 0.001). The concentration of the hydrochloric acid was kept constant at 0.6 M in 25% acetonitrile in water.